Paleomagnetic Secular Field Variation
and Rock Magnetism of Some Early
Holocene (≤9900BP) Postglacial
Lacustrine Sediments Near Thunder Bay
Northwestern Ontario, Canada

by

Bjarne Sven Gustav Almqvist

Lakehead

UNIVERSITY

OFFICE OF GRADUATE STUDIES

NAME OF STUDENT: Bjarne Sven Gustav Almqvist

DEGREE AWARDED: Master of Science

ACADEMIC UNIT: Department of Geology

TITLE OF THESIS: Paleomagnetic Secular Field Variation and Rock Magnetism of some early Holocene (≤9900BP) Postglacial Lacustrine Sediments near Thunder Bay, northwestern Ontario, Canada.
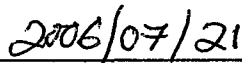
This thesis has been prepared

under my supervision

and the candidate has complied

with the Master's regulations.

Borradaile
Signature of Supervisor

2006/07/21
Date

Abstract

Paleosecular magnetic changes through a 1.5m section of post-glacial lacustrine deposits are strongly influenced by mineralogy and differential compaction. The sediments chiefly comprise clay and, in the lower one third part of the section, rhythmites which vary from ~2mm to ~5cm in thickness. 125 paleomagnetic specimens were collected in total from the 1.5m section. Anisotropy of magnetic susceptibility and anisotropy of anhysteretic remanent magnetization identify a magnetic fabric with maximum susceptibility parallel to the bedding plane of the sediments and with a preferred northwest-southeast axis, probably indicating paleo-current alignment. Minimum susceptibility represents the pole to bedding, due to grain alignment.

Incremental acquisition and demagnetization of isothermal and anhysteretic magnetizations and the orthogonal three-axis test indicate that the sediments contain two magnetic phases with different coercivities. Magnetic hysteresis measurements (clays n=226; silts n=37) show that clay is dominated by single domain magnetite and hematite (means of M_s=58.47±9.22Am^2, M_{rs}=17.12±27.22Am^2, H_c=21.09±7.69mT, H_{cr}=62.04±4.09mT) whereas silt is dominated by pseudo-single domain and single domain magnetite (means of M_s=681.0±395.9Am^2, M_{rs}=163.2±84.75Am^2, H_c=26.07±2.94mT, H_{cr}=56.08±3.17mT). The silt is dominated by magnetite, whereas the clay carries both hematite and magnetite.

Incremental alternating field demagnetization of clay, in 10 to 17 stages, successfully isolated three distinct remanence components, with different directions. A weak and spurious component that is due to handling magnetization, for example, was removed in early demagnetization steps. The two remaining components, isolated by further demagnetization, have geological significance. Mineral magnetic properties as well as differential compaction are responsible for the different directions of the two geologically significant magnetizations in the clay. One has intermediate coercivities (20 – 40mT) with a Fisher mean declination = 357.4° and Fisher mean inclination = 62.0°, approaching the present Earth's magnetic field (declination=356.7° and inclination=74.7°). The other has harder coercivities (>40mT) and represents a stable geological magnetization. The silt has a single component of magnetization carried by magnetite. Laboratory re-deposition of clay in large (125cm3) cubes accurately records the direction of the laboratory magnetic field; thus major inclination shallowing in natural sediments occurred subsequent to acquisition of original DRM.

A magnetostratigraphic record of the hard coercivity component over the 1.5 meter section reveals paleosecular variation of the Earth's magnetic field, with some complications due to compaction. A single westward drifting loop is recorded in the sediments, representing a time-

period of circa 600 – 2400 years, with declinations varying from 199.8° to 119.9° (Fisher mean=005.2°) and inclinations varying from -2.4° to 77.4° (Fisher mean=50.9°). In comparison the inclination of the geocentric axial dipole (GAD) for the study location is +66°.

Acknowledgements

Table of Content

List of Figures

List of Tables

Chapter 1: Introduction

The main portion of the Earth's magnetic field is generated in the fluid outer core in the form of a magnetohydrodynamic dynamo (Butler, 1992). Its generation is on such a complex scale that as of yet no mathematical model can fully explain the behavior of the geomagnetic field. The astatic nature of the Earth's field has been observed since the first established geomagnetic observatory some 400 years ago, although recorded knowledge of the geomagnetic field has existed since early Chinese and Arab scholars invented the compass. Simply put, the motion of the fluid outer core acts in a way to generate a giant dipole magnet with lines of flux that exit and enter Earth's South and North magnetic poles respectively. In fact, the geomagnetic poles are somewhat offset with regard to the actual South and North poles (the axis which Earth rotates about). However, because the outer core is fluid with eddies and currents interacting with the overlying mantle, it not only generates a regular dipole magnet, but also produces a non-dipole moment which corresponds to ~5% of the Earth's total field. Both the dipole and the non-dipole moments are responsible for short-term changes in the geomagnetic field, which is the main concern of this thesis. Short-term changes or paleosecular field variation (PSV) is commonly studied using semi-continuous sedimentary records, such as marine and lacustrine sediments, in order to obtain a wholesome picture of the behavior of the field (e.g. Lund, 1996; 1989; Lund et al., 1988; Creer, 1985). Archaeomagnetic data (e.g. from hearths and fired brick) and lava flows have also been successfully used for studying the short-term behavior, but are inevitably more intermittently spaced in time (e.g. Kovacheva and Zagniy, 1985; Batt, 1997).

I have studied a terrestrial glaciolacustrine deposit located in northwestern Ontario, from the early Holocene or possibly the late Pleistocene, in order to observe a detailed record of the short-term changes in the geomagnetic field together with the sediments' rock magnetic properties. The magnetic record provided by the studied section provides a rather complex history of the imprinting of the geomagnetic field and the physical and chemical processes that affect the record. The rock magnetic properties become crucial for any effort to describe and interpret the detailed record, especially in consideration to the presence of multiple ferromagnetic mineral phases. The objective is therefore set to unravel and describe the different contributions to the magnetic signal observed in the sedimentary section, in order for interpretation to become possible.

The thesis is divided into chapters that cover the relevant background information, process of data collection and data interpretation. Appendices are provided that include the raw data from the rock magnetic tests and demagnetization experiments. Chapter 1 introduces the

main theme of the thesis together with descriptions of the regional bedrock and surface geology of the study area. Chapters 2 and 3 introduce the topic of paleomagnetism through a brief account of fundamental rock magnetism and techniques used to analyze and obtain paleomagnetic data. Chapter 4 describes the characteristics of the geomagnetic field, with focus on paleosecular field variation. The techniques and instruments employed in the thesis study are introduced in Chapter 5. Chapters 6 and 7 provide the heart of the thesis, and contain the results and discussion of rock magnetic and demagnetization experiments. The overall interpretations of the results are summed up in Chapter 8, together with a concluding statement regarding the thesis.

1.1 Regional geology of northwestern Ontario

This section will briefly discuss the bedrock geology of northwestern Ontario as it applies to the area of Strawberry Creek, and the postglacial surface geology.

1.1.1 Bedrock geology

Northwestern Ontario and the area of Thunder Bay are dominated by Precambrian rocks. The earliest rocks occupying this area consist of Archean greenstone and granite terranes with patches of metavolcanic and metasedimentary deposits. The Archean rocks are overlain by early Proterozoic metasedimentary rocks such as slates and conglomerates, together with metavolcanic basalts and andesites (Burwasser, 1977). The early Proterozoic metasedimentary rocks consist of three distinct formations, collectively referred to as the Animikie Group. The three formations are known as the basal Kakabeka conglomerate, which is overlain by the Gunflint Formation which in turn is overlain by the Rove Formation. The Gunflint Formation houses important fossils from prokaryotic organisms and is recognized as one of the world's most diverse biotic communities during the early Proterozoic. A number of absolute dates exist for the Animikie Group (particularly for the Gunflint Formation), but most of these are based on whole rock samples and range in age from 1.556 to 2.111 Ga (Fralick et al., 2002). Recently, euhedral zircons from volcaniclastic beds in the upper portion of the Gunflint Formation were dated at 1878.3±1.3 million years (Fralick et al., 2002).

The Animikie Group is unconformably overlain by the Sibley Group, which is still in need of age constraint but with a maximum age of 1537(+10/-2) Ma (Davis and Sutcliffe, 1985). Toward the end of the Mesoproterozoic, the basement rocks were intruded by sills and dikes of diabase and gabbro. The sills and dikes in the area of Thunder Bay and Nipigon communities are collectively known as the Logan sills or the Nipigon and Logan sills. They are dated at ~1110Ma and are related to the Mesoproterozoic Keweenawan midcontinent rift system (Green, 1983).

1.1.2 Surface geology

The surface deposits present in northwestern Ontario are exclusively influenced by Quaternary glaciation, especially through the ice movements during the late Pleistocene and early Holocene. During this time period the ice margin fluctuated back and forth in the Strawberry Creek area. Several terminal moraines exist in the area as a result (Prest et al., 1968). Further, parts of northwestern Ontario and much of northern North America was occupied by glacial Lake Agassiz, one of the largest freshwater lakes known to have existed on Earth. Movement of water between Lake Agassiz and Lake Superior has greatly affected the surface deposited sediments throughout northwestern Ontario. Early in its history during the late Pleistocene, Lake Agassiz had its overflow removed south through the Minnesota River valley since northern drainage pathways were blocked by ice (Teller and Thorleifson, 1983). Once the ice margin had retreated northward new drainage channels were opened that allowed the water level of Lake Agassiz water to drop through overflows into the lower elevation Kashabowie-Seine River valleys west of Thunder Bay, into the Superior basin. The ice continued to recede and the lower elevation eastern outlets into Lake Nipigon were gradually opened (Figure 1.1). The activation of the lower drainage channels meant that Lake Agassiz fell to the lowest level of its existence.

The Marquette glacial advance, during the Emerson phase of Lake Agassiz (~9900BP; Teller and Thorleifson, 1983) once more blocked off the northerly Nipigon outlets (Figure 1.1, Figure 1.2). Glacial Lake Kaministikwia formed between the present day Marks moraine and the Dog Lake moraine (Figure 1.3, Figure 1.4). Overflow took place into Lake Agassiz from the Superior basin, via Lake Kaministikwia. Red clay characteristic of the Superior basin was introduced throughout parts of northwestern Ontario during this event (Rittenhouse, 1934; Antevs, 1954; Zoltai, 1965; 1963; 1961; see Figure 1.5). The Hartmann moraine served as the northern boundary for the spread of red clay. Once the ice margin started to retreat the northern drainage channels between the Lake Agassiz and the Lake Nipigon basin were once more opened. The deep and wide drainage channels that were cut through Proterozoic sills, together with the presence of large boulders in the upper reaches of the channels are suggested as evidence for catastrophic overflows with discharge of large amounts of water in short times (~100,000m^{3}s^{-1}; Teller and Thorleifson, 1983). As retreat of the ice margin continued north of the Nakina moraines (Figure 1.3), the spillways between Lake Agassiz and Lake Nipigon were abandoned, as water preferentially began to drain from Agassiz into the northeasterly Lake Ojibway.
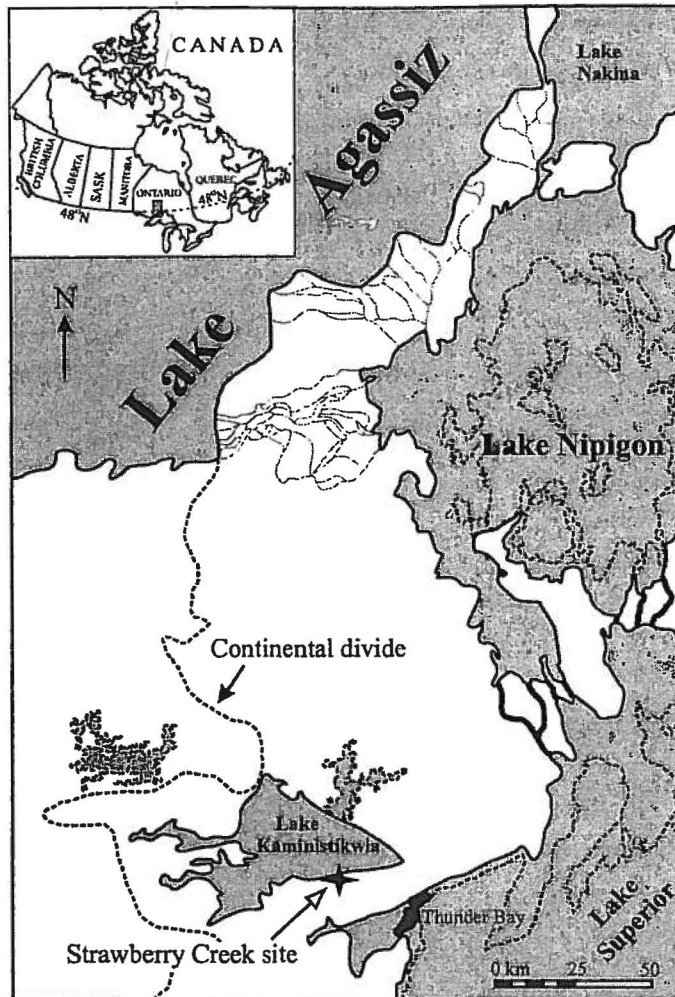
(Modified from Teller and Thorleifson, 1983)

Figure 1.1 Postglacial map of northwestern Ontario, showing the extent of glacial Lake Agassiz, Lake Nipigon and Lake Kaministikwia in solid lines. Modern day shore-lines are indicated by dashed lines, for Lake Superior and Lake Nipigon. Major glacial spillways are indicated by heavy black lines from Lake Agassiz to Lake Nipigon to Lake Superior. (Redrawn from Teller and Thorleifson, 1983).

1.1.3 The Strawberry Creek area

The sedimentary section studied from Strawberry Creek is situated about 30 kilometres west of Thunder Bay along Highway 17, on the north side (Figure 1.1). The best description for the surface geology of this area has been provided through the work of Zoltai (1961; 1963). The location served as a gravel pit, and is now owned by Lafarge construction and materials. The area is contained by the Dog Lake and Marks moraines which possibly served as a dam for glacial Lake Kaministikwia. Most of the surface deposits in the area consist of rolling tills with mixed amounts of sand, together with clay lake sediments (Zoltai, 1963: figure 3). The eastern part of the area (the wedge created by the Dog Lake and Marks moraines) is occupied by a gently

dipping deltaic sand plain that developed as sandy sediments spilled into Lake Kaministikwia from the Superior basin. Zoltai (1963; 1961) identified two common types of glaciolacustrine deposits in the area of Strawberry Creek. The first are deltaic deposits, which occur mainly in two areas: the lower Kaministikwia River and south of Hazelwood Lake. The second prevalent deposit consists of lacustrine clays and silts, which is the dominant deposit at the location studied in this thesis. Zoltai (1963) observed both massive deposits of clay and silt, and varved deposits of clay. Calcium carbonate is common in the clays and silts, and can constitute up 15% of the total sediment weight. The clays generally have a reddish colour, and occur prevalently in the Kaministikwia river valley; massive clays generally overly varved clays throughout the river valley.
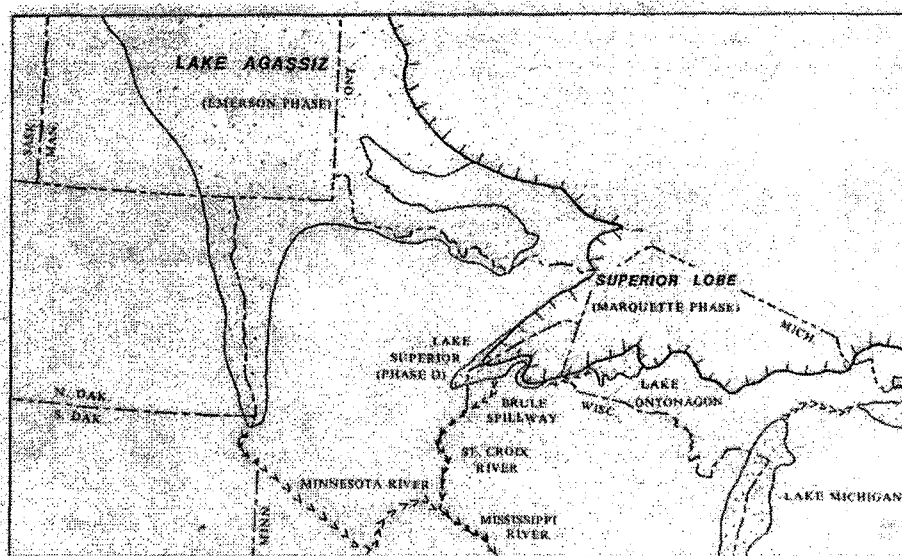
Figure 1.2 Sketch map illustrating the extent of the ice margin during the Emerson phase of Lake Agassiz (Marquette glacial re-advance) at ~9900BP (from Clayton, 1983).

It is a challenge to determine the age of deposition of the Strawberry Creek sediments, but clearly the deposition took place during the early Holocene. Similar red clays as those found at Strawberry Creek have been located in the western parts of northern Ontario (e.g. Dryden and Atikokan) (Teller and Thorleifson, 1983; Teller, pers. comm., 2004). The deposition of the red clays encountered in northwestern Ontario appears to be related to a singe event when overflow from the Lake Superior basin entered glacial Lake Kaministikwia and the eastern basins of Lake Agassiz (Minning, 1994). Further, Minning et al. (1994; also see Warman, 1991) state that red clays from the basins of Wabigoon, Lake Kaministikwia and Fort Frances show distinct geochemical

similarities which support their relation. Zoltai (1965) notes that the "band" of red clay that spread through northwestern Ontario probably originated from Lake Kaministikwia. Nielsen et al. (1982) obtained radiocarbon dates from mollusks at two locations southwest of Fort Frances, which were stratigraphically related to the red clays. After correction for a reservoir effect, Nielsen et al. (1982) found a calibrated radiocarbon age of 10,000±100 BP. from the mollusk associated with the red clay. This date coincides with the Emerson Phase of Lake Agassiz, and compares with radiocarbon ages of Arndt (1977), obtained from wood fragments. Further, Nielsen et al. (1982) argue that the red clay was deposited at the beginning of the Emerson Phase, when the ice margin was stationary and formed the Hartmann, Dog Lake and Marks moraines. This means that the red clays at Strawberry Creek must be ≤9900BP (or ≤10,000BP).
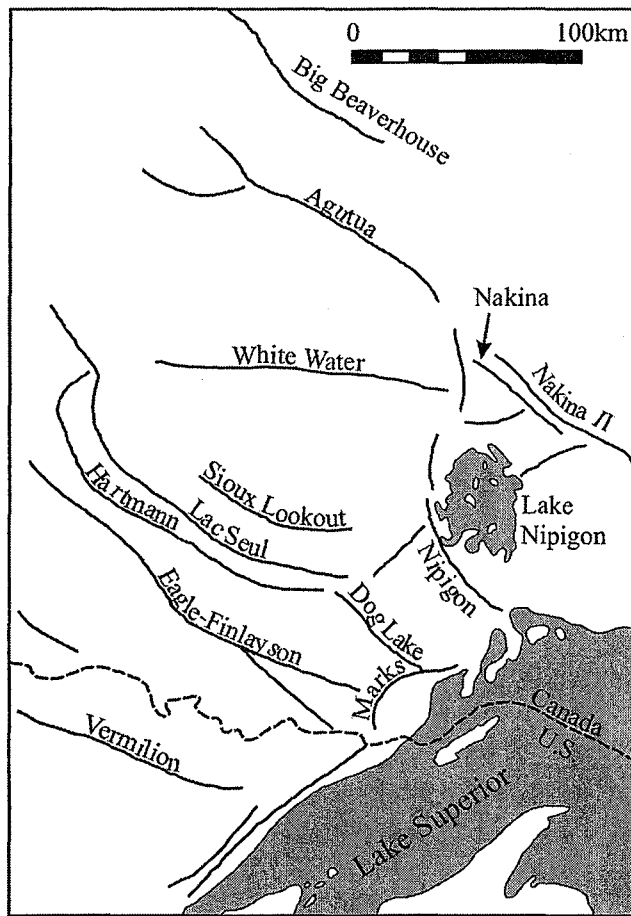
(Modified from Zoltai, 1965b)

Figure 1.3 Geomorphologic map of northwestern Ontario displaying the major moraines deposited in the area after retreat. (Redrawn from Zoltai, 1965).
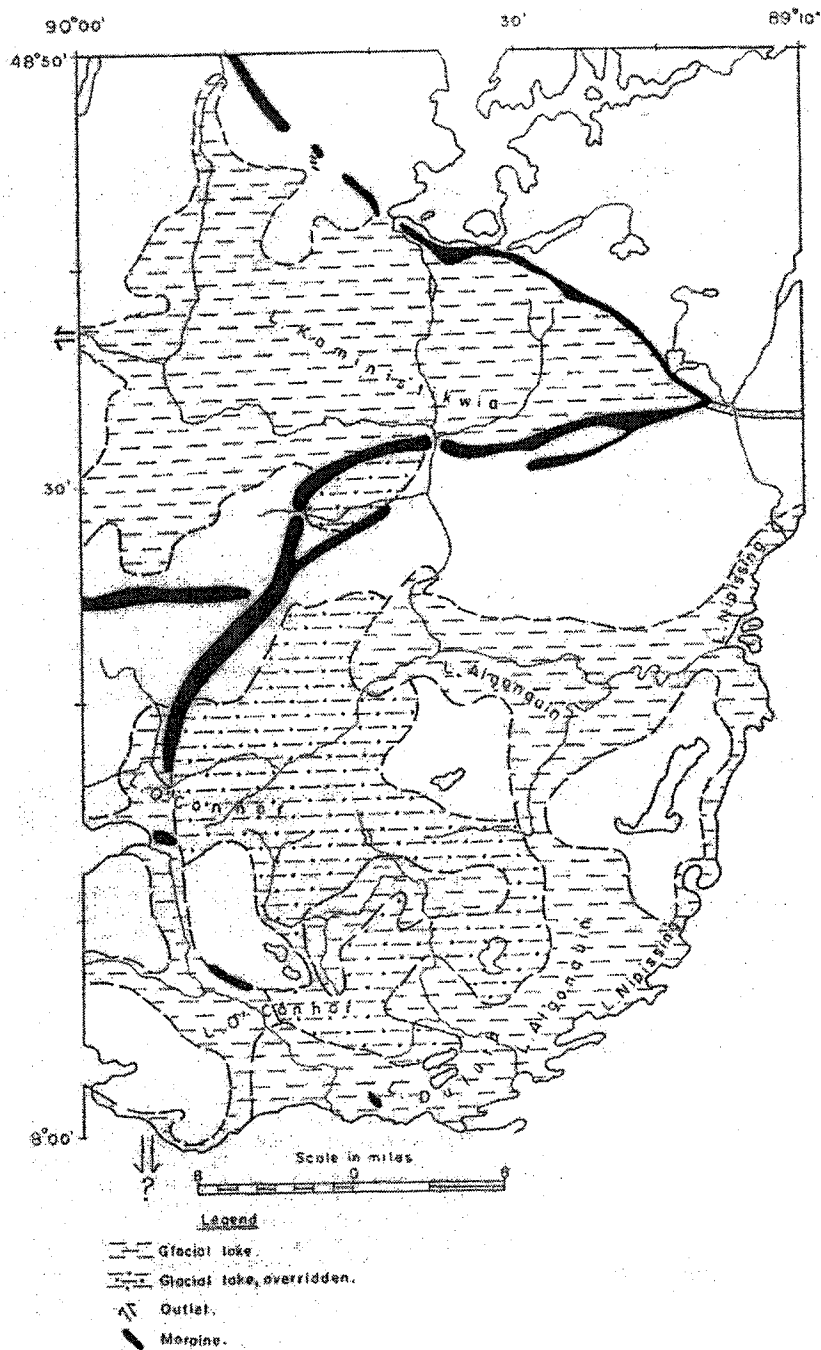
Figure 1.4 Glacial Lake Kaministikwia, located between the Marks and Dog Lake Moraines (from Zoltai, 1963).

For sake of ease, I choose to refer to the site studied simply as Strawberry Creek (even though it actually refers to the stream crossing Highway 17 in the vicinity of the study location). A vertical section was dug into the slope of a hillside facing southeast (Figure 1.6a and b) that had previously been cleared using machinery. The entire slope is coloured red as the overlying

red clay overburden has crept down slope over time. The upper portion of the section contains red massive clays followed by underlying red rhythmic deposits of clay and silt (most likely annually varved sediments, Figure 1.7a). These deposits are free of coarser sediments such as pebbles or gravel sized material, however some organic carbon staining occurs together with minor root disturbance. The varved couplets of clay and silt range in thickness from ~1-2mm to ~5 cm, and are dipping slightly (<5°) towards the east. Below the varved clays and silts are coarser sediments in the form of climbing ripples of sand (Figure 1.7b). A layer of hardpan calcium carbonate is deposited between the rippled sand and rhythmic clay and silt. A sandy till with dispersed large cobbles is deposited below the rippled sand, which makes up the bottom section of the excavated trench (Figure 1.8).

A trench with a vertical face was dug using a shovel, in steps (Figure 1.9), from the top to the bottom of the slope. Samples were collected only from the top 1.5m as the sandy till at the bottom half of the trench was unsuitable for fine scale paleomagnetic studies. Oriented troughs of stainless steel with a U-shape were used to extract sediments from the vertical cut face (Figure 1.10). The edges of the troughs were sharpened in order to easily insert them into the compacted sediments. These samples were wrapped in thin plastic and tinfoil in order to preserve them for later sub-sampling in the laboratory. Once in the laboratory, each of the troughs were cleaned and prepared for sub-sampling, mainly by creating a smooth surface in which regular 2x2x2cm plastic cubes could be pushed into. Care was taken not to disturb the sediments when the smooth surface was produced as this would affect the results of paleomagnetic measurements.
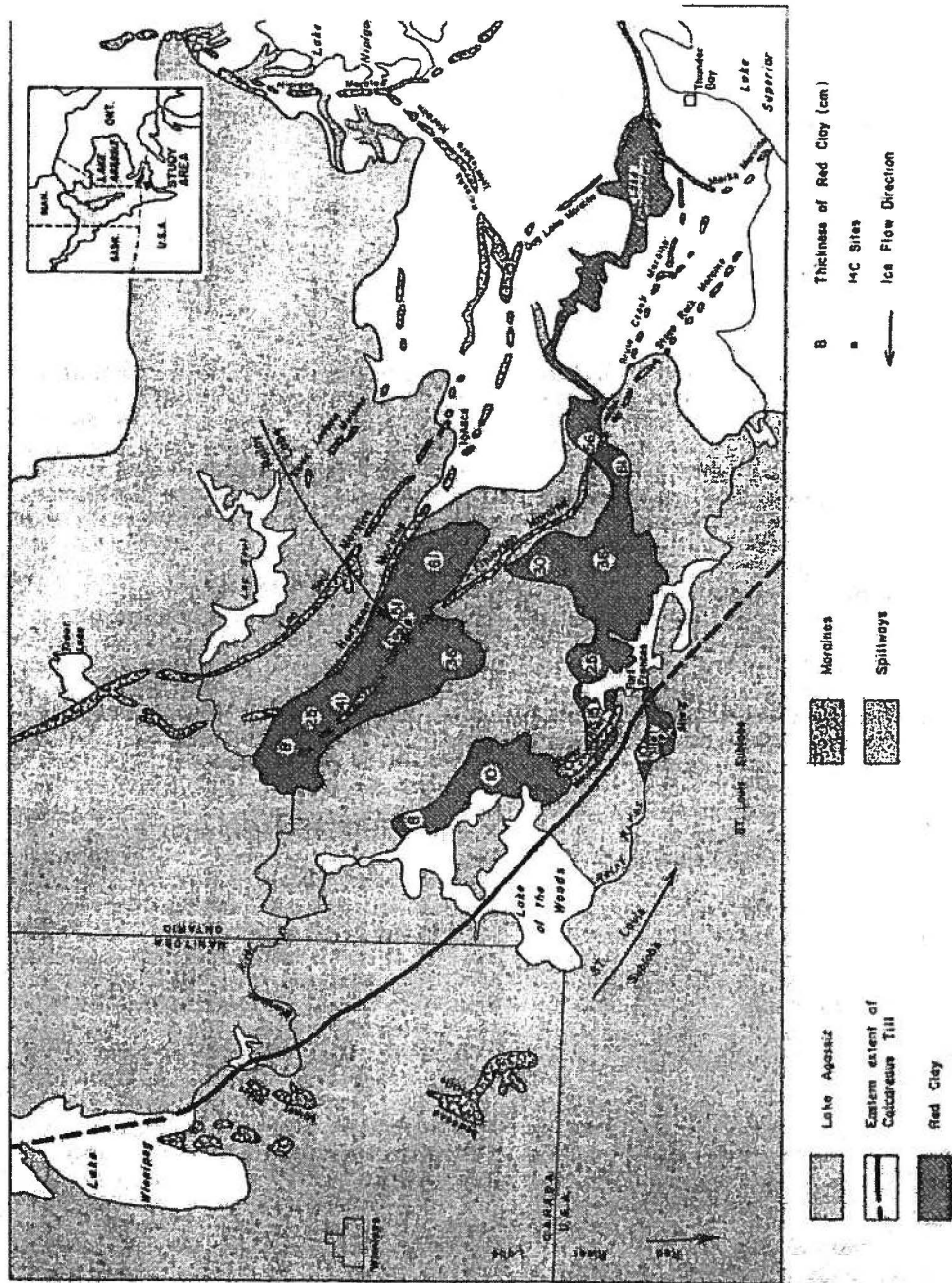
Figure 1.5 Spread of red clay throughout northwestern Ontario, together with other prominent surface deposits in the same area (from Nielsen et al., 1982).
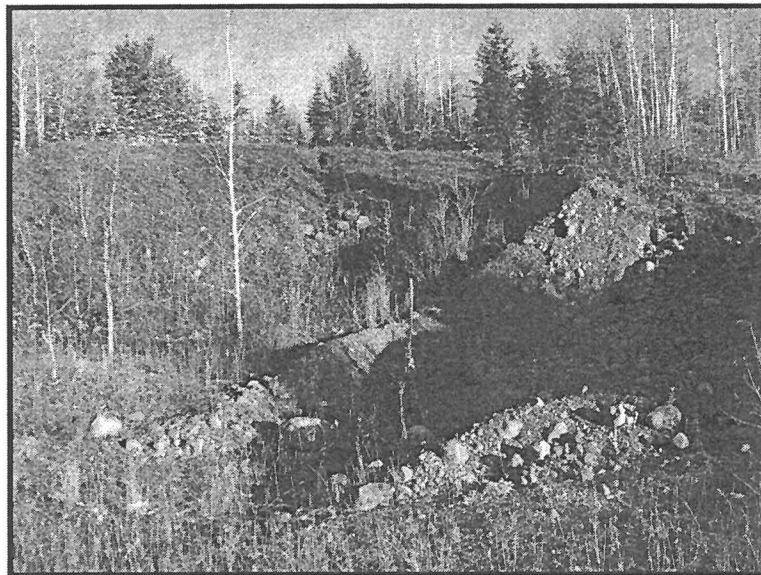
Figure 1.6 Photographs of the Strawberry Creek section. (a) Sedimentary section prior to the trench being dug. (b) Area to the right of picture in (a) showing where the sediments were moved by machinery.
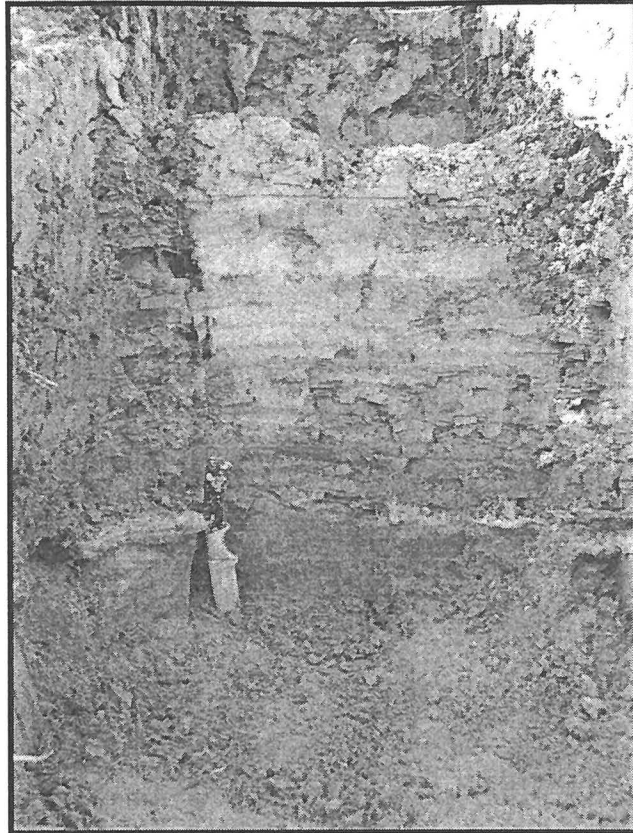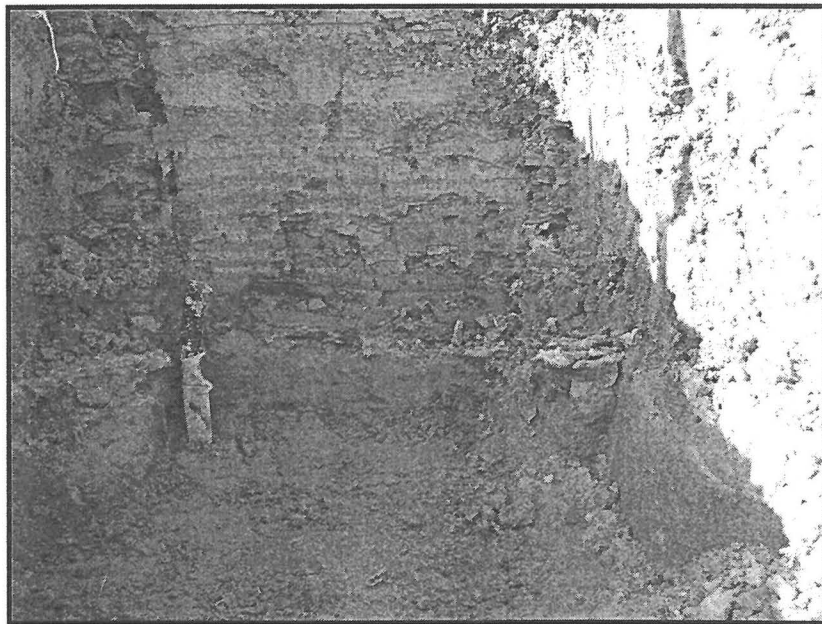
Figure 1.7 Detailed photographs of the sediments after the trench had been excavated. In (a), a large portion of the section is displayed with massive red clay at the top, followed by alternating (varved) layers of red clay and grey silt. Bottom of photograph in (a) shows the hardpan calcium carbonate layer and the climbing sand-ripples. (b) is a close-up of the middle portion of the section. Knife is shown for scale.
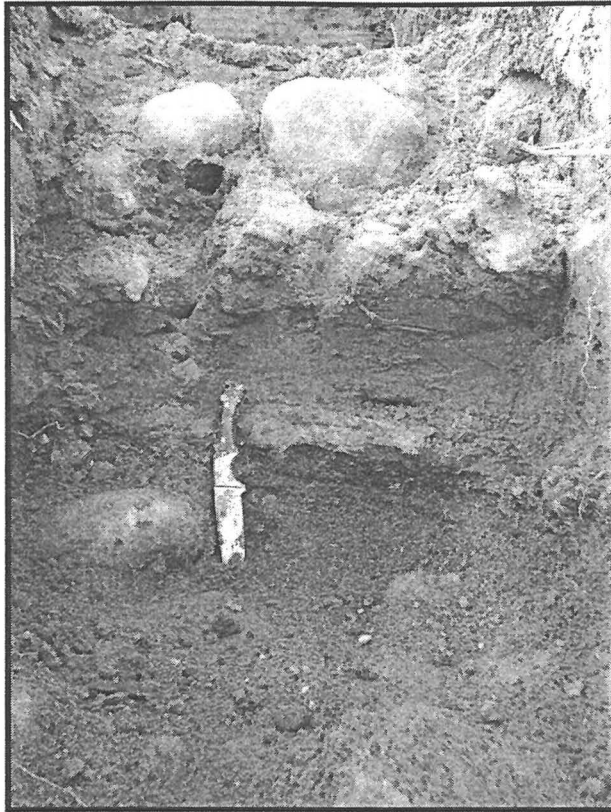
Figure 1.8 Photograph of the sandy till at the bottom of section (no paleomagnetic samples were extracted from this part of the section).

Figure 1.9 The completed trench at Strawberry Creek, about 3m deep. Note the transition from fine-grained sediments at the top to till material towards the bottom.
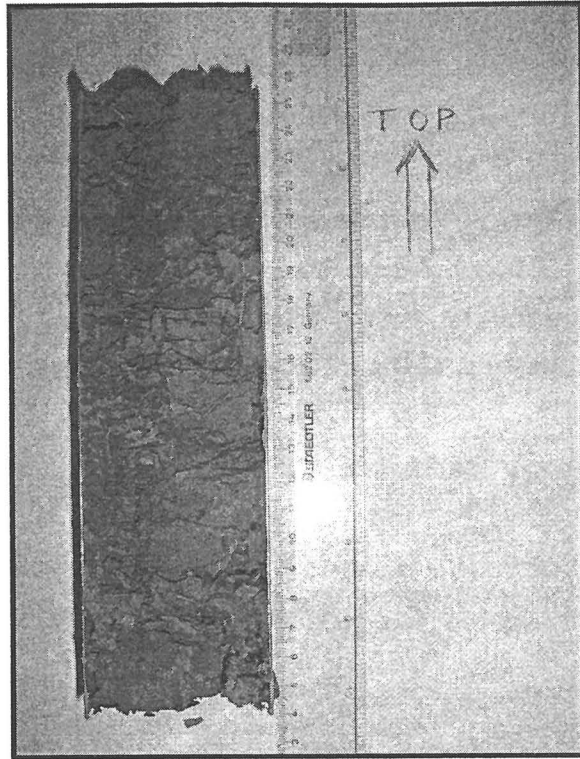
Figure 1.10 U-type channel used to extract samples of sediment that were later sub-sampled with 2x2x2cm plastic cubes.

Chapter 2: The principles of rock magnetism and the origin of magnetic remanences

2.1 The magnetic moment

The properties of the electron in an atom give rise to the magnetic moment in two ways. The first involves the orbital motion of the electron around the nucleus of the atom, and this is simply called the orbital magnetic moment. The second manner entail the spin moment produced by the rotation of the electron about its own axis, and is referred to as the spin magnetic moment (Chikazumi, 1964).

A single magnetic moment, μ, is defined either as a pair of electric charges (m) separated by a distance (l), or as a loop of electrical current (I) with an area (A) producing a vector, $\mathbf{n}$ (Butler, 1992). In this discussion bold faced letters refer to vectors. The latter definition is useful in explaining the magnetic moment that arises from the electron orbiting the nucleus of an atom, and the current loop model is a useful model in general since all magnetic moments are created through electrical currents.

The microscopic magnetic moment, or dipole (μ), described above produces a magnetic field ($\mathbf{H}$). $\mathbf{H}$ is described by the force it exerts on a physical object (Dunlop and Özdemir, 1997). The magnetization, $\mathbf{M}$, is the sum of all μ per unit volume, or the net magnetic dipole moment (Butler, 1992) or the magnetic intensity. Hence $\mathbf{M}$ considers a volume containing n atoms, each with a dipole moment (μ). The sum of H and M describes the augmented field ($\mathbf{B}$) such that

$$\mathbf{B} = \mu_0(\mathbf{M} + \mathbf{H}).$$ [Eqn. 2.1]

Since $\mathbf{M}$ considers a volume of atoms with their respective dipole moments, $\mathbf{B}$ can only be resolved on a macroscopic level (Dunlop and Özdemir, 1997). $\mathbf{B}$ is also dependent on the constant permeability of free space, $\mu_0 = 4\pi \times 10^{-7}$ H/m. The force exerted by a magnetic field, $\mathbf{H}$, on a volume carrying n atoms, each with a dipole moment will produce a magnetization ($\mathbf{M}$), dependent on the magnetic susceptibility (χ) of the dipole moments, such that

$$\mathbf{M} = \chi\mathbf{H}$$ [Eqn. 2.2]

The magnetic susceptibility is the ability of a material or substance to become magnetized. When an outside magnetic field, such as the $\mathbf{H}$ in [Eqn. 2.2] is applied to the substance, an induced magnetization is created ($\mathbf{M}_i$). A more in-depth discussion of fundamental magnetic properties in relation to paleomagnetism and rock magnetic studies are provided by Dunlop and Özdemir (1997), Stacey and Banarjee (1974) and Chikazumi (1964).

2.2 Diamagnetism, paramagnetism and ferromagnetism

All solid materials respond to an applied magnetic field. This response can be diamagnetic, paramagnetic or ferromagnetic. In paleomagnetic studies, only materials or minerals displaying the latter response are of interest, but in many rock magnetic experiments (e.g. anisotropy of magnetic susceptibility, hysteresis and the Curie balance) the former two responses can be very important.

Diamagnetism arises when the orbitals of electrons are altered due to an applied magnetic field (Butler, 1992). The diamagnetic response is a property of all solid materials, and the moment that is produced opposes the direction of the applied magnetic field (Figure 2.1a). The diamagnetic response has its origins in the orbital rotation of electrons and lacks the electron spin moment. Susceptibilities (χ) are usually very weak, around 10^{-6} SI; because the induced magnetic moment in a diamagnetic solid is weak; it is outweighed by the paramagnetic and ferromagnetic response. The diamagnetic moment is independent of temperature. Common diamagnetic minerals include quartz, calcite and plagioclase feldspar.

Paramagnetic solids possess a spin magnetic moment and the application of a magnetic field creates an induced magnetization parallel to the direction of the field (Figure 2.1b). The paramagnetic response is linear with respect to the strength of the applied field. Once the field is removed the induced magnetization disappears. The magnetic moments of a paramagnetic solid assume randomized orientations so that energy configurations are minimized when temperatures are greater than absolute zero and an applied magnetic field is absent. The magnetic moments are also assumed to be non-interactive (Dunlop and Özdemir, 1997). Paramagnetic solids have transition metals (e.g. Fe, Mg, Ti, Mn, Cr, Ni, etc.) incorporated in their molecular structure and common minerals that display paramagnetism include amphiboles, orthopyroxenes, siderite, pyrite and ilmenite (the latter is paramagnetic at room temperature). The magnetic susceptibility of a paramagnetic solid is on the order of 10^{-5} SI (Butler, 1992).

The distinguishing property of a regular household magnet is its ability to remain magnetized and adhere to other ferrous objects. This ability is retained in the magnet even when an applied magnetic field is not present. Magnets are ferromagnetic, and they manage to remain magnetized after an applied field is removed, in contrast to diamagnetic and paramagnetic materials in which **M** disappears when **H** is removed. The dipole memory is due to the exchange spin coupling of electrons, and interaction of the spin moments are the prominent feature leading a material to become ferromagnetic. The induced magnetization (**M**i) eventually saturates as an increasing magnetic field is applied to a ferromagnetic solid (Figure 2.1c), as all dipole moments

are aligned with the direction of the applied field. This is an important characteristic of all ferromagnetic substances, and the saturating field produces a saturation or spontaneous magnetization (M_s). Subsequently, when the field is removed, a measurable remanent magnetization (M_r) remain which is created by the exchange spin coupling (or magnetic memory) of the ferromagnetic dipole moments. The ferromagnetic response is temperature dependent and increasing temperatures leads to decreasing M_s. An increase in temperature leads to excitation of the atomic structure and disruption of the exchange couplings that gives rise to ferromagnetism. The loss of magnetization is gradual until the Curie temperature (T_C) is reached where $M_s=0$ and no spin exchange couplings remain (Dunlop and Özdemir, 1997: their figure 2.4). Since the atomic structures of individual materials are different from each other, each material has a separate T_C. This property is discussed below (section 2.3) for individual minerals.
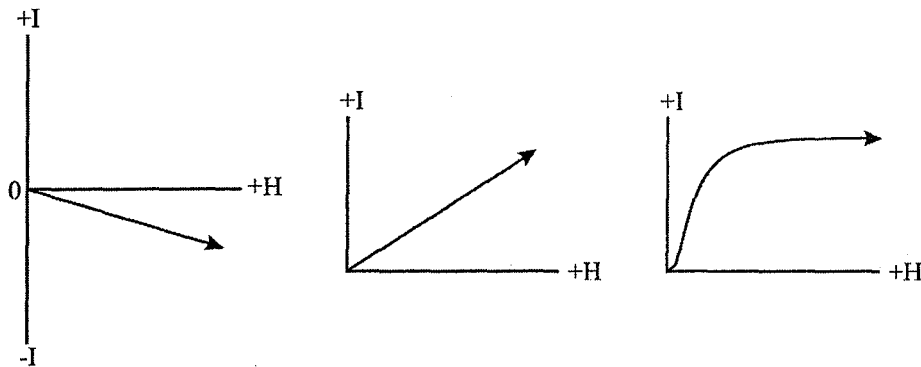
Figure 2.1 The induced response (I) to an applied magnetic field (H) in (a) a diamagnetic solid, (b) a paramagnetic solid and (c) a ferromagnetic solid.

The term ferromagnetism is used in two ways. As a general definition (*sensu lato*), ferromagnetism includes all forms of exchange-couplings that lead to the properties of saturation and remanent magnetization. Second, ferromagnetic properties also refer to a particular type of spin exchange-coupling exhibited by some substances (Figure 2.2c). The different kinds of spin exchange-couplings are shown in Figure 2.2(a-d). Four possibilities exist for the arrangement of the exchange-couplings: i) in ferromagnetic exchange-couplings all moments are coupled in a parallel fashion, leading to a large net M_s (Figure 2.2a); ii) for the case of antiferromagnetism the magnetic moments are coupled anti-parallel to each other with no net M_s (Figure 2.2b); iii) in ferrimagnetic materials exchange-couplings are anti-parallel, but of dissimilar strength in the opposing moments, leading to a net M_s (Figure 2.2c); iv) canted antiferromagnetism consists of anti-parallel exchange-couplings that are slightly offset to each other creating a net magnetization at near right angles to the direction of the magnetic moments (Figure 2.2d).

(a)   (b)   (c)   (d)
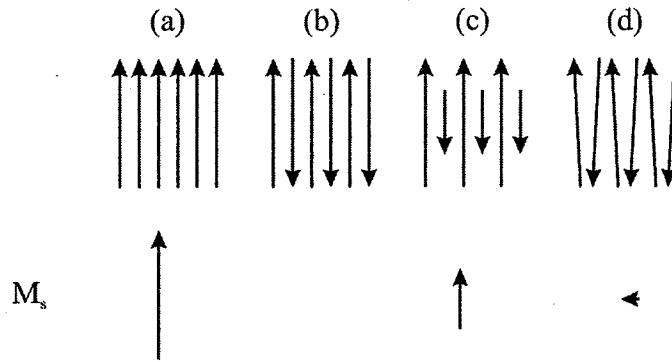
Figure 2.2 Exchange couplings displayed by ferromagnetic materials (*sensu lato*), (a) ferromagnetic couplings (*sensu stricto*), (b) antiferromagnetic couplings, (c) ferrimagnetic couplings and (d) antiferromagnetic spin-canted exchange couplings.

2.3 Magnetic mineralogy in sediments and sedimentary rocks

The most common magnetic minerals comprise iron-oxides, iron oxy-hydroxides and iron-sulphides. This section comprises a very general and brief discussion of the ferromagnetic minerals (*sensu lato*) important in sedimentary settings that can either be transported detrital grains or form authigenically in situ. For further detail on rock magnetic minerals see textbooks by Evans and Heller (2003), Dunlop and Özdemir (1997) and Butler (1992). The largest body of literature in rock magnetism concerns magnetite, although hematite in particular has also been extensively studied (e.g. Dekkers and Linssen, 1989; Dekkers, 1988; Dunlop, 1971; 1970)

2.3.1 Magnetite and its Titanium species

Magnetite (Fe_3O_4), together with hematite, is the most common magnetic mineral occurring in natural environments on Earth. It has an inverse spinel structure with A and B sublattices, containing different cations (Fe^{3+}, Fe^{2+}) at each site. The A-sites have tetrahedral coordination of oxygen ions and can hold the smaller Fe^{3+} cation, while the B-sites have octrahedral coordination of oxygen ions and hold the larger Fe^{2+} cations and the remaining Fe^{3+} cations. The magnetic moments of the sublattices oppose each other, however since the moment of Fe^{2+} will be unaccounted for (Fe^{3+} cations nearly cancel each others magnetic moment) a net magnetization will result. Magnetite is therefore ferrimagnetic and has M_s of 480 kA/m. The general formula used to characterize magnetite and its Ti-species is $Fe_{3-x}Ti_xO_4$; $x=0$ refers to magnetite and $x=1$ is the Ti equivalent called ulvöspinel. Intermediate compositions of x are possible and occur in certain types of environments. For example, titanomagnetite with $x=0.6$ (also called TM 60) is common in basalts that have undergone little or no oxidation. Saturation

magnetization and Curie temperatures decrease almost linearly as x increases. TM60 has a T_C of ~150-200°C and Ms ~125kA/m. Low-temperature experiments with liquid nitrogen and helium indicate that magnetite undergoes a crystallographic change at ~135K, from having a cubic lattice structure to a monoclinic structure (Evans and Heller, 2003).

2.3.2 Maghemite

Maghemite (γ-Fe_2O_3) forms as the oxidation product of magnetite. It has the inverse spinel structure; however every third Fe^{2+} cation is removed from the octrahedral B-lattice through oxidation, leaving this site vacant. As a consequence, maghemite is ferrimagnetic and has $M_s = 380$kA/m at room temperature (Dunlop and Özdemir, 1997), lower than that of magnetite. Before reaching its T_C the maghemite structure changes from the inverse spinel to hexagonal, thus creating hematite (α-Fe_2O_3). The T_C was determined by Özdemir and Banarjee (1984) to be ~645°C (see also Dunlop and Özdemir, 1997), although it is challenging to determine the T_C of maghemite experimentally since it irreversibly inverts to form hematite (i.e. structurally changes from inverse spinel to hexagonal framework) before it reaches its Curie temperature. Maghemite is a common weathering product of magnetite in soil formation processes.

2.3.3 Hematite

Hematite (α-Fe_2O_3), is a commonly occurring mineral in sediments and sedimentary rocks. Hematite is anti-ferromagnetic as a result of opposite spin directions of equal magnitude in alternating layers in the basal layers of its hexagonal structure (i.e. corundum structure; Figure 2.3a). The magnetic moments are perpendicular to the c-axis. However, the coupled magnetic moments are not exactly anti-parallel which leads to a canted or parasitic magnetization (Figure 2.2d; Figure 2.3a). Because of the spin canted origin of the magnetization, the intensity of Ms in hematite is much less compared to that of magnetite (~2.5 kA/m for hematite). Additionally, a defect magnetic moment is present in hematite that contributes to the M_s. The defect moment is not as well understood as the spin canted moment, but is thought to arise from lattice defects or impure non-magnetic cations (Butler, 1992). The Curie temperature (T_C) of hematite is ~675-680°C (Evans and Heller, 2003). Hematite is very coercive, and alternating field (AF) demagnetization is usually inadequate to remove the remanence carried by this mineral.

Hematite undergoes a crystallographic change when it is cooled to between -10 and -15°C, and the spin moments are pinned along the c-axis, with up- and down-spins in alternating layers of the crystal lattice (Figure 2.3b). Thus true anti-parallelism is achieved, and the spin

canted moment disappears. This crystallographic change is called the Morin transition (T_{Morin}). T_{Morin} is depressed or even absent in hematite that is of very small grain-size or contain titanium substitutions in its crystal lattice (Dunlop and Özdemir, 1997). The Morin transition is usually a useful indicator of hematite in a sample because most of the remanent magnetization in hematite is due to the canted moment. However, it can be difficult to observe this transition when hematite exists in combination with a high M_s mineral such as magnetite since the latter would simply overwhelm the net magnetic moment.

(a)   (b)
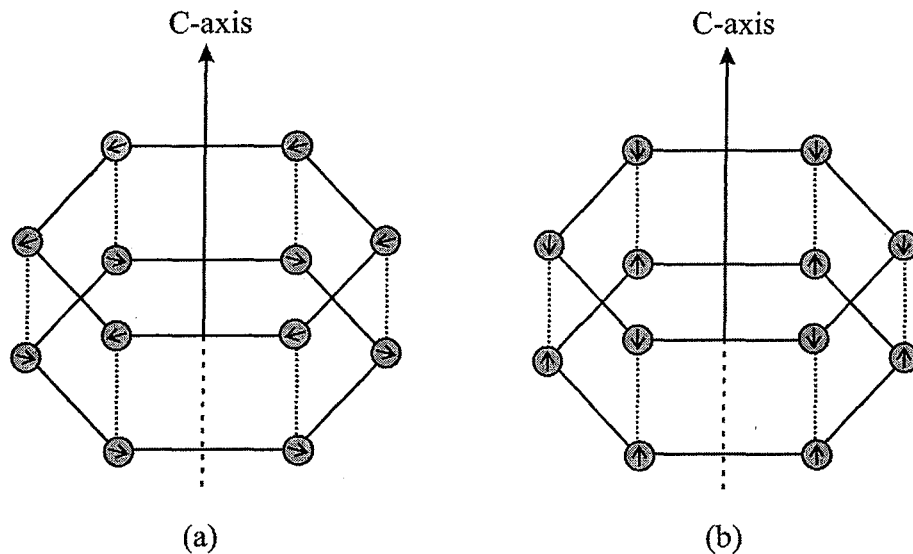
Figure 2.3 Simplified schematic of the exchange couplings in hematite, (a) shows the regular hexagonal lattice of hematite (corundum-structure), with arrows indicating the directions of spin moments by electrons. Spin moments are oriented perpendicular to the c-axis of the lattice, but also slightly offset in alternate layers, producing the spin-canted moment discussed in the text. (b) At temperatures below the Morin transition spin moments are oriented parallel and anti-parallel to the c-axis in alternating layers.

2.3.4 Iron oxy-hydroxides

Among the hydrous iron-oxides goethite (α-FeOOH) is the only magnetically significant mineral (Evans and Heller, 2003). It is common as a weathering product in soils and sediments, and can be an important contributor to the remanent magnetization in such environmental settings. Goethite is antiferromagnetic and has an orthorhombic structure, with coinciding Néel and Curie temperatures at ~120°C. The origin of M_s is not well understood in goethite but is thought to arise similarly to the defect moment that is present in hematite (Evans and Heller, 2003); the M_s is ~2kA/m, somewhat weaker than hematite. Dehydration of goethite produces hematite that is often very fine-grained (Dunlop and Özdemir, 1997). Lepidocroicite (γ-FeOOH) and ferrihydrite ($5Fe_2O_3 \cdot 9H_2O$; also known as limonite) are important hydrous iron oxides in

sedimentary environments in the sense that they may undergo chemical changes or dehydrate to magnetite and hematite.

2.3.5 Iron sulphides

Greigite (Fe_3S_4) and pyrrhotite ($Fe_{1-x}S$) are the two most significant iron sulphides contributing to magnetic properties in the sediments. Greigite has the inverse spinel structure, and is structurally the equivalent of magnetite, although S^{2-} is its anion rather than O^{2-}. It is a mineral that has become increasingly important in sedimentary environments during the last 15-20 years as a consequence of advanced in rock magnetic methods (Evans and Heller, 2003; Snowball 1997a, b), and usually form authigenically in anoxic sulphate-reducing environments or by magnetotactic bacteria in reduced sulfur-rich environments. The M_s of greigite is thought to be ~125kA/m based on measurements of synthetic samples (Evans and Heller, 2003), although Snowball and Torii (1999) argue that it is difficult to obtain enough pure natural material in order to establish the M_s. Greigite displays high magnetocrystalline anisotropy and often acquires gyroremanent or rotational remanent magnetism during alternating field demagnetization at high fields (Snowball, 1997a). Snowball (1997b) used the fact that greigite has a high magnetocrystalline anisotropy and acquires rotational remanence in order to identify and distinguish low concentrations of this mineral in natural settings from other magnetic minerals (Snowball and Torii, 1999). The T_C is ~330°C (Evans and Heller, 2003; Snowball and Torii, 1999) but greigite tends to disintegrate when heated to temperatures between 300-400°C. Similarly to magnetite, greigite shows a crystallographic change when exposed to low-temperature conditions (e.g. exposure to LN_2).

Pyrrhotite is more commonly identified as a detrital mineral than greigite, but can form authigenically under certain circumstances (Snowball and Torii, 1999). Monoclinic pyrrhotite (Fe_7S_8) is the only phase displaying ferrimagnetic properties, since the lattice is deficient in Fe^{2+} cations and therefore producing vacancies in the lattice (similar to the situation displayed by maghemite; Dunlop and Özdemir, 1997). This phase has an M_s of ~80kA/m, and the T_C is ~320°C.

2.4 Magnetic remanences in rocks and sediments

Natural remanent magnetization (NRM) is an umbrella expression for the range of observed remanent magnetizations contained by a specimen once analyzed in the laboratory. The NRM is acquired through a number of physical and chemical processes acting in nature, which do

not necessarily correspond in time. The most well studied remanence is thermoremanent magnetization (TRM) which involves the stabilization and alignment of the magnetic moments as the ambient temperature reduces below a specific temperature (i.e. the Curie temperature). TRM is the primary process of remanence acquisition in igneous rocks, but may also contribute to the remanent magnetization in metamorphic and sedimentary rocks as rocks are heated and cooled over time. Further, TRM is intimately tied to viscous remagnetization (VRM), as discussed later in this chapter. As the focus of this thesis concerns acquisition of remanence in Holocene glacio-lacustrine sediments most emphasis is placed on the possible mechanisms of remanence acquisition in this and similar settings (i.e. sediments and sedimentary rocks). For example, sedimentary and chemical acquisition processes at ambient temperatures are responsible for the magnetic remanences present in the Strawberry Creek sediments.

2.4.1 Magnetization of sediments

Sediments and sedimentary rocks are useful for studies in rock magnetism and paleomagnetism. Semi-continuous sedimentation through time provides an extended recording of the geomagnetic field as magnetic minerals are deposited and oriented according to the direction of the Earth's magnetic field. Sediments and sedimentary rocks have therefore been fundamental for studies of paleomagnetic field secular variation and magnetostratigraphy. The accuracy and completeness of this magnetic record is influenced by physical, chemical and biological processes (i.e. rate of sedimentation, compaction, diagenesis, bioturbation, etc.), which in turn are affected by climatic and environmental factors. As such, the rock magnetic record may also serve, in some respects, as an environmental and climatic proxy. For example, bulk magnetic susceptibility records of the paleosol and paleoloess deposits from the central loess plateau in China (Evans and Heller, 1994) have been used as indicators for separating cold and dry glacial periods against wet and warm interglacial periods.

During deposition of sediments, the magnetic particles settling from the water column are affected by the Earth's magnetic field. The total grain magnetic moment strives to relax parallel to the field vector, even after the grain has settled. This remanence acquisition process gives rise to detrital remanent magnetization (DRM). The alignment of magnetic grains continues even after deposition has taken place, and only at some specific depth in the sediment column are the magnetic grains finally locked into a stable position. In the study of detrital remanent magnetization (DRM), much attention in the last 20 years has focused on understanding the interplay between magnetic mineralogy and physical-chemical properties of sedimentation using rock magnetic methods and the resultant magnetic remanence in sediments. Hence, in order to

evaluate a semi-continuous sedimentary magnetic record it is crucial to understand the mechanisms that influence magnetic remanences in sediments, and what minerals carry that remanence.

Remanence acquisition in sediments is largely influenced by depositional conditions ranging from regional scale factors such as sedimentation in marine or lacustrine basins, to local scale factors such as effects of Brownian motion or bioturbation affecting individual magnetic particles. Acquisition of DRM is also governed by the magnetic properties of ferromagnetic minerals, such as their grain size (e.g. single vs. multidomain) and saturation magnetization.

2.4.1a Detrital remanent magnetization

The classical theoretical expression for depositional remanence developed by Nagata (1961) to describe the torque experienced by a spherical grain of magnetite in the presence of an applied magnetic field, with diameter d, is:

$$I\frac{d^2\theta}{dt^2} + \pi d^3 \eta \frac{d\theta}{dt} + \frac{\pi}{6}\mu_0 d^3 mH \sin\theta = 0 \qquad \text{[Eqn. 2.3]},$$

Where θ is the angle between the magnetic moment of the grain (m) and the applied magnetic field (H), I and η are the moment of inertia of the grain and the viscosity of fluid, respectively (see also, Dunlop and Özdemir, 1997, p. 426; Butler, 1992). The three terms in equation [Eqn. 2.3], from left to right, refers to inertial moment of the grain, viscosity of the fluid and the magnetic aligning torque. For small grains (≤10 μm), the magnetic and viscous torques are dominant, but for true multidomain grains (>10-20 μm) a mechanical torque, experienced by the grains as they settle on the bedding surface, surpasses forces of other torques. According to this expression, the magnetic moment of a grain moving down the water column aligns parallel to the Earth's field in less than one second, and the vertical distance traveled by the grain during this time is about 10^{-5} m (Katari and Bloxham, 2001; Nagata, 1961). Note that the inertial torque is relatively small, even for grains as large as 1 mm, because of the low viscosity of water (see figure 15.1 in Dunlop and Özdemir, 1997). Accordingly, for particles settling out from suspension, remanence should approach saturation based on the theoretical expression discussed above, however, this is never true in nature. Consequently, there has been considerable search for an explanation of why saturation of remanence in sediments does not occur. Clearly, if the unstable moments of multidomain grains are present saturation will not occur, but even with a

tightly constrained grain size group, such as exclusively single domains, saturation does not occur. Initial arguments were brought forward by Collinson (1965) and Stacey (1972), where they considered thermal agitations in water, or Brownian motion, such that the detrital remanence (M_{dr}) is given by

$$M_{dr} = (M_{dr})_{sat} L \left(\frac{\mu_0 V M_r H_0}{kT} \right)$$ [Eqn. 2.4],

where $L\left(\frac{\mu_0 V M_r H_0}{kT}\right)$ represents the Langevin function $(\coth[\frac{\mu_0 V M_r H_0}{kT}]-1/\frac{\mu_0 V M_r H_0}{kT})$ and V is the volume of each grain. The saturation DRM $(M_{dr})_{sat}$ assumes that all remanence moments (M_r) are aligned perfectly. The Langevin function thus represents a thermal randomizing influence on the magnetic moments, but as volume increases the effect of Brownian motion will decrease. Grains of small sizes would undoubtedly be affected by Brownian disturbances in water, although the upper grain size limit is yet to be determined. Stacey (1972) modified the expression developed by Collinson (1965), so that it included a uniform distribution of grain sizes (PSD, 0.1 – 0.2 μm). Although thermal fluctuation theory (Dunlop and Özdemir, 1997) probably is part of the reason why the experimental intensity of DRM is less than predicted by theory, it fails to completely explain a non-saturating DRM.

Beginning in the early 1990's and continuing to the present, much attention concerning the study of DRM has turned to electrochemical properties of water and their effect on remanence properties of magnetic particles in sedimentary environments (i.e. Lu et al., 1990; van Vreumingen, 1993a, b; Katari and Tauxe, 2000). Properties such as salinity, pH and electrostatic forces (e.g. London dispersion or Van-der-Waals forces) of water have been shown to affect the DRM of sediments, especially in the case of finer grained sediments that are incorporated in flocs before deposition. Since flocculation or coagulation of grains is controlled by water chemistry to a large degree, the acquisition of remanence in clay- and silt-rich sediments is also influenced by these conditions.

A laboratory experiment performed by van Vreumingen (1993b) showed that inclination error may also be related to the salinity of water. Flocculation of individual grains is favored at conditions of greater salinity, such that more magnetic particles are incorporated into flocs. In addition, van Vreumingen (1993b) noted that the intensity of magnetization decreased as flocculation was enhanced and the resulting magnetization was accompanied by shallower inclination. This was also observed by Katari and Tauxe (2000) from experiments using different water conditions of salinity and pH. In their work, they showed that intensities of magnetization

decreased with high salinities and low pH (the result of increasing size of flocs). In nature, a more important role may be played by organic matter, which creates a kind of biogenic "glue", which enhances flocculation. Conversely, at high pH, the opposite occurs, with a decrease in floc sizes when the solution becomes basic. An analogy in experiment would be ordinary grain size analysis, where a detergent or another base maybe used to de-flocculate or separate particles as they settle in the water column. Flocculation probably plays an important role in DRM, considering both affects on inclination and intensity of fine-grained sediments.

2.4.1b Post-depositional remanent magnetization

Once a grain has been deposited, it is possible that it will undergo post-depositional realignment. Consequently, as suites of magnetic particles are affected by post-depositional processes, a post-depositional remanent magnetization (pDRM) is formed. In natural sedimentary environments, pDRM is produced mainly by slumping, bioturbation, dewatering and compaction and it may represent the dominant remanence in some sediments and sedimentary rocks (Dunlop and Özdemir, 1997), while it is apparently absent in others (Katari et al., 2000). Note that bioturbation 1) has fixed depths, 2) is restricted to specific depositional environments and 3) is restricted to certain geological periods (e.g. bioturbated sediments are not found in Precambrian depositional environments).

Early laboratory experiments, using re-deposited deep-sea sediment, (Løvlie, 1974; Kent, 1973) illustrated that pDRM is acquired as small magnetic particles occupying interstitial pore spaces in the sediments rotate into alignment with the Earth's magnetic field. Løvlie (1974) suggested that acquisition of remanence can be delayed considerably after deposition, depending on rate of consolidation and grain size of sediments (especially size of magnetic particles). The extent to which pDRM contributes to the overall remanence of sediments is today a subject of some disagreement (see discussions in Roberts and Winklhofer, 2004; Katari et al., 2000; Hartl and Tauxe, 1996; Lund and Keigwin, 1994), especially regarding the rate of sedimentation and smoothing effects of pDRM. Vlag et al. (1996) suggest that smoothing of the geomagnetic recording in sediments is more prominent in depositional environments with a lower sediment accumulation rate, as compared with depositional environments of higher rates of sedimentation which may provide a greater resolution of the past geomagnetic field (as a consequence of more rapid lock-in of grains due to compaction). This kind of smoothing effect could be a reason why geomagnetic excursions are absent at some sites, while present at others, even though the two may be geographically related (Roberts and Winklhofer, 2004). However, as rate of sedimentation increases, so does the error of inclination (see below). It should be noted that the

smoothing effect of pDRM has never been quantified and therefore as of yet, just exists as a theoretical argument (Lund and Keigwin, 1994; Hartl and Tauxe, 1996).

The effect of pDRM is significant in sediments where the magnetic particles are substantially smaller than the non-magnetic grains (i.e. silicates). Since iron-oxides generally have a higher density than the rest of the grains, it is often the case that the magnetic constituent is more fine-grained than the remaining sediments. However, the property that influences pDRM most is pore water constituent. At a certain threshold when enough water escapes through the sediments, grains become immobilized and pDRM ceases.

2.4.1c The inclination error problem

Sediments deposited in laboratory experiments and nature sometimes exhibit different inclinations than the applied field at that site (i.e. geomagnetic field in natural sediments, or artificial field in a laboratory environment). The observed inclination is shallower than that of the applied field and this effect has been dubbed the inclination error. Shallower inclination is thought to originate from two physical processes; the first involves the roughness (or absence of roughness) of the bedding plane when a grain settles on the surface and the second occurs during compaction of sediments where grains rotate into the horizontal plane. The inclination error seems to be more prevalent in sedimentary environments undergoing rapid deposition, and the effect may even be absent in certain low energy environments (e.g. deep marine settings and far offshore in lakes). One possible reason for the absence of inclination error in sediments with low rates of deposition has been noted by Roberts and Winklhofer (2004). They suggest that sediments in low energy environments will undergo such substantial stirring (likely through bioturbation) that most magnetic particles which were initially affected by the mechanical torque of the bedding plane will realign relatively shortly after deposition which effectively leads to a post-depositional remagnetization. Shallower inclination is often observed in sediments that have been rapidly accumulated, while the opposite seems to hold for sediments with low rates of accumulation (Tan et al., 2002). This has led some authors (i.e. Roberts and Winklhofer, 2004; Lund and Keigwin, 1994) to suggest that the remanence signal in slowly deposited sediments is smoothed or increasingly affected by post-depositional remagnetization because of stirring effects (see discussion above). A shallower inclination might therefore be more prevalent in rapidly deposited sediments. Experimental results from Irving and Major (1964) showed that rotation of grains in large void spaces may occur as a post-depositional process, which effectively decreases the inclination error (see also Tauxe, 1993).

Tauxe and Kent (1984) illustrated that inclination of the magnetic field itself composed part of the problem in laboratory deposited sediments (Figure 2.4). At mid latitudes (~45°), the inclination error was most exaggerated, as can be seen in Figure 2.4, while at low and high values of inclination, the influence of field dependent error is less significant. Similar experiments were performed by Løvlie and Torsvik (1984), on laboratory re-deposited red sandstone with a considerable amount of hematite.
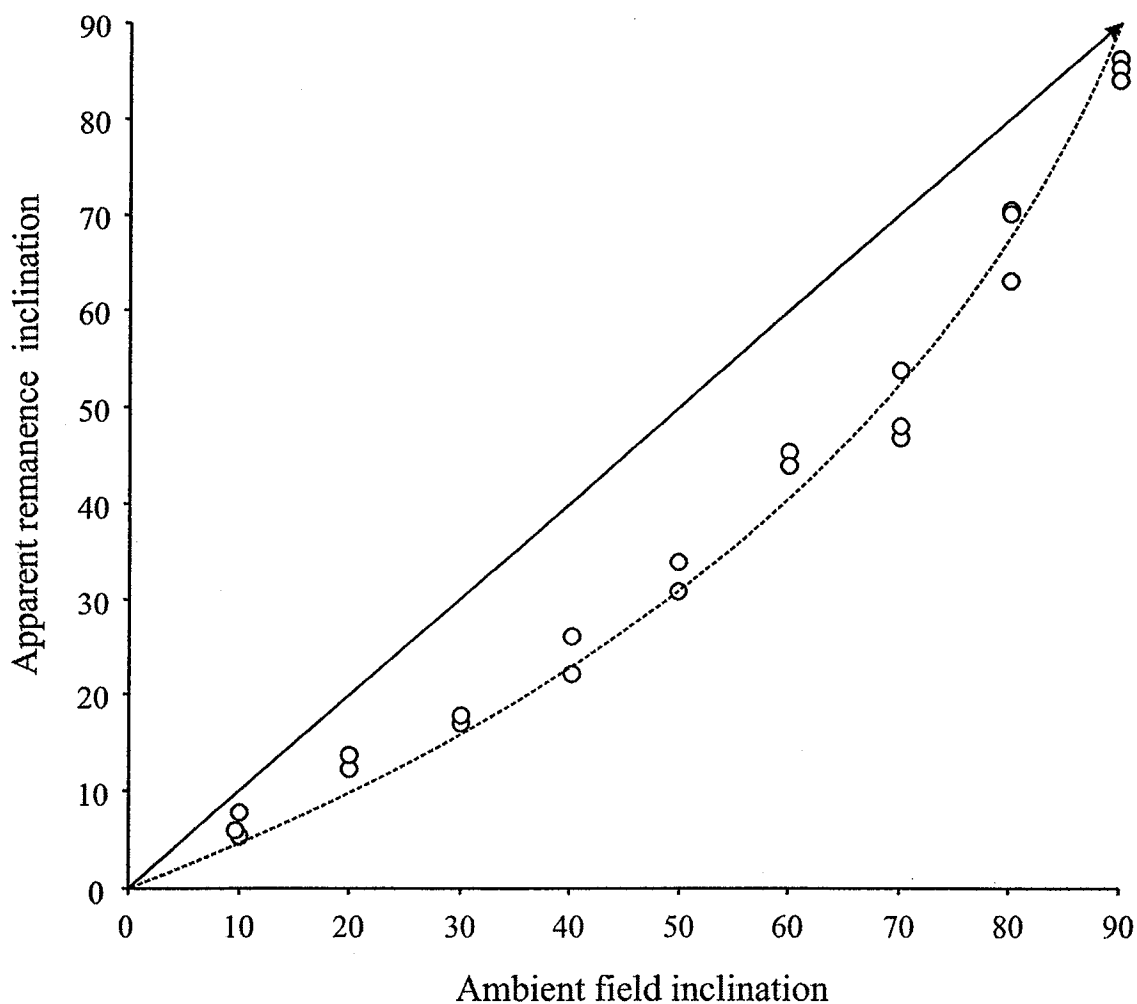
Figure 2.4 Laboratory redeposition experiment using natural river sediments, with hematite present, which illustrate an actual shallower remanence inclination than the inclination of the applied magnetic field. Solid line with arrow indicates the applied magnetic field. Dots indicate the inclination of individual samples. (Redrawn from Tauxe and Kent, 1984).

Aside from making similar observations as Tauxe and Kent (1984) regarding shallower remanence inclination, they also noted that the magnetic fabric of these sediments exhibited oblate ellipsoids with k_{min} distributed close to the vertical, while k_{max} and k_{int} were located close to the horizontal plane, showing some preference for direction. They observed coinciding k_{max} and

remanence direction, and concluded that the hematite was multidomainal, since single domain hematite theoretically should not show coinciding k_{max} and remanence direction.

2.4.1d Grain-size and anisotropy of magnetic susceptibility

The susceptibility ellipsoid in sediments and sedimentary rocks is often dependent on the grain size of the material. Greatest anisotropy belongs to sediment of small grain sizes, such as clay, since these are preferentially compacted in the horizontal plane. Consequently, magnetic minerals that are stuck together with clay particles through coagulation or flocculation also align their long axes in the horizontal plane (Lu et al, 1990; van Vreumingen, 1993b; Figure 2.5a). Larger particles, which are less affected by flocculation, may still experience alignment of grains, as they are affected by the bedding plane of the sediment surface and also aligning forces stemming from the water current (Tarling, 1983; Butler, 1992; Borradaile et al., 1999; Figure 2.5b). Since shape anisotropy dominates minerals such as magnetite, the magnetic moment overwhelmingly dominates the horizontal plane and thus the maximum susceptibility (k_{max}), while the vertical axis contains the minimum susceptibility (k_{min}). In coarse-grained sediments or sedimentary rocks, such as sand or sandstone, anisotropy is not as pronounced. Magnetic particles larger than single and pseudo-single domain-size are still dominated by shape anisotropy unless grains are strictly euhedral. The maximum susceptibility of single domain grains of magnetite is greatest perpendicular to their long axis, because the magnetic moment of these grains are always parallel to the long axis in the absence of an applied field, because this is the favourable energy configuration. The magnetic moment is already saturated in the long-axis of a grain giving a small susceptibility in this axis, whereas the moment will rotate slightly when susceptibility is determined in axes perpendicular to the long axis, giving a larger value of susceptibility. Single domain grains will therefore show a susceptibility ellipsoid which is opposite (inverse) to that displayed by multidomain and pseudo-single domain magnetite.

2.4.1e Biogenically produced magnetic minerals in lacustrine and marine sediments: a carrier of stable DRM?

In the last 30 years it has been discovered that organisms that produce ferromagnetic minerals are important contributors to the magnetic remanence in oceanic and freshwater sediments (i.e. Blakemore, 1975; Kirschvink and Lowenstam, 1979; Chang and Kirschvink, 1989). The most significant organisms, presently known, producing these minerals are bacteria and their contribution to remanent magnetism in natural sediments has become well documented

since their discovery in the mid 1970's (Blakemore, 1975). Magnetotactic bacteria produce magnetic grains of shapes and sizes that are specific to their species, and are known to intracellularly form magnetite and greigite (Fe_3S_4) depending on aerobic or reducing (anoxic) conditions. Dissimilatory iron-reducing bacteria, on the other hand, produce magnetite with a variety of grain sizes and shapes (Lovley et al., 1987), with a considerable amount in the super-paramagnetic (SPM) size range (<35 nm), but also of single domain (SD) size.
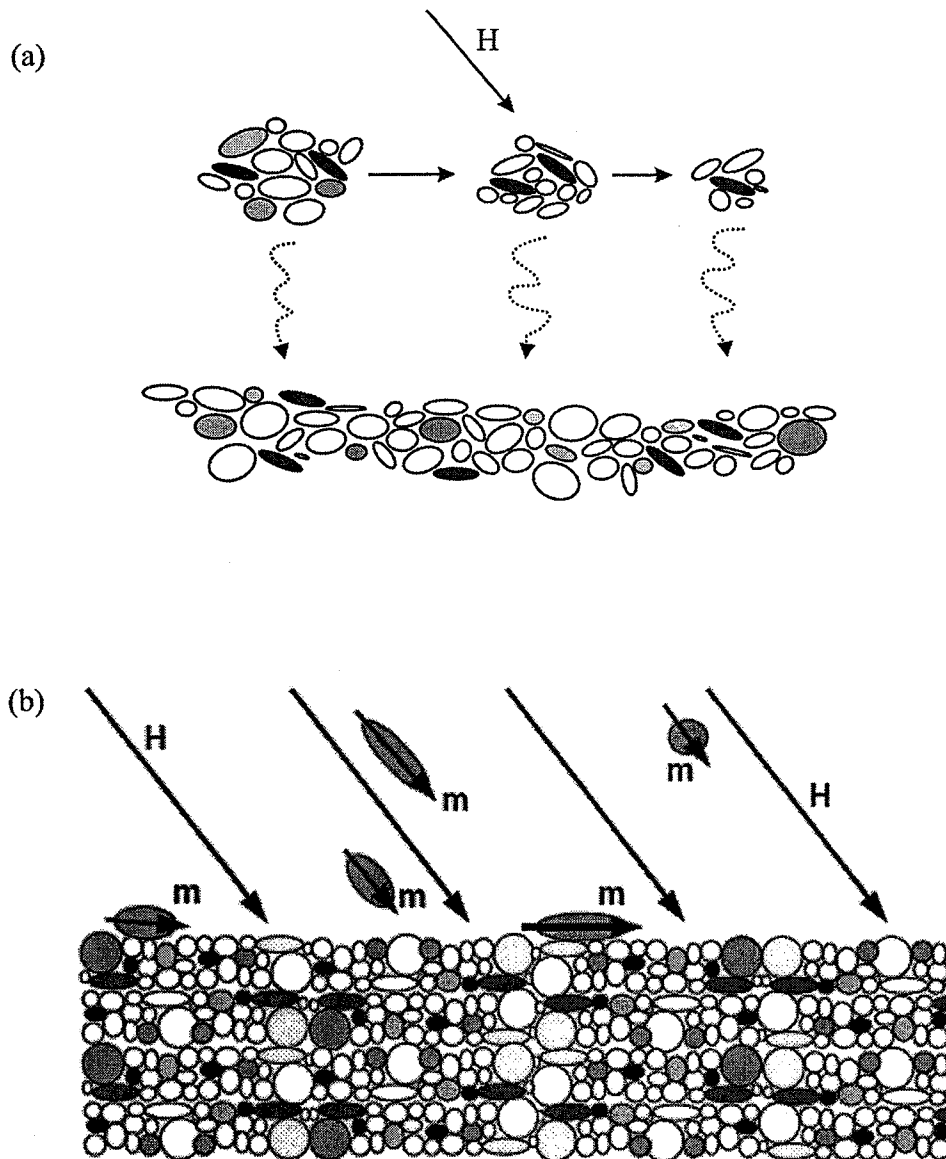
Figure 2.5 Schematic diagrams showing possible causes for inclination shallowing of magnetic grains in natural sediments. (a) Magnetic particles are incorporated into flocs of fine particles in the water column. (b) elongated magnetic particles are deposited at the sediment bedding plane such that their long-axes (and corresponding easy-axes of magnetization) are deposited parallel to the bedding plane (redrawn from Verosub, 1977).

A comprehensive review of the nature and formation of magnetosomes in magnetotactic bacteria is given by Bazylinski and Frankel (2004). The bacteria appear to thrive and be most abundant at the oxic-anoxic boundary of water bodies.

Moskowitz et al. (1993) have provided a useful test for detection of biogenically produced magnetite in rocks and sediments. They used low-temperature magnetization experiments, with and without the presence of an applied magnetic field while samples cool from room temperature (~300K) to about 10K. Thus, samples experience field-cooling (FC) and zero field-cooling (ZFC), and the ratio of their acquired remanence is indicative of shape and grain-size of the magnetite. Even slight oxidation of the magnetite produced by bacteria can skew the results of the low-temperature magnetization experiments (Weiss et al., 2004; Pan et al., 2005), to ratios which are indicative of non-biogenically produced magnetite. Other helpful rock magnetic methods include hysteresis, thermomagnetic measurements (e.g., Curie temperature) and coercivity remanence spectra for IRM and ARM acquisitions, but Pan et al. (2005) suggest that in order to unambiguously identify bacterial magnetite, transmission electron microscopy (TEM) observations should be used.

A clear distinction should be made, in the case of bacterial production of magnetite, between magnetosomes found in a living cell compared with fossil biogenic magnetite (which may be preserved after the cell itself has deteriorated). The chain-structure produced inside the cell may not preserve once the cell has been destroyed, and thus the rock magnetic characteristics may change. It is however, unclear to what extent biogenically produced magnetite contributes to the overall remanent magnetization of sediments. Since most grains are in the SD range, their high surface area to volume ratio makes them susceptible to dissolution after deposition in the sediment column as has been observed by Snowball (1997b). He showed that increased dissolution of SD magnetite of probably biogenic origin was noticeable with greater depth down the sediment column (see also Pan et al., 2005).

2.4.1f The case of red bed magnetization

Red sedimentary rocks have been widely used in paleomagnetic studies because 1) they are widespread and 2) they often carry a very stable NRM (ChRM). Hematite is the responsible mineral for the stable magnetization of these rocks. However, the origin and timing of red bed magnetization is disputed and two extreme views persist today (Butler, 1992). The first argues that the red beds magnetize as a DRM; the remanent magnetism is acquired contemporaneously or close in time to the deposition of sediments. This view favours the possibility that hematite is

of detrital origin. In this scenario red beds give a true representation of the paleomagnetic field at the time of sedimentation. The alternative extreme explanation of remanence acquisition in red beds favours the idea that remanence is acquired over a long period of time. In this case the red beds do not record an instant imprinting of the Earth's field but rather a prolonged period of remanence acquisition. An example would be a chemical remanent magnetization where hematite crystals form continually over time, due to diagenesis of the sediments. Clearly, detrital and chemically formed grains can exist together in a sedimentary setting, so it is possible that both processes described above contribute to the remanence signal. Therefore each red bed depositional setting has to be considered individually. Red bed magnetization is also affected by the magnetic properties of hematite. This mineral is usually dominant volumetrically in red sediments (although not necessarily dominant with regard to the magnetic intensity), and due to its high coercivity it tends to maintain a stable magnetization and faithfully record the direction of the Earth's magnetic field.

2.4.2 Chemical remanent magnetism

When new minerals are formed, at relatively low temperatures (below their Curie temperature) and in the presence of an applied field, they may acquire a chemical remanent magnetization or crystallization remanent magnetization (McElhinny and McFadden, 2000). If the volume of the grain grows until it surpasses the superparamagnetic threshold (~0.03μm), the grain will acquire a stable remanence. In some situations this may create a primary remanence, if the rock or sediment formed through chemical precipitation. CRM is also a common secondary remanence formed either through chemical precipitation of minerals in an existing rock or sediment or growth of grains already existing in the rock. When these grains grow through their blocking volume (i.e., exceed superparamagnetic grain size), they gain a stable magnetic remanence. Reorganization of the lattice of a mineral, as happens when maghemite (γFe_2O_3) inverts to hematite (αFe_2O_3), is not caused by a chemical change but rather is due to a crystallographic change, and this process has been appropriately named crystallization remanent magnetization (McElhinny and McFadden, 2000). Secondary CRM (either crystallization or chemical) can be harder to identify than a VRM (or vpTRM) and natural IRM, because of its overlapping coercivity or blocking temperature spectra with primary remanent magnetizations such as TRM and DRM.

2.4.3 Viscous remanent magnetism

A viscous remanence (VRM) is acquired at ambient temperatures, but it is really part of an acquisition spectrum, where TRM forms one end point (at high temperature) and VRM forms the second end point (at stable surface temperatures). If the temperature of a rock or sediment is kept more or less constant, then duration or time exposure becomes the significant factor, as can be observed from equation [2.1]. If one considers a group of single domain grains that have constant magnetic properties (i.e. B_c, J_s and v are constant), then the rate at which the magnetic moments of these grains will relax to a newly applied field can be likened to the decay of a radiogenic element (i.e. the relaxation time is probabilistic). If the temperature changes, then the relative relaxation times of these grains will also change. Of course, a distribution of nearly perfectly similar grains will not likely exist in nature, and therefore the acquisition of VRM in a range of grain sizes becomes a complicated phenomenon. VRM is very common, and is almost universally present in any sample collected for paleomagnetic purposes, although the contribution of VRM to the sample will vary depending on its magnetic mineralogy and time exposure to the ambient magnetic field. When a rock becomes exposed to elevated temperatures for prolonged periods of time, it acquires a partial thermoremanence (pTRM) or viscous partial thermoremanence (vpTRM; Van der Voo, 1993; Butler, 1992; Middleton and Schmidt, 1982). The significance of a vpTRM is that it will be rather resistant to demagnetization since, as has been shown by Pullaiah et al. (1975), this remanence has been acquired at elevated temperatures where τ is effectively reduced. Once uplifted and exposed to ambient temperature conditions, the rocks will carry a very stable secondary remanence that may be difficult to clean.

2.4.4 Stress remagnetization and piezoremanence

Effects of pressure are not as significant as accompanying changes in temperature. Low stability remanences may form during exposure to hydrostatic pressures comparable to those in the upper crust of the Earth (Tarling, 1983; Pearce and Karson, 1981). A remanence acquired by pressure has traditionally been called piezoremanent magnetization (Stacey and Banarjee, 1974). Since temperature will influence the remanence acquisition in a rock (acquiring a vpTRM), Borradaile (1996) performed remagnetization experiments on magnetite dispersed in a cement mixture induced by hydrostatic and differential stresses. He found that grains of low coercivity are most susceptible to remagnetization during applications of both kinds of stresses, but interestingly he also found that grains with high coercivities (>55 mT) remagnetize towards the direction of the applied field during the experiment. The original remanence, before deformation occurred, was remembered by grains with intermediate coercivities (~25 − 50 mT). It is likely

that loose domain walls in MD grains reorient during stressed conditions, and magnetization within the grain changes towards the locally applied field, which would explain remagnetization in the low coercivity grains. For the high coercivity component, SD or small PSD grains may rotate during the stressed conditions (shortening of the vertical axis), and thus have their magnetic moments moved and preferably align with the applied field (Borradaile, 1996). The results also showed that differential stresses (P_1 - P_3 >20 MPa) were more effective at remagnetizing specimens than hydrostatic stress ($P_1 = P_3$). In nature, remagnetization due to stress at low ambient temperatures may be most applicable to rocks undergoing low temperature metamorphism in the upper crust (Hudson et al., 1989), or perhaps for compaction of unconsolidated sediments (i.e. clays). Rapid application and removal of stress, as occurs with a meteorite impact, can either remagnetize rocks (Halls, 1978) or demagnetize them (Tarling, 1983).

Chapter 3: Paleomagnetic cleaning and separation strategies

Magnetic cleaning techniques enable the separation of paleomagnetic remanences found in rocks and sediments. They serve as a fundamental tool to the paleomagnetist in identification of characteristic or primary remanence components and secondary or overprinting remanence components. However, caution must be exercised to choose a proper cleaning technique depending on the rock magnetic properties and magnetic mineralogy of the material studied. Because of the difference in rock magnetic properties displayed by ferromagnetic minerals, every paleomagnetic study warrants an appropriate magnetic cleaning strategy in order to extract meaningful paleomagnetic data from the material. Simply applying a cleaning technique without considering the rock magnetic properties may serve to be more detrimental than beneficial to the paleomagnetist. It has therefore been suggested (Schmidt, 1993), that before a campaign of demagnetization begins, it is advantageous to have a thorough grasp of the mineral magnetic properties displayed by rocks or sediments investigated.

Over the span of geological time it is likely that the Earth's magnetic field will impose multiple remanence components in rocks as well as in unconsolidated sediment. Primary magnetic remanences are established during the formation of the rock or deposition of sediments and include thermoremanent magnetism (TRM), chemical remanence (CRM) and detrital remanent magnetism (DRM). The primary remanence is arguably of greatest interest to the paleomagnetist, since this component will allow insight to the ancient or "fossil" magnetization when the rock formed (e.g., As and Zijderveld, 1958). However, secondary magnetic remanences are significant, and are added subsequently to a rock or sediment and partially overprint the primary remanence, which results most likely in a deviation of the original magnetic vector, with changes in declination, inclination and also intensity of magnetization. Usually, in nature secondary remanences in rocks and sediments are produced by the steady acquisition of viscous remanence (VRM) due to the Earth's magnetic field or isothermally induced (IRM) through lightning strikes. CRM can also contribute as a secondary magnetization, when new minerals form or existing minerals grow through precipitation. Together, primary and secondary remanences define the natural remanent magnetism (NRM) which is the vectorial sum of all remanences combined (Dunlop, 1979). Prior to any magnetic cleanings, when dealing with hard rocks, it is useful to consider field stability tests (e.g., Graham, 1949; Kirschvink, 1978), as these can provide considerable insight to the age of magnetization and whether extensive remagnetization has occurred (see also, McElhinny and McFadden, 2000; Van der Voo, 1993;

Butler, 1992; Tarling, 1983). This chapter is divided into two sections, the prior concerns the different demagnetization techniques employed by paleomagnetists and the latter concerns the interpretation of the data obtained after demagnetization is complete.

3.1 Aspects and theory of the various cleaning techniques

The objective of incremental magnetic cleaning techniques is to remove remanent magnetizations in small steps to separate and identify their different components. Optimally, magnetic cleaning aims to "erase" the magnetic history in a rock or sediment starting with the most recent events (remagnetizations) and ending with the separation of the primary remanent magnetization. As ferromagnetic minerals have a wide range of blocking coercivities and blocking temperatures or alternatively unblocking coercivities and unblocking temperatures, therefore it is important to choose a proper cleaning strategy knowing the constituent magnetic mineralogy. This section addresses the various magnetic cleaning techniques, their underlying theoretical backgrounds, and their advantages and disadvantages. Alternating field demagnetization "removes" remanences of relatively low and intermediate coercivities while it is unsuitable to demagnetize the remanence of higher coercivity minerals. Although related to AF demagnetization and being a viable technique for magnetic cleaning, direct current demagnetization is not considered in this discussion. Complementary then, to alternating field demagnetization, is thermal demagnetization where magnetic minerals are demagnetized completely at their respective Curie temperatures (in a field free space). Next, chemical demagnetization or leaching is briefly discussed, and its application mainly to sedimentary rocks. Finally, low temperature demagnetization is addressed as it a useful complementary technique to either primary technique discussed (e.g. AF, thermal or chemical).

3.1.1 Alternating field demagnetization

Collinson (1983: p. 308) has defined alternating field (AF) cleaning in ferromagnetic studies as a method where "demagnetization is achieved by cycling the material through magnetic hysteresis loops of decreasing amplitude to randomize domain moment directions." AF demagnetization affects magnetic particles in rocks based on their coercivity. Ferromagnetic grains consist of either one, or more than one magnetic moment, referred to, respectively, as single domain (SD) and multidomain (MD) particles. In the former, the magnetic moment will always be finite (i.e. it will always have a direction and magnitude, dictated by either the shape or magnetocrystalline anisotropy of the grain), but in the latter magnetic moments are separated by

domain walls and within the grain they may counteract each other and completely cancel any net magnetic moment. It is likely however, that MD grains do a have a finite net magnetization even after AF demagnetization because this favors the lowest energy state conditions (Collinson, 1983). In other words, the demagnetization behavior in SD grains is controlled by rotation of the magnetic moment, while domain wall movement controls MD demagnetization behavior.

The foundation for AF demagnetization lies in the fact that magnetic minerals have physical properties of coercivity and coercivity of remanence (B_C and B_{CR}). For a magnetic single domain particle the microcoercivity is defined as the resistance of the particle's magnetic moment to be moved from one magnetic easy direction to another magnetic easy direction (i.e. the moment is positioned at a low energy state and rotated through an energy barrier until it reaches another low energy position). Bulk coercivity refers to a sample's ability to resist an applied magnetic field, until its remanence is reduced to zero. Theoretically, the magnetic moments of grains with microscopic coercive force, $B_c' < B\cos\theta$, (the applied AF, Figure 3.1) will follow the AF until the field strength decreases below B_c' (McElhinny and McFadden, 2000: p. 114). As the AF intensity is progressively increased, grains with greater coercivity will become affected. Laboratory equipment used for AF demagnetization can generally provide peak alternating fields from 100 – 200 mT. Once higher fields are produced there is an increased chance for acquisition of spurious ARM in the specimens due to instrumental problems (Collinson, 1983).
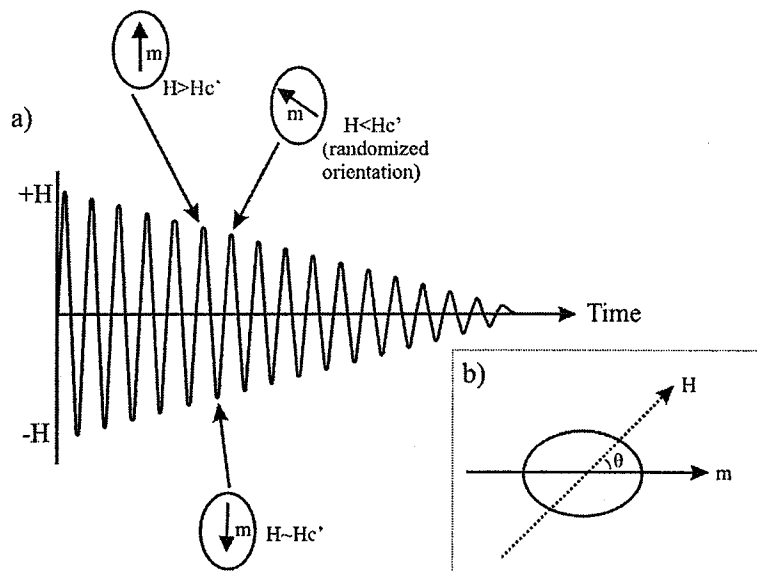
Figure 3.1 (a) An alternating field (AF) that oscillates between +H and –H, and decays with the passage of time. The magnetic moment, m, moves along the AF until its microcoercivity, Hc', is greater than the applied field, H. When Hc'>H, m is "locked" into its position (at some randomized position), (b) shows the angle θ between the applied field and the magnetic moment.

For unconsolidated sediments it is preferable to use AF demagnetization, since this is a less destructive method than thermal demagnetization. Although slight alteration of the magnetic minerals is possible during AF treatment (for example through rearrangement of domain walls in multidomain grains), this method does not cause chemical changes in the sediments as will occur during thermal demagnetization. Because of its non-destructive nature, a specimen treated with an AF can be reused for other experiments, for example the Lowrie 3-axis test discussed below. AF demagnetization is ideal in situations where most or all remanence is carried by low coercivity minerals, such as (titano-)magnetite, maghemite and in some cases iron-sulphides (i.e. greigite; Snowball, 1997b). However, when the remanence is dominated by high coercivity minerals, such as hematite and the hydrated iron-oxide, goethite, coercivities are generally too high to be affected by the AF, and hence thermal demagnetization (or chemical demagnetization) of these minerals is more viable (Özdemir and Dunlop, 1996; Collinson, 1967). The magnetic carriers in some sediments and sedimentary rocks can be heavily influenced by hematite, especially in the case of red sediments (Butler, 1992). Alternatively, it can be useful to use AF demagnetization in combination with another treatment, for example thermal demagnetization. This can be of use when multidomain magnetite is present as a spurious component in a rock, obscuring the primary magnetization. Low intensity alternating fields (≤ 20 mT) may serve to remove the noisy component of MD grains, followed by thermal demagnetization in order to identify the characteristic remanence or for the removal of high coercivity phases. A problem that may arise with AF demagnetization is when the primary remanence is actually removed before the secondary overprint(s), as has been observed by Buchan (1978). In his study of the Thanet complex (a multiple intrusion complex composed of diorites, metagabbros and gabbros), located in southeastern Ontario, he found in some samples that a thermally very stable remanence component (B, unblocked at a temperature range between 560 – 580°C) had lower coercivities, that were isolated during AF demagnetization, than the thermally less stable A component (which conversely displayed higher coercivities than the B component).

AF demagnetization is performed using two different methods. The first is static AF demagnetization (As and Zijderveld, 1958). In this technique a specimen is exposed to an equal strength AF in three successive treatments oriented at orthogonal axes (i.e. x, y and z), followed by measurement of the remaining remanence. The treatment is repeated with successively greater AF's. The second method uses a "tumbler" to slowly rotate the specimen during demagnetization, and results using this technique were first reported by Creer (1959). Tumbling the specimen requires sophisticated instrumentation, and even slight errors in the method may cause acquisition of an undesired ARM (called a rotational remanent magnetization).

A serious problem that may arise during AF treatment is the acquisition of spurious remanence, which may be acquired in two ways, 1) gyroremanent magnetization (GRM), due to properties of magnetic minerals in the sample (Stephenson, 1980a; 1980b; 1993; Dankers and Zijderveld, 1981) and, 2) as a superimposed ARM originating either from harmonics present in the waveform of the alternating field or if the specimen is not properly shielded from an outside influence of Earth's magnetic field. The acquisition of GRM during AF demagnetization has become documented more frequently during the last two decades (i.e. Stephenson, 1980a, 1980b; Dankers and Zijderveld, 1981; Snowball, 1997; Sagnotti and Winkler, 1999), and what may previously have been thought of as a spurious ARM acquired due to problematic instrumentation, may in fact have been due to GRM. The effect of both problems can be dampened, following AF demagnetization techniques which allows for the elimination of either spurious remanence. If a spurious ARM is induced during AF demagnetization, it may be necessary to adjust the instrumentation or use a demagnetization strategy that would eliminate the acquisition of the ARM (Figure 3.2). In order to avoid acquisition of a spurious anhysteretic remanent magnetism (ARM) from the AF, six successive treatments with an equal strength AF can be performed (again using the same orthogonal axes, but with six different directions). This experiment is also useful in order to detect possible acquisition of spurious ARM when AF demagnetization is performed in the regular static three successive treatments. GRM, on the other hand, may be acquired during tumbling of a specimen, and this remanence is termed rotational remanent magnetization (RRM). GRM acquired in this way can be reduced by reversing the tumbling sequence so that the specimen is rotated oppositely to the first episode of rotation (Hillhouse, 1977). GRM may also appear during static AF demagnetization, as a result of anisotropy in the rock specimens (and its magnetic mineralogy), as has been observed by Snowball (1997) in lacustrine sediments where greigite (Fe_3S_4) was the dominant remanence carrier (Figure 3.3).
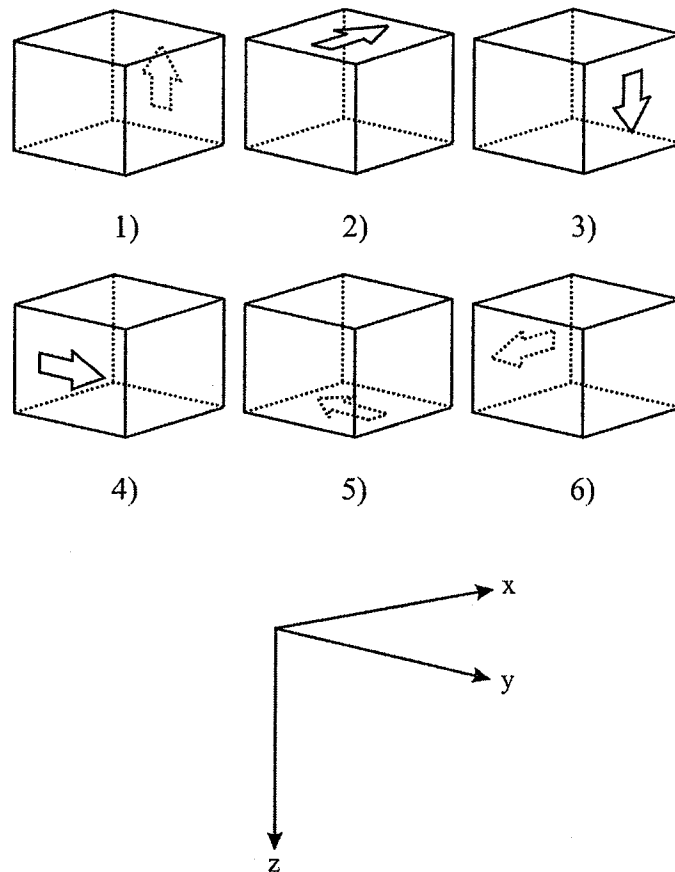
Figure 3.2 Alternating field demagnetization strategy used in order to attempt to remove spuriously acquired anhysteretic remanent magnetism. The cube specimen is demagnetized in six different orientations. The orientations are predetermined for the purpose of canceling spurious acquisition in all directions.

3.1.2 Thermal demagnetization

Another useful demagnetization method is heating the desired sample in a magnetic field-free environment. Agitation through thermal energy will interrupt the electron exchange interactions (the spin aligning interaction creating a magnetic moment). Each ferromagnetic mineral has an individual temperature where all exchange interactions are finally disrupted and no magnetic moment persists (i.e. the spontaneous magnetization is reduced to zero); this is the definition of a Curie temperature (McElhinny and McFadden, 2000: p. 35). The Curie temperatures for the most common ferromagnetic minerals are listed in Table 3.1. It should be noted that minerals exhibiting a high coercivity (i.e. resistance to an applied magnetic field) may not display a high Curie temperature. For this reason, the nature of demagnetization spectrums obtained through thermal and AF treatments may not necessarily be similar.
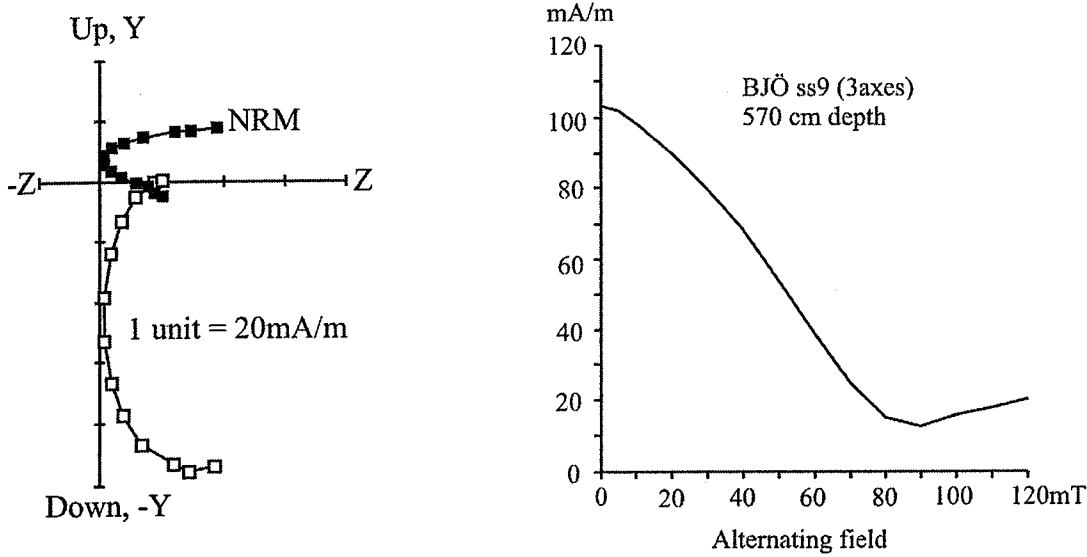
Figure 3.3 Acquisition of gyroremanent magnetization during alternating field demagnetization. At greater peak fields the demagnetization path shows steady curvature as well as a slight increase in intensity, indicative of GRM. Redrawn from Snowball (1997).

Table 3.1 Relevant rock magnetic properties of some common ferromagnetic (sensu lato) minerals

Mineral	Composition	Ms (kA/m)	Tc (°C)	Tn (°C)	Hcr (mT)*	Reference
Magnetite	Fe_3O_4	480	580	N/A	-	Dunlop and Özdemir, 1997; Borradaile, et al., 2004
SD				N/A	30 - 60	
PSD				N/A	10 -> 30	
MD				N/A	>10	
TM60	$Fe_{2.4}Ti_{0.6}O_4$	125	150	N/A	~200	Dunlop and Özdemir, 1997; O'Reilly, 1984
TM30			350	N/A	~100	O'Reilly, 1984
Maghemite	$\gamma\text{-}Fe_2O_3$	380	590 - 675	N/A	300	Dunlop and Özdemir, 1997; O'Reilly, 1984
Hematite	$\alpha\text{-}Fe_2O_3$	2 - 2.5	675	680	?500	Dunlop and Özdemir, 1997; Butler, 1992
Goethite	$\alpha\text{-}FeOOH$	~2	120	120	500 - 1000	Dunlop and Özdemir, 1997; Özdemir and Dunlop, 1996
Greigite	Fe_3S_4	~125	320	N/A	-	Dunlop and Özdemir, 1997
SD (#, †)				N/A	2.5 - 60	Diaz-Ricci and Kirschvink, 1992; Snowball, 1991
Pyrrhotite	Fe_7S_8	~80 - 130	320	320	500-1000	Dunlop and Özdemir, 1997; Butler, 1992; Clark, 1984; Dekkers, 1988

* - Mineral Coercivities
\# - Determined experimentally by Snowball, 1991
† - Determined theoretically by Diaz-Ricci and Kirschvink, 1992
Ms = Saturation magnetization
Tc= Curie Temperature
Tn = Neel Temperature
Hcr = Coercivity of remanence

A theoretical background for thermal demagnetization and acquisition of thermoremanent magnetization (TRM) has been provided by Louis Néel (1955). Simply put, each ferromagnetic grain has a relaxation time (τ), the time at which the grain's magnetic moment relaxes in the direction of an applied magnetic field. Some grains are stable over very long time scales (even for durations longer than the existence of Earth), while other grains relax almost instantaneously in the direction of the new applied field. The relaxation time, τ, is largely influenced by the ambient temperature conditions existing around it, and this time-temperature relationship for a ferromagnetic single domain grain has been mathematically expressed by Néel (1955) as

$$\tau = \frac{1}{C}\exp\left(\frac{Vj_sB_c}{2kT}\right)$$

[Eqn. 3.1]

where τ is the theoretical relaxation time of a single domain ferromagnetic grain; C is a unit-less frequency constant on the order of 10^9 - 10^{11} (Dunlop and Özdemir, 1997; Pullaiah et al., 1975); V is the volume of the grain; j_s is the saturation moment of the grain; B_c is the microcoercivity of the grain; k is Boltzmann's constant and T is the absolute temperature (expressed in Kelvin). From the expression in [3.1] it is clear that τ of a grain is exponentially dependent on its surrounding temperature, but also of the product in the numerator of the exponent (which includes microcoercivity of the grain). From [Eqn. 3.1], Pullaiah et al. (1975; see also, Butler, 1992) developed theoretical blocking curves for magnetite and hematite (showing the relationship between τ and temperature), which could be used to predict the potential stability, over geological time, of these magnetic phases. Further, [Eqn. 3.1] cannot be used to make inferences about τ in PSD and MD grains, as different physical conditions apply to these grains. Figure 3.4 displays the function of increasing volume and corresponding hypothetical relaxation times in SD, PSD and MD grains. When a rock acquires a thermoremanent magnetization (TRM) during cooling, the magnetic moments of the ferromagnetic minerals are successively "locked" into a position determined or influenced by the directions of all applied fields (e.g. in nature generally by the Earth's magnetic field, but also due to the influence of surrounding magnetic minerals that have already had their magnetic moments aligned). Hence, the acquisition of a TRM moves through a spectrum of blocking temperatures. If the cooling of the rocks is rapid, as in an extrusive rock, it is likely that the TRM is of a rather uniform remanence vector. Alternatively, if the rock is cooled slowly, as for igneous rocks rising slowly through the crust with high heat capacity, then the lock-in time of the remanence might be influenced by the wandering of the Earth's magnetic field. But, for very long cooling times the remanence vector might be rather uniform, as a consequence of the averaging effect of long term movement in the axial dipole moment (Merrill et al., 1998). Because of the discrete, and successive, blocking of magnetic moments in a rock during cooling,

one can consider destroying this remanence through heating in a laboratory magnetic field-free presence. The moments that were blocked during the last stages of cooling would effectively be the moments initially unblocked during heating. A ferromagnetic mineral, is therefore said to have an unblocking temperature (T_{ub}), where thermal energy breaks the spin interaction of its magnetic moment(s). Moments carried by minerals with $T_{ub}<T$, will be effectively disrupted, where T is the temperature of the heating interval; intensity of the remanence is progressively decreased with increasing temperature as less moments contribute to the magnetization. Because of the different physical properties of individual grains, there is a spectrum of unblocking temperatures. For a ferromagnetic mineral (*sensu lato*) all magnetic moments are unblocked at its Curie temperature.

There are practical benefits to thermal demagnetization compared to AF demagnetization. The problem of acquiring a spurious ARM during a demagnetization, as may occur during AF treatments, is avoided since thermal treatment is performed in a magnetically field-free space. Secondly, as Walton (1996) has indicated, alternating field demagnetization does not provide a guarantee that secondary or overprinted remanence, for example a viscous remanence (VRM), is
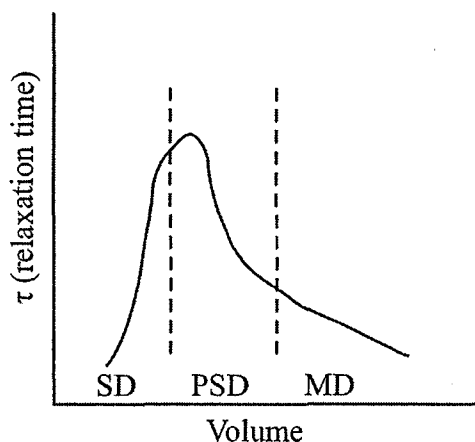
Figure 3.4 Hypothetical changes in relaxation time with increasing grain volume (considering all other variables in [Eqn. 3.1] are kept constant). Units in this case are arbitrary and as such the relationship between relaxation time and volume is not empirical. Redrawn from Merrill and McElhinny (1983).

removed initially during low intensity field treatments, which is usually desired. Walton (1996) explained that this is because an alternating field may affect a different spectrum of grains than thermal demagnetization does (considering all ferromagnetic phases). Thermal demagnetization, on the other hand, does provide a technique to remove the secondary remanence, due to the nature of the blocking temperature spectrum (removing the most recently acquired remanence at low heating temperatures, leaving the primary remanence isolated). In some cases AF demagnetization may activate, or demagnetize, the magnetic moments of grains that carry the

primary remanence, before it affects the grains carrying the secondary remanence (see Buchan, 1978). Ouliac (1976) recognized that a probable secondary VRM in folded red marls and breccias from southern France was difficult to remove using AF demagnetization, while heating of specimens from the same study area isolated the primary remanence at around 340°C. The argument can be further extended by considering that thermal demagnetization can affect the remanence of all ferromagnetic phases, given high enough temperature, while an AF, applied even to its highest capacity (~200 mT), may not be able to affect the high coercivity mineral phases, such as hematite or goethite.

3.1.3 Chemical demagnetization through acid leaching

Exposing rock specimens to dilute acids over gradually increasing time intervals will effectively dissolve ferromagnetic minerals and thus demagnetize a sample of rock or sediment (Butler, 1992). Samples are treated with acids for incrementally increasing periods of time, in order to successively remove minerals and decrease the remanence. Initial studies used concentrated hydrochloric acid to leach samples of red sandstone (Collinson, 1965). Roy and Park (1974) performed chemical leaching on red sedimentary rocks as well, and were able to identify three chemical remanence components, with origins from the formation of the rock: acquisition of CRM during or slightly after deposition, later acquisition of a CRM to fill in the pore space of the sediments and finally a CRM acquired during lithification of the rock. They combined chemical treatments with thermal treatments, and exposed their specimens to acid leaching for about half a year. Small grains are preferentially removed first by leaching since they have a high surface area to volume ratio (McElhinny and McFadden, 2000), which means that SP grains are destroyed first followed by small SD grains. If the magnetization is originally due to CRM, then small grains are likely to have acquired their remanence last, because they have not had the time to grow as large as some of the initially formed grains (which are the grains that carry the primary CRM). Small grains are also likely to carry a secondary remanence, which is thus removed initially during chemical demagnetization (analogous to thermal cleaning). To achieve a greater surface area to volume ratio in specimens collected (i.e. a cylinder or cube) it is possible to drill cuts or openings through the specimen in order to expose a larger area to the surrounding acids. Although a useful technique to remove remanent magnetization in sedimentary rocks, chemical demagnetization is inherently time consuming and can be a "messy" procedure, considering the use of acids and continuous cleaning of samples.

3.1.4 Low temperature demagnetization

The use of low temperature demagnetization in paleomagnetic studies relate to the physical properties of magnetic minerals, where rock magnetic studies have mainly considered magnetite (and titanomagnetites) and to a lesser extent hematite. By subjecting a crystal of magnetite to low temperature conditions (i.e. through submersion in liquid nitrogen), the crystal is cycled through the isotropic point and the Verway transition, thus changing its inherent remanent magnetization, coercivity and susceptibility (Dunlop and Özdemir, 1997). Initial studies on effects of low temperature characteristics (remanence and coercivity phenomenon) of magnetite were performed by Ozima et al. (1964), who showed that magnetic remanence decreased during cooling to 77K in liquid nitrogen. They also found that through low temperature cycling magnetite sometimes experienced a self-reversal of remanent magnetization below -150°C (123K), while upon warming back to room temperature a fraction of the original remanence was recovered. Around 123K, the remanence was reduced to zero. They attributed the remanence decrease (sometimes leading to self-reversal) and recovery phenomenon to the magnetostatic interaction of grains showing magnetocrystalline anisotropy. The recovered fraction mainly contained the remanence component with higher coercivities and therefore it was suggested that the magnetically soft (euhedral single domain magnetite and multidomain magnetite) had become demagnetized during the low temperature cycling. Although the use of liquid nitrogen is commonplace, this is not the only alternative used for low temperature treatments. In some cases, it might be desired to induce a strong magnetic field at very low temperatures (i.e. the boiling point of liquid helium) and then observe how the remanence behaves during warming of the material. Of course, liquid helium also serves to bring magnetite through its isotropic point and the Verway transition, but is a very expensive alternative to liquid nitrogen. In other circumstances it might be sufficient to use solid CO_2 for low temperature demagnetization purposes, especially in hematite rich rocks or sediments. Hematite undergoes a low-temperature transition at or below 260K, which is called the Morin transition. The benefit of using CO_2 (or dry ice) for unconsolidated sediments or rocks with significant amounts of pore water is realized when the freezing point of water is considered. Although the freezing point might be suppressed as low as 210K when water forms a thin film, coating the pores of rocks and sediments, this is still well above the boiling point of liquid nitrogen at 77K. Carbon dioxide has a sublimation point of -78.5°C (~195K), which is closer to the freezing point of thin film water. Borradaile (1994) found that use of liquid nitrogen for rocks and sediments with high pore water content could lead to ice-pressure demagnetization, where the pore water would freeze and thus reorient the grains and effectively demagnetize a sample. This is however, not always a desired effect,

sediments are usually much younger than hard rocks, both will be influenced by local and regional environmental factors that alter their physical and chemical properties. In other words, several magnetizations may have been introduced into the rocks or sediments with passage of time, due to physical or chemical processes (Van der Voo, 1993). Simply measuring the magnetic remanence of a collected sample may therefore be quite meaningless, unless, owing to the fortunate circumstance that only one, uniform, vector remanence exists in the sample. Generally, however, rocks and sediments carry multiple remanences which combine for a resultant vector of the natural remanent magnetism. The original or characteristic remanence that was acquired during formation of the sample is hidden by the secondary overprints (subsequent magnetizations). In most studies for paleomagnetic purposes it is generally the direction and magnitude of the primary or characteristic remanence that is desired. Nevertheless, the secondary overprints may reveal important information about a sample's history (Dunlop, 1979), for example, whether the rock has been exposed to subsequent heating or stresses after the formation of the rock (e.g. metamorphism), or if new minerals have formed in the rock or sediment (e.g. a secondary chemical remanence) or if an ambient temperature VRM overprints the part of the original magnetization. All of these scenarios create secondary remanences, which will obscure the primary remanence component. This section therefore involves a discussion on how to separate and identify different remanence vectors, whether they are primary or secondary and which techniques have been developed for these purposes.

Paleomagnetism would perhaps be a simpler subject if one did not have to consider the geological history of a rock. If remanences of only one origin existed within the rock or sediment, a sample could simply be measured with a magnetometer, and the apparent inclination and declination would reveal the direction of the ancient geomagnetic field. Alas, this is not so, since throughout the history of a geological specimen chemical and physical changes will undoubtedly affect it and new magnetic remanences form with their respective declinations and inclinations. The objective of the paleomagnetist therefore becomes to decipher the components of NRM (using various demagnetization methods) in order to understand the acquisition of remanence in geological specimens.

3.3 Separation and plotting techniques

One of the popular techniques for displaying the orientation vectors obtained from incremental demagnetization is the Zijderveld plot (Dunlop, 1979; Zijderveld, 1967; As and Zijderveld, 1958). This technique was developed by Zijderveld and As during some of their initial work using incremental AF demagnetization (As and Zijderveld, 1958). Paleomagnetic vectors

are plotted on two orthogonal planes (i.e. the X-Z plane and the X-Y plane), one being vertical and the other horizontal in order to display both inclination and declination. The Zijderveld technique also provides intensity of the orientation vectors; the intersection of the midpoint of the two planes marks the origin, where remanence is equal to zero. During incremental demagnetization as the intensity decreases, the remanence vector will move towards the origin. A simple example of a Zijderveld plot is illustrated in Figure 3.5a, where Holocene glacial silt has been demagnetized using incremental AF demagnetization, showing the decay of a single vector towards the origin. Note that the remanence is not completely demagnetized at the highest AF that could be produced by the instruments, so a small component of remanence is carried by high coercivity magnetic minerals. The majority of the signal is produced by minerals with a coercivity of remanence that is below 180 mT (the highest applicable AF), and is most likely carried by magnetite. The horizontal component (plotted on the X-Y plane; filled squares) is demagnetized successively towards the northeast, while the vertical component (plotted on the X-Z plane; open squares) is demagnetized successively upwards and to the north. The direction of acquisition of remanence is however opposite to the path of demagnetization. The actual direction of the paleomagnetic vectors in Figure 3.5a is southwest (horizontal) and steeply downward to the south. The classical Zijderveld plot is useful to separate components of multivectorial remanences (Dunlop, 1979), and Figure 3.5b gives an example where more than one remanence component is present in a sample that was thermally demagnetized. The NRM consists of two well-defined vector components, one initially unblocked between 20 and about 450°C, and a second component with higher unblocking temperature between 470 and 570°C. At 570°C the vector has moved to the origin and the remanence is completely removed. The two vector components in Figure 3.5b are almost antiparallel each other, and with initial demagnetization the vector moves away from the origin. If one were to simply measure the NRM in this sample it would give a resulting vector that would plot between the 20°C and the origin, which is very untruthful of the magnetization history of this sample. This example thus clearly illustrates the importance of incremental demagnetization. Another important piece of information gained from the Zijderveld plot in Figure 3.5b is the incremental loss of remanence (i.e. the intensity) when the sample has been demagnetized. Most of the remanence is lost after the turning point has been reached around

(a)

(b)
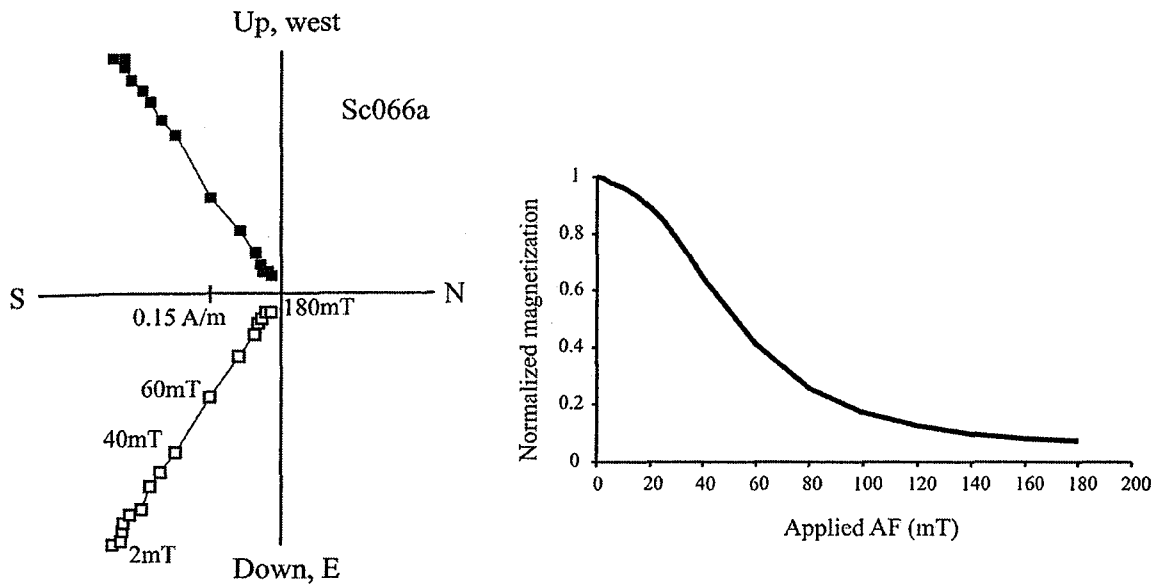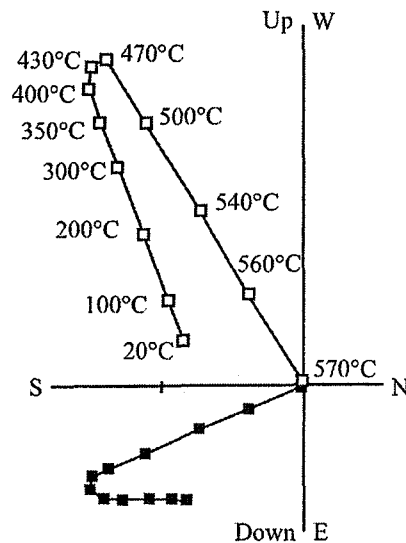
Figure 3.5 Zijderveld plots, (a) shows a simple case where only one paleomagnetic vector is present, while (b) shows a slightly more complicated case, where the sample contains two paleomagnetic vectors roughly anti-parallel to each other. Closed (open) squares refer to projection on the horizontal (vertical) plane. Figure 5(b) has been redrawn from Van der Voo (1993: p. 47).

450°C, which would suggest that the remanence is dominated by minerals with blocking temperatures above 450°C. Since all the remanence is lost before 580°C, the Curie point of magnetite, it is likely that most remanence is carried by this mineral. Whereas declination is always represented truthfully in a Zijderveld plot with axes representing N-S and E-W creating a 360° circle, the same is not true for the inclination. The main drawback of the plot becomes the

illustration of inclination, as the perspective view (either N-S or E-W, or some other arbitrary axis) cannot truly represent the real inclination, unless observed at a perfect right angle to the declination of the demagnetized remanence. However, even if this is the case, the declination usually changes so that a right angle is unachievable. The resulting inclination will therefore become distorted, either through appearing too steep (when the axis is more or less parallel to the overall declination of the sample) or too shallow.

The second technique commonly employed to plot remanent magnetization components uses equal area stereonets (e.g. Figure 3.6). Vector points plot on a spherical surface, where the vertical axis is represented by the center of a hemisphere and the horizontal is located along the circumference of that hemisphere. This can be likened to looking down into a bowl and observing points on the inner surface of the bowl. Inclination is then a measure of how "deep" into the bowl a point lays. The circumference of the bowl is 360°, which determines the position of a point's declination. Since all points lie on the surface of the sphere, they have no magnitude (i.e. intensity). Stereonets have been widely utilized in paleomagnetism to address directions of remanent magnetizations (e.g. Hoffman and Day, 1978; Halls, 1976; 1979). If vector points cluster around a single location on the sphere, the remanence component is uniform in one direction. More complex situations arise when vector points plot at different positions on the sphere (see Figure 3.6b). The latter happens when there is some overlap in coercivities or blocking temperatures of grains in a sample, and this will be discussed further in the next section. Figure 3.6a shows the directions from AF cleaning (incrementally to a peak field of 180 mT, in 17 steps) with a tight clustering in the SW quadrant with a moderate inclination downward. The declination has not been corrected for the orientation toward geographic north, but the figure display the true inclination. In Figure 3.6b, specimen SC067a has been induced with three remanence components in three orthogonal axes and subsequently demagnetized to a peak AF of 180 mT (in 19 steps, see section on Lowrie 3-axis test in chapters 5 and 6). The z-component was induced vertically and removed first with relatively weak AF to a peak around 30 mT. There is a rather sharp turning point between the z- and y-component. The y-component formed the intermediate magnetization in the sample (between 30-60 mT). Note that when the y-component has been removed the vector stabilizes in the direction of the induced x-component.

N

Sc066a (n=17)

Fisher statistics
mean= 244.1/43.2
a95%=0.5
Fish-k=4571.4

(a)

x (>60 mT) N

y (30 - 60 mT)

z (0-30 mT)

Sc067a (n=19)

Fisher statistics
mean= 019.6/09.2
a95%=9.3
Fish-k=13.9

(b)
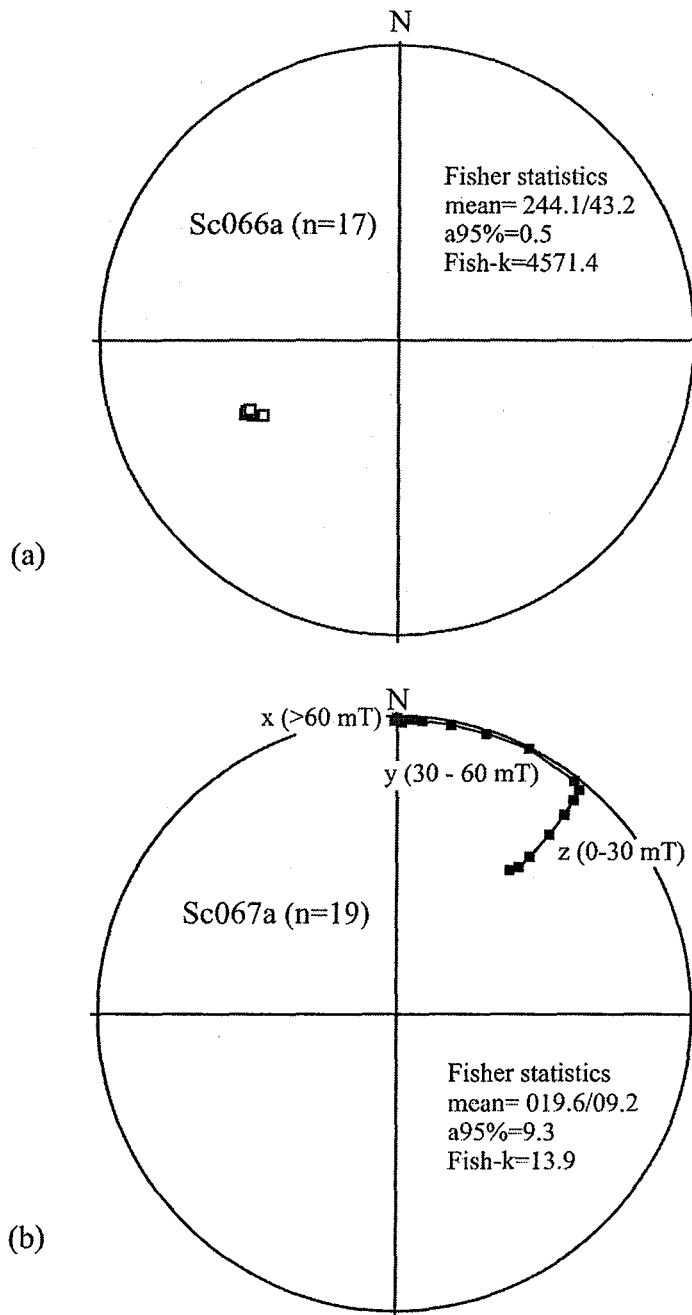
Figure 3.6 Equal area stereonets displaying paleomagnetic vectors at different stages of demagnetization. (a) Progressive AF demagnetization of a specimen carrying a single remanence vector, (b) AF demagnetization of a specimen carrying multiple remanence vectors (note that in (b) the Fisher statistics are not as useful to describe the sample population, since multiple vectors are analyzed).

3.3.1 Overlapping coercivities and blocking temperatures: the "smearing" problem

Consider a sample with two components of magnetization. In either vector component there are grains with similar unblocking temperatures or coercivities. During demagnetization, either thermal or AF, the magnetic moments of grains carrying both directions of remanence may

become activated (i.e. they become unblocked). The resultant vector is an average of those grains that were unblocked. The coercivities or unblocking temperatures of these grains are overlapping, and as a consequence both remanences are demagnetized synchronously (Figure 3.7a). Instead of two separate vectors, as displayed in Figure 3.7b, overlapping remanences may merge and form a curved path on a Zijderveld diagram, and consequently it becomes difficult or impossible to determine directions of the remanence components (Figure 3.7b, cases 2 and 3). This is particularly the case in older rocks, with complicated histories of magnetization. Hoffman and Day (1978) were able to circumvent the problem of overlapping remanences by using the
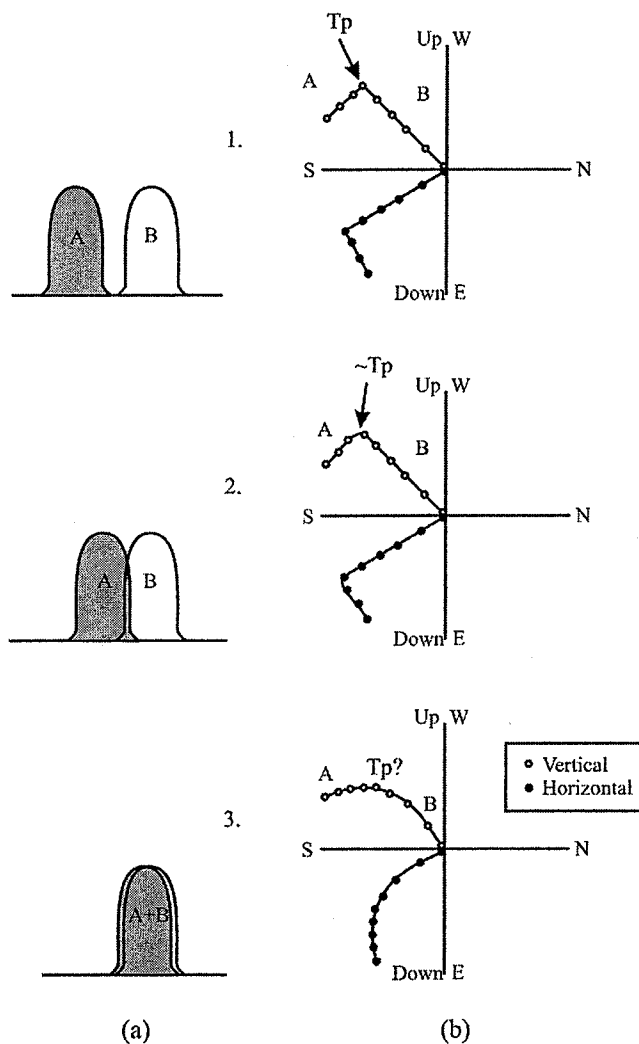
Figure 3.7 Simple hypothetical scenario, where in (a) different degrees of overlap are shown between component A and component B, and (b) shows the corresponding Zijderveld plot. In the first case there is no overlap between A and B and the vectors show clear separation. In the second case there is slight overlap between A and B, which is shown in the plot as curvature between the vectors, but they are still separable. In the final scenario there is almost complete overlap between A and B and it is impossible to separate vectors A and B in the Zijderveld plot. Tp = Turning point.

difference vector path (vector subtraction) of the demagnetization data. From the difference vector data they plotted best fit great circle paths along the data points. AF demagnetization of Jurassic basalts from Port San Luis, California, showed that the difference vector data yielded two great circles with three components of magnetization (Hoffman and Day, 1978: figures 6 and 7). It was not possible to separate any of these components using the corresponding Zijderveld plot. Instead the intersection of the two great circles on the stereonet identified the direction of the intermediate remanence, while the primary (called the stable) remanence was identified as the final vector difference on the great circle (vector subtraction of the applied field at 440 and 460 Oe).

Halls (1979) illustrated that through a combination of difference and resultant vectors, one could obtain paleomagnetic directions that were unobtainable using difference vectors alone (see Figure 3.8). He analyzed Precambrian igneous mafic rocks from Slate Islands of northern Lake Superior. The rocks contained a primary remanence since their formation, and a secondary shock induced remanence obtained from a meteorite impact and finally a soft VRM from the Earth's present field. Zijderveld plots could not be used to readily separate vector components, and instead Halls used a modified version of the Hoffman-Day method. Using only vector subtraction did not significantly improve Halls data, but when difference vector and resultant vector analysis were combined on the same stereonet it was possible to recognize separate remanence directions. Again, the intersection of the great circles (see Figure 3.8) defines the direction of the intermediate magnetization (as was shown by Hoffman and Day, 1978). In certain situations it is possible to reduce the effect of overlapping remanences, using low temperature treatments, as discussed previously.

3.4 Principal component analysis (PCA)

Kirschvink (1980) used principal component analysis (PCA) to estimate a best least-squares fit for paleomagnetic samples. PCA provides a method to calculate the directions of paleomagnetic linear points (demagnetized from one discrete magnetic component) and planar points (demagnetized from more than one discrete magnetic component). Based on the multivariate technique, PCA takes into account all available data obtained from incremental demagnetization. The obvious variable that is considered in PCA is intensity, while this property is excluded in difference and resultant magnetization vector techniques. It is not possible to consider intensity in the latter techniques since they use stereonets. PCA is unlike vector subtraction, which only takes into account the first and last vector points in a magnetic component or remagnetization different vector paths which excludes use of intensity (Kirshvink,

1980). Of course, the remanence components have to be separated before PCA can be used, by either the Zijderveld plot, Hoffman and Day's (1978) vector subtraction technique or Halls' (1979) combined resultant and difference vectors.
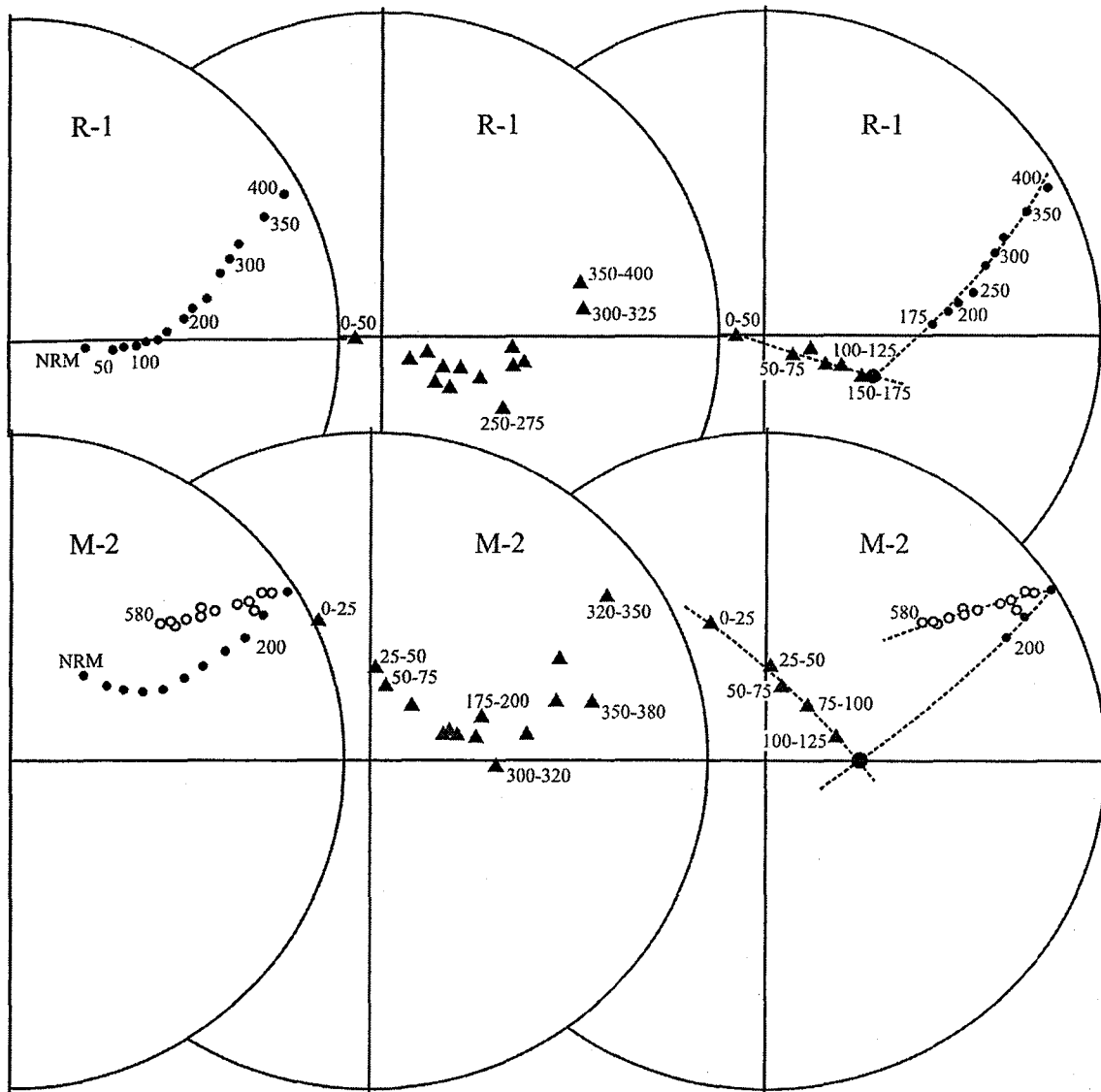
Figure 3.8 Stereonet plots of resultant vectors (circles) and difference vectors (triangles), and their combination for specimens R-1 and M-2. Open (closed) circles have upward (downward) directions. Alternating fields is measured in oersteds. The intersection of the great circle paths are marked with a larger circle indicating the direction of an intermediate shock induced remanent magnetization. Figure is redrawn from Halls (1976).

3.5 Summary

Procurement and interpretation of demagnetization data form the foundation for paleomagnetic research, whether on short timescales (e.g. Holocene sediments) or in old rocks (e.g. Proterozoic igneous rocks). It is therefore vital to understand what cleaning methods and strategies may benefit the paleomagnetist, and subsequently what techniques can be employed to understand the collected data. The relevant cleaning techniques include:

1) Alternating field demagnetization – by which an alternating current is used to progressively higher peak fields in order to preferentially align magnetic moments in grains to cancel each other.

2) Thermal demagnetization – by which thermal energy is used to disrupt the aligning spin exchange interactions of electrons that give rise to remanent magnetism. A sample is heated incrementally to higher temperatures in a magnetic field free space, in order to randomize moments upon cooling back to ambient temperatures.

3) Chemical demagnetization – by which paleomagnetic specimens are exposed to leaching acids for progressively longer time intervals, dissolving the ferromagnetic minerals and effectively removing the remanent magnetization.

4) Low temperature demagnetization – by which a specimen is exposed to low-temperature conditions (i.e. submersion in liquid nitrogen, or liquid helium), reducing the remanence contribution of polydomain grains, thus usually making it easier to identify the primary remanent magnetization.

The second part of this chapter addressed the relevance of secondary magnetizations and how to separate these from primary magnetizations. The separation methods include:

1) The Zijderveld plot – which illustrates direction and intensity of paleomagnetic data on two orthogonal planes, one showing the horizontal demagnetization plot and the second showing the vertical demagnetization plot.

2) Stereonet plotting – which uses the Hoffman and Day (1978) technique of difference vector analysis or the improved method of Halls (1979) where difference vector analysis is combined with resultant vector analysis.

3) Principal component analysis – which was introduced by Kirschvink (1980) in order to provide an objective estimate of the best fit lines and planes for paleomagnetic directions, including as much of the original paleomagnetic data as possible.

Chapter 4: Earth's magnetic field and Paleosecular variation

Paleomagnetic field secular variation or paleosecular variation (PSV) and magnetostratigraphy provide records for short ($10^2 - 10^4$ years) and long term ($>10^4$ years) behavior, respectively, produced by dipole and non-dipole effects in the Earth's interior. More specifically, PSV is the study of the "general spatial and temporal variability of the Earth's internal magnetic field during periods of stable magnetic polarity" (Lund, 1989: 876). Emphasis is placed on periods of stable magnetic polarity in the case of PSV studies, as this indicates the behavior of the dipole and non-dipole field in the absence of magnetic reversals. In contrast, magnetostratigraphy involves the study of geomagnetic reversals, using mainly sedimentary and volcanic stratigraphic records (e.g. the mid-oceanic spreading ridges). PSV data is provided by archaeological materials, such as kilns and fired bricks (e.g. archaeomagnetism; Batt, 1997; Kovacheva and Zagniy, 1985; Kovacheva et al., 1998; Sternberg, 1983) and volcanic lava flows (see Figures 4.1 – 4.3). The magnetization of volcanic rocks and archaeological materials is dominantly of thermoremanent magnetic (TRM) origin, which is usually very stable at ambient temperatures and geomagnetic field conditions and provides clear paleomagnetic and archaeomagnetic data for instances in geologic time. Data from archaeomagnetic and volcanic materials have been used for paleointensity measurements with fair success (Merrill et al., 1998). Unfortunately, the records provided by these are intermittent in and not always dispersed favourably through space and time. For example, there is a large bias of archaeomagnetic data gathered from locations in Europe, Middle-East, North America and eastern Asia, while data from other parts of the world is lacking. Semi-continuous sedimentary records from lacustrine and marine settings have become widely available through extensive studies particularly in Europe and North America and can be beneficial for establishing a wholesome PSV picture (e.g. Figure 4.3) (Lund, 1996). This chapter addresses the properties of the Earth's magnetic field of internal origin and the fluctuations in the field over time due to the geomagnetic dipole and non-dipole moments. This discussion is brief and only superficially describes the complex subject of geomagnetism and origin of the Earth's magnetic field. More comprehensive discussions on these subjects are provided by Tarling (1983), Merrill et al. (1998), Lowrie (1997) and McElhinny and McFadden (2000). Statistical and chronological methods involving the Earth's field are also briefly considered, in conjunction with paleomagnetic data produced from lake sediments of North America.
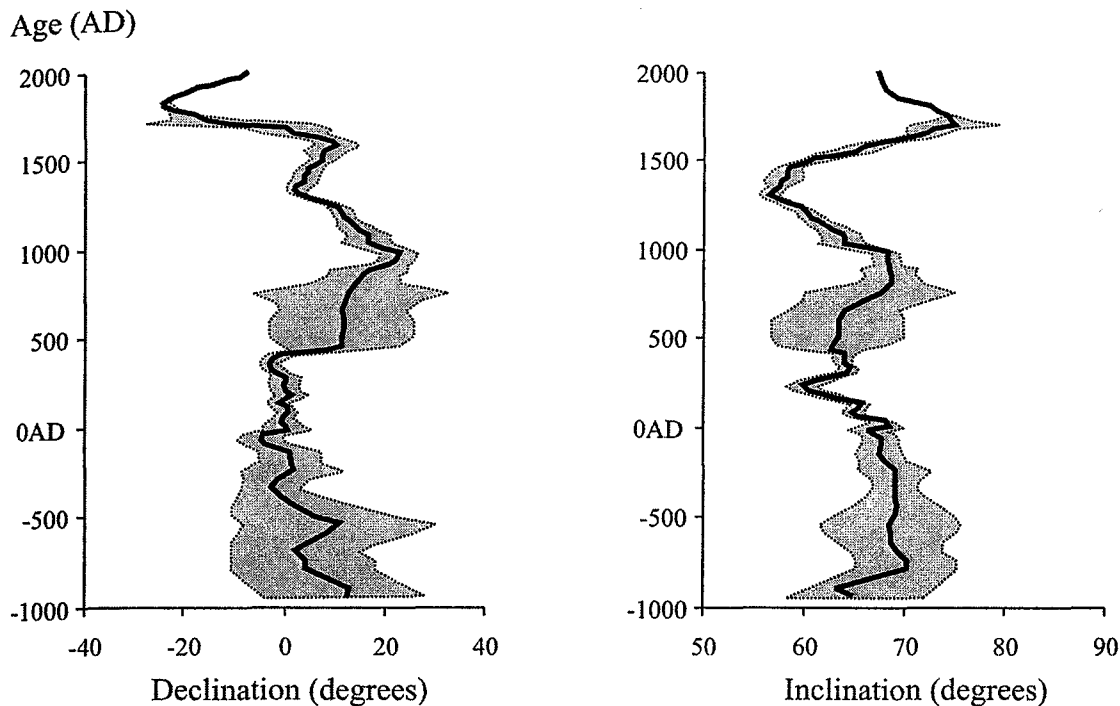
Figure 4.1 The revised British archaeomagnetic secular variation curve, 1000BC – 2000AD (Batt, 1997). The shaded gray area represent the 95% confidence limit.
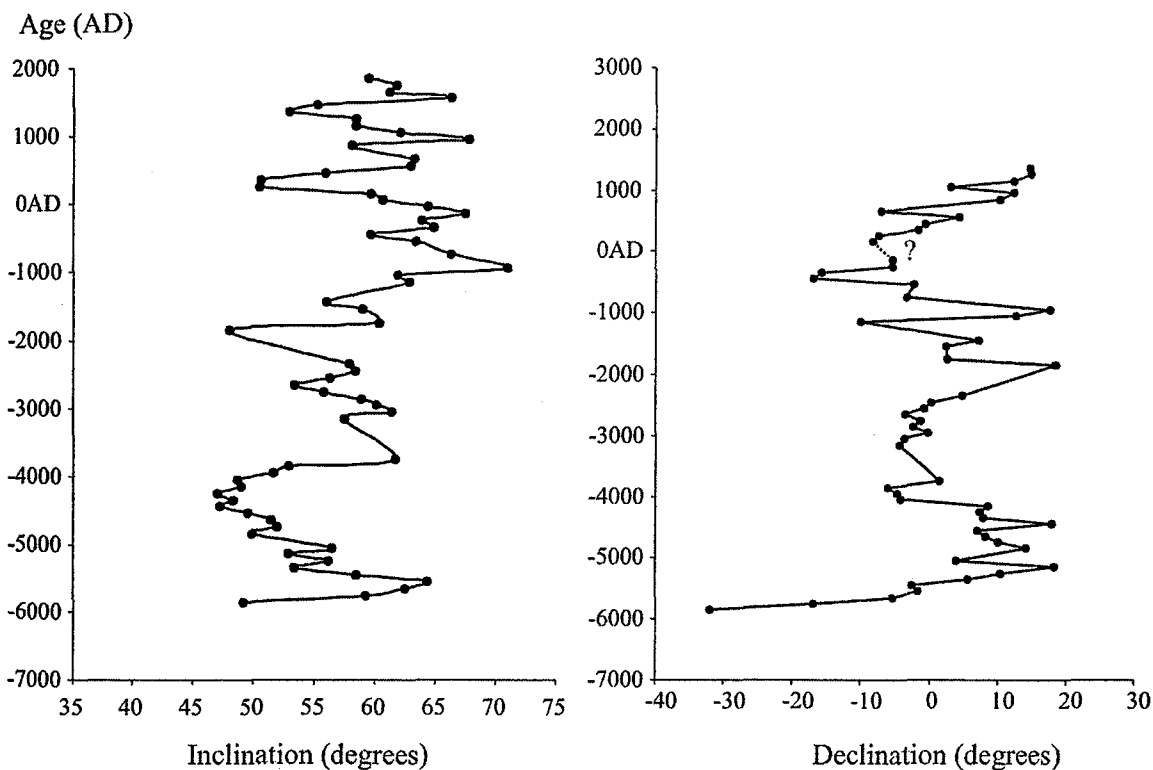
Figure 4.2 Archaeomagnetic secular variation curve from Eastern Europe (Kovacheva et al., 1998).
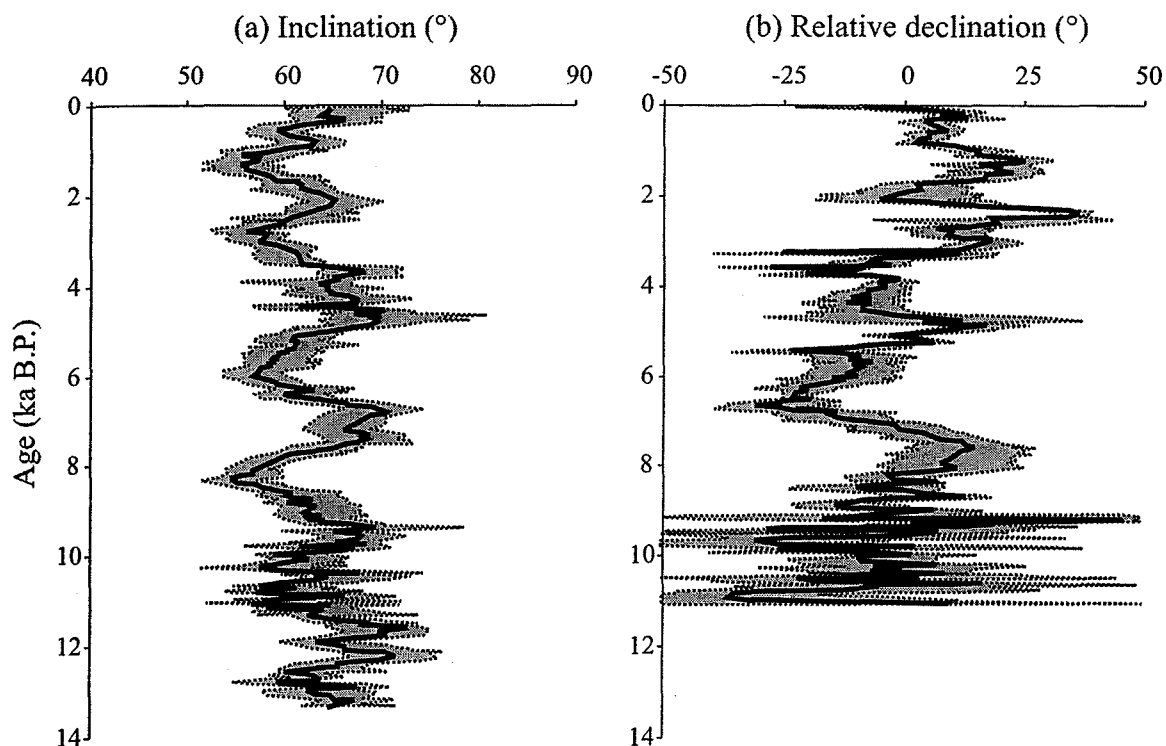
Figure 4.3 (above) Paleosecular variation curve of central North America based on lake sediment records from Lake Superior, Lake Huron, Lake St. Croix and Kylen Lake (Creer and Tucholka, 1982). The shaded gray area represents the 95% confidence limit.

4.1 Earth's magnetic field

Mathematically, the Earth's magnetic field of internal origin is best described through the use of spherical harmonic functions (Lowrie, 1997; Merrill et al., 1998), although any detail regarding spherical harmonic models of the field are beyond the scope of this chapter. Instead, it is useful to provide a descriptive discussion about the Earth's field. As was mentioned in the introduction, the main portion of the Earth's magnetic field is generated from within the planet. The most likely source for the generation of the geomagnetic field is the fluid outer core, which acts as a magnetohydrodynamic dynamo. More than 90% of the total Earth's magnetic field can be explained through a magnetic dipole that originates within the Earth, which is a first order effect using spherical harmonic analysis. The remaining portion of the field is described through a non-dipole field component (second or higher order spherical harmonic effect, also of internal origin) and external sources such as from the ionosphere and magnetosphere (Lowrie, 1997). There is also a contribution to the Earth's field from the remanent magnetization of rocks in the crust. The Earth's dipole is tilted somewhat with respect to its axis of rotation. The poles where field lines exit and enter the Earth's surface are called the geomagnetic poles, and each pole is antipodal to the other, or exactly opposite. The addition of the non-dipole portion produces

magnetic poles that are not exactly opposite each other, since the non-dipole effects arise from local sources at the core-mantle boundary.

4.2 Geomagnetic secular variation

The Earth's magnetic field appears to exhibit three regular, innate temporal characteristic variations on time scales longer than one year (Evans and Heller, 2003), that all originate from the interaction between the Earth's core and mantle (i.e. generation of the dipole and non-dipole field). In order of longevity, they are 1) geomagnetic polarity reversals, 2) secular variation and 3) excursions. One could also consider variations in external sources of the magnetic field, beyond the Earth's surface, contributed by the ionosphere and the magnetosheath for example. However, most external magnetic sources fluctuate rapidly with time periods much less than one year, with the exception of the solar winds. Geomagnetic secular variation describes Earth's prehistoric magnetic non-dipole field variability from historic time into the Neogene time period. Historic field secular variation (HSV) describes the Earth's non-dipole field variability as recorded from observatory measurements for the last ~450 years (Lund, 1989). The most prominent evidence of secular variation has been the westward drift of the geomagnetic field during historic time (Hagee and Olson, 1989; Bullard et al., 1950), and in fact secular variations are experienced by both the dipole and the non-dipole field components. During the last 450 years, the intensity of the geomagnetic field has been reduced on average by 3.2% for every century (Barton, 1989; Lowrie, 1997), and the rate of decrease in intensity appears to accelerate during the last century. The decrease in intensity has been explained to be due to secular variation in the dipole moment, and archaeomagnetic paleointensity measurements over the last 10,000 years support this argument (Lowrie, 1997; Merrill et al., 1998). The decrease in intensity of the dipole moment will lead to a greater influence of the non-dipole field. It is uncertain how this affects the overall geomagnetic field, but it is thought that a decrease in the dipole moment could be related to excursions of the magnetic field, and perhaps even magnetic reversals. It has also been suggested that excursions may arise as a consequence of an increase in the non-dipole magnetic moment. An increase in the ratio of the non-dipole to the dipole moment would also affect secular variation in the Earth's field.

Paleomagnetic field secular variation (PSV) is primarily used in order to gain further understanding of the core-mantle interaction and develop the mapping function between observed spatial and temporal variations of the geomagnetic field (Lund, 1989), but the PSV records are useful in other regards as well. PSV (and HSV) reflect what is happening in the interior of the Earth, specifically in the liquid outer core. However, PSV is also used to test the validity of the

geocentric axial-dipole (GAD) hypothesis, which is a crucial component for application of paleomagnetism. The direction and intensity of a single paleomagnetic measurement of a rock or sediment is affected by all the sources that give rise to the Earth's magnetic field, including PSV. A single paleomagnetic measurement may therefore not represent the past position of the studied location (i.e. paleo-latitude and paleo-longitude). Instead, it is appropriate to continuously sample a location until a suitable amount of time has been covered to present an average paleomagnetic field, or time averaged field (McElhinny and McFadden, 2000; Figure 4.4). In its simplest form, the GAD hypothesis predicts that sampling over a sufficient amount of time should produce a dipole that is aligned parallel to the Earth's axis of rotation (instead of being inclined with respect to that axis). PSV is also very useful in correlation of stratigraphic sequences (as is discussed below), for example from lake and ocean sediment cores, in conjunction with other methods such as stable isotope data or magnetic susceptibility records.
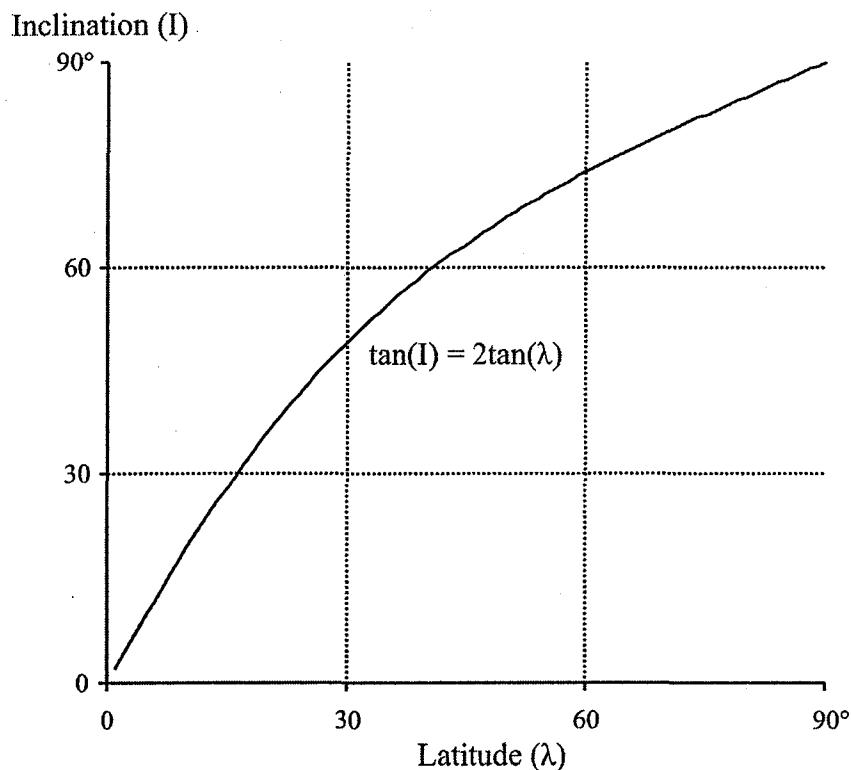
Figure 4.4 The geocentric axial dipole model. The inclination of the Earth's magnetic field is determined by site latitude; the relationship between latitude (λ) and the inclination (I) of the Earth's magnetic field is described by tan(I)=2tan(λ).

Resolution of data is very important in PSV studies, since the objective is to present short-term changes in the Earth's magnetic field. As noted in the beginning, PSV can be studied using sedimentary records, volcanic rocks and ash, and archaeological materials (e.g. hearths,

kilns and heated bricks). Each of these has both advantages and drawbacks. Volcanic and archaeological materials provide a truly instantaneous recording of the geomagnetic field, since they acquired a TRM upon rapid cooling, but due to their nature, recordings are usually dispersed intermittently throughout time. Alternatively, sediments often provide a more continuous recording of the geomagnetic field behavior through time, although caution should be utilized since pitfalls arise during their study. The following is a list of possible contributors that may give rise to complication in the interpretation in the PSV record:

1) Rate of deposition – In some ocean basins, depositional rate is too low to register the fine resolution needed in regards to short-term changes in the Earth's magnetic field. This leads to a smoothing effect in the PSV record, and possible absence of geomagnetic excursions (Roberts and Winklhofer, 2004; Lund and Keigwin, 1994). Slow depositional rate is generally not a problem in lacustrine deposits, since large amounts of sediments are transported into lake basins over short periods of time, compared to oceanic basins. Slowly deposited sediments may also be re-magnetized through processes such as bioturbation to a greater extent than rapidly deposited sediments. Although theoretically sound (Lund and Keigwin, 1994), there is no quantitative proof as of yet that smoothing occurs because of low rates of deposition (Katari et al., 2000).

2) Time constraint – It may be difficult to absolutely determine ages of sedimentary deposits, mainly because of a lack of time indicators (in contrast to archaeological materials and volcanic deposits). For example, in lacustrine sediments ^{14}C-dating is often hampered by the influence of older recycled, detrital carbon (unless macro-fauna can be identified and separated from the sediments), or the absence of datable organics. In addition for radiocarbon dating, water-logged organic material needs to be corrected for a ^{14}C reservoir effect.

3) Inclination shallowing and compaction – As discussed above, during deposition it is likely that magnetic particles are affected by the bedding plane, or the roughness of the sediment surface. Elongated grains may therefore orient themselves so that their long-axes preferentially settle in the horizontal plane (see Figure 2.5b). Thus, the magnetic moment of such grains will be shallower than the actual geomagnetic field (except at geographically low latitudes where the field is already shallowly inclined). Further, compaction of sediments will affect the inclination, and possibly also declination, of the imprinted magnetic field (see chapter 2, section 2.4.1c). Tauxe and Kent (1984) illustrated that the inclination of an applied field is important for the observed inclination of laboratory deposited sediments, and is most significant for mid-latitude

angles (~45°; see Figure 2.4), while van Vreumingen (1993a, b) and Katari and Tauxe (2000) have shown that water chemistry influences inclination, as well as the intensity of magnetization.

4) A possible contributor to deviant behavior between the recorded signal in the sediment and the actual geomagnetic field lies in the magnetic mineralogy carrying the remanence. Due to inherent shape and magnetocrystalline anisotropy in some magnetic minerals, particularly hematite, the remanence can be deflected away from the direction of Earth's magnetic field (Tan et al., 2002). Possible examples of these magneto-mineralogical properties are provided in chapters 6 and 7. As the sample is demagnetized, a curved vector component is discovered due to overlapping coercivity spectrums of more than one mineral phase. The remanence signal shallows or becomes sub-parallel to the horizontal plane as one approaches the origin at high peak alternating fields.

4.3 Time-series analysis and Paleosecular variation

This section follows the outline given by Lund (1989), regarding the use of time-series modeling of PSV records. Paleomagnetic studies of lake sediments do not generally yield regularly spaced, discrete data points which complicates the use of time-series analysis (with the possible exception of varved sedimentary sequences). However, it is possible to consider high-resolution paleomagnetic records as continuous time-series, rather than discrete. Three categories of time-series techniques have mainly been utilized for PSV studies: 1) waveform analysis, 2) spectral analysis and 3) statistical analysis (Lund, 1989). Waveform analysis considers the high-resolution data obtained from a paleomagnetic record, such that it can be used to make waveform comparisons within the record, between two different paleomagnetic records and finally between PSV and HSV records. Within record waveform observations identify recurring patterns in the high-resolution data, and an interesting example is provided by the results from Mono Lake (Lund et al., 1988). The paleomagnetic record of Mono Lake has been studied in detail by many workers, and a recurring pattern has been identified to repeat itself every 2400-3500 years, for at least 15,000 years. It is thought that the observed pattern stems from the Mono Lake excursion, which suggests that recurrence in the waveform refers to long-term memory in the core-dynamo process (at least on a regional scale). This is a great example of how a high-resolution paleomagnetic record (in this case sampled from outcrop of Holocene and Pleistocene sediments from Mono Lake) can contribute to further understanding the nature of short-term core-dynamo processes. The waveform PSV pattern can be compared between two or more paleomagnetic records over a limited region, when the records overlap in time. In North America, Lund (1996) and Hanna and Verosub (1988) have compared lake sediments ranging in space from the east to

the west coast with consistent results, within the Holocene (~0 - 10,000 years ago). Lund (1996) proceeded to use waveform analysis to look at looping or circularity behavior of inclination and declination features in the records from the North American lakes. The sites used in his study are well spaced longitudinally (with a range of almost 4000km, or ~40° longitude), while they are more constrained with latitude (~20° - 40°N). Generally, when comparing or correlating PSV records a region spanning 3000 km is justifiable (Lund, 1989), since at greater distances different sources in the core-dynamo process may affect the individual PSV patterns.

Spectral analysis is used to observe power frequency distributions within the PSV record, and has suggested that secular variation in the Earth's magnetic field is a band-limited phenomenon. The PSV appears stationary, in a statistical sense, for time intervals greater than 10,000 years. The stationary nature of PSV is crucial, since it is one of the underlying assumptions of the axial-dipole hypothesis (which in itself is fundamental to the studies of paleomagnetism and plate tectonics). Barton (1982) identified two bands within the time-period 100-10,000 years with different intervals. A short-period interval is identified at 500-3500 years, while a long-period interval occurs at 7000-10,000 years. These bands maybe linked to different processes in the core-dynamo, where the former arises from non-dipole behavior and the latter from dipole behavior.

Statistical analysis of PSV provides a method to give a time-averaged record of secular variation. The calculated average can then be tested against the axial-dipole hypothesis in order to observe the stationary Earth's magnetic field, over time-periods longer than PSV. A question that often arises in paleomagnetism is whether a geological site has been sampled over adequate time for the averaged PSV pattern to approach the theoretical axial-dipole. The longest period displayed by PSV is thought to be ~10ka (Lund, 1989), and often a data set collected from a single locality (or small region) covering 10^5 to 10^6 years is adequate for paleomagnetic purposes. Empirically, the averaged PSV does not show a strict spherical distribution of data but rather an elliptical distribution (Lund, 1989) and the deviation of the mean inclination (I) from the theoretically determined dipole results in an inclination anomaly. Over at least the past 5ma it has been found that the mean inclinations of the averaged PSV vary with latitude and are consistently shallower than predicted by the axial-dipole hypothesis (Merrill and McElhinny, 1977). The inclination anomaly (of shallower than predicted inclinations) has been observed in several studies during the latter Pleistocene from both sediments and lava flows, and virtual geomagnetic poles (Lund, 1985).

4.4 Paleosecular variation as a chronological tool

When a PSV record has been established, with adequate chronological control, it is possible to use this record as a correlation tool for other PSV and archaeomagnetic records. Well developed PSV master curves for the United Kingdom and other parts of Europe (Turner and Thompson, 1981; Kovacheva and Zagniy, 1985; Clark et al, 1988; Batt, 1997; Evans and Hoye, 2005) and North America (e.g. Lund, 1996; Verosub and Hanna, 1989; Creer and Tucholka, 1982) are examples of high resolution magnetic records gathered mainly from archaeomagnetic data and some lacustrine and marine sediments (see Figures 4.1 - 4.3). Secular variation exhibits an irregular cyclical pattern of swings in declination and inclination with specific time intervals and as such the reproducibility is not exact every time the pattern is repeated. This is often useful when using PSV as a tool for age correlation, since the uniqueness of certain cycles may be helpful to infer where a point or record on the PSV master curve may fit. Paleomagnetic data obtained from lake sediment cores, archaeological monuments and volcanic sequences are steadily increasing and thus their use for correlation is improving. ^{14}C and geochronological dating methods are most common in establishing the ages of the PSV record, although historical dates can be used for some archaeological materials. Due to the nature of these methods, problems with uncertainties may arise, sometimes obscuring the pattern of secular variation with error margins in time that may cover entire cycles or loops in the PSV record. In certain cases for lake sediments that have annual characteristics, such as varves, it is possible to obtain very precise chronologies for the paleomagnetic records (e.g. Ojala and Saarinen, 2002; Ojala and Saarnisto, 1999).

4.5 Paleosecular variation records from Central North America

The paleomagnetism and PSV of lake sediments from northwestern Ontario and Minnesota have been studied in some detail (Mothersill, 1979; 1985; 1988; Banarjee et al., 1979; Creer and Tucholka, 1982; Lund and Banarjee, 1985; Sprowl and Banarjee, 1989). The earliest studies were provided by Mothersill (1979) and Banarjee et al. (1979) on lake sediments from Lake Superior and a couple of lakes in eastern Minnesota, all of which showed clear patterns of PSV. Later studies of Mothersill (e.g. Mothersill, 1985; 1988) have mainly dealt with establishing stratigraphic relationships and rates of sedimentation through paleomagnetic measurements in the Lake Superior basin, rather than placing an emphasis on identifying PSV patterns in these sediments. Creer and Tucholka (1982) produced a compilation of paleomagnetic data obtained from lake sediments in the Great Lakes area of North America and smaller lakes from Minnesota (Mothersill, 1979; 1981; Banarjee et al., 1979), in order to construct a type secular variation

master curve for inclination and declination of east-central North America (Figure 4.3). Establishing accurate radiocarbon dates for sediments in northwestern Ontario (particularly Lake Superior) has been a challenge, mainly due to lack of macro-organic material from these sediments but also because older reworked carbon tends to become incorporated into the sediments which displace radiocarbon dates for bulk samples of sediment. However, lake sedimentary records from Minnesota (Banarjee et al., 1979) have yielded accurate radiocarbon dates which were used by Creer and Tucholka (1982) to establish the chronology for Lake Superior sediments and paleomagnetic record. The type curves for inclination and declination in Figure 4.3 are reproduced from Creer and Tucholka (1982) and are based on the paleomagnetic and radiocarbon records of sediments from Lake Superior (Mothersill, 1979), Lake Huron (Mothersill, 1981) and lakes St. Croix and Kylen from Minnesota (Banarjee et al., 1979). Note that declination is reported as relative since true declination could not be obtained from the lake coring process. Creer and Tucholka (1982) also note that core "twisting" is evident in some records which may be the cause for the large standard deviation in the bottom portion of their stacked declination record (Figure 4.3b).

Lund and Banarjee (1985) have provided one of the most detailed studies concerning Lake St. Croix at the border between Minnesota and Wisconsin and Lake Kylen located in northeastern Minnesota. Through careful sampling of paleomagnetic samples and use of time-series analysis (including power spectrum analysis and waveform morphology) they found evidence for long-term, ~10,000 year, and shorter-term, ~2400 year, wavelengths present in the extracted paleomagnetic record. They attributed the long-term component, which had the lowest frequency, being due to the Earth's dipole. Because the long-term dipole feature stretches across almost the entire recorded paleomagnetic record of Lake St. Croix and Lake Kylen it is difficult to assess its reliability. The short-term behavior was explained as drift of the non-dipole field, and wavelengths of shorter nature were found with periodicities of 600, 800, and 1200 years, but with a most common frequency of ~2400 years. The short-term wavelength data can be readily observed from the filtered data for Lake St. Croix (Lund and Banarjee, 1985: figure 20) with regularly recurring wavelengths every ~2400 years. Further, from their work Lund and Banarjee (1985: figure 21) suggests that during the last 8000 years before present (B.P.) the non-dipole moment in central North America has experienced clockwise or westward drift, whereas prior to this the non-dipole drift has been predominantly counterclockwise movement (but this is not necessarily evidence for eastward drift).

Chapter 5: Methods used to study the Strawberry Creek Sediments

Rock magnetic methods are used to study and interpret magnetic mineralogy present in rocks, unconsolidated sediments and soils. Indirectly, the results of rock magnetic measurements are useful for application in paleomagnetism and for verification of results gained from paleomagnetic measurements. All magnetic minerals exhibit specific rock magnetic properties, and criteria have been established to identify individual minerals using magnetic methods. Whether a rock or sediment is suitable for paleomagnetic study is, therefore, one of the questions that rock magnetic analysis aims to answer (Schmidt, 1993). A direct application of rock magnetism is considered when magnetic minerals are used to proxy some environmental effect, where minerals reflect physical, chemical or biological processes. For example, as an intrusive dike cools in a host rock one can infer its flow directions from the AMS ellipsoid, or magnetic minerals themselves can be direct indicators of depositional conditions in lacustrine or marine settings (i.e. anoxic versus aerobic conditions). The rock magnetic laboratory at Lakehead University offers a range of equipment useful in studies of magnetic mineralogy. The whole range may not be applicable to any one project or study, but each instrument is in itself useful to deduce information about mineral magnetic properties in a sample and acts as a compliment to other instruments. The methods used in the current study are presented in the following sections.

5.1 Alternating field demagnetization

All specimens analyzed in the study of the Strawberry Creek sediments had a measurable remanent magnetization, on the order of $\geq 10^{-3}$ A/m; measurement noise level of the instrument could be disregarded ($\sim 10^{-4}$ A/m). An AF demagnetizer with 200mT maximum achievable AF and capability to induce ARM from Sapphire instruments was used to stepwise demagnetize specimens. Thermal demagnetization was deemed inappropriate due to the nature of the sediments, as heating the specimens would likely dehydrate and chemically alter the magnetic mineralogy during consecutive heating intervals. The process of heating could also damage and deform the plastic specimen holders. Due to at least one high coercivity phase, AF demagnetization failed to completely remove the remanent magnetization in some specimens, although it was possible to extract paleomagnetic data from every specimen used in the study (using PCA; Kirschvink, 1980). Also, due to resistance within the coils producing the AF, the highest achievable AF was closer to 180mT. During long periods of experiments the maximum

achievable AF continues to degrade as the coils heat and resistance increases. A three and six axis orientation method was used for the AF demagnetization of specimens (see Figure 3.2, chapter 3).

5.2 Anisotropy of magnetic susceptibility and magnetic fabric

Magnetic susceptibility is a property exhibited by any material, whether it is diamagnetic, paramagnetic or ferromagnetic. Diamagnetic and paramagnetic materials display linear responses to an applied magnetic field such that $M=\chi H$. As previously discussed (see Chapter 2) diamagnetism is a weak response to an applied magnetic field in every material and χ is negative. Paramagnetic materials also exhibit the diamagnetic response, but are far more influenced by the positive χ. The response to an applied weak field in ferromagnetic materials is also linear, but as the field becomes more intense, the ferromagnetic moments eventually saturate. The benefit of using low-field measurements for investigating magnetic susceptibility is that all properties described above exhibit a linear response to the applied field, based on what minerals are present in a rock or sediment and their respective amounts. The magnetic fabric refers to the shape and orientation of the susceptibility ellipsoid (Hrouda, 1982) which is determined from the physical properties of the minerals (e.g. shape, magnetocrystalline anisotropy and magnetostriction). Magnetic susceptibility was measured using an SI2 Sapphire susceptibility bridge. The anisotropy of magnetic susceptibility (AMS) ellipsoid is obtained through a seven-orientation measurement scheme, with three orthogonal axes and four body diagonals (Borradaile and Stupavsky, 1995; Nye, 1957; see Fig. 5.1a). This measurement scheme has been shown to give low experimental errors during determination of the AMS ellipsoid, when susceptibilities are $\geq 100\mu SI$ (Borradaile and Stupavsky, 1995), and thus achieve a good approximation of the susceptibility anisotropy. AMS provides valuable information on the susceptibility ellipsoid (i.e. an oblate, prolate or neutral ellipsoid; Figure 5.1b), and indicates directions of maximum, intermediate and minimum susceptibility (k_{max}, k_{int}, k_{min}, respectively). The bulk susceptibility of a sample can be calculated from the AMS data in two ways:

1) the arithmetic mean of the susceptibility directions (see for example Hrouda, 1982)

$$k_{bulk} = \frac{k_{max} + k_{int} + k_{min}}{3} \qquad \text{[Eqn. 5.1]}$$

2) the geometric mean of the susceptibility directions

$$k_{bulk} = \sqrt[3]{k_{max} \cdot k_{int} \cdot k_{min}} \qquad \text{[Eqn. 5.2]}$$

[Eqn. 5.2] was used to calculate bulk susceptibilities in this study.
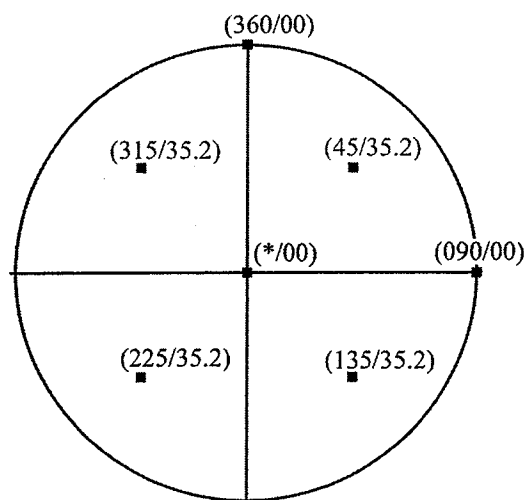
(a) Measurement scheme for AMS and AARM
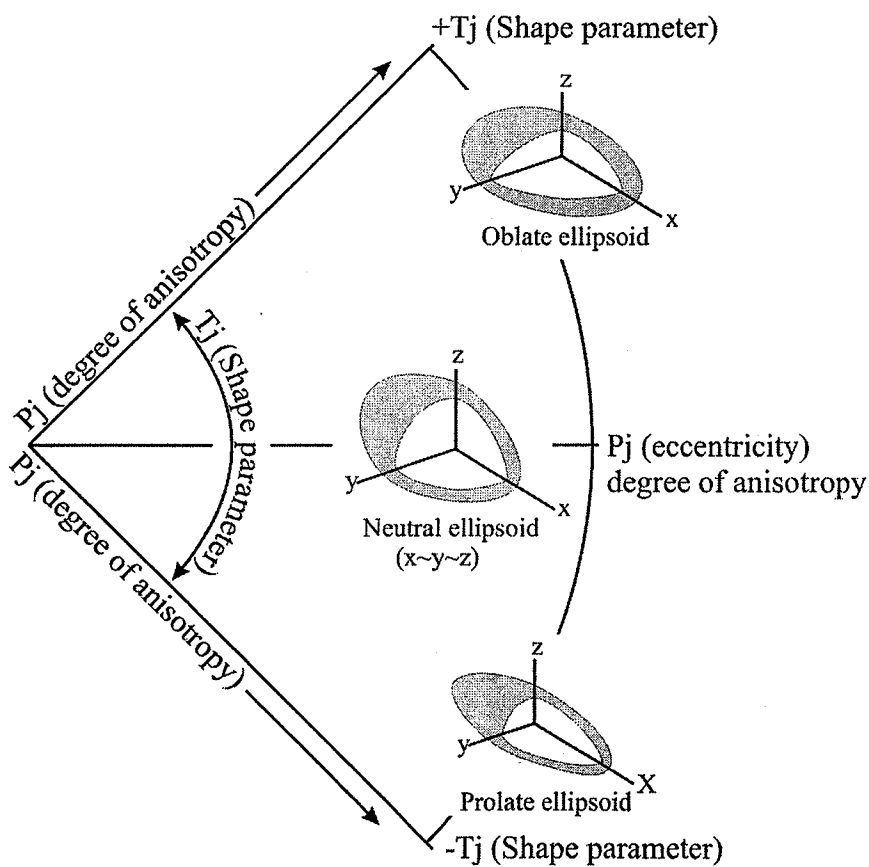
(b) The modified Jelinek plot (Borradaile and Jackson, 2004)

Figure 5.1 (a) Stereonet showing the measurement scheme for the determination of the susceptibility tensor (Borradaile and Stupavsky, 1995), (b) the susceptibility tensor provides an ellipsoid with maximum, intermediate and minimum susceptibility. The modified Jelinek plot (Borradaile and Jackson, 2004) illustrate the shape (Tj) and degree of anisotropy (Pj) of the susceptibility ellipsoid; a positive Tj indicates an oblate susceptibility ellipsoid, while a negative Tj indicates a prolate susceptibility ellipsoid.

5.3 Isothermal remanent magnetization

A magnetic remanence obtained from a high field over a short amount of time at steady temperatures is called an isothermal remanent magnetization (IRM). In nature an IRM is usually produced through lightning strikes, but laboratory instruments can artificially produce this remanent magnetization. A direct current is used to align the magnetic moments of grains and if the direct current is strong enough to influence and align all the magnetic moments parallel with the applied field, a saturated IRM is produced (SIRM). A pulse magnetizer was used for the purpose of experiments which demanded application of isothermal remanent magnetization (IRM). The saturating field or SIRM that can be produced by this instrument is 1.2T. Due to the inherent high coercivity of some iron oxides (e.g. hematite/goethite), the largest available field of the pulse magnetizer may not be enough to saturate the specimen. All magnetite (SD, PSD and MD) should attain saturation with fields ≤300mT (Evans and Heller, 2003; Thompson and Oldfield, 1986). Magnetic moments aligned in this fashion are only at equilibrium during the time for which the field is applied. Once the field is removed, they are no longer in equilibrium and the moments rearrange themselves in order to reach a stable energy configuration. Single domain moments are most influenced by their shape and magnetocrystalline anisotropies, while for multidomain magnetite the main factor becomes a stable orientation of domain walls. An IRM does not represent a good example of remanence acquisition in nature (with the exception of lightning strikes).

IRM's were used in two ways for the study of the Strawberry Creek sediments: 1) incrementally increasing IRM intensities to eventually achieve saturation magnetization which was followed by AF demagnetization (Figure 5.2), and 2) an orthogonal three-axis test (Lowrie, 1990; Figure 5.3). In the first experiment a specimen is initially demagnetized, followed by exposure to a small DC-field. The intensity of DC-magnetization is increased subsequent to measurement of the remanence and the process continues until the saturation field has been reached (1T in our study). This kind of experiment has frequently been used to distinguish magnetic mineralogy and grain size (i.e. Dunlop, 1986; Dunlop and Özdemir, 1997; Robertson and France, 1994; Symons and Cioppa, 2000). Useful information about grain size and mineralogy is acquired when acquisition is plotted versus the AF demagnetization. This test was popularized by Cisowski (1980), who used it to interpret whether magnetic grains are interacting. The diagram has therefore been named the Wohlfarth-Cisowski. Another name is the cross-over plot, insinuating the intersection of the IRM acquisition curve and the AF demagnetization curve (Symons and Cioppa, 2000). The value where the acquisition curve crosses the decay curve is

called the R-value, and usually a value of ≥ 0.5 indicates no significant interaction of the ferromagnetic moments of the minerals. A value of R<0.5 suggest significant interaction of magnetic moments, and the lower the cross-over value, the more significant is the interaction between grains in the sample. The median destructive field (MDF) is the field necessary to remove half of remanence (0.5), either in an artificial or natural remanent magnetization. The coercivity of the minerals present in the sample determines the shape of the acquisition and demagnetization curves which is the reason this method can be used to help identify rock magnetic mineralogy.
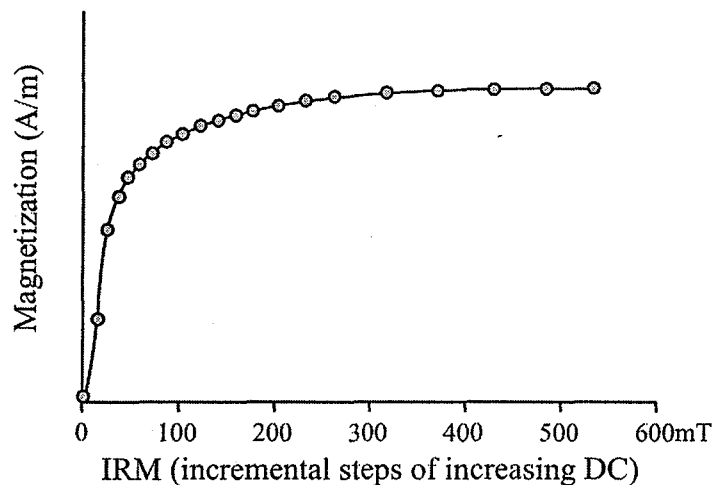
Figure 5.2 Isothermal remanent magnetization acquired over incrementally increasing steps of applied direct currents (in mT). Magnetization increases with the intensity of the applied DC, until the material is saturated and magnetization plateau.

The second experiment, involved inducing IRM of different and non-overlapping coercivities in three orthogonal directions. This technique for separating fractions of coercivity was initially used by Lowrie (1990), in order to identify magnetic carriers in a Swiss limestone. Demagnetization of the artificially induced orthogonal remanences (here referred to as the x-, y-, and z-components) is performed through regular AF treatment. Lowrie (1990) used thermal demagnetization to unblock the remanence in his limestones; however, for unconsolidated sediments this is not preferable. Changes in direction and intensity of remanences during demagnetization signify unblocking coercivities, and the length of each x-, y-, and z-vector indicate an amount or fraction of coercivity carried by each vector. This method therefore acts as a very effective means of isolating coercivity ranges in a sample, and thus giving an indication of magnetic mineralogy. Borradaile et al. (2004) used Lowrie's (1990) method to study the magnetic mineralogy of Proterozoic diabase from sills related to the Proterozoic rift system in the Lake Superior region. They selected coercivity ranges from <15mT, 15-30mT and >30mT (Figure 5.3),

which corresponds relatively well with domain-sizes of MD, PSD and SD magnetite, respectively (Borradaile et al., 2004; D. Dunlop, Pers. Comm., 2004).
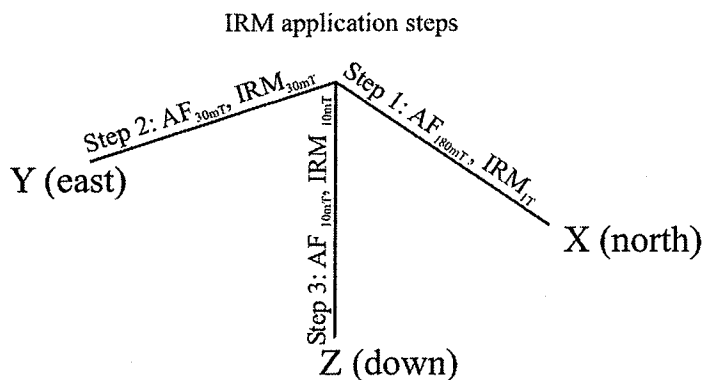
Figure 5.3 The orthogonal three-axis test. The axes used in the test carry remanent magnetizations with separate and non-overlapping coercivities.

5.4 Anhysteretic remanent magnetization

Anhysteretic remanent magnetization (ARM) is produced by placing a sample in the presence of an alternating field together with a small steady bias field (usually on the order of the geomagnetic field, 0.05- 0.1mT). An ARM is a better model for NRM acquisition, mimicking TRM in particular, but avoiding chemical changes that would occur during heating (Evans and Heller, 2003). The alternating field acts as thermal agitations during cooling of a rock, and similarly to acquisition in a TRM, moments are locked in once the AF reduces below their specific blocking coercivities. Consequently, the resultant magnetization of an ARM is more stable than an IRM in ambient conditions. Anhysteretic remanent magnetism (ARM) is often used to avoid heating rocks or sediments, but to simulate the natural acquisition of a thermal remanent magnetization. The alternating field acts as thermal vibrations during the remanence acquisition process, and the decay of the field simulates reduction in temperature. Meanwhile, the weak background DC acts as the Earth's magnetic field. The ARM is produced using the Sapphire AF demagnetizer, with a steady background DC (0.1mT) and a window (the points where the DC-field is initiated and subsequently terminated) at an AF usually of 60mT. An alternative treatment with ARM is through incrementally increasing the window, from initially very small initial AF's until the window equals the AF peak field. This is in sorts similar to the acquisition of incremental IRM described above. Moments that are responsive (i.e. react with the switching field) within the window are preferentially aligned with the background DC field. Subsequent increases in the window thus leads to an increase in remanence acquisition. The amount of

remanence acquired between changes in the window reflects coercivity ranges present in the sample and is therefore indicative of magnetic mineralogy.

The incrementally increasing background window creates a partial ARM (pARM) that is most useful when observed with a coercivity spectrum (Jackson et al., 1991). A pARM is useful to distinguish coercivity ranges of the magnetic minerals present in a sample and serves as a tool for identifying the magnetic mineralogy. The drawback of using an ARM is the limited range over which the background AF can be applied; spurious magnetizations may be produced once the AF reaches values >200mT. Induction of ARM's and pARM's are useful for many common magnetic minerals (e.g. magnetite, pyrrhotite, maghemite), but falls short of affecting high coercivity minerals that sometimes dominate the magnetic mineralogy of certain lithologies (e.g. hematite and goethite). The results for pARM acquisition are shown for clay and silt samples in chapter 6.

5.4.1 Anisotropy of anhysteretic remanent magnetization

Anisotropy of anhysteretic remanent magnetization (AARM) is a method used to determine anisotropy of magnetic remanence (AMR) solely contributed from ferromagnetic particles. Whereas AMS affects all mineral grains in the sample that is measured, AARM only considers particles that are able to carry a magnetic remanence. Measurements are performed with a magnetometer in zero field condition. Artificial remanences are induced using an ARM technique applied in three orthogonal directions and four body diagonal directions (Borradaile and Stupavsky, 1995; Jackson, 1991; McCabe et al., 1985). The anisotropy of the magnetic remanence is usually greater than that of the magnetic susceptibility as a consequence of inherent anisotropy of magnetic moments in ferromagnetic minerals that are due mainly to factors of shape, crystallography and the internal stress of individual magnetic particles (Jackson, 1991).

The main drawback with measuring AMR is time consumption of the experiment. The AMS of a specimen can be readily obtained in about three minutes, whereas the measurement of AARM for that same specimen may take nearly five to ten times as long depending on measuring scheme and available equipment. The value of the AARM measurement should not be underestimated however. Knowledge regarding the anisotropy of a remanent magnetization is crucial when studying changes in the Earth's magnetic field (i.e. PSV) and reconstructions of past continental and ocean floor movements using paleomagnetism. Even slight anisotropies of magnetic particles will affect the outcome of resulting remanences induced by the geomagnetic field. AARM is very useful in complementing AMS when studying sediments and DRM, to elucidate the possibility of inclination error and field refraction of magnetic particles. It is well

known that the inclination of a DRM may be shallower than the actual applied field inclination ($I_{DRM} < I_F$; see discussion on DRM and pDRM in Chapter 2), as a consequence of depositional mechanisms and compaction. Further, AARM has been used to investigate the anisotropy in low susceptibility rocks, containing mainly diamagnetic minerals such as limestone, where AMS may be less informative regarding the anisotropy of a rock (e.g. McCabe et al., 1985).

The method used for determination of AMR is outlined as follows: 1) a specimen is demagnetized with a 160mT peak AF, 2) an ARM is imparted on the specimen, with 0.1mT background DC field over a window stretching from 60-0mT AF, 3) the ARM is measured and subsequently demagnetized by a peak 160mT AF, and 4) The procedure is repeated for the remaining directions (the measurement scheme is shown in the description for AMS measurements; Figure 5.1a) for a solution of the anisotropy tensor (Borradaile and Stupavsky, 1995; Nye, 1957).

5.5 Magnetic hysteresis

Magnetic hysteresis was performed using a Princeton measurements Micromag 2900 with capable saturation field to 1.4T. From hysteresis, a large amount of data is collected in a comparatively short amount of time, which makes this an efficient tool for analyzing rock magnetic properties. A hysteresis loop consists of the magnetization plotted against the applied field (Figure 5.4). Initially the field is continuously increased in the forward direction to a maximum saturating positive field, theoretically at which point all magnetic moments are parallel to the applied field. Saturation in the forward direction is followed by a reversal of the applied field in the opposite (negative) direction, bringing the applied field through zero on the vertical axis to saturation in the negative field direction. Consequently, at this stage in the loop, all magnetic moments are now parallel to the opposite field direction. The field is again applied in the forward direction through zero on the vertical axis to saturation in the positive field direction. Finally, the field is reduced to zero, thus completing a full loop (Figure 5.4b). Saturation magnetization (M_s), saturation remanence magnetization (M_{rs}) and coercivity (H_c) is obtained from a single experimental run (Figure 5.4). Coercivity of remanence (H_{cr}) is obtained by applying backfields to a sample in increasing increments. Measurements are done in the absence of an applied field. H_{cr} corresponds to the backfield that effectively reduces M_{rs} to zero (e.g. no remanence moment remaining in the sample in the absence of an applied field). Therefore the coercivity of remanence of a specimen is always greater than its coercivity.

A slope correction is necessary in order to remove the paramagnetic contribution. Figure 5.4b shows a regular hysteresis loop with a large paramagnetic moment that does not saturate

with application of 1T (the maximum field used in our study). Figure 5.4c displays a sample with the corrected loop, and illustrates the characteristic saturation magnetization plateau of ferromagnetic materials. Notice that the magnetization is substantially reduced due to the removal of the paramagnetic component. Rarely, the loop can display a negative slope at saturation fields because of the dominant presence of minerals that solely possess a diamagnetic response to an applied magnetic field (e.g. quartz and calcite). This is not common, since the paramagnetic moment significantly outweighs the diamagnetic moment.
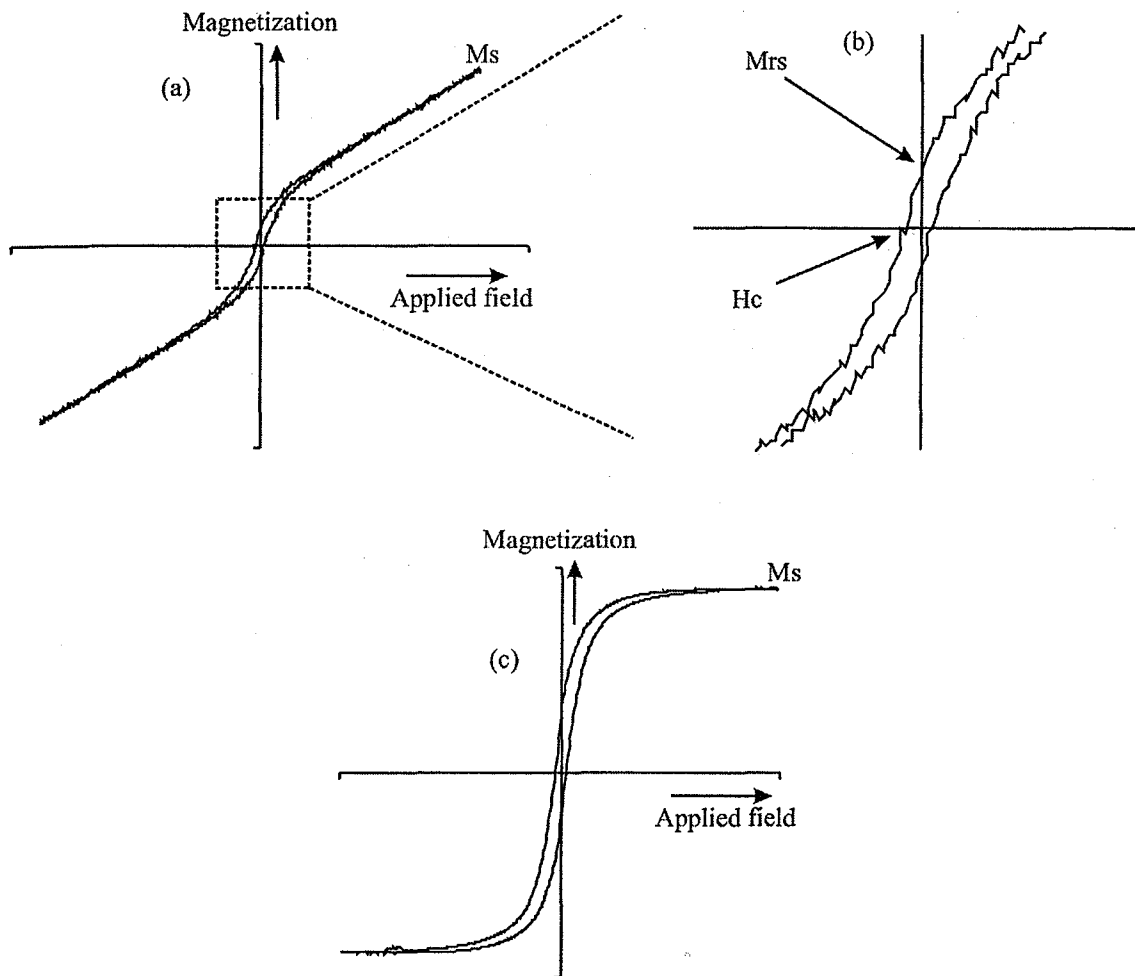
Figure 5.4 (a) Hysteresis loop showing the directions of the applied field and the corresponding magnetization. M_s is the saturation magnetization displayed by the loop at the greatest applied field. (b) Close-up of the center of the hysteresis loop, showing saturation remanent magnetization (M_{rs}) and coercivity (H_c). (c) The hysteresis loop after paramagnetic slope correction.

Chapter 6 Results and discussion of rock magnetic experiments

In this chapter the results from rock magnetic experiments of Strawberry Creek sediments are shown and discussed. Section 6.1 details the magnetic fabric determined using anisotropy of magnetic susceptibility (AMS) and anisotropy of anhysteretic remanent magnetization (AARM). Experiments involving IRM, partial ARM (pARM) and 3-axis induced IRM's are discussed in section 6.2. Section 6.3 deals with results from hysteresis experiments. Sections 6.4 and 6.5 concern low temperature and high temperature experiments respectively.

6.1 The magnetic fabric of the sediments from Strawberry Creek

6.1.1 Results and interpretation of AMS measurements

The sediments contain an oblate magnetic fabric as is illustrated in Figure 6.1, with its maximum principal axis (and magnetic foliation) close to the horizontal plane and the minimum principal axis through the vertical plane. Clay minerals clearly influence the magnetic fabric, and the red clays have a more eccentric oblate fabric (P_j>1.20) than the silts (P_j<1.10), as is illustrated by the modified Jelinek plot. The eccentricity or degree of anisotropy of the fabric in the rhythmic sediments is similar to that of a metamorphosed slate (Borradaile and Jackson, 2004). Ising (1942) originally discovered that magnetic fabrics of clay could have a similar degree of anisotropy as metamorphosed slate. The fabric displays maximum susceptibility along a SE-NW axis, which is a probable indicator of a grain-aligning paleo-current flow. It is notable that this alignment axis coincides with the slight dip of the bedding plane, a few degrees towards the E-SE. Frequency histograms of the bulk susceptibility from the Strawberry Creek specimen show a bimodal distribution with peaks at ~500 μSI and ~3400 μSI (Figure 6.2a); the bimodal distribution illustrates that the silts have higher bulk k than the clays. The mean bulk k of all specimens is 715 μSI with a standard error of 95 μSI. Figure 6.2b show the bulk susceptibility (k) with the x-axis on a base 10 logarithmic scale. In the case of the red clays, AMS is probably particularly indicative of the clay mineral fabric, as a consequence of both the weak magnetic remanence of the clays and the high concentration of paramagnetic clay minerals. In contrast, silts are probably dominated by diamagnetic calcite, which is greatly outweighed by the ferromagnetic susceptibility of magnetite. The differences of susceptibilities in clays and silts are readily observed by the bimodal distribution in the susceptibility histogram (Figure 6.2).
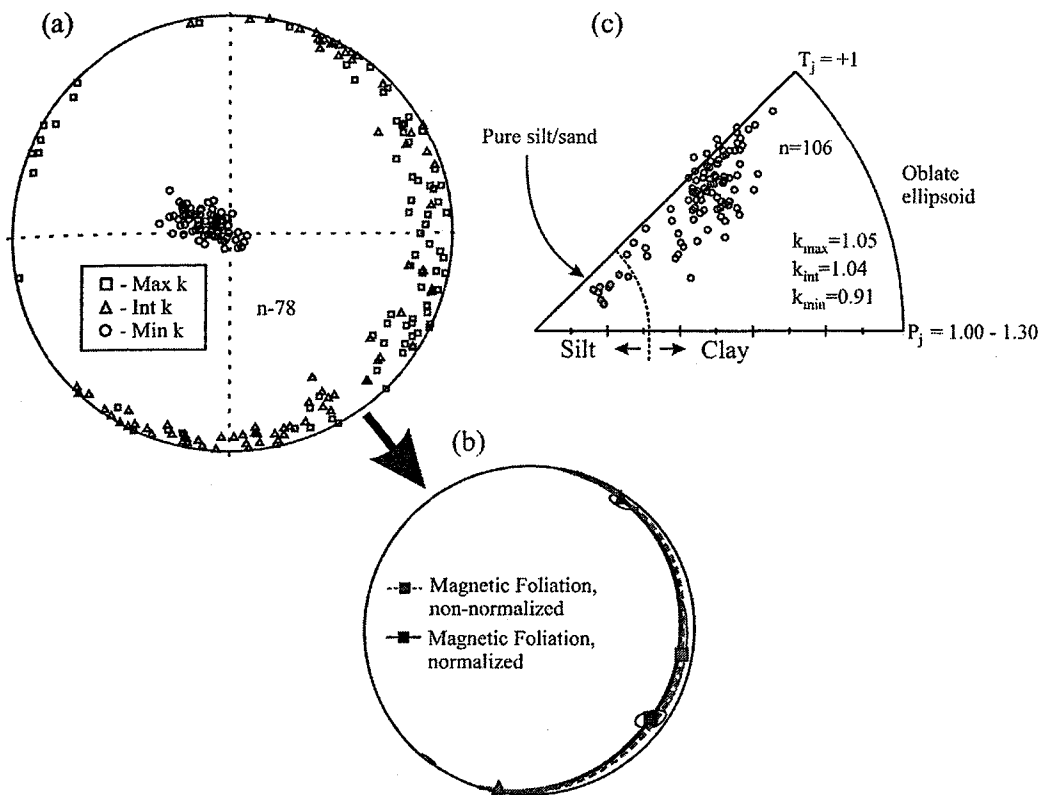
Figure 6.1 Anisotropy of magnetic susceptibility for the Strawberry Creek specimens. In (a) k_{max}, k_{int} and k_{min} are plotted on a equal-area stereonet. Minimum susceptibility is oriented perpendicular to the bedding plane (in the vertical axis), while intermediate and maximum directions are located in the bedding plane of the sediments; (b) show the directions of non-normalized and normalized average directions of k_{max} and k_{int}, which together define the plane of magnetic foliation; in (c) a modified Jelinek diagram (Borradaile and Jackson, 2004) is used to illustrate the shape ellipsoid of the magnetic susceptibility. T_j represents the shape of the ellipsoid, with positive values indicating an oblate fabric while negative values have a prolate fabric; P_j is the eccentricity of the fabric. Note a clear oblate fabric with greater eccentricity of the red clay than in the grey silts.

6.1.2 Results and interpretation of AARM measurements

Anisotropy of anhysteretic remanent magnetism (AARM) is used to understand the fabric among the magnetic minerals as the method isolates the ferromagnetic component; measurements of ARM are performed in the absence of an applied field as compared to AMS, which is measured in the presence of an applied field (see Chapter 5, section 5.2). AARM measurements in seven different directions (measurement scheme devised by Borradaile and Stupavsky, 1995; see Figure 5.1) reveal that there is preference for sub-horizontal alignment of the magnetic minerals in some Strawberry Creek clay samples (Fig. 6.3). ARM's imparted in orthogonal directions are deflected slightly to the left in the stereonet, although it is not clear whether field refraction or shallower inclination occurs from these measurements. ARM's applied at a bout 35°

angles illustrate field refraction in the sediments as the magnetization depart towards the horizontal plane from the applied field. Interestingly, applied ARMs are deflected towards the left in the stereonet, which could probably be explained by a slight dip of the bedding plane. The magnetic foliation (determined from AMS measurements) illustrates this offset from the X-Y plane (horizontal) and is consistent with a slight dip to the E-SE which was also observed in the field (Figure 6.2). It is likely that field refraction occurs as a consequence of near horizontal clay particles deflecting the field, as well as the preference for sub-horizontal alignment of hematite (e.g. flakes of hematite maintain their magnetic moment perpendicular to their c-axis). Shape anisotropy in magnetite, i.e. oblate or prolate grains with their long-axes preferentially aligned towards the horizontal plane, would also impact refraction of remanence in the sediments. In contrast, there is no hematite present in the silts but there is still deflection of the remanence at 45° inclination, although not as significant. Larger grain-size particles, than in the clay, are also compacted and oriented preferably with their long axes in the horizontal plane, which is most likely the explanation for refraction of the remanence in the silts.
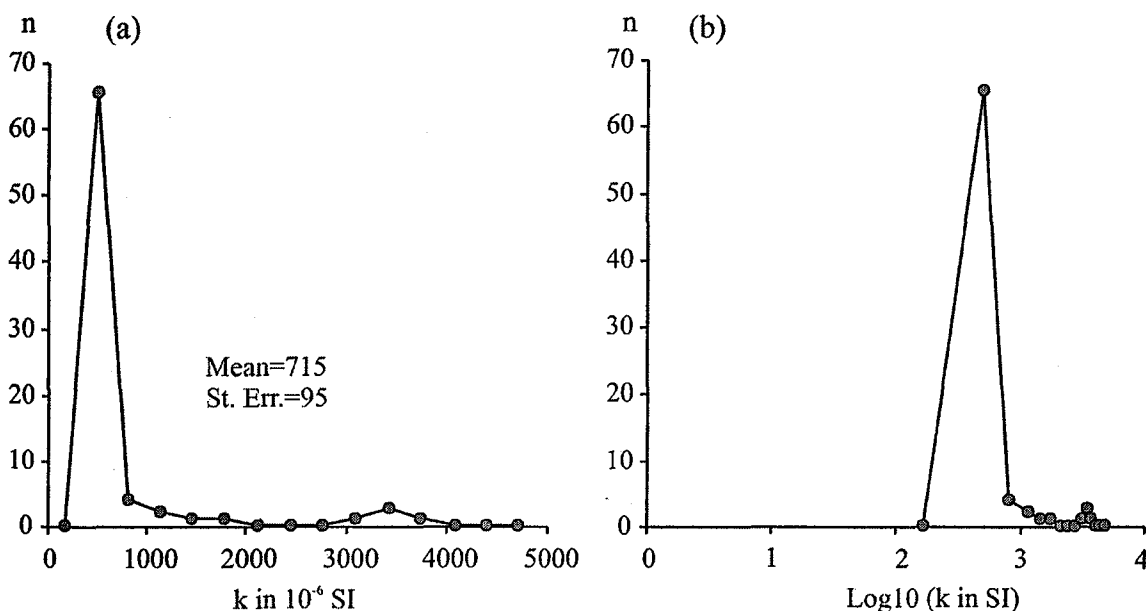
Figure 6.2 (a) Bulk susceptibility frequency histogram of the Strawberry Creek sediments. The mean susceptibility = 715×10^{-6} SI, standard error of the mean = 95×10^{-6} SI. (b) Illustrates the same results as in (a) but with k (x-axis) on a Log 10 scale.

The orientation of the applied ARM and its intensity of anisotropic remanence have some interesting properties (Table 6.1). The intensities of ARM in the clays are greatest in the horizontal plane (x, y), with minimum intensity along the vertical axis and intermediate intensities when inclination of the applied field is intermediate between the vertical and

horizontal (α=35.26°). This is contrasted in the silt-dominated specimens, where maximum intensity of ARM is found to lie in the vertical axis (*/90 = 766.32μSI) and when the specimens are oriented at the angle 225/35 (decl/incl; intensity = 841.51μSI). The explanation for this phenomenon must be that grains of magnetite in the silt are oriented with their long axes or magneto-crystalline anisotropy sub-parallel to the vertical axis and alignment of grains closer to the inclination of the Earth's magnetic field, while the opposite is true for hematite and magnetite in clay (where the magnetic moment preferentially lies sub-parallel to the horizontal plane). Consequently, this would have a significant impact on the original NRM of the sediments, leading to shallower inclination in the clays.
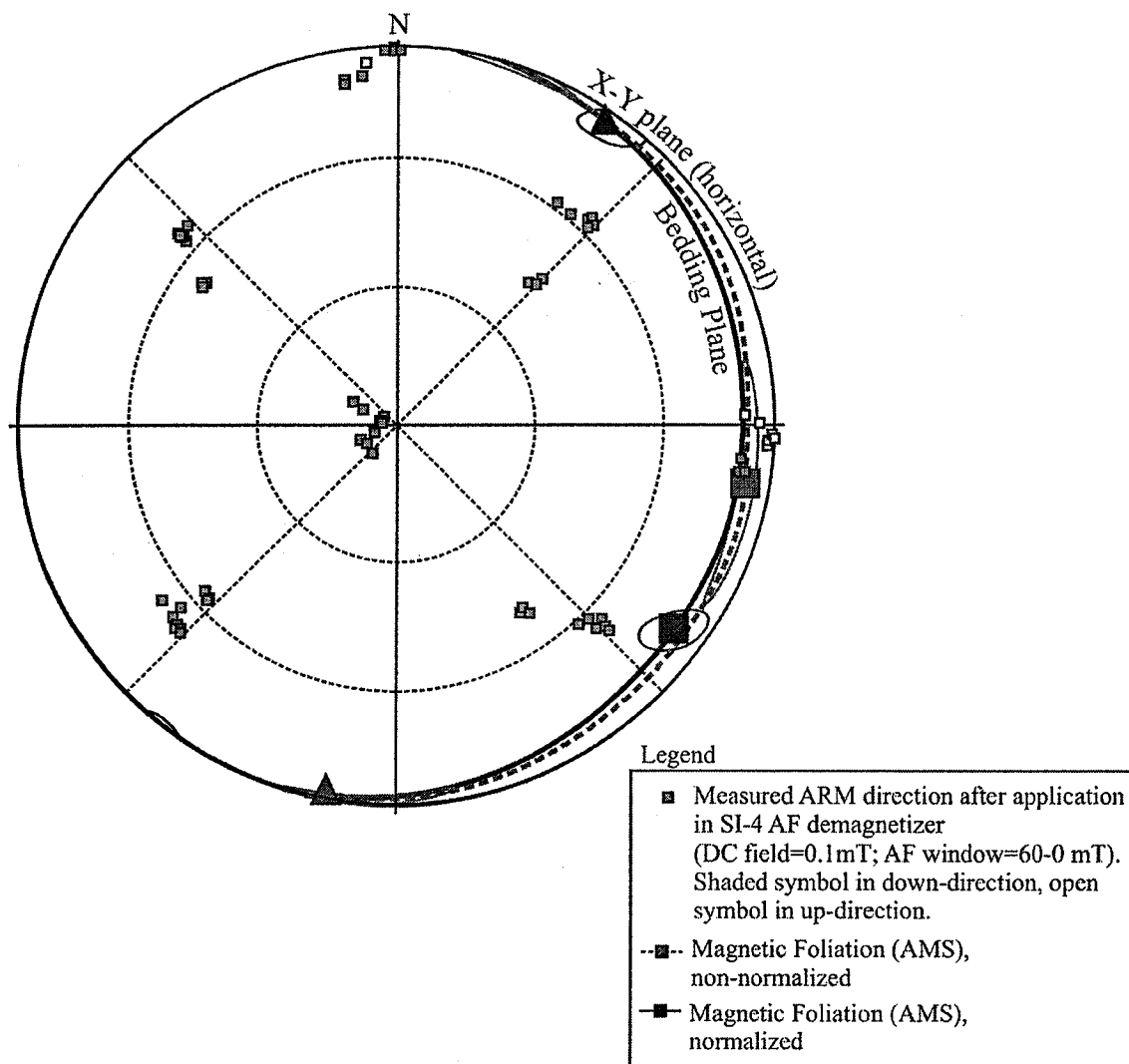
Figure 6.3 Stereonet showing results from ARM's induced in seven different directions (Borradaile and Stupavsky, 1995); ARM's measured in three orthogonal directions four body diagonals. Anisotropy of the magnetic particles is evident as ARM's are deflected (especially in the case of body diagonals) towards the horizontal or bedding plane.

The grains of magnetite in the silt might not have experienced the effect of compaction and post-depositional rotation to the same extent as the clay. Alternatively, the magnetite is not dominated by shape anisotropy of the grains (e.g. grains are more euhedral than elongate). Because the easy axis of magnetization in hematite is oriented perpendicular to the c-axis the magnetocrystalline anisotropy of hematite may be important in the clays, contributing to the shallow inclination of the red clays.

Further evidence for anisotropy of magnetic remanence is illustrated in Figure 6.4 and Table 6.2. ARM's applied in the horizontal plane (x-axis) and the vertical plane (z-axis) are markedly different as their ratio is not close to unity (Figure 6.4). The ratio of ARM_X/ARM_Z is greater than 1.2 which suggests the preferential alignment of magnetic moments (grain long-axes or magnetocrystalline anisotropy) parallel or nearly parallel with the horizontal plane. Table 6.2 lists values of ARM_X and ARM_Z through the stratigraphic column. It is notable that the ratio of ARM_X/ARM_Z approaches unity as the silt content increases. Unlike the results in Table 6.1 however, no specimens show ratios that are less than one. The ratio increase in the clays is likely due to the preferential compaction of clay compared to the lesser compaction of silt, resulting in the increase. However, hematites coating the clay particles or possible oxidation of clay particles to hematite are also possibilities for explaining the greater ARM anisotropy of the clay. The mean of ARM_X is 248.18±132.58 mA/m, while the mean of ARM_Z is 164.69±93.48 mA/m. The standard error of mean $(\sigma/[n]^{1/2})$ for ARM_X = 15.62 mA/m and for ARM_Z = 11.02 mA/m. The mean ratio of ARM_X/ARM_Z indicates that a horizontal magnetization of the sediments outweighs a vertical magnetization by approximately 1.5 (Table 6.2). However, since the remanence anisotropy is dependent on lithology, the distribution of ARM_X/ARM_Z may be bimodal, although this is not clearly illustrated in a frequency distribution which shows a single mode (Figure 6.5), perhaps because samples of silt are underrepresented in the stratigraphic column.

Table 6.1 AARM measurements (x, y and z axes)

Specimen	lithology	ARM(X+Y)/2 (mT)	ARM(Z) (mT)	ARMh/ARMz
Sc203	Silt	675.7	785.1	0.86
Sc204	Silt	667.3	765.5	0.87
Sc205	Silt	637.9	748.3	0.85
Sc30504b	Clay	217.0	147.0	1.48
Sc30505a	Clay	208.6	144.0	1.45
Sc30505b	Clay	215.2	147.1	1.46
Sc30506a	Clay	246.4	168.4	1.46
Sc30506c	Clay	286.4	198.3	1.44
Sc30510a	Clay+silt	497.3	391.7	1.27
Sc30510b	Clay+silt	680.5	525.1	1.30

ARMh=ARM(X+Y)/2
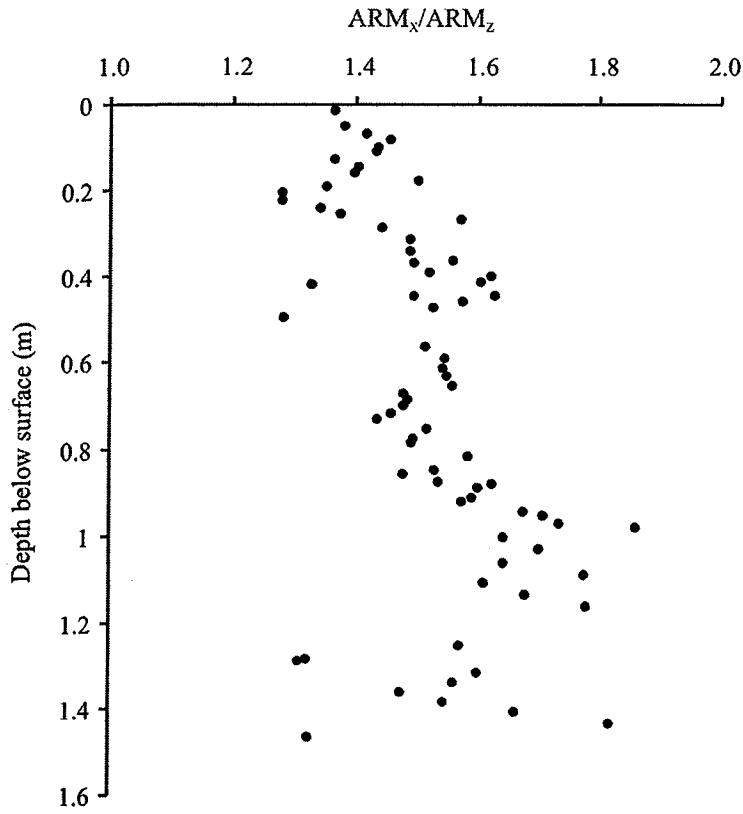
Figure 6.4 The ratio of ARM's applied in the horizontal plane (x-axis) and the vertical plane (z-axis) are presented against stratigraphic depth (depth below surface in meters). The details of the ARM's are given in Table 6.2.
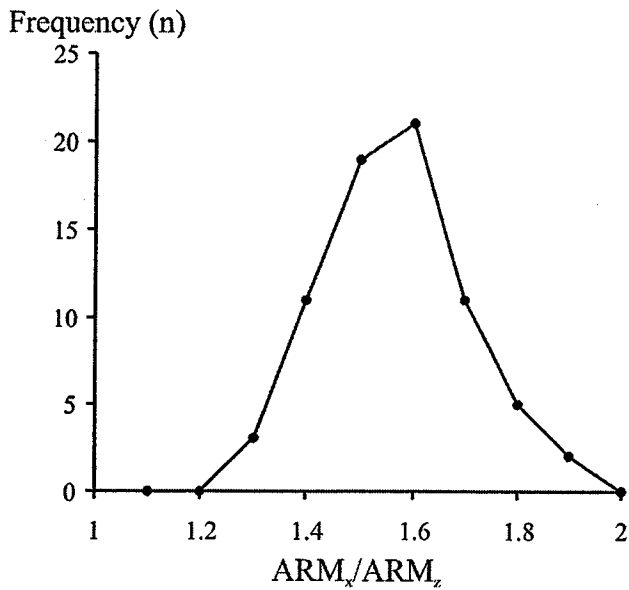
Figure 6.5 Frequency distribution for samples used to determine the ratio ARM_X/ARM_Z.

Table 6.2. ARM$_X$ and ARM$_Z$ expressed with depth and lithology.

Specimen	lithology	Depth below surface (m)	Int x* (mA/m)	Int z** (mA/m)	Ratio x/z
SC001A	clay	0.013	199.32	146.33	1.36
SC003A	clay	0.051	190.48	137.94	1.38
SC004A	clay	0.07	190.07	134.28	1.42
SC005A	clay	0.081	150.23	103.23	1.46
SC006A	clay	0.098	190.00	132.26	1.44
SC007A	clay	0.111	183.68	128.17	1.43
SC008A	clay	0.129	180.36	132.32	1.36
SC009A	clay	0.143	174.36	124.17	1.40
SC010A	clay	0.159	179.41	128.47	1.40
SC011A	clay	0.179	178.36	118.80	1.50
SC012A	clay	0.192	198.08	146.55	1.35
SC013A	clay	0.206	190.00	148.45	1.28
SC014A	clay	0.224	182.82	142.91	1.28
SC015A	clay	0.238	193.32	144.21	1.34
SC016A	clay	0.253	198.62	144.63	1.37
SC017A	clay	0.267	198.82	126.39	1.57
SC018A	clay	0.285	202.67	140.72	1.44
SC019A	clay	0.311	192.65	129.58	1.49
SC020A	clay	0.338	187.90	126.49	1.49
SC021A	clay	0.364	192.31	123.48	1.56
SC022A	clay	0.397	197.44	121.99	1.62
SC023A	clay	0.413	204.52	127.56	1.60
SC024A	clay	0.443	210.66	140.99	1.49
SC025A	clay	0.471	193.44	126.89	1.52
SC026A	clay	0.495	180.70	140.84	1.28
SC027A	clay	0.369	200.41	134.23	1.49
SC028A	clay	0.392	193.03	127.17	1.52
SC029A	clay	0.416	191.55	144.26	1.33
SC030A	clay	0.442	187.24	115.18	1.63
SC031A	clay	0.457	191.89	121.79	1.58
SC032A	clay	0.564	203.25	134.45	1.51
SC033A	clay	0.59	193.09	124.85	1.55
SC034A	clay	0.614	188.10	122.10	1.54
SC035A	clay	0.629	200.72	129.59	1.55
SC036A	clay	0.652	183.60	117.88	1.56
SC037A	clay	0.673	201.28	136.14	1.48
SC038A	clay	0.684	206.48	139.25	1.48
SC039A	clay	0.697	201.72	136.42	1.48
SC040A	clay	0.716	198.91	136.55	1.46
SC041A	clay	0.732	206.36	143.73	1.44
SC042A	clay	0.752	196.16	129.33	1.52
SC043A	clay	0.773	201.37	134.75	1.49
SC044A	clay	0.786	208.45	139.88	1.49
SC045A	clay	0.814	201.18	126.95	1.58
SC046A	clay	0.846	225.54	147.49	1.53
SC047A	clay	0.88	220.10	135.70	1.62
SC048A	clay	0.912	222.56	139.78	1.59

SC049A	clay	0.953	216.95	126.95	1.71
SC050A	clay	0.981	227.20	122.09	1.86
SC051A	clay	0.856	220.35	149.04	1.48
SC052A	clay	0.873	224.12	145.85	1.54
SC053A	clay	0.89	238.59	149.15	1.60
SC054A	clay	0.921	225.63	143.24	1.58
SC055A	clay	0.945	216.04	128.90	1.68
SC056A	clay	0.971	235.69	135.84	1.73
SC057A	clay	1	226.21	137.73	1.64
SC058A	clay	1.027	223.65	131.53	1.70
SC059A	clay	1.062	237.07	144.18	1.64
SC060A	micro-rhythmite	1.09	244.87	137.95	1.78
SC061A	micro-rhythmite	1.105	199.55	123.87	1.61
SC062A	micro-rhythmite	1.135	236.86	140.97	1.68
SC063A	clay	1.159	199.00	111.88	1.78
SC069A	clay	1.253	379.70	241.59	1.57
SC070A	silt	1.281	727.72	550.34	1.32
SC071A	silt	1.289	665.04	508.04	1.31
SC072A	mixed clay/silt	1.313	364.78	227.70	1.60
SC073A	mixed clay/silt	1.339	447.24	286.29	1.56
SC074A	mixed clay/silt	1.36	456.23	309.83	1.47
SC075A	mixed clay/silt	1.381	425.07	275.31	1.54
SC076A	mixed clay/silt	1.405	333.85	200.82	1.66
SC077A	mixed clay/silt	1.432	798.46	439.02	1.82
SC078A	silt	1.462	735.64	554.73	1.33
mean			248.18	164.69	1.52
st. dev.			132.58	93.48	0.13
st.error			15.62	11.02	0.02

Note: Specification of the applied ARM
Peak alternating field = 100mT
window alternating field = 60 - 0.1 mT
Direct current field = 0.1mT

* x-axis: horizontal plane
** z-axis: vertical plane

6.2 Rock magnetic mineralogy in the Strawberry Creek sediments

6.2.1 Incremental IRM acquisition and decay

Figure 6.6(a, b) shows incremental acquisition of IRM to a saturating field of 1T, for the silt and clay portions of the glaciolacustrine section. Saturation was almost certainly achieved in the silts as is shown by the plateau developed at higher fields in Figure 6.6b. The pattern of remanence acquisition is significantly different in the clay, and complete saturation is not achieved at 1T. Remanence is more than an order of magnitude higher in the silt than in the clay (133.0A/m and 6.8A/m respectively). The slope of the acquired remanence is shallower in the clay demonstrating the presence of minerals with high coercivity, while the silt saturates in fields of ≤300mT.

Cross-over plots for magnetite and hematite, based on incremental acquisition and demagnetization curves such as shown in Figure 6.7, are useful for identification of magnetic mineralogy since their coercivities are dependent not only on the kind of ferromagnetic mineral but also on their domain size and structure. Reference curves for different mineral phases and domain sizes have been developed based on research of IRM magnetization and demagnetization,
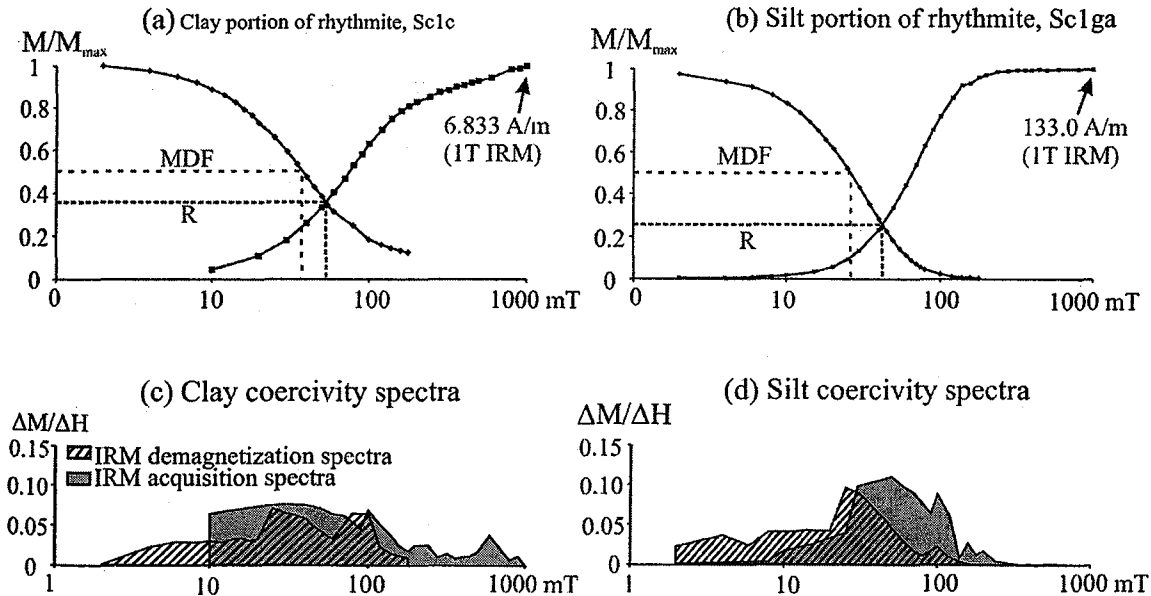
Figure 6.6 Incremental IRM acquisition and demagnetization diagrams for (a) red clay and (b) grey silt; magnetization is indicated against the particular field strength of either the magnetizing DC-field or demagnetizing AF. Incremental acquisition of IRM was applied to 1.2T maximum field, while the highest AF achieved was 180mT. The median destructive field (MDF) and the cross-over value (R) between the DC acquisition curve and AF demagnetization curve are indicated. In (c) and (d) the magnetization (shaded) and demagnetization (hatched) spectra are shown for clay and silt, respectively.

particularly the seminal work of David Dunlop (Dunlop and Özdemir, 1997; Dunlop, 1986; Fuller et al., 1988; Cisowski, 1981). Symons and Cioppa (2000) provided useful reference curves (fields) for acquisition and demagnetization of magnetite and hematite, and their different domain sizes (shaded areas in Figure 6.7a, b). Symons and Cioppa (2000) used a saturating field of 900mT which is relatively close to 1T, which was used for the clays and silts from Strawberry Creek.

For the silts it is possible to identify that the IRM magnetization and AF demagnetization curves clearly lie within the SD field for magnetite (Figure 6.7a, b). Clays are complicated due to their high coercivity during acquisition and demagnetization of the IRM. The curves for clay in Figure 6.6a and b overlap different domain sizes of magnetite (PSD, SD) and approach the reference fields for hematite at higher applied IRM's and AF's. The red colouration, together with the high coercivity of the ferromagnetic minerals in the clays suggests the presence of hematite. The acquisition and demagnetization curves for the clay also indicate the presence of PSD and SD magnetite. Without thermal experiments (i.e. thermal demagnetization or Curie balance), it is not possible to rule out the additional presence of goethite as a high coercivity component, although an attempt to discern the presence of goethite in the sediments is described later in this chapter (section 6.5). The crossover method for identification of magnetic mineralogy does not readily separate hematite and goethite for IRM magnetization and AF demagnetization because both these minerals have high coercivities; only identification of a high coercivity mineral is possible. It is not possible to achieve the high fields needed to completely magnetize or demagnetize samples containing these high coercivity minerals. The incremental IRM applied to the clay displaces the acquisition curve towards the right (compared to the silts) and indicates the presence of a higher coercivity mineral than magnetite (Figure 6.6a, clay). A displacement towards higher coercivities is true for AF demagnetization as well (Figure 6.6b).
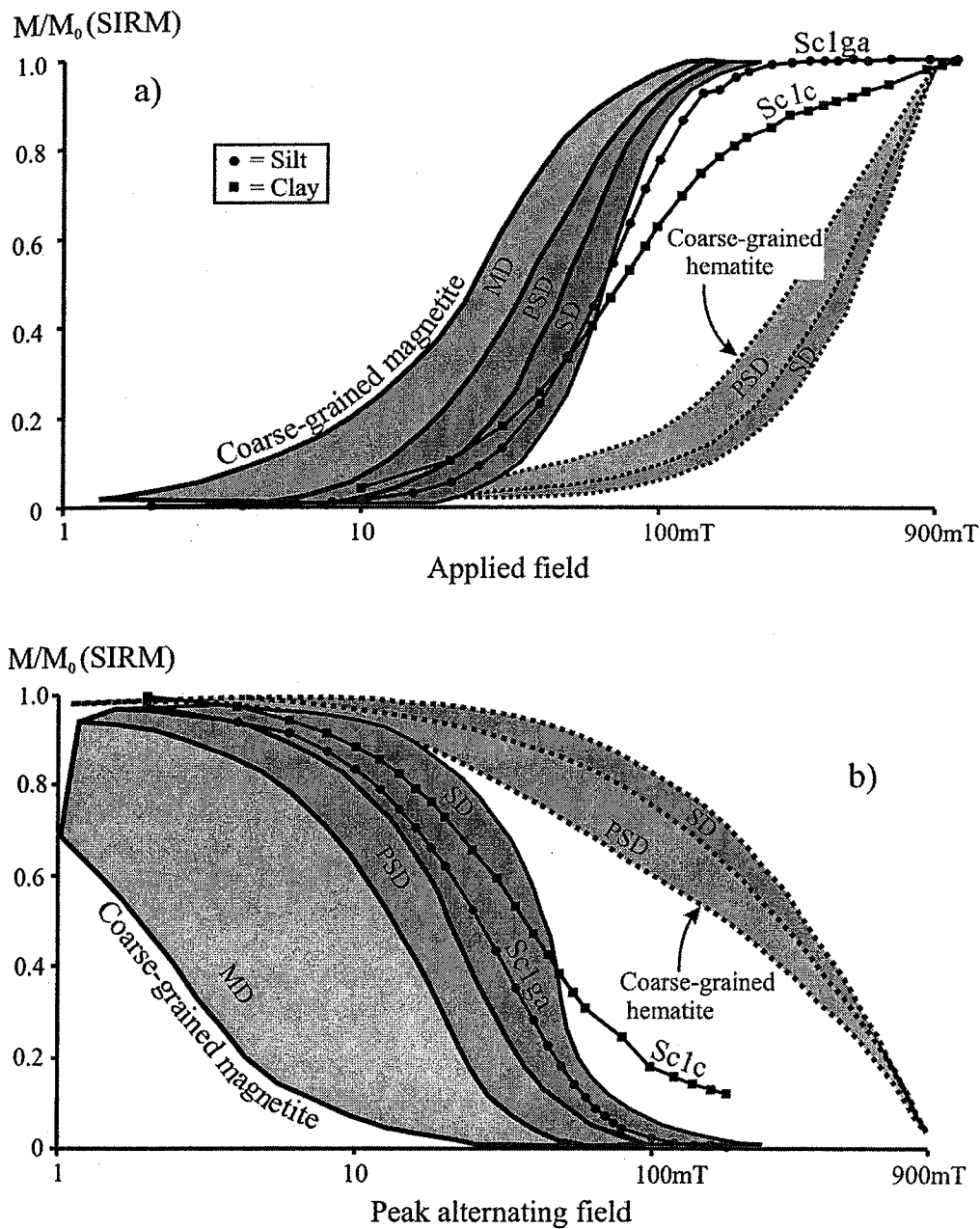
Figure 6.7 IRM acquisition (a) and AF demagnetization (b) curves for clay and silt samples with background reference fields for different domain sizes of magnetite and hematite (from Symons and Cioppa, 2000). Background fields with closed borders refer to magnetite, while fields with open, dotted borders represent hematite. Note that magnetization is normalized in the diagrams (M/M$_0$). In the silts magnetite dominates the magnetic signal whereas magnetite and hematite are both significant contributors to the remanence in the clay.

6.2.2 ARM acquisition and decay

The crossover plot is also useful in illustrating acquisition of incremental ARM, when using a flexible AF window. This is shown in Figure 6.8(a, b), for ARM acquired in a clay and a silt from the rhythmic portion of the section. ARM is gradually acquired as the AF window increases in intensity (from 5 – 160mT). The background DC-field was held constant at 0.1mT. The contrast of ARM acquisition in the clay versus silt is not as pronounced as in the experiments with IRM, but there are some notable differences. The acquired remanence over a window of 160mT is significantly higher in the silt (584.9mA/m) than in the clay (177.7mA/m; Fig. 6.8). The crossover value is slightly lower in the silt, and in both graphs the R-value is close to 0.4. However, whether the crossover value in ARM acquisition and decay implies significant interaction of the magnetic constituent in the samples is not as clear as with IRM acquisition (Cisowski, 1981). It is unlikely that a contribution from high coercivity hematite influences the intensity of the acquired ARM in the clay, since the highest applied AF is 160mT (much lower than hematite's coercivity). It is more likely that the intensities of the ARMs are due almost exclusively to magnetite. From the intensities stated above this means that silt contains by volume more magnetite than the clay, or grain-sizes are different in the two sediments (e.g. coarser grained silt contains more MD magnetite than finer grained hematite). ARM is a sensitive indicator of the magnetic moments of finer grained particles, whereas IRM (or sIRM) activates moments from a larger range of grain sizes (0.04 - 400μm; Evans and Heller, 2003). Comparing the ratios of ARM/sIRM(1T) for clay and silt therefore provides an indicator of grain-size in the sediments. For the clay ARM/sIRM = 0.026 (based on the values presented in Figures 6.3 and 6.8), while for the silt ARM/sIRM = 0.0044, which leads to the conclusion that the red clays contain finer ferromagnetic grain-sizes than the silts. It should be noted that a sIRM may influence the magnetic moments of both hematite and magnetite, while an ARM (with AF window = 160mT, DC = 0.1mT) will likely not affect moments of hematite. Nevertheless, a comparison of ARM/sIRM in the clays and silts demonstrates a clear difference in grain sizes since the saturation remanence of magnetite (480kA/m) is vastly greater than that of hematite (~2.5kA/m).

The benefit of gradually increasing the width of the AF window is acquisition of partial ARM. An ARM that is acquired over different coercivity intervals activates magnetic moments in grains of specific coercivities. As the AF window is widened, more coercive minerals are included in the ARM. Figure 6.8(a, b) illustrates this by calculating the spectrum of acquired remanence between successive ARM applications, with progressively wider AF windows (shaded gray and hachured area of Figure 6.8). Noticeably, the same magnetic moments are not activated

at the same AF field strengths during acquisition and demagnetization. In both silt and clay, acquisition of ARM is observed from the complete spectrum of the AF's, from 5-160mT, while demagnetization is more constricted and tends to have peak values around 40mT AF. It is clear though, that most ARM is acquired at an AF window <80mT in clay, and <120mT for the silt. This means that the ARM continuously increases in intensity with wider applied AF window (up to 160mT) in both the clay and the silt. The same magnetic moments are easily demagnetized and reach a stable plateau at rather low AF's (~100mT). An explanation for this behavior could be

(a) Clay portion of rhythmite, Sc05009

M/M_{max} (ARM)

M_{max} = 177.7 mA/m

ARM demagnetization spectra
ARM acquisition spectra

(b) Silt portion of rhythmite, Sc05004

M/M_{max} (ARM)

M_{max} = 584.9 mA/m

Hard remanence aligned in opposite direction, which leads to initial demagnetization

ARM demagnetization spectra
ARM acquisition spectra
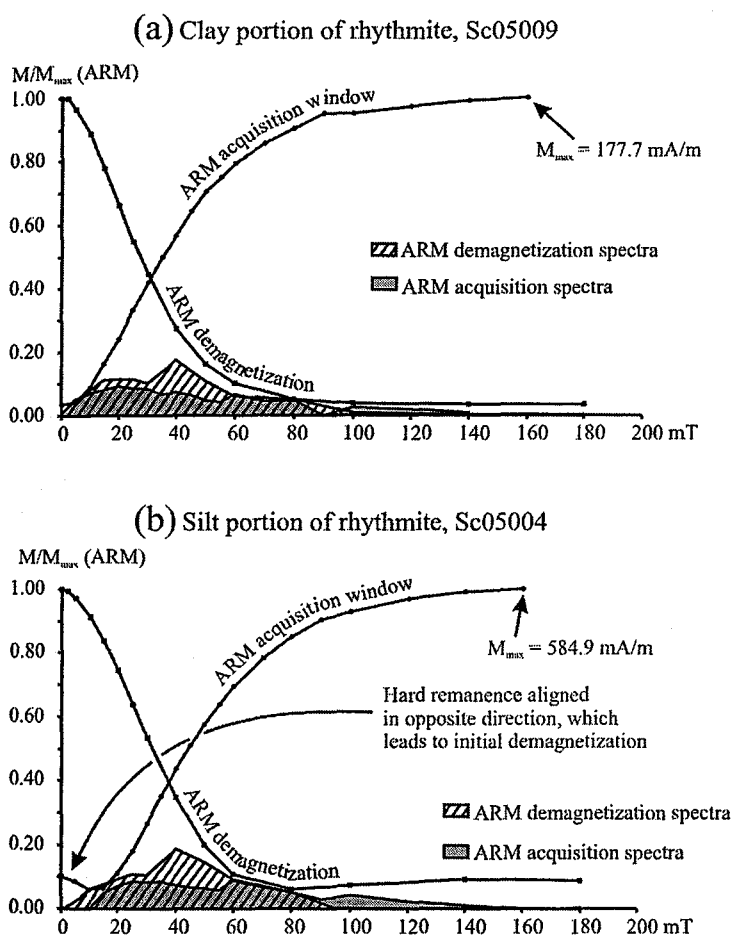
Figure 6. 8 Incremental ARM acquisitions for (a) clay and (b) silt. The applied AF is 160mT, with a background DC-field of 0.1mT. The ARM window (the portion of the AF where the DC-field is applied) is flexible and increased in increments from initially 5 - 0mT to a final 160 - 0mT. Acquisition and demagnetization spectra are shown for the (a) clay and (b) silt. Note the initial demagnetization during acquisition in the silt, which stems from an oppositely aligned remanence which was not successfully removed during AF cleaning to 180mT before ARM acquisition was performed.

interaction of magnetic moments such that continuous magnetization occurs with wider AF windows, perhaps from MD or PSD magnetite.

6.2.3 Orthogonal three-axis test

The effectiveness of the orthogonal 3-axis test to separate components of coercivity in samples is illustrated in Figure 6.9. Nine specimens (Figure 6.9b-j) have been given non-overlapping artificial IRM's in three orthogonal directions (fields corresponding to <10mT, 10 – 30mT and >30mT; with the exception of Figure 6.9c, where the fields corresponded to <5mT, 5-15mT and >15mT). Eight of the specimens used for this experiment show similar characteristics during demagnetization and they constitute clays and silts originating from the Strawberry
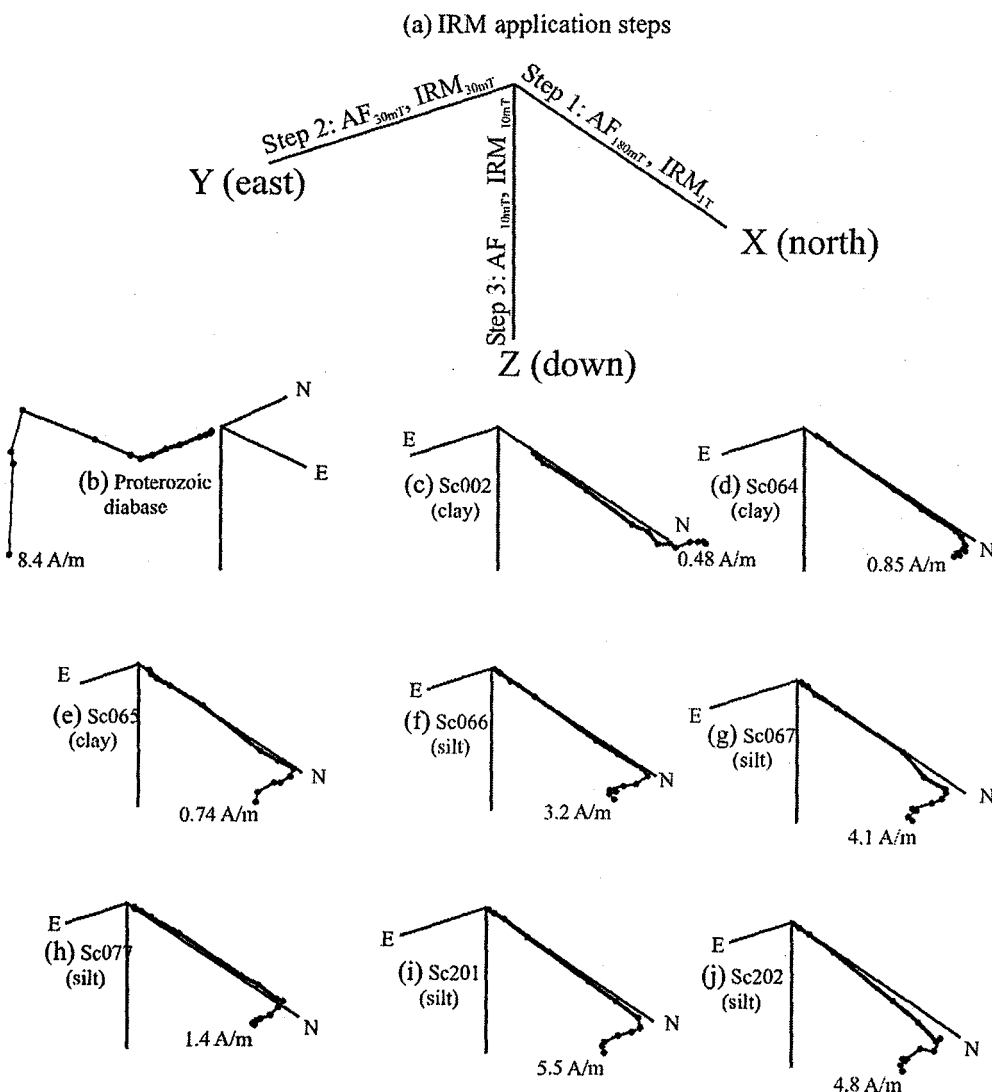
Figure 6.9 Orthogonal three-axis tests for a suite of different specimens; specimens carry artificial magnetizations of different intensities in different directions. Demagnetization is performed using an AF. The intervals of magnetization used in each direction as indicated (a), z: <10mT; y: 10 – 30mT; x: >30mT, with the exception of 6.9(c) which used intervals of, z: <5mT; y: 5 – 15mT; x: >15mT. The saturating field used in the x-direction is 1T. (c)-(e) are specimens of red clay; (f)-(i) are grey silt; (b) is a sample of Proterozoic diabase from the Thunder Bay district.

Creek glacio-lacustrine profile. For comparative purposes the orthogonal three-axis test was applied to a Proterozoic diabase near Thunder Bay (Fig. 6.9b), which greatly contrasts with the other samples, having a known magnetic mineralogy dominated by MD magnetite (Borradaile et al., 2004). The dominant ferromagnetic mineral for all specimens is magnetite, but clearly the glacio-lacustrine sediments carry multiple domain states, whereas the diabase is dominated by low coercivity MD magnetite. The Lowrie 3-axis test thus provides a powerful technique of separating and identifying what magnetic minerals are present in a sample, as well as their domain state (in the case of magnetite). Most of the remanence in the Proterozoic diabase is carried by low-coercivity magnetite, mainly MD with some PSD (>0.1μm), while in the glaciolacustrine clays and silts the majority of remanence is carried by SD magnetite, high coercivity PSD magnetite and possibly a minor constituent of hematite (based on previous experiments, as well as from hysteresis, hematite is more common in the clay). The presence and importance of hematite (or any other high coercivity phase such as goethite) is difficult to gauge from Figure 6.9, although hypothetically, a Lowrie 3-axis test using high coercivity intervals could possibly separate hematite from magnetite (e.g. using a major axis >300mT, and a minor axis ≤300mT). However, even the highest possible inducing DC (1.2T) available might not be enough to activate the hematite (or goethite which has even greater coercivity). Thus, in practice this is not possible since M_s for hematite (~2.5 kA/m) is very low and very high for magnetite (~480kA/m), and hematite is so coercive that the maximum laboratory field available (1.2T) cannot saturate it.

The red clay and the grey silt from Strawberry Creek can be distinguished using the three-axis test using different coercivity intervals in order to identify which domain-states dominate[1] (Figure 6.10). High coercivity phases dominate both the clay and the silt, as is apparent since the majority of the remanence is lost at ≥60mT. The silts are dominated by SD and coercive PSD magnetite, with a very small contribution of MD magnetite. The red clays are complicated by the addition of hematite, which masks the presence of SD and PSD magnetite. Hematite has a very high coercivity, but contributes very little to the remanent magnetization in the clay compared to magnetite. From the three-axis plots of both silts and clays it is apparent that there is a bias against MD magnetite, a consequence stemming from where the magnetite originates, and

---

[1] It is important to note that domain state is affected by internal (due to impurities or inclusions) and external stresses on a grain, the chemical composition of the grain (i.e. substitution by elements), and its shape. Magnetite grain-size is only equivalent to domain state if the grain is totally stress-free and pure (stoichiometric and inclusion free), such as for pure biogenic, hydrothermal or synthetic magnetite (Dunlop and Özdemir, 1997). The origin of grains is therefore extremely important when considering grain-size and domain state.

it is likely that both sediments contain magnetite of the same origin. The clay may contain somewhat finer grain-size than the silt.
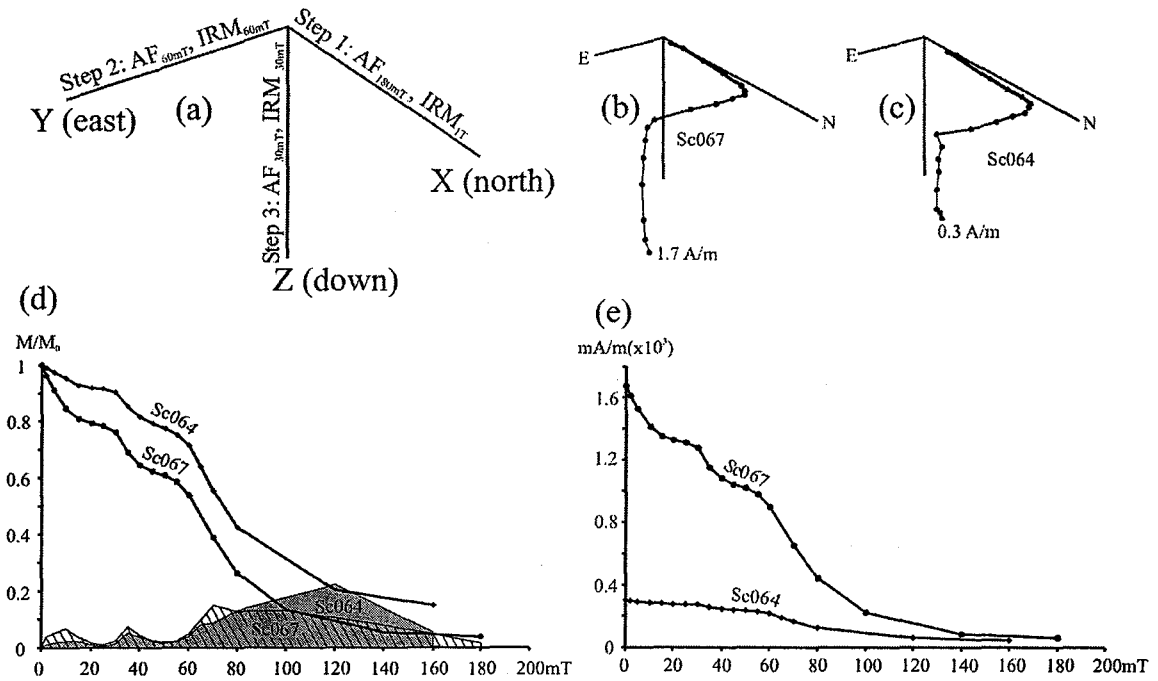
Figure 6.10 Orthogonal three-axis tests for silt (a) and clay (b), as described in Figure 6.9. The intervals of magnetization used in each direction of (a) and (b) are, z: <30mT; y: 30 – 60mT; x: >60mT. The saturating field used in the x-direction is 1T. (c) Shows the normalized intensity of the silt and clay during AF demagnetization, while (d) shows the non-normalized results. The characteristic "humps" in (d) and (e) represent demagnetization of the specific coercivity intervals.

A final orthogonal three-axis test was performed with different coercivity intervals in order to try and determine the importance of high coercivity hematite in silt and clay. The results for this experiment are shown in Figure 6.11. The experiment used two directions of induced magnetization with different coercivity intervals: the positive x-direction (chosen arbitrarily) carried an induced remanence with coercivity >120mT, whereas the positive y-direction (respective to the x-axis) carried a remanence of ≤120mT. Hypothetically, most magnetite present in the samples should achieve saturation before 120mT and therefore separate the higher coercivity minerals from magnetite (although a very small portion of magnetite may still not have achieved saturation at fields of 120mT due to magnetic properties of the magnetite). As can be seen in Figure 6.11, only a fraction of remanence remains after AF demagnetization to 120mT; less than 10% of the remanence remains in the clay after AF demagnetization, whereas the silt

sample is indistinguishable from the origin after demagnetization. The contribution to remanent magnetization of hematite is therefore very small in the clay (<10%) and minute in the silt.
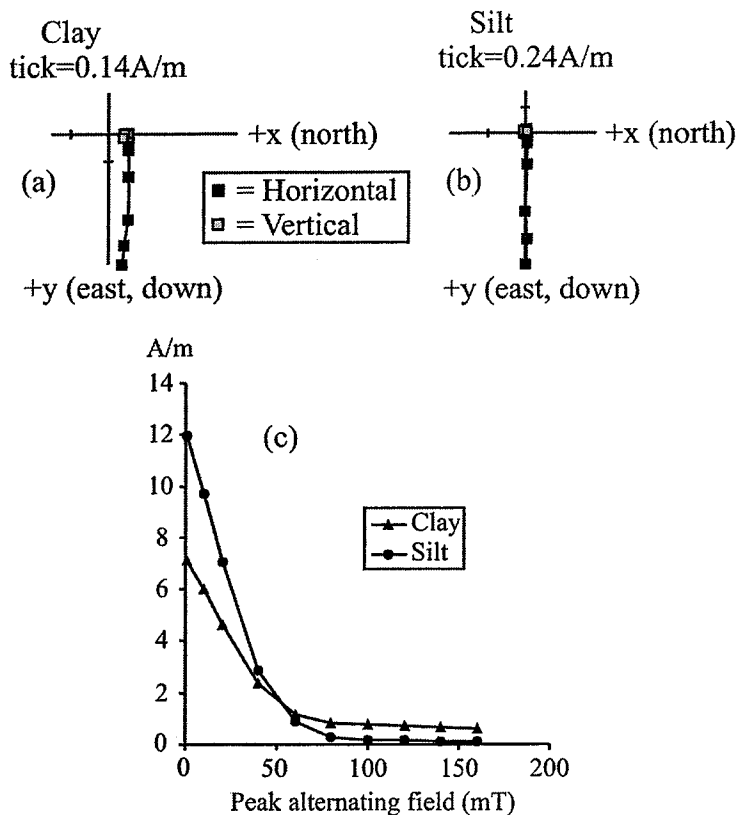
Figure 6.11 Orthogonal two-axis tests for (a) clay and (b) silt, displayed using Zijderveld plots. The intervals of magnetizations used in each direction for the samples are x: >120mT and y: ≤120mT. (c) Shows the normalized intensities for clay and silt during AF demagnetization.

6.3 Hysteresis experiments

The parameters of M_s, M_{rs}, H_c and H_{cr} (discussed in chapter 5) provide valuable information on the rock magnetic properties of a sample. These parameters can be expressed and compared in several different ways to gain an inference regarding rock magnetic mineralogy (e.g. Day et al., 1977; Dunlop, 1986 ; Tauxe et al., 1996; Pike et al., 1999; Roberts et al., 2000; Dunlop, 2002a; 2002b; Wang and Van der Voo, 2004). The result of three hysteresis loops from samples of Strawberry Creek sediments are shown in Figure 6.12 before and after the paramagnetic slope correction. Note that the red clay (Sc018a) is dominated by paramagnetic clay minerals, as the original non-corrected Ms is decreased by almost half the value prior to slope correction (5.94×10^{-8} Am^2 to 3.44×10^{-8} Am^2). Interestingly, when Sc018a has been slope corrected it shows some evidence of a "wasp-waist" (i.e. the loop pinches near the origin along the x-axis). A wasp-waist is usually an indication of the presence of more than one magnetic

phase in the specimen with very contrasting magnetic properties. Wasilewski (1973) showed in an early experiment that a mixture of hard and soft coercivity components is an overall reduction in H_c.

Prior to slope correction   After slope correction
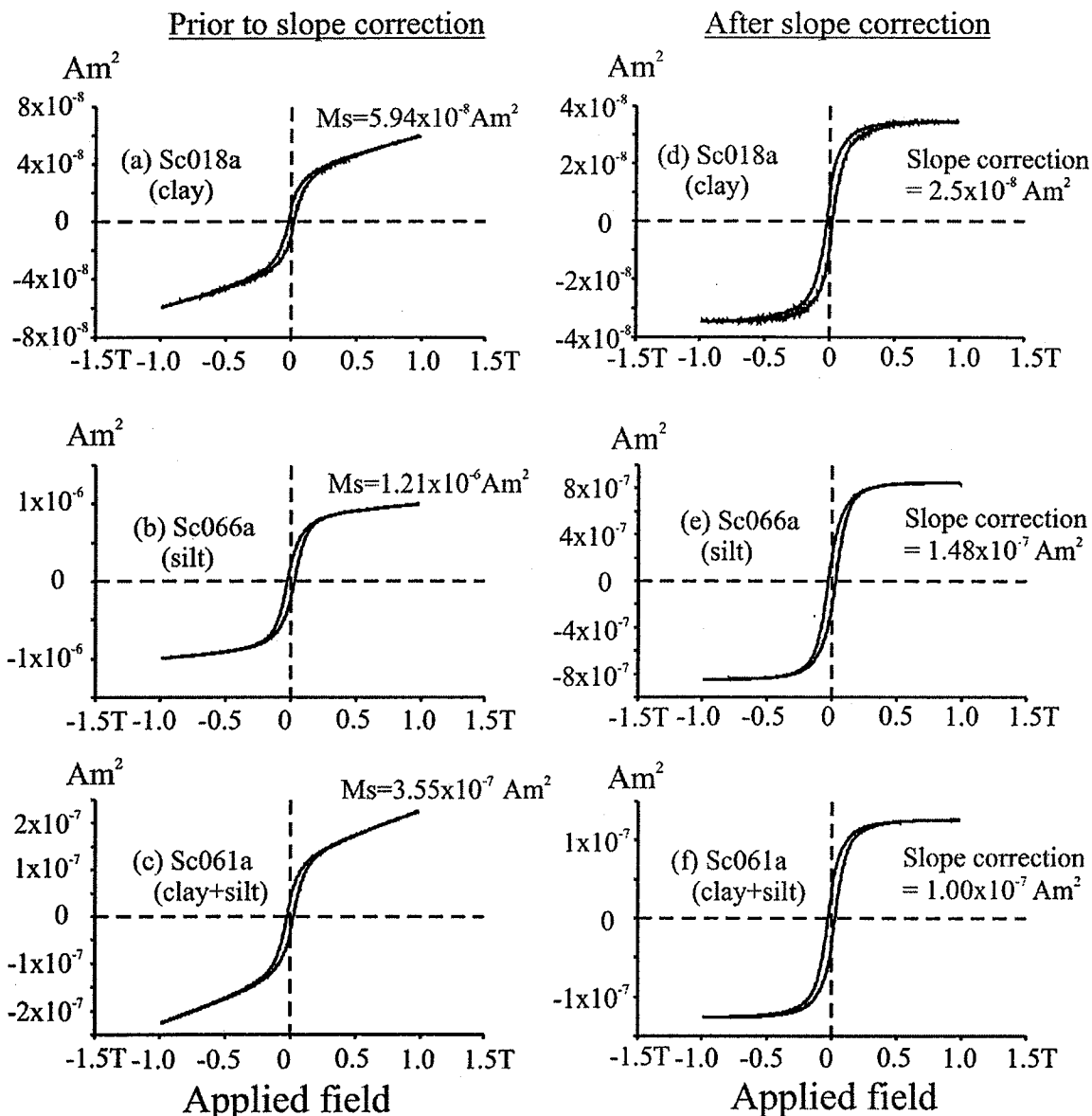
Figure 6.12 Sample hysteresis loops for (a) clay, (b) silt and (c) thinly, ~1-2mm, laminated alternating silt and clay, uncorrected for the contribution of paramagnetic and diamagnetic minerals. The same three samples are shown in (d) – (f) for hysteresis loops that have been corrected for paramagnetic and diamagnetic contributions.

The constriction at the origin occurs because H_c reflects the magnetically soft (low coercivity) component in the sample, while H_{cr} reflects the hard component (Roberts et al., 1995). In Sc018a the loop likely represents the contributions of SD, PSD magnetite (soft H_c component) and

hematite (hard H_c component). However, for this to be apparent, and displayed in a hysteresis loop, hematite needs to constitute about 100 times the volume of magnetite in the sample (Roberts et al., 1995; Dunlop and Özdemir, 1997: p. 323). The silt (Sc066a) has a substantially higher M_s than the clay, before and after slope correction, likely because of the dominance of magnetite in these specimens. About one tenth of the original non-corrected M_s is removed by slope correction (M_s changes from 1.21×10^{-6} Am^2 to 1.06×10^{-6} Am^2). Notably, the paramagnetic contribution in the silt is considerably larger than in the clay. The micro-rhythmite specimen Sc061a has an intermediate M_s between clay and silt. The slope correction for paramagnetic contribution accounts for a substantial part of the M_s (3.55×10^{-7} Am^2 to 2.55×10^{-7} Am^2). Sc066a and Sc061a do not display pinching of the hysteresis loop near the origin, as in the clay which suggests that a single magnetic phase dominates (outweighs) the magnetic signal of silts and the mixture in the micro-rhythmites. In few cases the slope was negative as a response to the applied field in which case the majority of the minerals were diamagnetic in the specimen. This was mainly observed when the specimen size was small. The sediments are carbonate-rich, so it is possible that diamagnetic calcite can dominate the signal when other minerals are absent or present in only minor amounts, thus creating a hysteresis loop with negative slope at high applied fields.

The hysteresis parameters (M_s, M_{rs}, H_c and H_{cr}) were compiled for all slope-corrected loops for clays and silt and averaged in order to produce stacked hysteresis loops (Figure 6.13). A total of 220 clay specimens and 35 silt specimens were included in the stacked loops, the sizeable difference being a consequence of sampling strategy in the sedimentary column. Specimens were collected close to every two centimeters in the upper massive red clays and each horizon of the underlying rhythmites was sampled individually where possible (e.g. each clay and silt portion of a rhythmite were sampled individually). Micro-rhythmites (~1mm thickness) were sampled but not included in the stacked hysteresis loops because of the possibility for overlapping signal of the ferromagnetic minerals from the clays and the silts. The mean, standard deviation and standard error of the sample mean for the collective of clays and silts have been compiled in Table 6.3. Results in Figure 6.13 show very contrasting magnetic properties between clays and silts. Most obvious, the M_s differ by an order of magnitude, which can be identified from the two loops. This reflects the greater concentration of magnetic minerals in the silts, and likely the dominance of magnetite. Differences in the remaining parameters are observed in Table 6.3. As expected, M_{rs} is much greater in the silts, reflecting the high M_s. Ratios based on the mean of M_{rs}/M_s are nevertheless similar in clays and silts (silts = 0.25; clays = 0.29) and standard errors of the mean (for M_s and M_{rs}) are small for both types of sediment indicating that this is a truthful

relationship. The volume independent parameters, H_c and H_{cr}, have values that are similar in clays and silts, however a two-tailed null hypothesis test rejects the possibility that the sample means for H_c and H_{cr} in clays and silts are equal at the 95% confidence level ($z > |1.96|$). H_c is somewhat greater in the silts, while the opposite is true regarding the H_{cr}. This means that it is easier to use an applied field to reduce the magnetization to zero in the clays (H_c). H_{cr} is however harder in the clays, where the field is reduced to zero before measurement takes place.
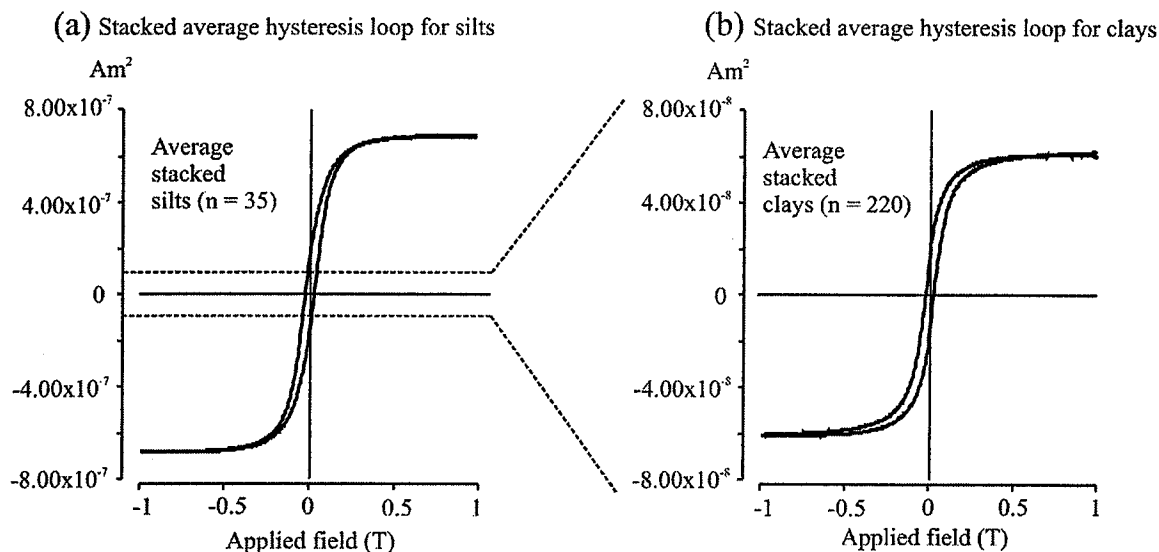
Figure 6.13 Stacked (average) hysteresis loops, corrected for paramagnetic and diamagnetic contributions, for all specimens of (a) silt, n=35, and (b) clays, n=220.

Table 6.3 Statistics of hysteresis parameters

	Silts		Clays	
	mean±s.d.	s.error	mean±s.d.	s.error
$\overline{M}_s$*	681.9±395.9	66.9	58.47±9.22	1.84
$\overline{M}_{rs}$*	163.2±84.75	14.3	17.12±27.22	0.62
$\overline{H}_c$†	26.07±2.94	0.50	21.09±7.69	0.28
$\overline{H}_{cr}$†	56.08±3.17	0.54	62.04±4.09	0.52

Ms= Saturation magnetization; Mrs= Saturation remanent magnetization
Hc= Coercivity; Hcr= Coercivity of remanence
* Units for Ms and Mrs are Am^2
† Units for Hc and Hcr are mT

It is possible that different grains are activated with and without the applied field, leading to the results seen in Table 6.3. In any case it is clear that erasing the remanence in clays

is harder than in silts, as is also observed during acquisition and demagnetization experiments above (i.e. IRM, ARM).

6.3.1 The Day plot

The magnetic properties of a material greatly influence its magnetic characteristics. Whether a material is useful for paleomagnetic studies is therefore a consequence of its rock magnetic mineralogy and grain-size. Day et al. (1977) set out to determine rock magnetic characteristics on known grain-size fractions in order to establish criteria necessary for identification of different grain-sizes in a sample based on its rock magnetic properties (M_s, M_{rs}, H_c and H_{cr}). They used synthetically grown titanomagnetites. As was noted above, during the discussion of the orthogonal three-axis test, domain states are affected by their geological histories which means that magnetic properties may not give conclusive evidence of the grain-size, and artificially produced minerals may not be representative of natural grains. Nevertheless, Day et al.'s (1977) method allows for comparison of the squareness ratio M_{rs}/M_s against the coercivity ratio H_{cr}/H_c, with boundary values for SD, PSD and MD magnetite. Using the criteria of Dunlop (2002a) all samples analyzed lie within the PSD field (M_{rs}/M_s=0.2-0.5, H_{cr}/H_c=2-5; Figure 6.14). The magnetite plots on the upper left side of the PSD field of the revised Day plot (Dunlop, 2002a) along the theoretical mixing curve of SD-MD magnetite although the distribution is readily constrained, suggesting limited grain-size distribution, as mentioned above. However, even though the silts have coarser grain sizes than the clays, it is unlikely that a large component of MD magnetite is present in the silts, as is demonstrated from the results of the three-axis tests (see Figures 6.9 and 6.10). Dunlop (2002a, b) also mathematically modeled theoretical mixing curves, based on proportions of different grain sizes of magnetite, and incorporated these into the Day plot. Mixtures of grain sizes (SD, PSD and MD) will result in curves moving through the domain sizes. If superparamagnetic (SP) magnetite is present the mixing curves are further complicated, leading to increased values of the ratio H_{cr}/H_c consequently moving results toward the right on the Day plot (Figure 6.14). The data obtained from Strawberry Creek can be separated into the red clays, which plot in the upper right portion of the PSD field, and the silts which plot on a steeper curve on the left side of the PSD field. In other words,

the decrease in M_{rs}/M_s with increasing H_{cr}/H_c is not as drastic in the clays as in the silts. The presence of highly coercive hematite (and possibly goethite) could divert the magnetite curve of clays up and to the right in the PSD field, similarly to the presence of SP magnetite. For example, mixtures of magnetic minerals with greatly contrasting magnetic properties (magnetite and hematite) have been identified by Yamazaki et al. (2003) in marine sediments from the Sea of Japan. They observed that all measurements fell into the area of PSD magnetite on the Day plot, although the values are continuously displaced from the SD+MD mixing curve (Dunlop, 2002a) down-core, making a semi-circle towards the upper part of the PSD area (Figure 6.15a). A zone of dissolution (1.2 – 1.6m) was suggested based on decreasing intensities of ARM, SIRM and bulk susceptibility (Figure 6.15b) indicating that magnetic material is removed from the sediment in this zone. Hence they attributed the displacement on the Day plot to increasing dissolution of magnetite down-core, which would gradually increase the magnetic contribution of dissolution-resistant hematite. Results from Figure 6.14(a, b), together with the shape of a hysteresis loop from above the zone of dissolution indicate the dominance of magnetite (Figure 6.14c), while a wasp-waist appearance of a hysteresis loop below the zone suggests the presence of two minerals with contrasting magnetic properties (Figure 6.15d).
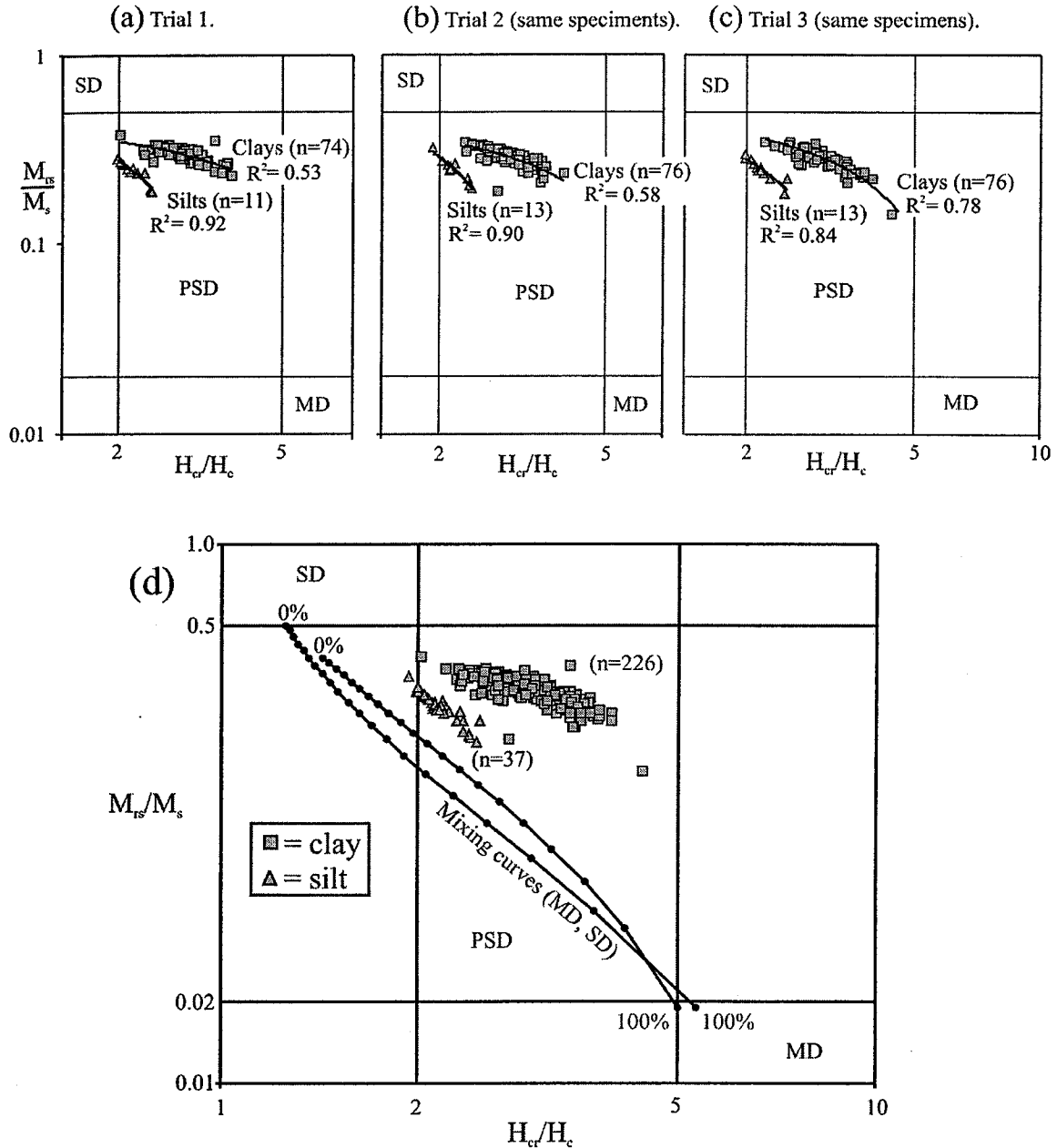
Figure 6.14 Day plots (Day et al., 1977) for three trials (a) – (c) of hysteresis measurements from the Strawberry Creek sediments. M_{rs}/M_s and H_{cr}/H_c boundary parameters for SD, PSD and MD fields are taken from Dunlop (2002a, b). The same specimens were used for the three trials in (a) – (c). All points of data, n=263, are included in (d) together with the theoretical mixing curves of Dunlop (2002a). Each dot on the line represents the MD contribution in 5% increments, from 0 – 100%.
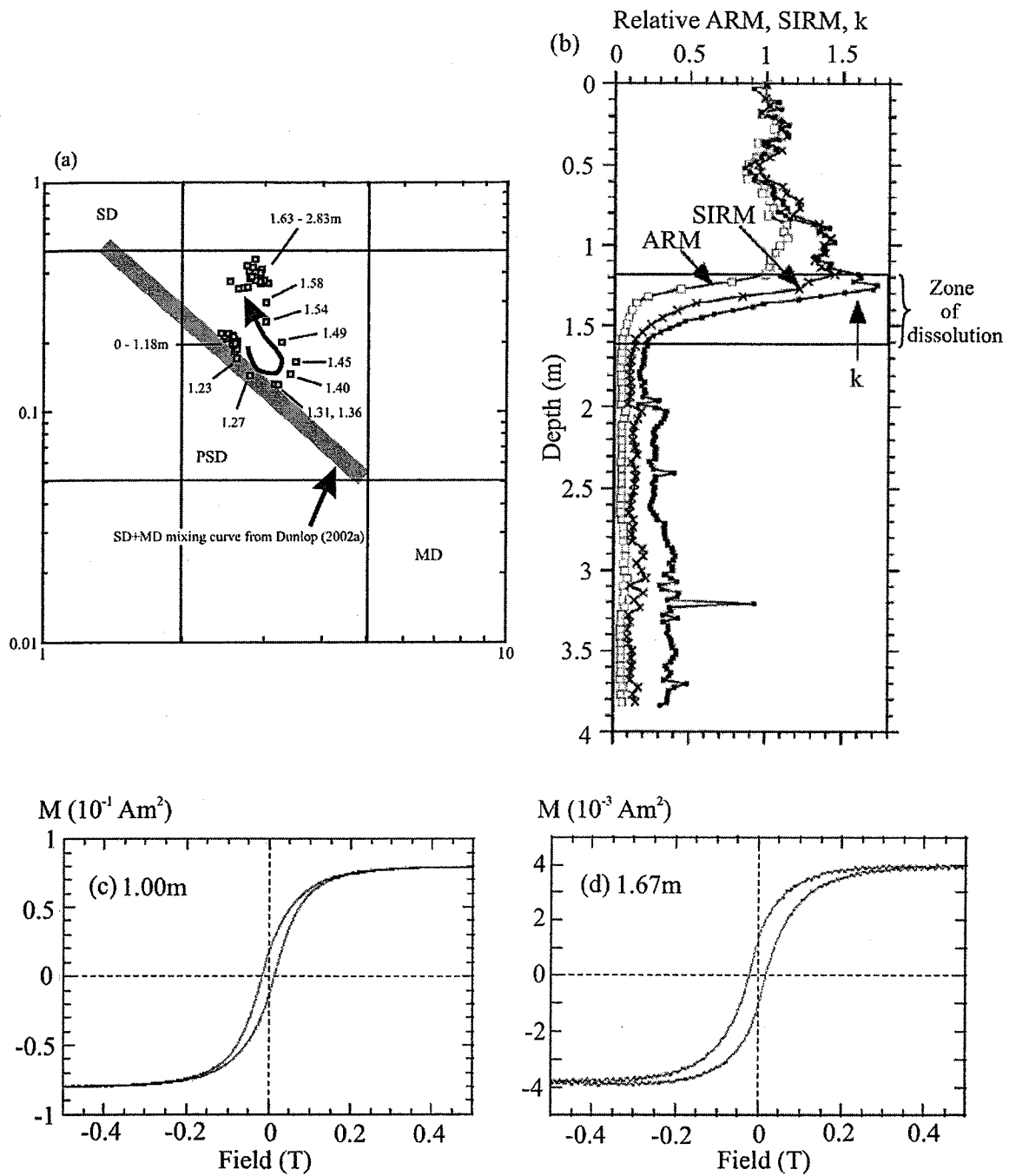
Figure 6.15 Rock magnetic data from a 4.4m core of Japan Sea sediments from the study of Yamazaki et al. (2003). (a) Day plot of samples with corresponding depth intervals. (b) ARM, SIRM and k, with values normalized to the top of the core specimen. Hysteresis loop measurements are from sediments sampled (c) above the zone of dissolution (1.2 – 1.6m), while (d) is from below the zone (1.67m).

6.3.2 Squareness (M_{rs}/M_s) versus coercivity (H_c)

The M_{rs}/M_s ratio, also called the "squareness" ratio (Tauxe and Bertram, 2002), can be graphed against H_c and provides a method for establishing what magnetic minerals are present in the material (e.g. Wang and Van der Voo, 2004; Hodych, 1996; Wasilewski, 1973). Non-oxidized titanomagnetite ($Fe_{2.4}Ti_{0.6}O_4$) will plot as a straight line intersecting with the origin (Figure 6.16). The greater the amount of Ti, the steeper is the line drawn through the origin. Figure 6.16 illustrates the case of near pure magnetite (Fe_3O_4) and titanomagnetite (TM60: $Fe_{2.4}Ti_{0.6}O_4$). The experimentally determined values for pure magnetite and TM60 are from Wang and Van der Voo (2004), and the data from the Strawberry Creek silts shows that the composition contains near pure magnetite (in the case for PSD and MD).
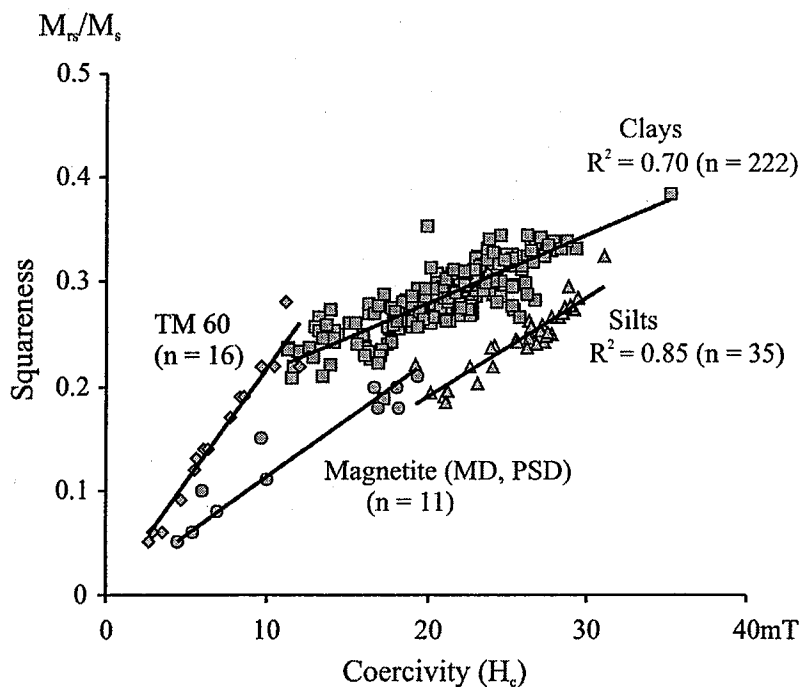
Figure 6.16 M_{rs}/M_s ("squareness") versus coercivity (H_c) for clays (n=222) and silts (n=35). The regression lines for clays and silts have a significant linear correlation at the 95% confidence level (Borradaile, 2003: Table 7.3), and clearly belong to two different populations based on their magnetic mineralogy. MD and PSD magnetite and titano-magnetite (TM 60) data are used for reference, and are taken from Wang and Van der Voo (2004). TM 60 = $Fe_{2.4}Ti_{0.6}O_4$ (x = 0.6).

The linear relationship between squareness (M_{rs}/M_s) and coercivity (H_c) arises from the approximations

$$Mrs = \frac{Hc}{N}$$

[Eqn. 6.1]

and

$$\frac{Mrs}{Ms} \approx \frac{Hc}{N \cdot Ms}$$

[Eqn. 6.2]

where N is the demagnetizing factor. If the ratio of M_{rs}/M_s exceeds 0.5, i.e. SD magnetite is present, the linear relationships of [6.1] and [6.2] are not maintained (Wang and Van der Voo, 2004). The linear relationship disappears in SD grains because of differences of Hc, Ms and N between SD and MD/PSD grains (Dunlop and Özdemir, 1997). However, linear relationship remains true for identification of titanomagnetites ($Fe_{y-x}Ti_xO_4$) that are of PSD and MD grain-size.

As the magnetic minerals are oxidized they move away from the line through the origin, and intersect the y-axis at a value greater than zero, as happens with titanomaghemite. The magnetic minerals in the red clay are similarly displaced from a line through the origin, reflecting the presence of hematite. The slope of the line for clays is shallower than that for the silts and intersects the M_{rs}/M_s axis above the origin.

6.3.3 Coercivity (H_c) versus coercivity of remanence (H_{cr})

The final method used here to compare parameters obtained from the hysteresis experiments is a simple coercivity against coercivity of remanence plot (H_c vs. H_{cr}; Figure 6.17). Again, the populations of magnetic minerals in silts and clays plot separately, and are best described through empirical power law curves. Backward forecasting is used for descriptive purposes, and brings both curves close to the origin, although they do not lie on the same path. The H_{cr} is higher in the clay than in the silt, while H_c in the two sediments are comparable. Wasilewski (1973) suggested boundary parameters for the domain-sizes of magnetite, which are illustrated in Figure 6.17 as hachured lines; both silts and clays fall within the PSD grain-size range which agrees with the Day plot in Figure 6.14.
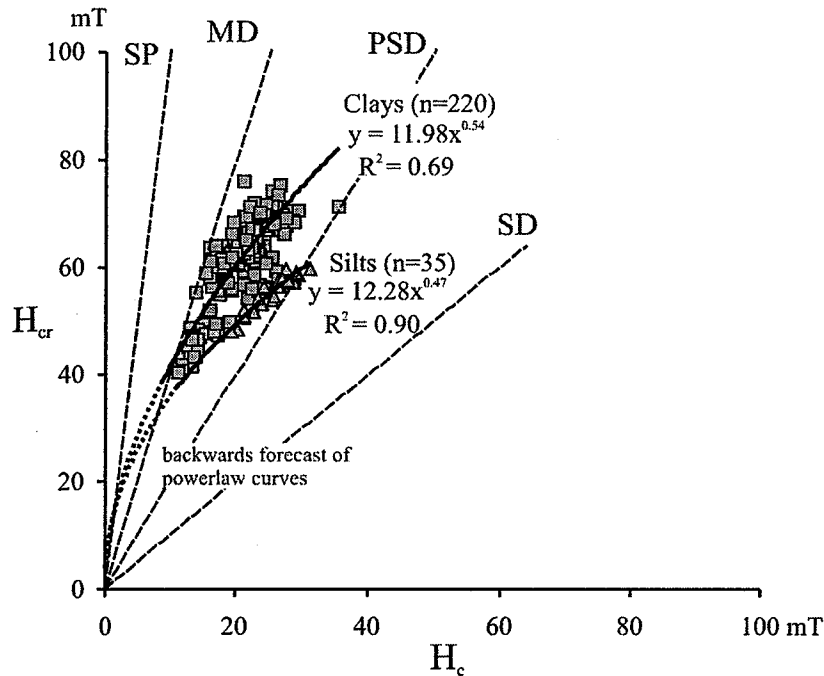
Figure 6.17 Coercivity (H_c) is plotted against coercivity of remanence (H_{cr}) for clays (n=220) and silts (n=35). A power law curve is fitted to the data of the clay and the silt. Backwards forecasting curves are for descriptive purposes only. The dashed lines indicate domain-size ranges suggested originally by Wasilewski (1973).

6.4 Low-temperature experiments using liquid nitrogen

A couple of experiments using low-temperature treatment with liquid nitrogen (LN_2) of a silt and clay were performed. The specimens were simply covered with LN_2 in a stainless steel dewar flask with negligible field inside the container, and were allowed to rest in the LN_2 until they had equilibrated. They were then removed from the container and mounted in the holder of the spinner magnetometer. As the specimens warmed towards room temperature in the magnetometer their remanence was automatically measured every 15 seconds using a special computer program, until no noticeable change in remanence could be observed (i.e. until specimens had reached internal temperatures close to room temperatures). The initial NRM was 61.4 mA/m prior to treatment with LN_2, and 57.2 mA/m following treatment. The results of this experiment for a clay-rich specimen are shown in Figure 6.18, which illustrates that as the specimen initially warms it looses remanence until it approaches the original NRM where it levels off until the final time of measurement, after almost 4000s. Note that no measurement of temperature is available using this method, although it can be assumed that as the specimens are initially moved to the magnetometer they are at equilibrium with the LN_2 at close to 77K. The specimens will warm quickly at first, following Newton's law of cooling, in order to equilibrate

with room temperature and should pass through the Verweij transition (~135K) shortly after they have been put in the holder of the magnetometer.
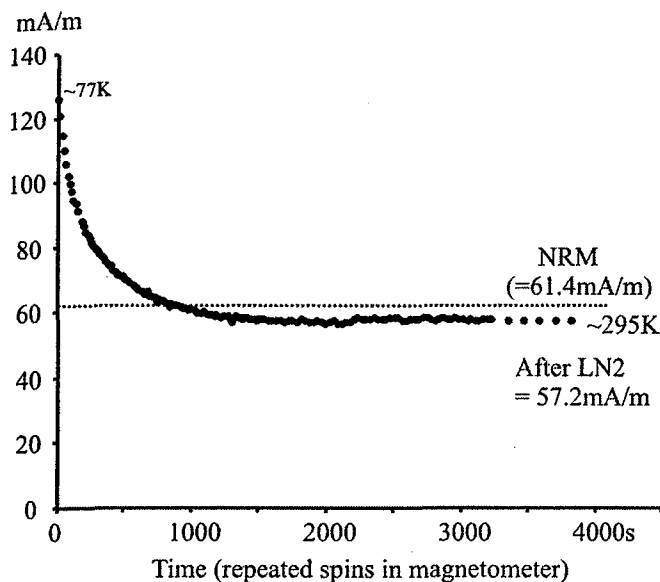
Figure 6.18 Specimen Sc214 (red clay) was submerged in liquid nitrogen (LN$_2$) inside a stainless steel dewar flask. The magnetization of the specimen is continuously measured upon removal from the LN$_2$ with a molspin spinner magnetometer. Initial and final temperatures are estimated based on equilibrium temperature of the LN$_2$ and final temperature of the specimen at the end of the experiment.

Interestingly, as the clay specimen (Figure 6.18) warms it does not appear to move through the Morin transition (about -10°C for hematite). As illustrated in earlier sections of this chapter hematite is an important remanence carrier in the red clays. However, because of the large difference in magnetization of magnetite (Ms=480kA/m) and hematite (Ms=~2.5kA/m), any evidence of the Morin transition is suppressed. Alternatively, albeit unlikely, the hematite is very fine grained or possibly impure so that the Morin transition is severely suppressed. In very fine particle hematite (e.g. of diagenetic origins) the transition can be depressed to below 100K, and can be completely absent in grains with sizes ≤0.1μm (Dunlop and Özdemir, 1997; O'Reilly, 1984; Bando et al., 1965). It is difficult to assign grain-sizes for the pigmentary hematite of the red clay, however it is possible that single domain sizes of these particles are very small. Another possibility is that the MT is very subtle and hard to identify in Figure 6.18.

6.5 Thermal demagnetization in automotive engine oil

In order to try to determine whether goethite is complementing hematite as a high coercivity mineral in the Strawberry Creek sediments, a partial thermal demagnetization

experiment was attempted. A specimen of red clay (with NRM=60.1 mA/m) was submerged in a glass beaker filled with automotive engine oil. The oil principally serves as a medium in which the specimen is heated while it was also insulated and partly protected from oxidization. The beaker containing the oil was then heated and the temperature was carefully monitored using a thermometer. The beaker was removed from the hotplate at ~130°C and inserted into a mu-metal shield, and subsequently allowed to cool in a field free environment. This temperature was chosen because goethite has coinciding Curie and Néel temperatures around 120°C (Dunlop and Özdemir, 1997). Therefore, at 130°C any remanence carried by goethite should effectively be randomized when the specimen is cooled in a shielded environment. The result for the experiment is shown in Figure 6.19, and illustrates that the test was partly successful in discriminating against any contribution of goethite in the specimen. Initial measurement of the specimen indicates that a viscous remanence (1423.9 mA/m) was acquired during the heating (and probably not randomized after insertion into the mu-metal shield). Progressive AF demagnetization easily removes the VRM (<50mT) which is most likely carried by very fine grained SD magnetite or MD magnetite, but as with previous AF demagnetization, fails to remove the magnetically coercive component. This may be an indication that goethite is not a significant remanence carrier in the red clays.
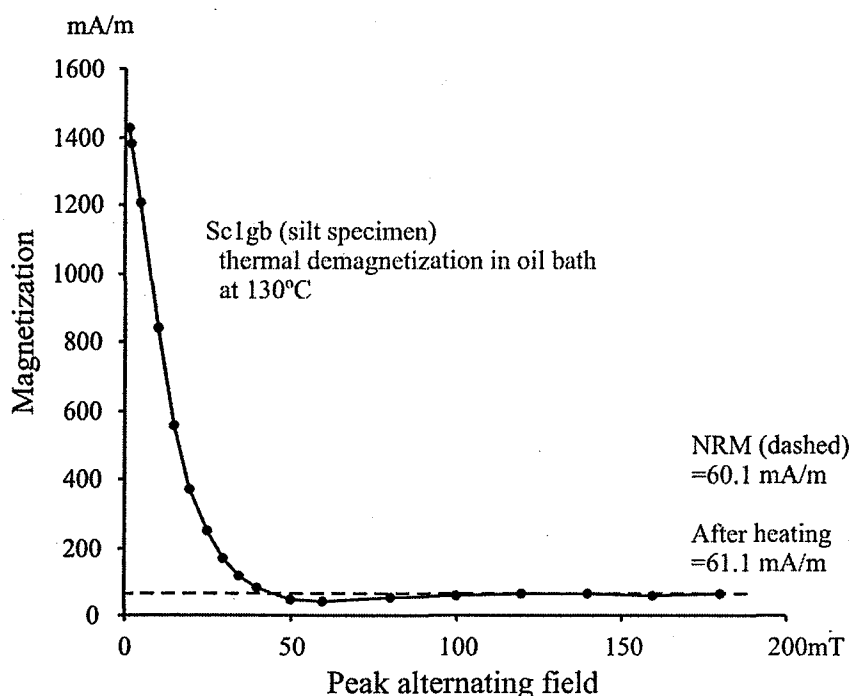
Figure 6.19 Intensity of magnetization is measured during AF demagnetization after specimen Sc1gb (silt) has been submerged in automotive engine oil and heated to ~130°C, for the purpose of detecting the presence of goethite (see text for details of the experiment). The hatched line is the original NRM (60.1mA/m). The solid line represents AF demagnetization of remanence after the specimen was heated in oil.

6.6 Rock magnetic parameters expressed with depth

Another method of analyzing results from the rock magnetic experiments is plotting the data against depth of the sedimentary profile. This is done for a variety of parameters (Fig. 6.20a-f) including χ, χ_{arm}, χ/χ_{arm}, Intensity of NRM, M_{rs}/M_s and H_{cr}/H_c. The rock magnetic parameters are relatively uniform through the top meter of massive red clay, but fluctuate rapidly in the lower part of the section that contains the alternating clay and silt rhythmites. Bulk susceptibility (χ; Figure 6.20a) shows that silts have high susceptibility compared to the clays. The volume of magnetic minerals is greater in the silts. The susceptibility of ARM (Figure 6.20b; χ_{ARM}) similarly show greater values in the silts, but also higher values in relation to the susceptibility profile of Figure 6.20a. This is demonstrated by the low ratio of χ/χ_{ARM} in Figure 6.20c. The ratio approaches unity in the silt-rich layers and the micro-rhythmites, indicating the influence of larger grain-sizes of the magnetic minerals in the silts. Simply put, the χ_{ARM} is a sensitive indicator of SD magnetite, as ARM preferably activates the magnetic moments of remanence-carrying SD magnetite, since grains containing domain walls relax to a lower energy state once an applied field is removed (Evans and Heller, 2003). A continuously applied field as used for χ preferably measures the magnetization of grains with domain walls, which could help explain why ratios of χ_{ARM}/χ are lower in the silts, because of coarser grains in this sediment. As the intensity of ARM is also volume dependent (Figure 6.20d) and it shows that the silts contain more magnetic material than the clays. The ARM together with the NRM is further discussed in chapter 7. Results for ratios of M_{rs}/M_s and H_{cr}/H_c are displayed for specimens through the section in Figure 6.20e and f; each solid line represents a single experimental run. The noise is rather more substantial in the upper part of the section, containing the massive clays. Results for both M_{rs}/M_s and H_{cr}/H_c are fairly uniform in the rhythmic portion of the lower part of the section. M_{rs}/M_s (Figure 6.20e) shows a slight tendency towards decreasing values in the lower portion of the section, reflecting the increasing abundance of coarser grain-size material in the silts (including magnetic minerals). The ratio of H_{cr}/H_c readily reflects changes in the lithology with depth, as is evident from the saw-tooth pattern in the lowest part of the section; the ratio is higher in the clay than in the silt.
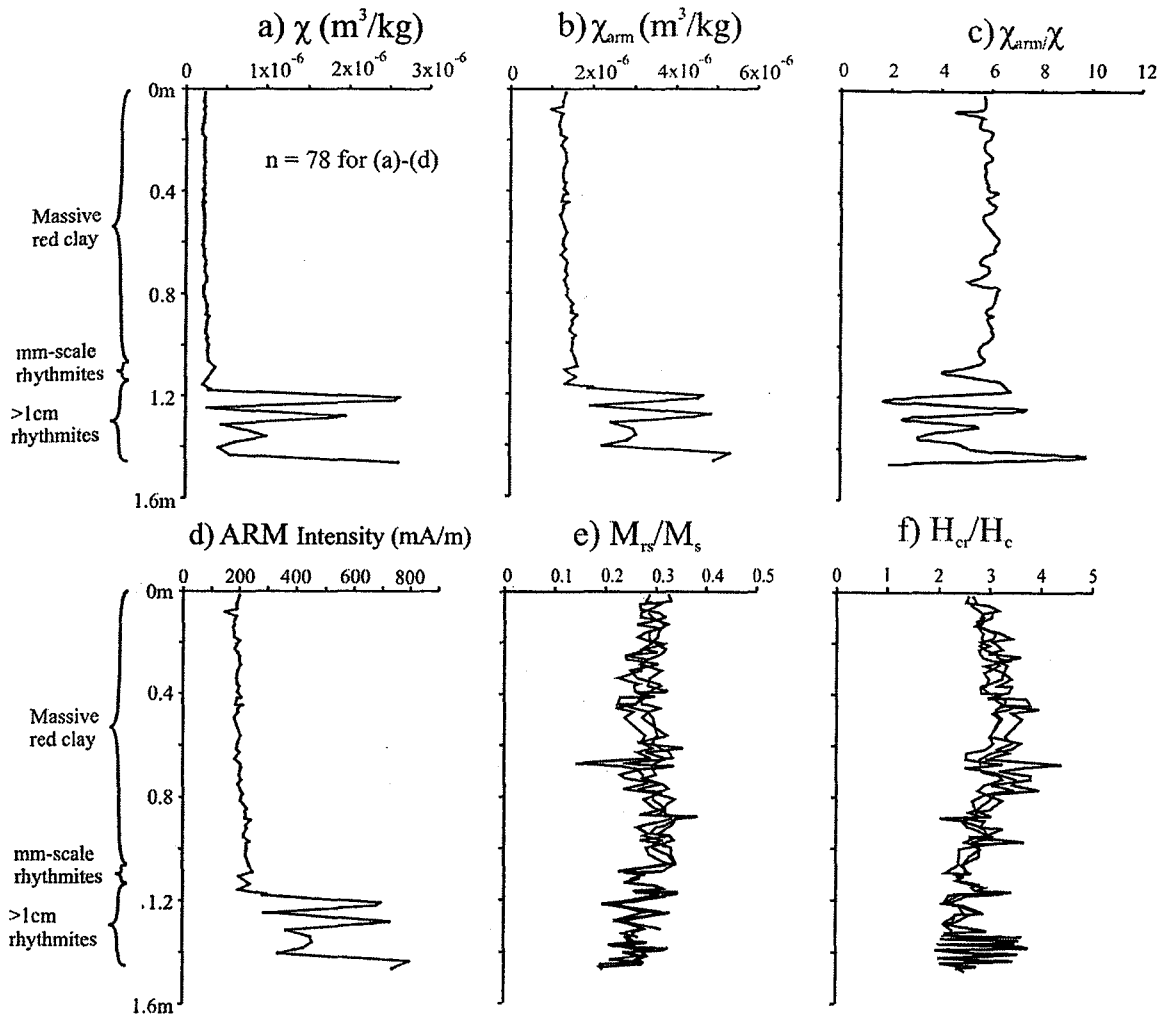
Figure 6.20 Several different rock magnetic quantities are plotted against the stratigraphy of the Strawberry Creek site. The quantities are: (a) low field susceptibility (χ); (b) mass normalized per unit field (m^3/kg), ARM susceptibility; (c) Ratio of low field susceptibility to ARM susceptibility; (d) intensity of NRM; (e) Ratio of M_{rs}/M_s ("squareness"); (f) Ratio of H_{cr}/H_c.

Chapter 7. The natural remanent magnetization and paleosecular variation

This chapter details the results from alternating field (AF) demagnetization from the Strawberry Creek samples. The results are discussed in context with the stratigraphic profile and lithological properties. The magnetostratigraphy displays paleosecular variation (PSV) of the Earth's field.

A cautionary remark should be made about the number of significant figures displayed in tables and appendices concerning the data points of inclinations and declinations. Values for declinations and inclinations are reported to one decimal point, obtained from measurements with the molspin spinner magnetometer. This level of accuracy is probably not feasible due to sampling errors in the field and laboratory, as well as measurement errors due to manual reorientation of the specimens. The latter error is reduced significantly with use of sample cubes, which are held firmly in place during each measurement. However, carrying one decimal point is common practice in paleomagnetic studies, and the practice has therefore been exercised in this study as well.

7.1 The natural remanent magnetization

The properties of natural remanent magnetism (NRM) in the Strawberry Creek sediments are dictated by their lithology. Particularly, differences are noted between samples of red clay and grey silt. The distribution of intensities of NRM's is contrasting (Figure 7.1), and serves as evidence for the argument above (see chapter 6 for a detailed discussion on the rock magnetic properties). The concentration displayed at low intensities in Figure 7.1 constitutes specimens of red clay, while silts are dispersed across a range of greater intensities. Some specimens contain a mixture of clay and silt, usually when the thickness of each layer of the rhythmite was less than 2cm. Mixed samples carry intermediate NRM intensities and fall between the extremes of low intensity clays and high intensity silts. The total number of specimens in Figure 7.1 (n=116) include 85 clay specimens, 23 silt specimen and 8 specimens of mixed clay and silt. In a plot of NRM against stratigraphy (Figure 7.2a) the upper massive clays have fairly uniform intensities (mean=46.63mA/m; st.d.=18.83mA/m; st.error.=2.35mA/m; n for clays in the column=61). In the lower part of the section intensities fluctuate, because of the introduction of micro-rhythmites (mm-scale) and larger rhythmite couplets (>1cm). Clay and silt alternations are recognizable in the thicker rhythmites by peaks of low and high intensity, respectively. Other rock magnetic parameters similarly display fluctuations due to the alternation of clays and silts (see chapter 6,

Figure 6.17). Figure 7.2b displays the ARM acquisition of the same specimens measured for NRM. For the ARM's, an AF was applied to 100mT, with a background DC field of 0.1mT applied over a window of 60 – 0.1mT. ARMs also reflect changes in the lithology, but generally have higher intensities in clays than NRMs. Contrastingly NRMs are more intense in the silty portions of the rhythmites (notably in the thicker rhythmites). Magnetic particles in clay react differently to the ARM than particles in the silt and the ratio of NRM/ARM clearly illustrates these differences (Figure 7.2b). In all clays NRM/ARM<1, while in the lower section, silty portions of each rhythmite have NRM/ARM>1.
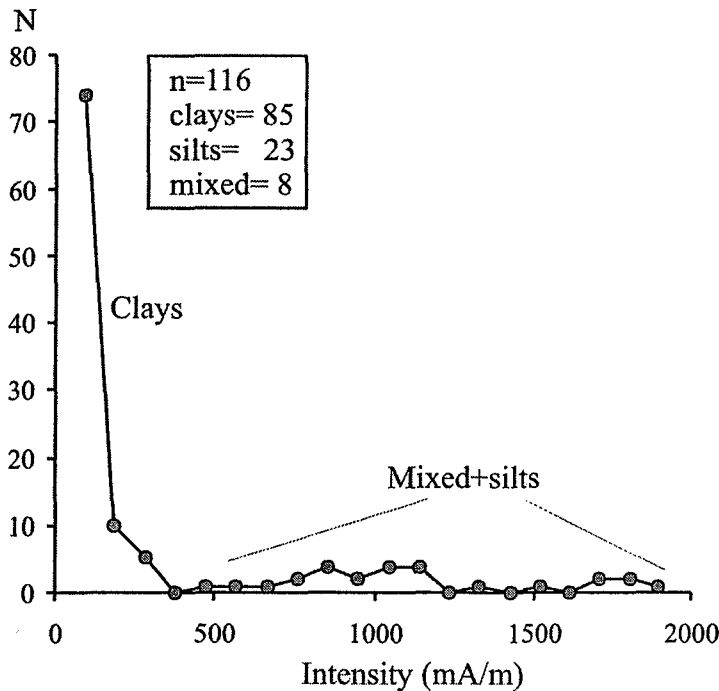
Figure 7.1 A frequency histogram with the distributions of NRM intensities (in mA/m) for clays, silts and a mixture of clays and silts (the clay/silt mixture is referred to as mixed in the diagram).

7.2 The magnetic remanence components

Alternating field (AF) demagnetization reveals that the glaciolacustrine sediments carry a single, two or three remanence components, depending on the nature of the particular specimen. The NRM therefore consists of multiple remanences contributing to the overall measured NRM vector, such that

$$NRM = M_A + M_B + M_C \qquad \text{[Eqn. 7.1]}$$

where M_i represents magnetic remanence components that are separable during demagnetization, and therefore identified as an individual magnetization event. Often these individual components
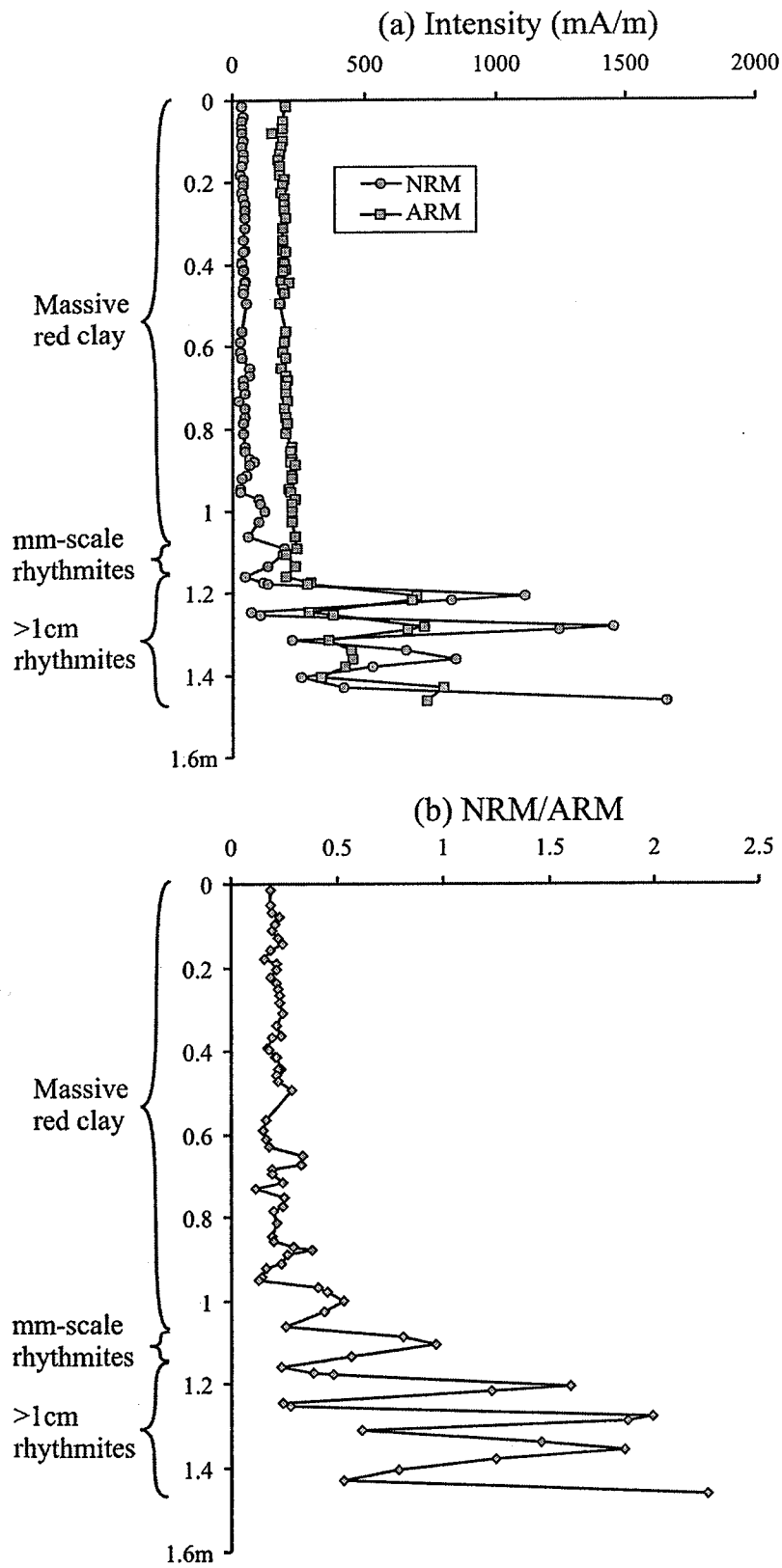
Figure 7.2 Intensity measurements (in mA/m) for NRM and ARM are compared in (a). The ratio of NRM/ARM is displayed in (b).

are classified as either a characteristic remanence (ChRM) or secondary remanences (Butler, 1992; also see discussions on remanent magnetizations in chapter 2 and demagnetization in chapter 3). A theoretical relationship between the remanence vectors in [Eqn. 7.1] is illustrated in Figure 7.3(a), where $H_{cr} = M_A > M_B > M_C$. The path of the NRM is the vector sum of the individual remanence vectors (Figure 7.3a; [Eqn. 7.1]). Figure 7.3(b) shows a hypothetical scenario with a set of samples containing the remanence vectors in Figure 7.3(a), displaying a range of unblocking coercivities.
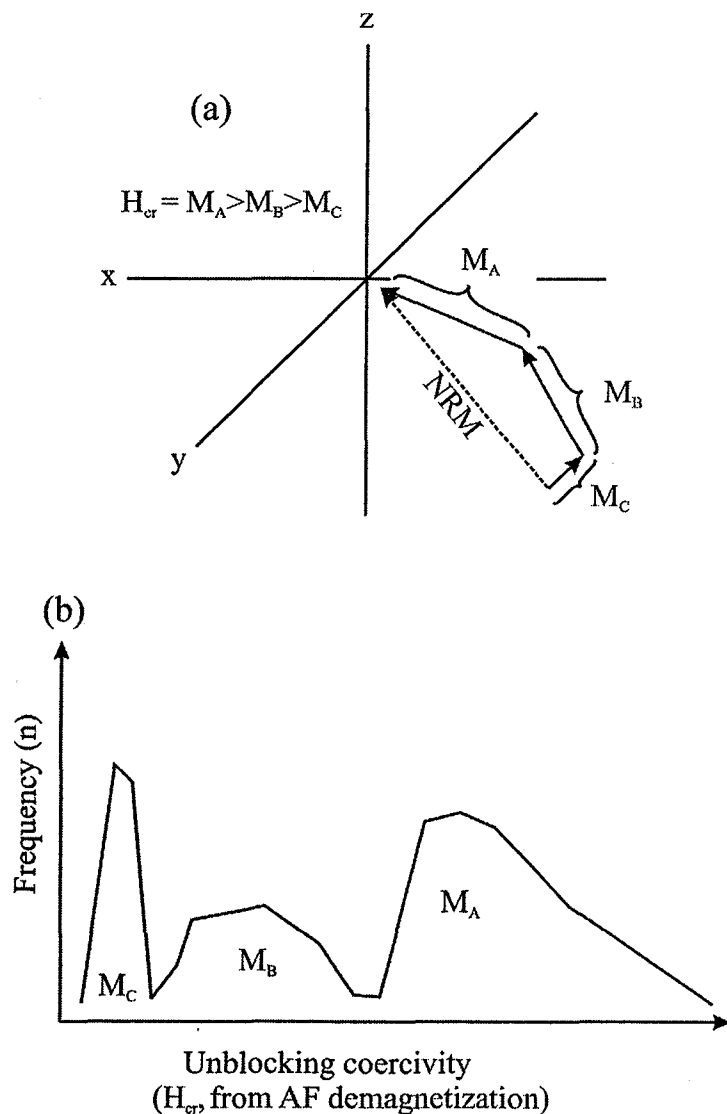
Figure 7.3 Theoretical relationship between the remanence vectors M_A, M_B and M_C of different coercivities, as they are demagnetization towards the origin (a). $H_{cr} = M_A > M_B > M_C$. (b) hypothetical distribution of unblocking coercivities for a sample set containing the three remanence vectors in (a).

A single vector component of remanence is identified in 10% of the samples; two vector components of remanence are identified in 47% of all specimens; three vector components are identified in 43% of all specimens. Further, these remanences were separated depending on their coercivity intervals and by considering the low coercivity fraction as the soft remanence component (M_C), the magnetically coercive fraction as the hard remanence component (M_A) and intermediate coercivity fraction (M_B), which could not be assigned to either of the first two, as the intermediate remanence component. It is commonly assumed in paleomagnetic research that these components follow a chronological order, from magnetically young (soft remanences) to magnetically old (hard remanences). Thus, a hard remanence would be primary and a soft remanence would be secondary. This is a hazardous statement when considering multiple magnetic phases in a sample, especially concerning magnetite and hematite which have very different magnetic properties (i.e. coercivity). The red clay often carries two and sometimes three components of remanence, which is attributed to the presence of hematite and magnetite in the clays, each mineral being responsible for a different remanence component. Magnetite has low coercivities relative to hematite, and therefore corresponds to the presence of soft and intermediate remanences. However, coercive magnetite (SD, PSD) and hematite are likely to carry the hard remanence component in both silts and clays. Two components of remanence or more are present in at least ~85% of the clay specimens studied from the section (n=77), while almost half of those specimens has a third component of remanence as well (Figure 7.3). Some specimens of clay show curved unblocking coercivities at higher AF's without sharp turning points (Figure 7.4a), as a product of overlapping coercivities (Figure 7.3; Butler, 1992). The unblocking coercivity of specimen Sc041a is difficult to identify from its curved appearance in Figure 7.4a. More than 20% of the remanence still remains after AF demagnetization to 180mT in this specimen (Figure 7.4b) which is a clear indication that a high coercivity component remains. Silts generally show simpler demagnetization histories, with soft remanences unblocked at low AF's followed by a stable remanence that is demagnetized towards the origin (often with <10% remanence remaining). The low coercivity or soft remanence is demagnetized at low AF's (≤10mT) and is probably due to handling or laboratory acquired remanence and is not considered further.

The two prominent remanence components are isolated at alternating fields >10mT and represent real remanences acquired *in situ*. The more coercive remanences are separated into the intervals of 20-40mT (referred to as the intermediate component=IR), and >40mT (referred to as the hard component=HR) and as mentioned previously these divisions reflect the coercivities of the magnetic minerals carrying each component of remanence (MD, PSD, SD magnetite and

hematite in order of increasing coercivity). A suite of samples showing "typical" AF demagnetization histories shown in Figure 7.5 for clays, silts and mixtures of clay and silt.
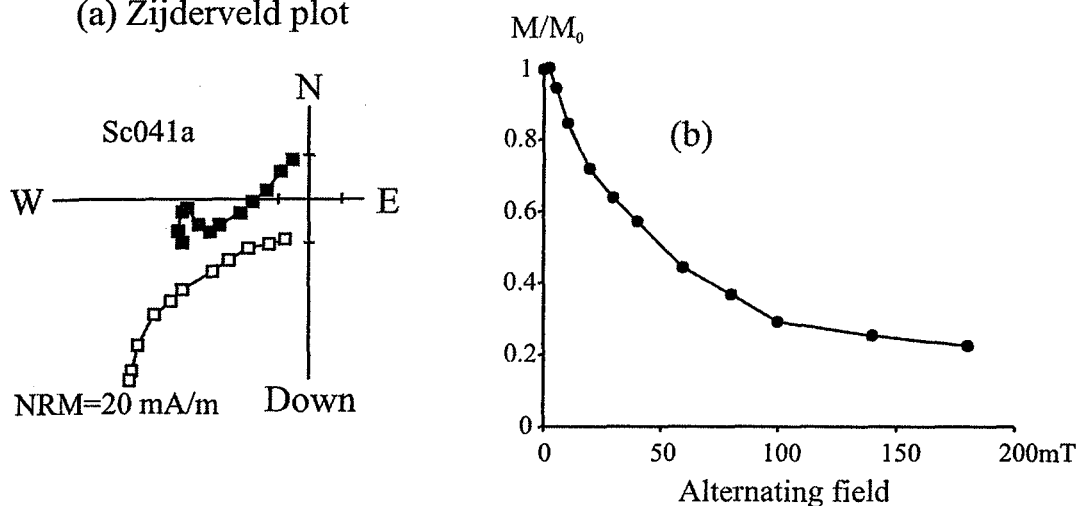
Figure 7.4 (a) Zijderveld diagram for demagnetization of specimen Sc041a, with open (closed) symbols representing plots on the vertical (horizontal) plane, (b) shows the corresponding normalized intensity during AF demagnetization. AF demagnetization steps were 0, 2, 5, 10, 20, 30, 40, 60, 80, 100, 140 and 180mT.

Samples of clay often show a two-component remanence (Figure 7.5a-c) and have large portions of remanence remaining after AF cleaning to 180mT (Figure 7.5g), close to 30% of the original NRM intensity in some cases. Many specimens showing a high coercivity component do not clearly demagnetize towards the origin. Unblocking coercivities are generally distinguishable but can be difficult to identify. Samples with a dominant composition of silt only carry a single component remanence that is effectively demagnetized to the origin, usually with less than 10% remanence remaining after application of AF demagnetization to 180mT (Figure 7.5d-g). The NRM intensities of the silt samples are much greater than the clays, sometimes by almost two orders of magnitude in difference. Any contribution of hematite to the remanent magnetization in the silts is diminished because of the dominance of magnetite. The inclination is steeper in silts as compared to clays, resembling the intermediate component identified in most red clay specimens. From rock magnetic experiments (hysteresis, cross-over plots and orthogonal 3-axis tests) it is clear that the magnetic mineralogy is different in silts versus clays, or at least clay is supplemented by a small amount of hematite. From the rock magnetic experiments it is evident that both lithologies are dominated by high coercivity minerals, although in the case of silts this likely represents the presence of SD and PSD magnetite, while in clay substantially more coercive hematite is influencing the remanence together with fine grained SD magnetite.
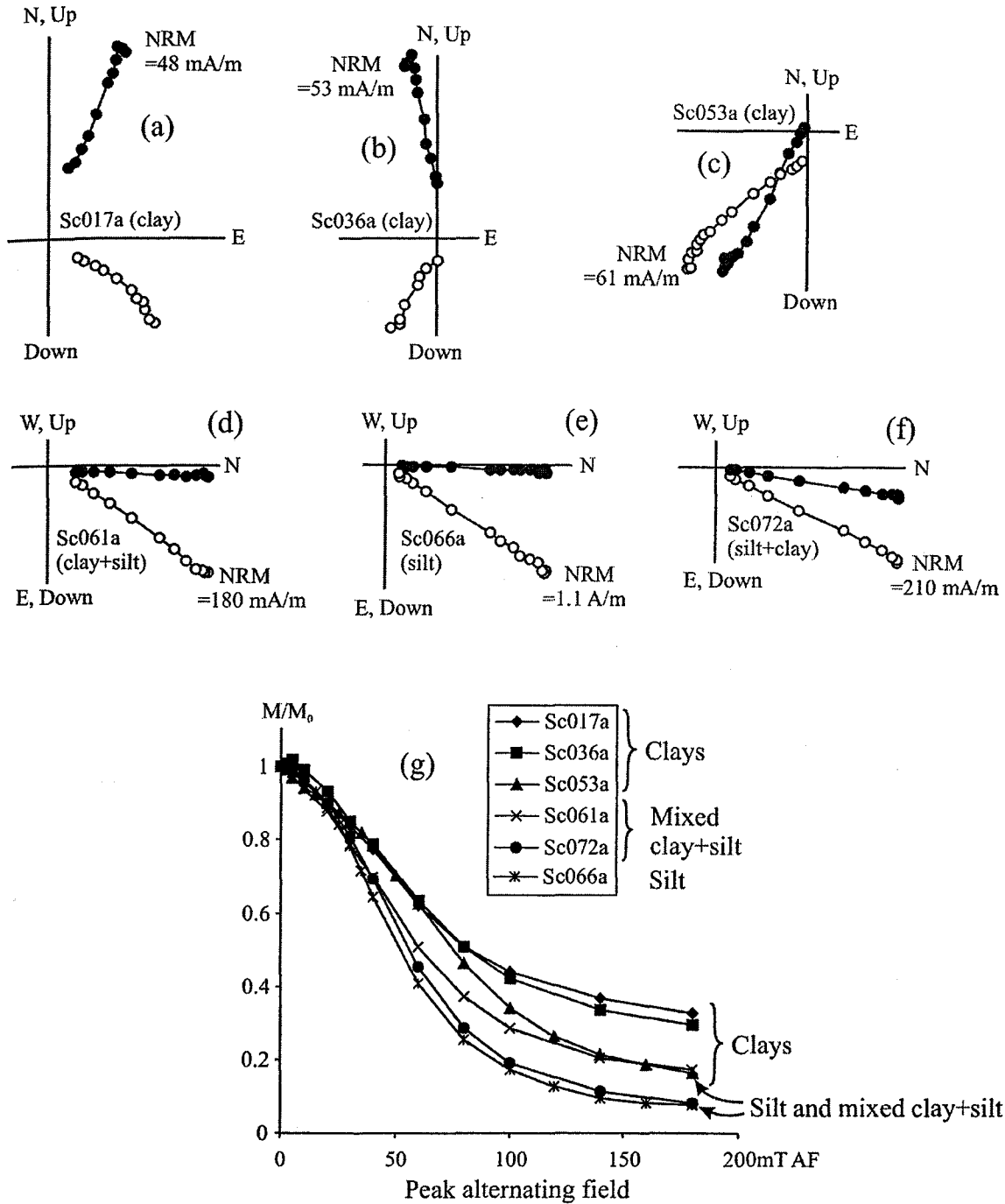
Figure 7.5 (a)-(f) Several Zijderveld diagrams of demagnetization for specimens with different lithology (clay, silt, and mixture of clay and silt). The NRM is indicated for each specimen. Open and closed symbols as in Figure 7.4. (g) Normalized intensities for the respective specimens of (a)-(f). AF demagnetization steps were 0, 2, 5, 10, 20, 30, 40, 60, 80, 100, 140 and 180mT.

Different demagnetization histories are evident even within a single couplet of silt and clay of a thicker rhythmite (Figure 7.6a and b). The clayey top portion of the rhythmite shows a curved

demagnetization with respect to the vertical plane, whereas the silt portion has a single stable component of remanence demagnetized towards the origin.
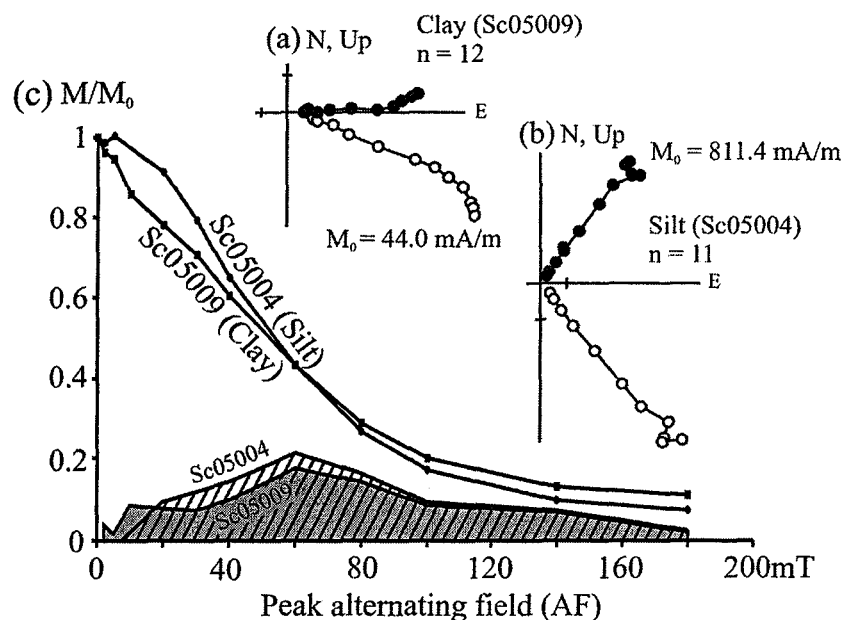
Figure 7.6 (a) and (b) show Zijderveld diagrams for clay (Sc05009) and silt (Sc05004) specimens, respectively (M_0=NRM). Symbols as described in Figure 7.4. (c) Normalized intensities during demagnetization with accompanying coercivity spectra. Peak alternating field =180mT.

As the coercivity window of 20-40mT is surpassed during AF demagnetization the remanence begins to curve into a more parallel orientation with the horizontal plane which nearly coincides with the bedding plane of the sediments (e.g., Figure 7.5 and Figure 7.6). This shallowing of inclination could represent an effect of compaction of the high coercivity minerals present in the sediment column, such as rotation of elongate fine-grained magnetite (SD, PSD), or anisotropic hematite, which preferably aligns its magnetic moment with the bedding plane of the clay minerals. Another reason for horizontal alignment of grain long-axes is current alignment. Even though the sediments of Strawberry Creek were deposited in a low-energy, calm environment (judging from lithology and grain size) AMS demonstrates that maximum susceptibility (k_{max}) lies approximately in the NE-SW axis (Figure 6.1) suggesting a paleo-current flow either towards the northeast or southwest. The magnetic fabric illustrated by the anisotropy of remanent magnetization and AMS also show that the bedding plane is displaced somewhat to the west from the horizontal plane, is another indicator of grain alignment in the sediments.

7.3 Large specimen versus small specimen measurements

The homogeneity of magnetic remanence in the red clay was tested using oriented large specimens of red clay ($125cm^3$ cubes) which were measured with a special molspin magnetometer designed for large specimen measurements ("BigSpin" by Molspin Ltd, UK). Each large cube was subsequently split into eight smaller oriented cubes with the standard $8cm^3$ volume, which were measured using a regular molspin magnetometer. A compilation of the directions of large and small specimens is shown in Figure 7.7(a, b). The majority of specimens for both large and small specimens plot in the northeast quadrant, with shallow inclinations (as indicated by α_{95} confidence cones for means of large and small specimens). The directions of large and small specimens coincide rather well with the directions of the red clay in the magnetostratigraphic profile (see section 7.4 below). The results for individual large cubes together with their smaller specimens are displayed in Figure 7.8(a-e). The confidence cones for mean and sample of large and small specimens coincide well. In specimens Sc1a1 and Sc1a2 the large cubes have similar ChRM vectors to the directions obtained from the individual small specimens (e.g. Figure 7.8a, b). Further, the smaller sub-specimens from Sc1a1 and Sc1a2 have somewhat scattered ChRMs, with smaller Fisher-k values and greater angles of the α_{95} confidence cones. The remaining specimens (Sc2; Figure 7.8c-e) have homogenous ChRM vector directions, for large specimens and smaller sub-specimens. For Sc2 specimens the Fisher-k values of samples are large (>80) and the α_{95} confidence cones are small (<21°).

Demagnetization for the large specimens was performed using regular AF demagnetization in the Sapphire Instruments SI-4 static demagnetizer. However, due to their size it was not possible to fit the large specimens inside the coil of the AF demagnetizer. Instead the specimens were placed at the entrance of the AF coil in six different orientations in order to receive AF demagnetization. The field at the mouth of the coil is much reduced compared to the actual applied field produced within the coils (the field reduces in intensity as a function of the cube root of the distance from the coil). Therefore the set AF value of the instrument exaggerates the actual applied alternating field received by the specimens. A set field of 180mT AF removes between 25 − 35% of the intensity of the original NRM of large specimens at the mouth of the coil. In smaller specimens, using conventional inside-coil AF demagnetization, this corresponds to an AF roughly between ~30 − 40mT, which may more accurately represent the true AF to which the large specimens are exposed. In three of the larger specimens a shallower characteristic (compacted) inclination becomes apparent subsequent to AF demagnetization (Figure 7.8). In general, it appears as if the homogeneity of the remanent magnetic signal in small and large specimens coincides well, and represents the recording of the Earth's magnetic field. As

with the NRM and hard remanence component described in Section 7.2, the remanent magnetic signal in the red clay has undergone significant inclination shallowing.
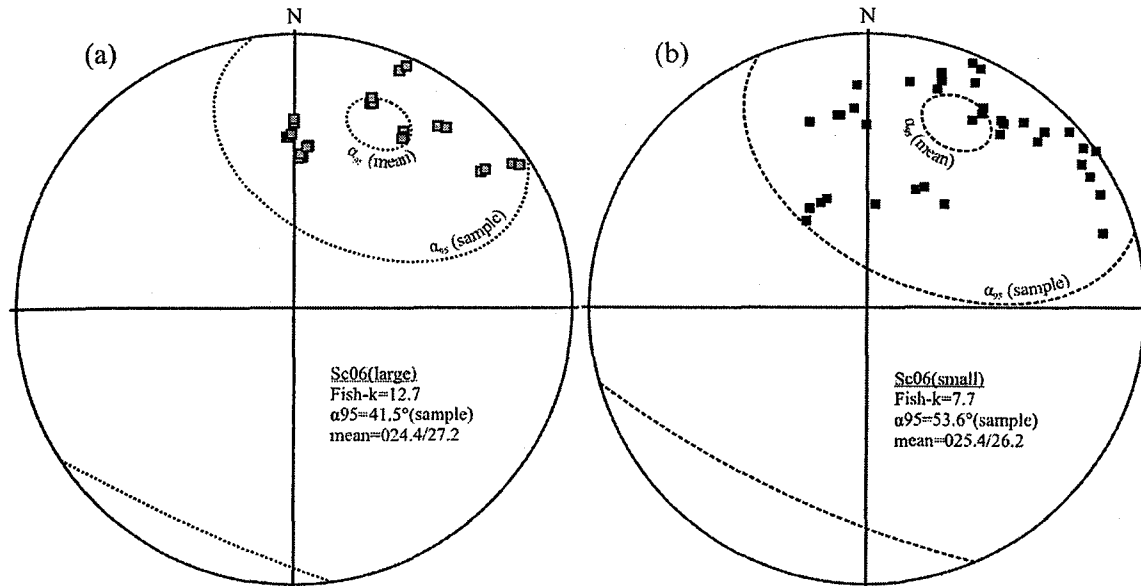
Figure 7.7 A compilation of remanent magnetic vectors for (a) large specimens and (b) small specimens. Shaded squares refer to directions of large specimens, whereas closed squares refer to small specimens. α95 confidence cones are shown for the sample and mean of large and small specimens.

7.4 A re-deposition experiment of the red clay

To isolate the possible contribution of DRM on the magnetic remanence in the clay, a re-deposition experiment was performed using red clay collected from the Strawberry Creek site. Pieces of the red clay were allowed to dry thoroughly, and subsequently disaggregated using a mortar and pestle. The powdered clay was then mixed into a beaker containing distilled water. The beaker was placed in an ultrasonic bath for about an hour to further disaggregate the particles. The slurry was stirred using a stainless steel rod during and after the ultrasonic treatment. A small amount of the slurry (a few centiliters) was transferred into plastic cubes daily over a two-week period. Four cubes with a volume of $8cm^3$ and four cubes with a volume of $125cm^3$ were used for the experiment. Some specimens developed cracks in the sediments, although this did not seem to affect their overall remanent magnetization directions or fabric. Once the cubes were filled and the sediments solidified sufficiently for movement not to disturb the sediment, they were measured using molspin magnetometers designed for $8cm^3$ and $125cm^3$ specimens. The results for small and large cubes are shown in Figure 7.9(a, b).

(a)

N

α₉₅ (mean)

α₉₅ (sample)

Sc1a1 (125cm³)
Fish-k=1424.0
α₉₅=04.5 (sample)
mean=003.2/42.8
Sc1a1 (8x8cm³)
Fish-k=19.9
α₉₅=35.1 (sample)
mean=002.8/41.7

(b)

N

α₉₅ (mean)

α₉₅ (sample)

Sc1a2 (125cm³)
Fish-k=800.4
α₉₅=06.1° (sample)
mean=359.0/35.7
Sc1a2 (8x8cm³)
Fish-k=9.5
α₉₅=52.7° (sample)
mean=356.9/38.5

(c)

N

Sc2a1(125cm³)
Fish-k=81.8
α₉₅=19.0°(sample)
mean=021.7/14.7
Sc2a1(4x8cm³)
Fish-k=235.1
α₉₅=12.0°(sample)
mean=022.6/07.6

(d)

N

Sc2a2(125cm³)
Fish-k=147.0
α₉₅=14.1°(sample)
mean=054.9/12.3
Sc2a2(8x8cm³)
Fish-k=58.8
α₉₅=20.5°(sample)
mean=056.0/07.2

(e)

N

Sc2b(125cm³)
Fish-k=138.1
α₉₅=14.6°(sample)
mean=034.7/23.0
Sc2b(8x8cm³)
Fish-k=123.5
α₉₅=14.1°(sample)
mean=035.9/18.3

Figure 7.8 Individual large samples are displayed together with their corresponding smaller specimens. Directions for large specimens are shown by shaded gray squares, whereas directions for small specimens are given by closed squares. Dotted (striped) lines represent the confidence cones of large (small) specimens.

The remanent magnetizations of all cubes are consistent with the direction of the PEF in the laboratory as measured with a dip-meter (laboratory field inclination 78±2°).

The directions displayed on the stereonets in Figure 7.9 suggest that the DRM of the re-deposited red clay is close to the magnetic field inclination in the laboratory, with similar declination. All eight specimens are tightly grouped with a small values of α_{95} confidence cones (small cubes = 3.8°; large cubes = 4.1°), and large Fisher-k values (small cubes = 582.0; large cubes = 510.5). Fisher statistics for the re-deposition experiment are summarized in Table 7.1. The experiment indicates that the DRM is acquired close to the ambient magnetic field, and verifies that most inclination shallowing recorded in outcrop must be due to post-depositional effects (such as compaction, chemical alteration or viscous acquisition of remanence in the sediments subsequent to deposition). The re-deposition experiment does not replicate the shallow inclinations of the hard remanence component encountered in the naturally deposited red clays. Rather, the inclinations of the re-deposited sediments are closer to the inclination of the intermediate remanence component, although there is no certainty that the two inclinations reflect the same process of acquisition. The re-deposition experiment does however provide proof that the red clays acquire remanent magnetizations that reflect the direction of the Earth's present magnetic field during DRM.
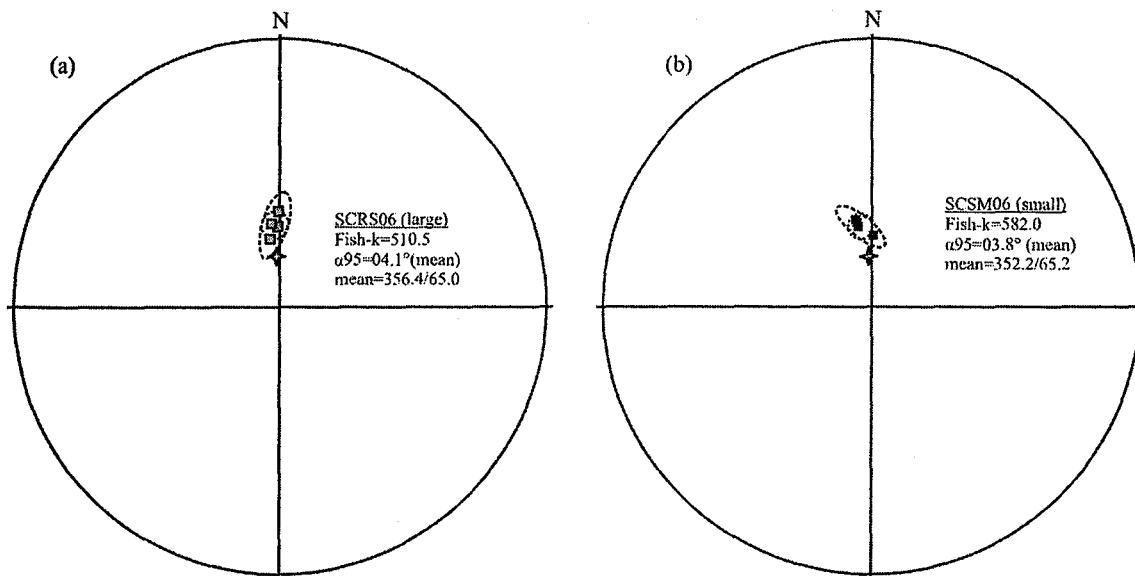
Figure 7.9 Results from re-deposition experiments with (a) large cubes and (b) small cubes. Directions for large specimens are given by the shaded squares, whereas directions for small specimens are given by closed squares. The star represents the direction of the ambient laboratory magnetic field.

Table 7.1 Fisher statistics of the re-deposition experiment

Sample	Fisher-k	α95(mean)	α95(sample)	mean decl.	mean incl.
SCRS06 125cm3 (n=4)	510.5	04.1°	08.1°	356.4	65.0
SCSM06 8cm3 (n=4)	582.0	03.8°	07.6°	352.2	65.2

7.5 The magnetostratigraphic record

The primary purpose for studying the paleomagnetic signature of Strawberry Creek sediments is to investigate their magnetostratigraphy and possibility for imprinting of paleosecular variation (PSV) originating from the non-dipole portion of the geomagnetic field. Continuous or semi-continuous deposition of sediments should act as a continuous recording of variations in the geomagnetic field. This task is complicated by evidence for two stable remanent magnetizations which were discovered during AF demagnetization. As illustrated above and in chapter 6, an intermediate remanence is carried by PSD magnetite (and possibly some MD and SD magnetite), while a hard remanent magnetization is carried by SD and PSD magnetite, as well as hematite. These two remanences show a similar stratigraphic variation of declination, whereas their inclinations are substantially different (Figure 7.10). Large variations in both declination and inclination are observed in the magnetostratigraphic profile. Declination varies more than 240° through the entire section, although the largest peaks in Figure 7.10a are abrupt and major changes in declination are noticeably at ~0.6m and ~0.9m. Large swings (>100°) of declination occur in less than 3cm of the deposited record, and the same feature is obvious with inclination showing rapid swings from high values to low values, and back again to high values. The rapid switching in declination and the shallow inclination is a matter involving a number of reasons and it is probable that compaction and paleo-current alignment of the sediments play a significant role, as do the inherent magnetic and physical properties of the ferromagnetic minerals involved. Abrupt changes in inclination and declination as shown in Figure 7.10 are more likely than not unrealistic for representation of true paleosecular variation, and the true paleomagnetic signal represented by the Earth's field is influenced by other effects.

The magnetically hard component is shallowly inclined compared to the intermediate magnetization and follows the pattern of the NRM closely throughout most of the profile (although it is probably more appropriate to conversely say that the NRM follows the pattern of the hard remanence component). As with declination, variations in the field diminish in the lower portion of the profile. The mean inclination of the intermediate remanence (~62.0°) is more than 10° steeper than the hard remanence inclination (~50.9°). These stable remanence components can be compared to a time-averaged geomagnetic field, such that short-term non-dipole effects are subdued and only the Earth's dipole moment is considered. This model is referred to as the geocentric axial dipole (GAD; McElhinny and McFadden, 2000; see discussion in chapter 4). At the latitude of Thunder Bay (48°22'N) the GAD has an inclination of ~66°N (Figure 4.4; 7.10; 7.11). In comparison, the present Earth's field (PEF) direction considering the latitude and

longitude of Thunder Bay (48°22'N, 89°19'W) has declination 356.8° and inclination 74.7° (calculated using the 10th generation of the International Geomagnetic Reference Field).
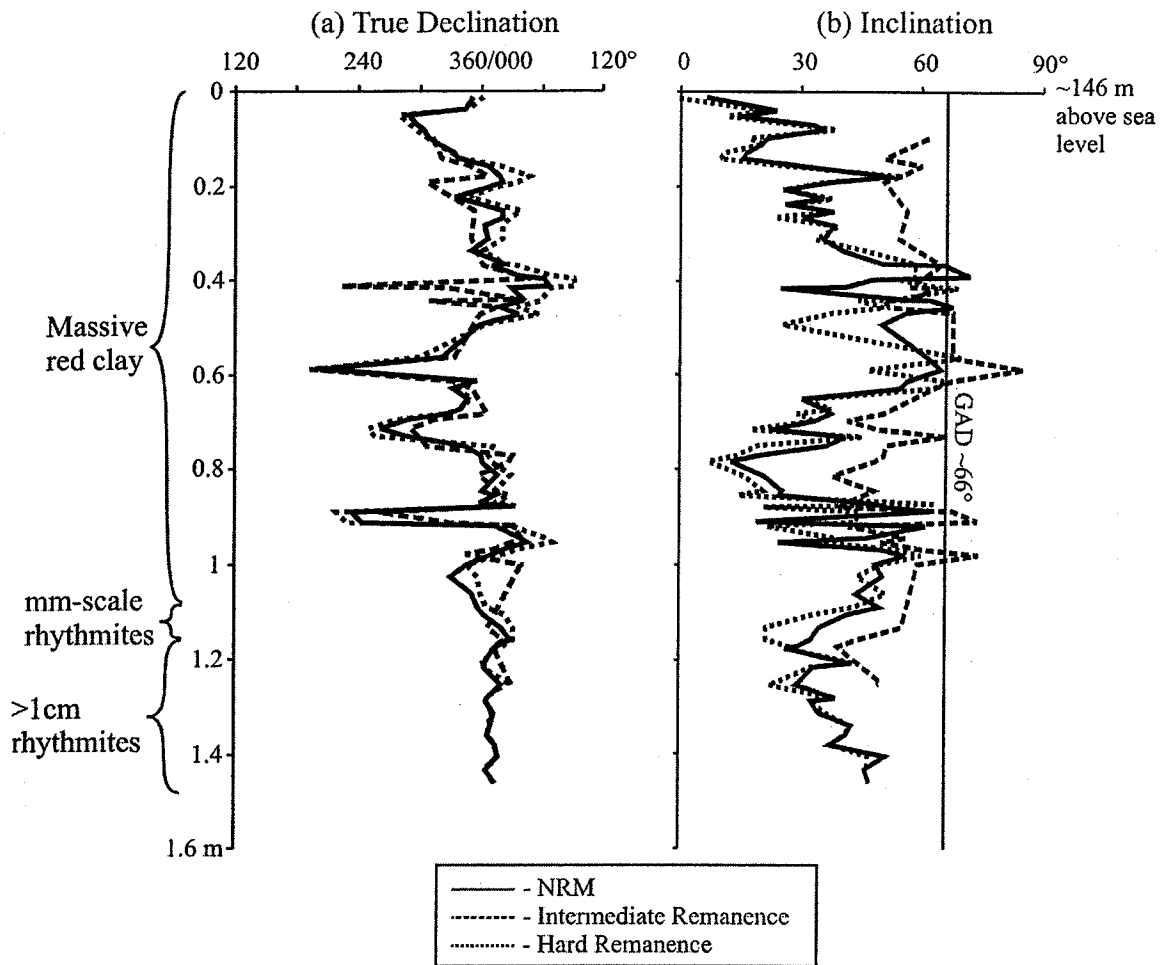
Figure 7.10 Magnetostratigraphic profiles for (a) declination and (b) inclination. The lithology of the section studied is indicated on the left-hand side. The top of the section (0m) corresponds with an elevation of ~146m above the sea level. Each profile contain the record for NRM, intermediate remanence component (Hcr=~20-40mT) and the hard remanence component (Hcr>40mT). The geocentric axial dipole (GAD) is shown with the profile for inclination for the latitude of the city of Thunder Bay, Ontario, Canada.

Both the intermediate and the hard components are therefore shallower than the GAD and PEF. The extreme shallow inclination is basis for skepticism as values sometimes drop below 20°, which separates the inclination of the sediments from the GAD by more than 40°. Rapid changes to very low inclinations are unreasonable for the latitude of northwestern Ontario and Thunder Bay, even when taking into account secular variation. Because
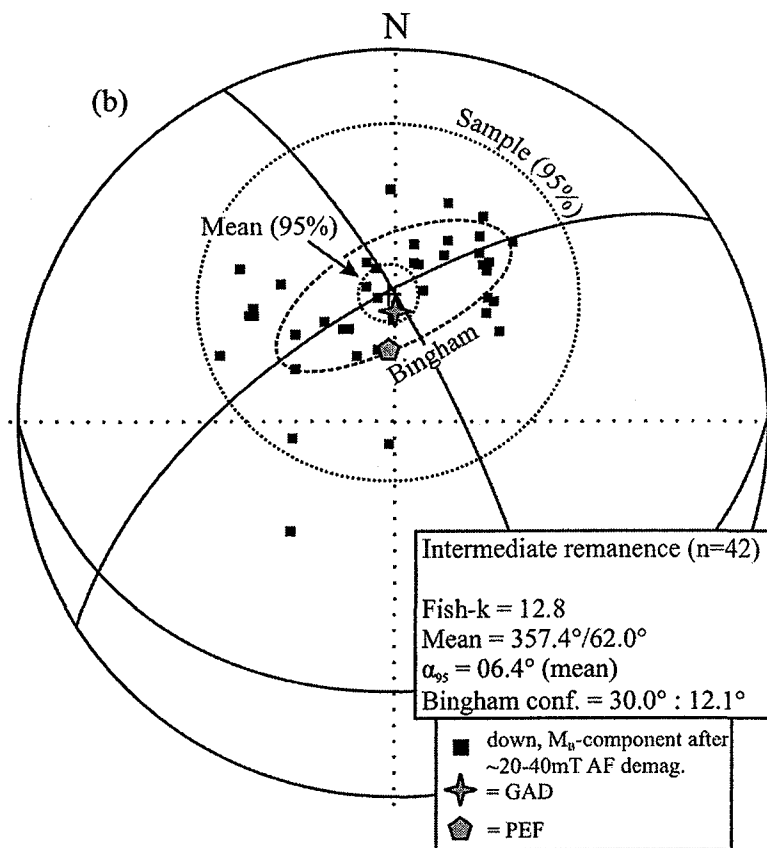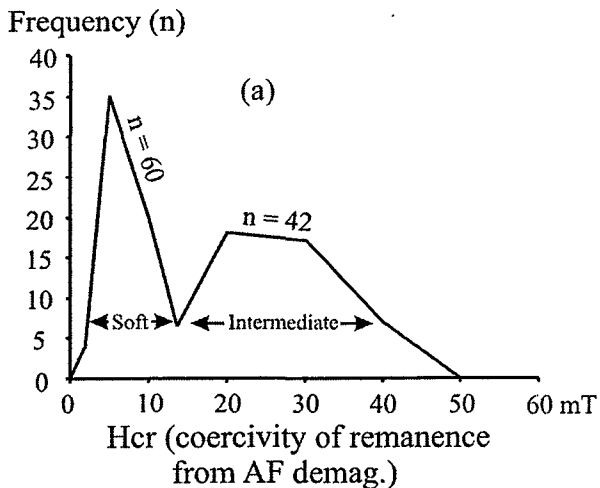
Frequency (n)

Figure 7.11 (a) Frequency histogram of unblocking remanence coercivities (mT) for the specimens shown in Figure 7.7; soft remanence component has Hcr≤10mT, intermediate remanence component has Hcr>10mT (~20-40mT). (b) Stereonet with individual intermediate remanences (n=42), accompanied by Fisher and Bingham statistics. All directions are downward (positive inclinations). The geocentric axial dipole (GAD) and the present Earth's field direction (PEF) are illustrated for reference. The solid lines within the stereonet refer to the Eigen-symmetry planes.

of short-term fluctuations in declination and inclination of the geomagnetic field, the α-95 confidence cones are large for the HR and IR samples, as shown in Figures 7.11 and 7.12. A majority of specimens (n=60) from the Strawberry Creek carries a soft or spurious remanence, over a narrow range of low coercivities (Figure 7.12a). More than half of the specimens (n=42) carry a remanence with intermediate coercivity (~20-40mT). Directions of the IR component are somewhat clustered (Fisher-k= 12.8; Figure 7.12b), and the GAD lies within the 95% confidence level of the Fisher mean. Application of Bingham statistics indicates that the distribution of IR directions is elliptical rather than spherical. The HR directions are shallower than the IR (Figure 7.10). Fisher and Bingham statistics are not as useful in describing the HR, because of the greater variation in directions displayed (Fisher-k=4.3). However, the Eigen-symmetry planes show similar orientation for the intermediate and hard remanence.

The nature of the "short-term" features is suspicious and may represent depositional characteristics of the sediments rather than the actual imprinting of the Earth's magnetic field. It is unlikely that they are evidence for some geomagnetic feature such as excursions, since there would be accompanying swings in both declination and inclination which is not evident from Figure 7.10b. Neither has there been documentation of excursions occurring during the Holocene in North America, even though many studies of Holocene paleosecular variation have been conducted using lake-sediment and terrestrial records (e.g. Lund, 1996; Banarjee et al., 1979). There is less variation in declination towards the bottom of the section, likely since the rhythmic deposits do not extend over the same amount of time as the overlying red clays. It is appropriate to apply moving averages to the data in Figure 7.10, as a low-pass filter to remove or lessen the effect of abrupt and short-term effects in the magneto-stratigraphic record. Simple moving averages (MA's) may be useful to explain long-term patterns in a time-series or a continuous data series (Borradaile, 2003), such that

$$ym_i = \frac{\sum_{i-k}^{i+k} y_i}{2k+1} \qquad \text{[Eqn. 7.2]}$$

where 2k+1 has to be an odd value. [Eqn. 7.2] is the general form for any moving average model where ym_i is new value created by the moving average. The value of k decides the order of the moving average (e.g. k=1 is a 3-point moving average, k=2 is a 5-point moving average). y_i represent the data points included in the moving average, ±k values in front and behind of y_0. The MA provides a clearer image for the patterns in declination and inclination, especially in the hard remanence data (Figure 7.13a, b; 7.14a, b, 7.15). Wave-like patterns are apparent for both the declination and inclination records, after the MA's have been applied. One complete wavelength

is present in the 5-point MA declination record (Figure 7.13b) while the 5-point MA of inclination (Figure 7.14b) also shows a wavy pattern, with almost two complete wavelengths. The intermediate component of declination (Figure 7.13c, d) and inclination (Figure 7.14c, d) do not show the same clear patterns as the hard remanence. Noticeably, the IR inclination is steeper in the 3- and 5-point MA's, as was observed in the original magneto-stratigraphic record (Figure 7.10b).
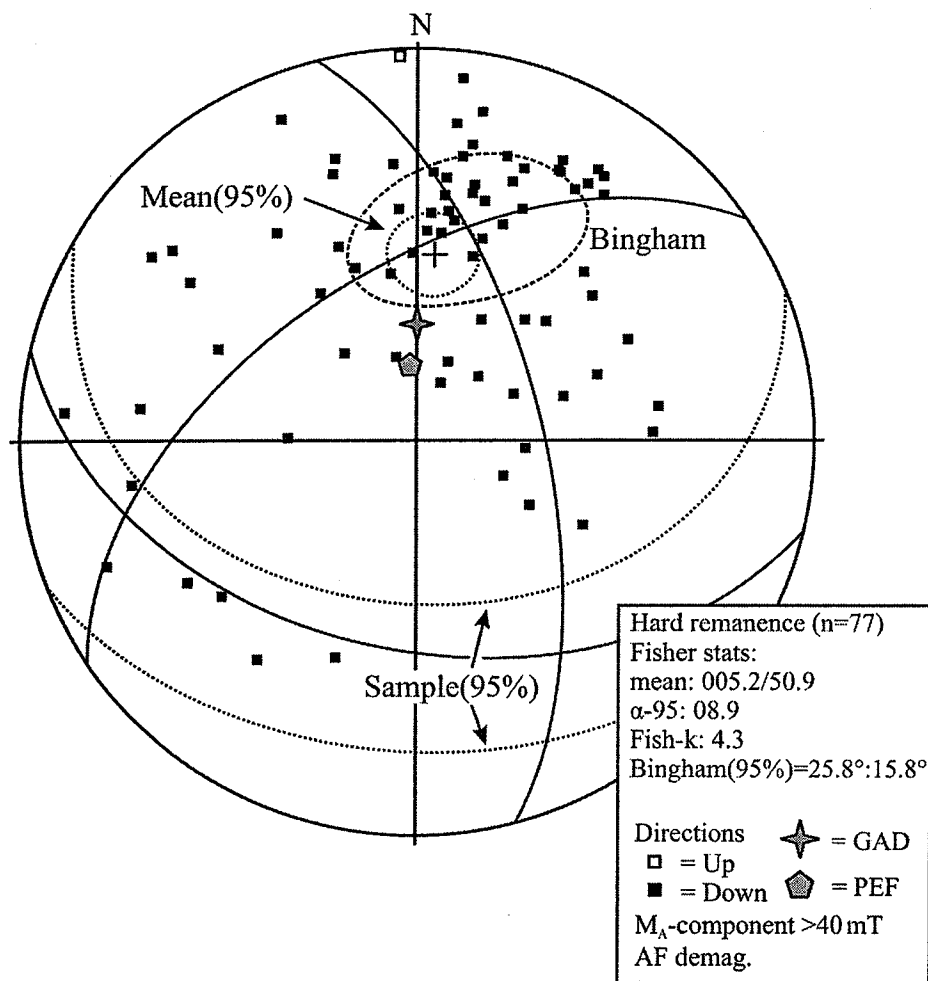
Figure 7.12 Stereonet indicating individual directions of the hard remanence, accompanied with Fisher and Bingham statistics (for 95% confidence levels of mean and sample). Open (closed) symbol denotes direction is upward (downward). Mean direction is indicated by a cross. The geocentric axial dipole (GAD) and the present Earth's field direction (PEF) are illustrated for reference. The solid lines within the stereonet refer to the Eigen-symmetry planes.
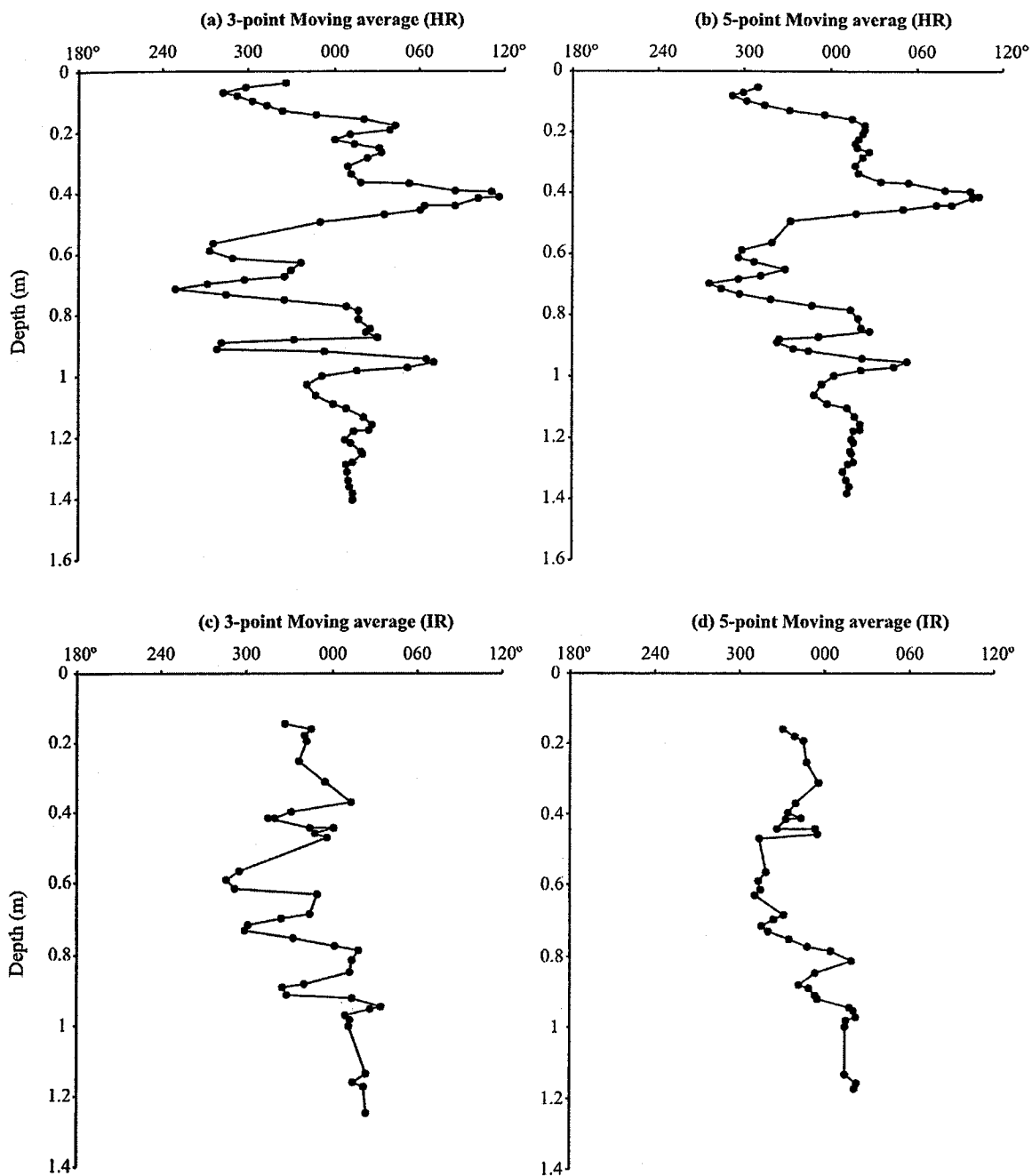
Figure 7.13 Moving averages for declination. (a) 3-point and (b) 5-point moving averages for the hard remanence component of declination. (c) and (d) are 3- and 5-point moving averages, respectively, for the intermediate remanence component of declination. HR= hard remanence; IR= Intermediate remanence.
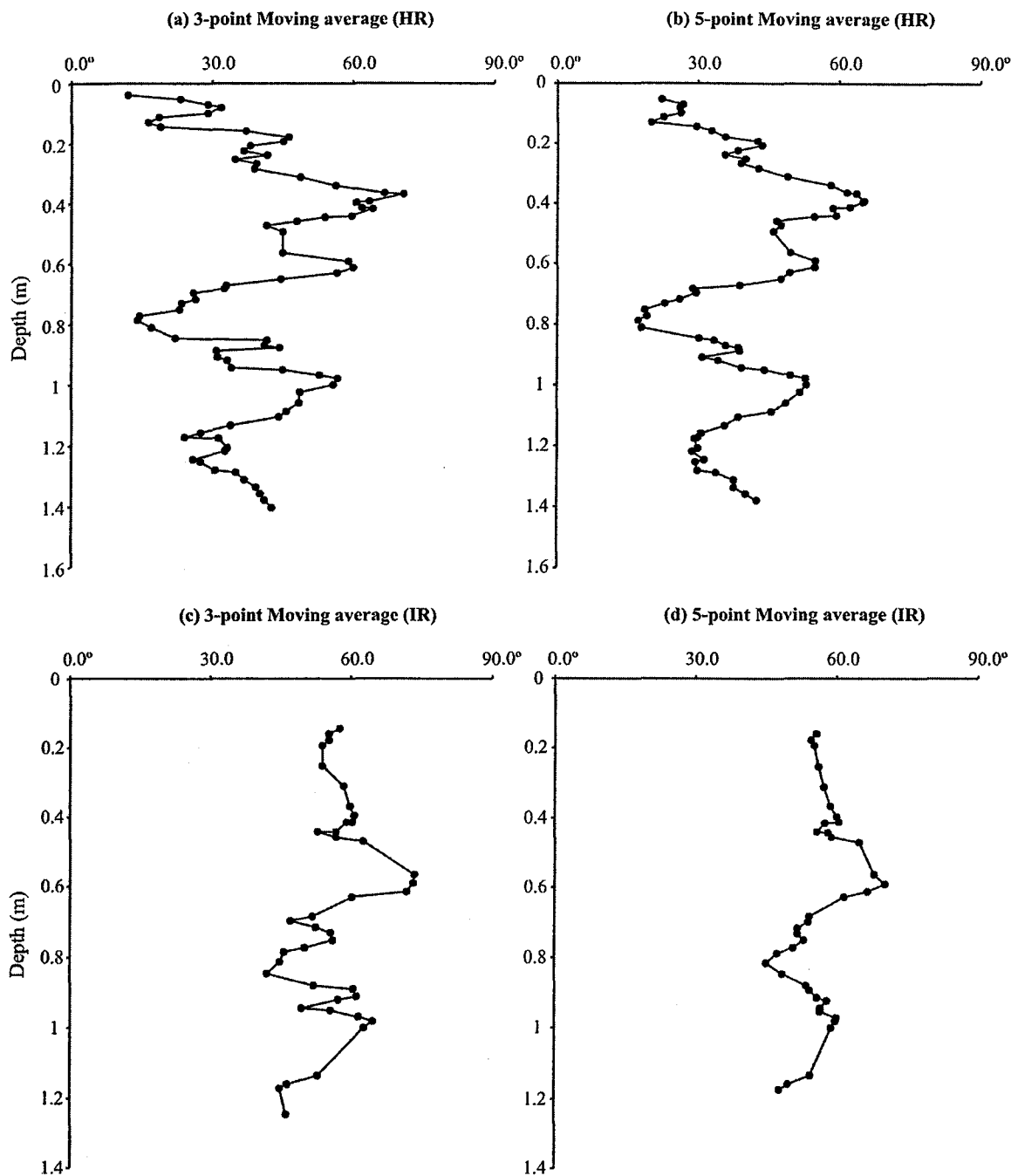
Figure 7.14 Moving averages for inclination. (a) 3-point and (b) 5-point moving averages for the hard remanence component of inclination. (c) and (d) are 3- and 5-point moving averages, respectively, for the intermediate remanence component of inclination. HR= hard remanence; IR= intermediate remanence.

Interestingly, the wave-like pattern observed in the HR is partially preserved in the IR, which may have some important consequences regarding the timing of remanence acquisition (discussed below). Declinations in the MA (3- and 5-point) show some differences between the HR and IR in the upper part of the profile. The HR swings toward the east rather drastically in comparison

with the IR. In the lower part of the profile there are not substantial differences in the MA's between the HR and IR declinations.

7.6 The timing of remanence acquisition: contemporaneous or asynchronous?

The similar declinations of the intermediate and hard remanence components suggest that they were acquired at similar or closely spaced times, together with the similar MA waveforms of the intermediate and hard inclinations. If this is this case, it is probable that separate ferromagnetic mineral phases are responsible for the intermediate and the hard remanence. Rock magnetic experiments illustrated that silts and clays have different magnetic properties. Silts have an almost exclusive influence from magnetite and only display a single vector component after demagnetization (disregarding the spurious remanence with $H_{cr} \leq 10mT$). Clays on the other hand often display two stable magnetic remanences that could originate separately from magnetite and hematite. Thus, magnetite of MD and mainly PSD size would be responsible for the intermediate remanence, while SD magnetite and mainly hematite would influence the hard remanence. It is therefore suggested here that although two components of remanence are present in the clays, they were acquired close in time, based on their magnetostratigraphic records. Tan et al. (2002) demonstrated through laboratory experiments that a mixture of coarse-grained (specularite) and fine-grained (pigmentary) hematite particles displayed two components of remanence after deposition and compaction had occurred. The hematite particles were mixed in a clay-sized matrix, and grains were deposited in the presence of a laboratory produced magnetic field and subsequently compacted. They found that the finer particles of pigmentary hematite carried a signal that resembled the actual inclination of the laboratory field, whereas the coarser-grained hematite suffered from severe inclination shallowing, by as much as 23° displaced toward the horizontal plane. The horizontal displacement becomes more severe with increasing demagnetization temperatures or alternating fields, indicating that specularite has a higher unblocking temperature and coercivity. Two important factors that influenced their results consisted of the rate of deposition and the grain-size of the sediments. The presence and amount of clay-sized particles may be one of the most influential effects on the recorded remanent magnetization of sediments (Lu et al., 1990; Deamer and Kodama, 1990; Anson and Kodama, 1987). It is likely that the presence hematite is related to the clay minerals. Hematite could be deposited as a detrital component together with the clay or it may have formed through oxidation of iron-bearing clay minerals and silicates or possibly magnetite, in the massive clays and clayey portions of the rhythmites.

(a) True declination
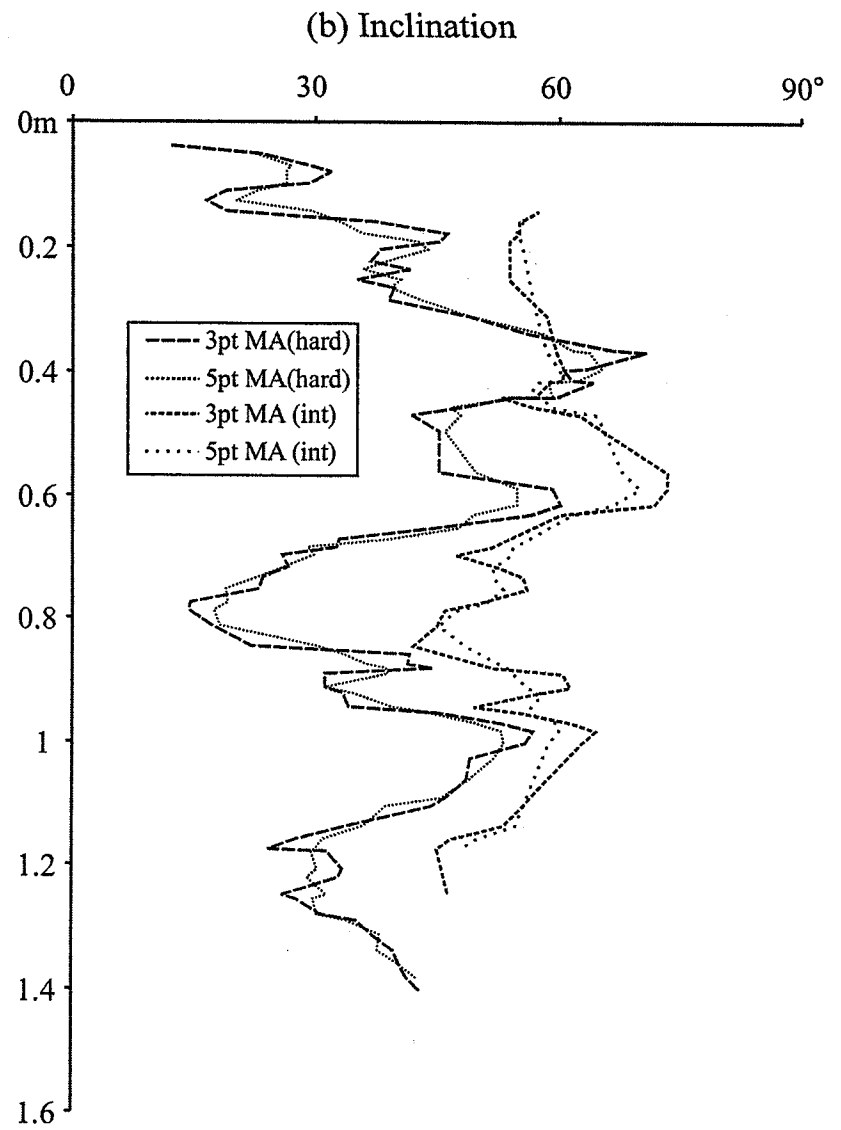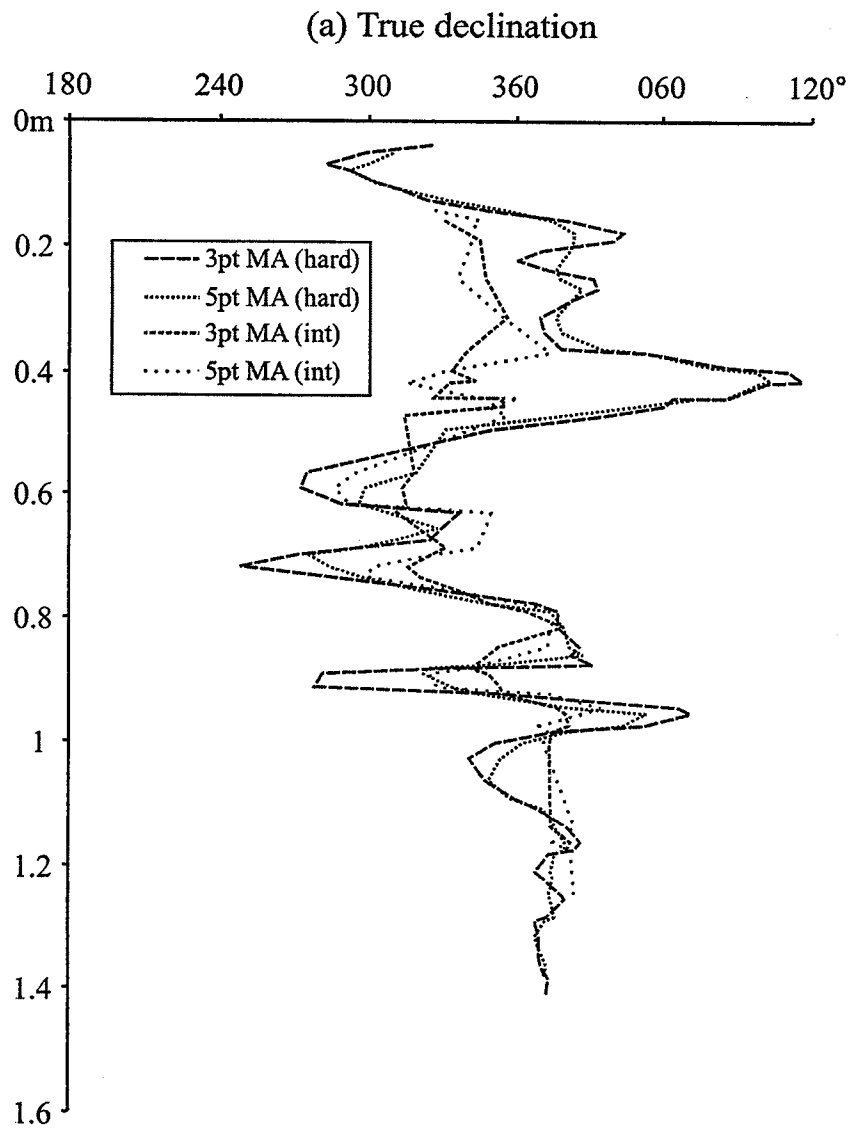
(b) Inclination

Figure 7.15 (previous page), (a) 3-point and 5-point moving averages for the declinations of the hard and intermediate remanence components. (b) 3-point and 5-point moving averages for the inclinations of the hard and intermediate remanence components.

In either case, it is clear that the any amount of hematite present in the Strawberry Creek clays is related to the hard, shallow remanence component. The alternative explanation to the timing of remanence acquisition is that one of the remanence components (HR or IR) represents a ChRM or primary magnetization while the other is a secondary remanence, acquired at a later stage. This could be the case if hematite forms diagenetically in the sediments, as a chemical remanent magnetization (CRM) or if low to intermediate coercivity magnetite (MD, PSD) acquired a viscous remanent magnetization (VRM). A chemical remanent magnetization is possible, but as shown in the magnetostratigraphic record (Figure 7.7) it is sometimes challenging to indicate the difference between the HR and IR, especially for declinations. A viscous remanence is no doubt carried by the low coercivity minerals; however, it is unusual to expect coercivities between ~20-40mT due to viscous acquisitions for the relatively short lifetime of the sedimentary sequence at Strawberry Creek (viscous remanence unblocking). In some cases, VRM has shown to acquire relatively coercive remanences during historical time periods, as has been demonstrated by elevated unblocking temperatures (rather analogous to elevated unblocking coercivity or H_{cr} in magnetite) of VRM in archaeological monuments (Maher et al., 2000; Borradaile and Almqvist, 2006).

7.7 Paleosecular variation in the Strawberry Creek section

The non-dipole moment originating in the Earth's outer core is often displayed in magnetostratigraphic records with sufficient time-resolution (i.e. sediments are deposited over a time frame which resolves the detail of paleosecular variation). Moving averages of the magnetic stratigraphy of Strawberry Creek illustrate waveform patterns which would suggest that PSV recording is preserved (Figures 7.13-15). The MA inclination record displayed in Figure 7.14 (a, b) show almost two complete wavelengths beginning from the lower portion of the profile. A wave-like pattern is less apparent in the declination MA, but can be identified showing at least one complete wavelength (Figure 7.13a, b). Intermediate remanence vectors (Figures 7.13c, d; 7.14c, d) are generally constricted around their mean value in the stratigraphic profile, compared to the hard remanences (e.g. see Figures 7.11 and 7.12). In other words, the hard remanence shows greater amplitude than the intermediate remanence. The MA inclination of the IR resembles the HR inclination, which might suggest that these two remanence vectors were acquired during the same time period and have recorded the same features of secular variation as

the hard remanence. The pattern of PSV can also be illustrated by comparing declination and inclination (5-point MA: Figure 7.13, 7.14). In Figure 7.16 the declination and inclination of NRM are plotted against each other. A rather complicated pattern is apparent, although there is coherency in the path of declination and inclination, as larger and smaller loops are distinguishable. A plot of the hard remanence declination versus inclination (Figure 7.17) illustrates a pattern of loops, with recurring loops towards the upper right (westerly declinations and steeper inclinations). A large and more undefined loop is produced in the lower left portion of Figure 7.17, towards an easterly declination and shallower inclination. Note that the loops are exaggerated towards the top of the section (e.g. extend over a larger area) compared to more constricted loops in the lower part of the section.

Another method of realizing the effect of secular variation is through application of Fisher statistics (Fisher, 1953). By calculating the Fisher means for small groups of specimens it is possible to determine average directions in relation to the position in the section. Based on the HR directions (Figure 7.12), a Fisher mean was calculated for groups of directions; each group consisting of ten specimens each, up through the profile (Figure 7.18). The groups are partially overlapping with the next, usually by five specimens, such that a coarse moving average of the Fisher mean directions is produced (e.g. the mean for specimens 1-10 are initially calculated, followed by a calculation for the mean of specimens 5-15, and so on). The resulting moving averages shown in the stereonets of Figure 7.18(a-c) illustrate that the Fisher means move in a major loop with anticlockwise drift, upwards through the section; an entire completed loop is apparent. The cones of confidence for each mean are illustrated in Figure 7.18(a, b), and the path of the actual means is shown in Figure 7.18(c). The means are displaced towards the X-Y plane of the stereonet in comparison with the PEF and GAD, because of the shallow inclinations obtained from the hard remanence component.
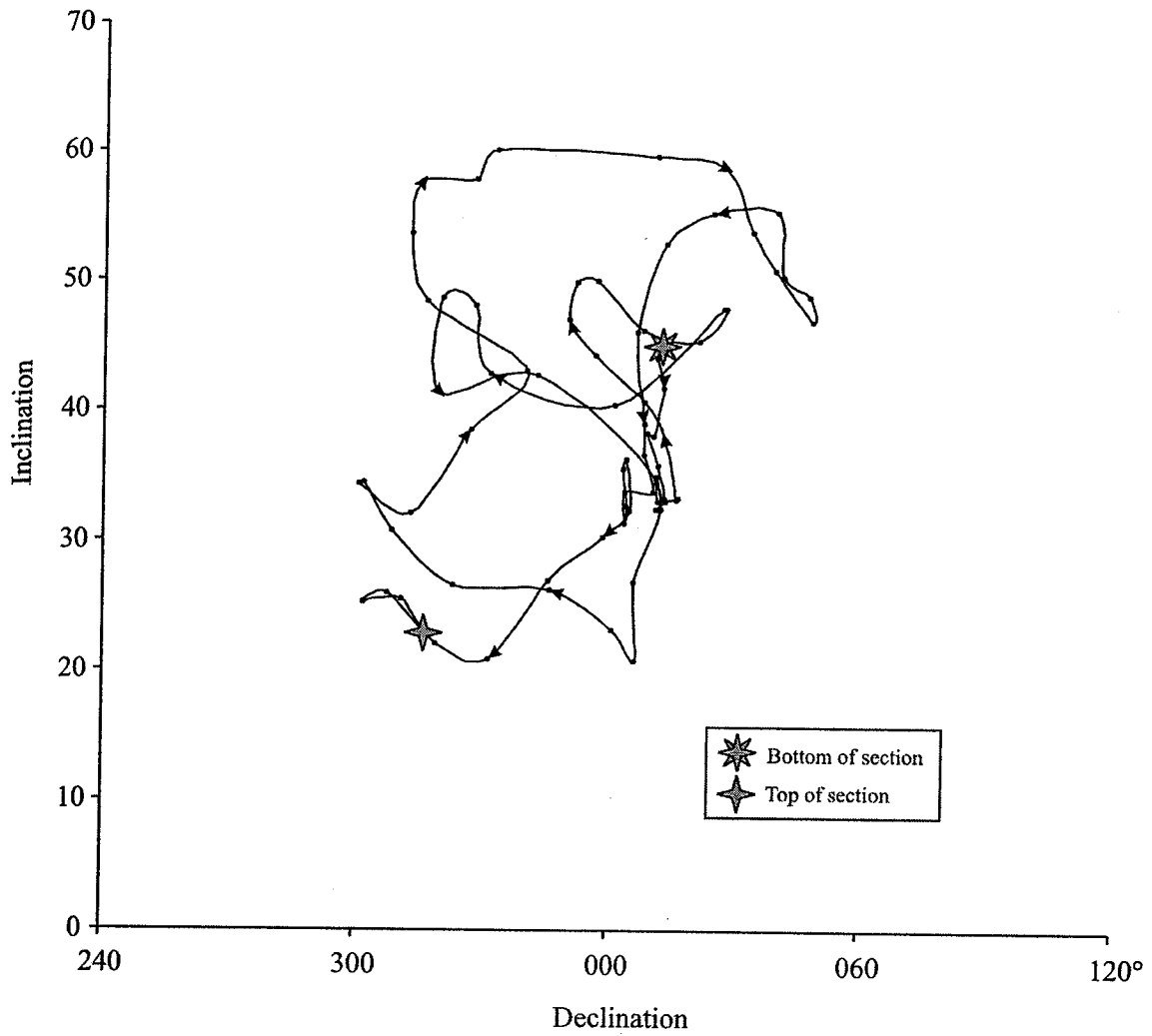
Figure 7.16 The declination and inclination of the NRM are plotted against each other. The top and bottom of the Strawberry section are given by symbols. Arrows indicate the direction towards the top of the section.
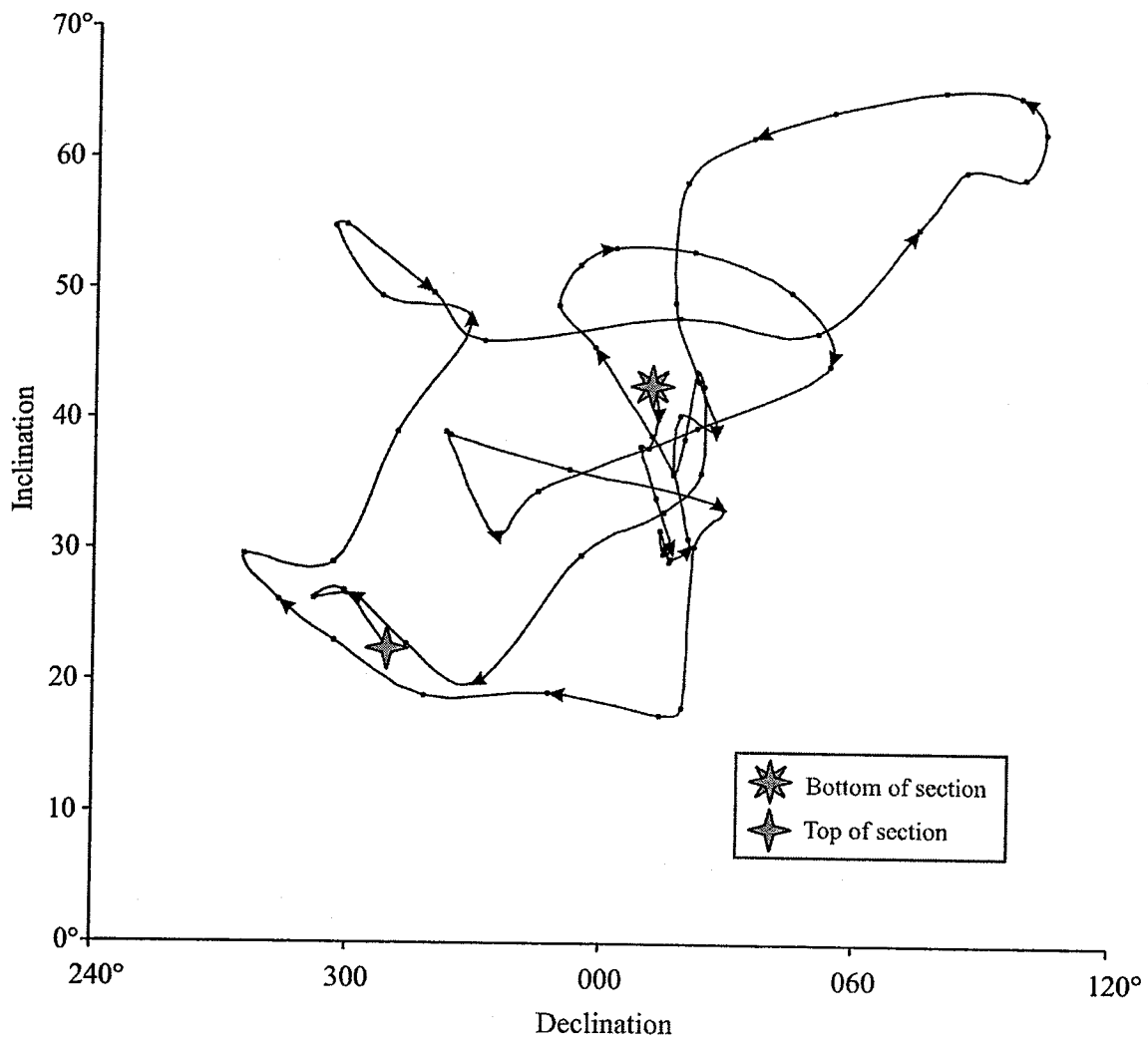
Figure 7.17 The declination and inclination of the hard remanence are plotted against each other. The top and bottom of the section is given by symbols. Arrows indicate the direction towards the top of the section.
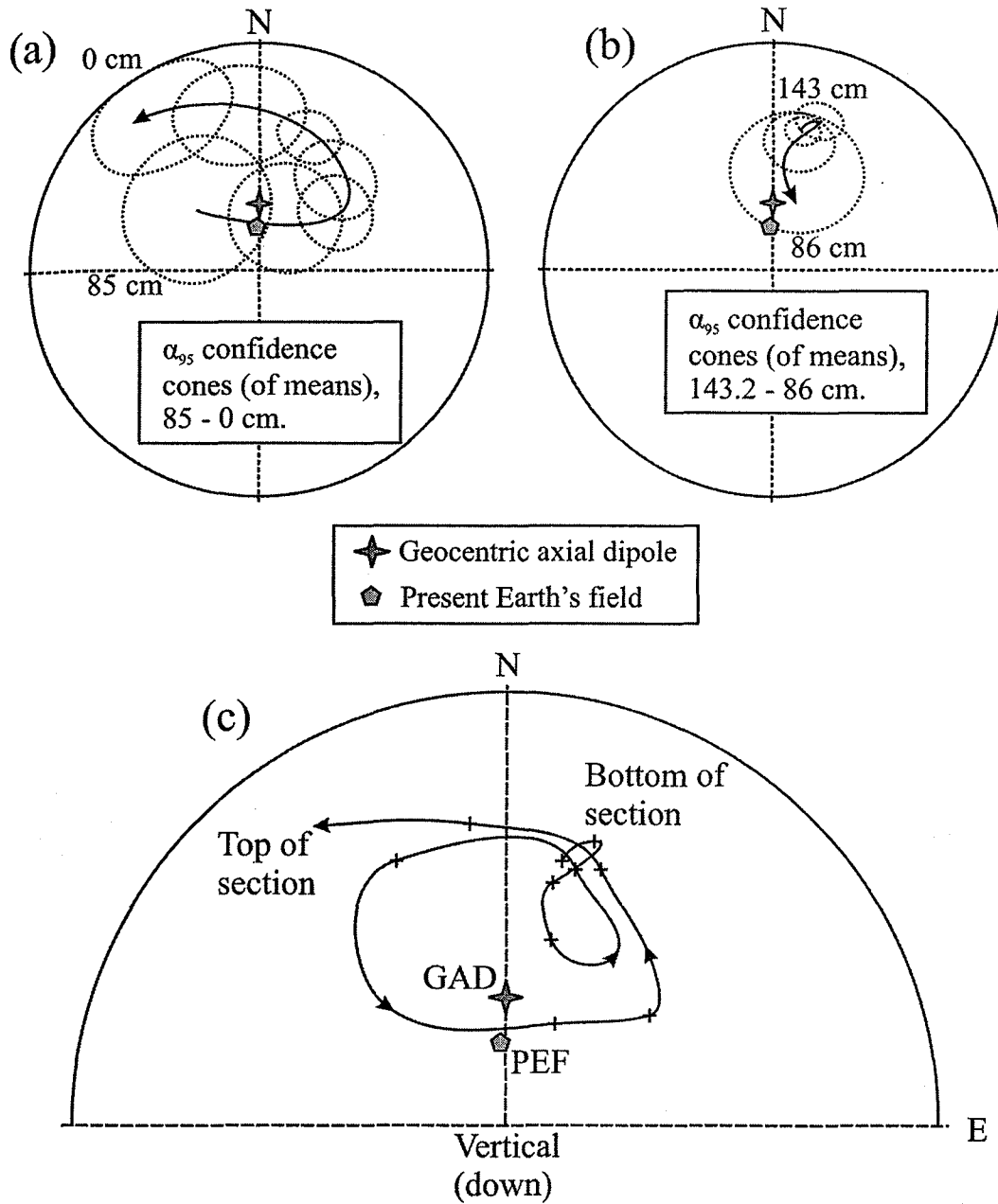
Figure 7.18 Coarse moving average of the hard remanence, using partly overlapping Fisher means (see text for explanation). The confidence cones of the samples (at 95% confidence level) are shown for (a) 0 – 85cm and (b) 86 – 143cm. (c) Shows the directions and path of the Fisher mean directions for each sample. The direction of the geocentric axial dipole (GAD) and present Earth's field (PEF) are shown by symbols.

Chapter 8: Conclusions

The study of PSV recorded by lacustrine sediments provides a measure of the geodynamo behavior at one location through time, and a correlation tool for stratigraphic and paleoclimate studies. In order to obtain this desired information it is necessary to understand (1), the magnetic mineralogy and (2), the true characteristic remanent magnetization and effects of inclination shallowing. Simply using the "raw NRM" is not appropriate to determine the characteristic remanent magnetization, and can in the worst scenario produce misleading results as has been the case in some previous studies (see Thompson and Berglund, 1976). A dry land exposure of sediments (as in this study) provides the benefits of decreased fabric disturbance as well as true declinations. Studies using lake-cores have difficulties because they use wet sediments and disoriented declinations.

Based on previous work (e.g. Zoltai, 1967; Arndt, 1977; Nielsen et al., 1982) the age of the red clays throughout northwestern Ontario is ≤9900BP, having been deposited during the Emerson Phase of lake Agassiz to the northwest and the Marquette glacial re-advance from the east (Teller and Thorleifson, 1983; Clayton, 1983). The geochemical signature of the red clay suggest that a single depositional event and common provenance is responsible for the spread of the red clays (Minning et al., 1994). At the time of deposition of the red clay flow of water was westerly from the Lake Superior basin into the Lake Agassiz basin, through the intermediary glacial Lake Kaministikwia (see Figures 1.1 – 1.4).

8.1 The magnetic fabric

AMS and AARM indicate a strong magnetic fabric in the sediments, which approaches an oblate shape ellipsoid (Figure 6.1). AMS gives the total fabric of all minerals (diamagnetic, paramagnetic and ferromagnetic). Magnetite is most important ($k_{magnetite}$ is ~1000 times larger than $k_{hematite}$), and its role is detected by comparing the normalized AMS tensor to the non-normalized AMS tensor. AARM isolates exclusively the fabric of the magnetic particles, particularly that of magnetite in this study. The

technique does not allow for the isolation or recognition of the hematite fabric, since the applied fields necessary to activate the magnetic moments of hematite cannot be achieved in the AF demagnetizater. Clays have a more eccentric AMS ellipsoid than silts. Maximum susceptibility is located in the bedding plane which nearly coincides with the horizontal plane. Minimum susceptibilities cluster around the vertical axis. Mean tensors for normalized and non-normalized susceptibilities show a preferred alignment of grains in the SE-NW directions, which is the probable paleo-current axis. This axis agrees well with the paleo-hydrology of this location at the beginning of the Holocene, as the event that led to the deposition of the characteristic red sediments throughout northwestern Ontario is related to Lake Superior overflowing northwestwardly into glacial Lake Agassiz. Bulk susceptibility (Figure 6.2) is greater in silt than in clay, as more magnetite (possibly coarser-grained) is incorporated in silts. From the AARM measurements it is evident that the ferromagnetic minerals are oriented preferably along the bedding plane. AARM and AMS also show that the bedding plane is offset a few degrees from the horizontal plane, dipping slightly to the E-SE.

8.2 The rock magnetic mineralogy

IRM is used only to verify the magnetic mineralogy because it uses a saturating magnetic field, effectively producing the maximum response of every magnetic mineral. IRM acquisition experiments show that the magnetic mineralogy comprises at least two magnetic phases, one with low and intermediate coercivities and a second with high coercivity (Figures 6.4 – 6.6). Coercivity spectra display that acquisition and demagnetization is greatest between 10 – 100mT for both silt and clay. Silt tends to saturate before 300mT indicating the presence of a low to intermediate coercivity ferromagnetic component, whereas clay continues to magnetize above 300mT, indicating a high coercivity phase. The ARM experiment (Figure 6.6) fails to illustrate the presence of hematite in the clay, but does however clearly indicate the presence of SD and PSD magnetite in both silt and clay.

Orthogonal three-axis tests (Lowrie, 1990) further constrain the choices for magnetic mineralogy and may indicate the potential contribution of different domain-structures to the NRM. Using several experimental runs with different coercivity intervals

applied along different axes the experiments suggest that SD-PSD (fine-grained) magnetite dominates in silt, whereas a small extra contribution from hematite composes the NRM in clay. Both silt and clay contain a minor component of MD magnetite (H_{cr}<10mT).

Hysteresis experiments show on average that silt is more magnetic than the clay (from M_s and M_{rs}; Figures 6.9; 6.10 and Table 6.3). Coercivity is greater in silt, but coercivity of remanence is less on average in the silt. Slight constriction (wasp-waisting) of the hysteresis loops, together with the higher coercivity of remanence in the clay corroborates the presence of two magnetic phases (magnetite and hematite). The feeble constriction is likely due to the high coercivity phase (hematite) being underrepresented compared to the low-intermediate coercivity phase (magnetite). The Day-plot (Figure 6.11) and comparison of H_c and H_{cr} (Figure 6.14) show that all magnetic minerals fall inside the parameters for PSD magnetite. Clay specimens are displaced to the right of the theoretical SD-MD mixing curves presented by Dunlop (2002a) which is most likely due to the influence of hematite (e.g. Yamazaki et al., 2003). The "squareness" (M_{rs}/M_s) versus H_c plot (e.g. Wang and Van der Voo) shows that silt responds as PSD and MD magnetite (Figure 6.13). The different magnetic properties displayed by clay and silt are apparent when examining the rock magnetic properties over depth (Figure 6.17). In particular, χ_{ARM}/χ distinguishes the coarser grain-size of magnetic particles in silt versus the finer particle size present in the clay.

8.3 The NRM and separation of the characteristic remanent magnetization

Alternating field demagnetization is necessary to identify and verify a characteristic stable vector-component in the NRM. Thermal demagnetization is not applicable in this case since unwanted chemical alteration of magnetic minerals may occur during demagnetization experiments and the unconsolidated sediment is too fragile and hydrous. Three magnetic remanences with different vectors are revealed through AF demagnetization. This isolates remanence vectors with different coercivity ranges; referred to as the low- (≤10mT), intermediate- (~20-40mT) and high coercivity (>40mT) components. They are usually clearly separable using the spin05.exe program software.

The low-coercivity component represents spurious magnetization, most likely acquired in the laboratory and has no geological importance. The intermediate remanence directions cluster about the present Earth's field (PEF) vector, although on average the inclination of the intermediate remanence component is slightly shallower than the PEF. PSD and less coercive SD magnetite are the likely remanence carriers in the case of the intermediate remanence component. The hard remanence component is shallowly inclined, much shallower than any expected field inclination at this latitude and oriented sub-parallel to the bedding plane. SD, PSD magnetite and hematite are likely responsible for this remanence component.

Large (125cm^3) specimens of clay were collected and measured with a large-specimen spinner magnetometer ("bigspin" by Molspin Ltd, UK). After measurements, the large specimens were cut into smaller cubes (8cm^3) and measured in a regular specimen-size Molspin magnetometer. Results (Figures 7.7 and 7.8) illustrate that vector directions of small specimens are consistent with large specimens, and the majority of specimens have directions plotting within the northeast quadrant of an equal area stereonet. This verifies the homogeneity of magnetic moment over the sampling scales. The large specimens were AF demagnetized prior to subdivision into smaller cubes, but demagnetization barely changed vector directions, whereas remanence intensities decreased approximately 25 – 35% from the original NRM. Small specimens coincide well with the directions of their corresponding large specimens, and α_{95} confidence cones are small (with large Fisher-k values).

Re-deposition experiments of clay in four 125cm^3 and four 8cm^3 cubes each accurately recorded the direction of the laboratory magnetic field (Figure 7.9). Sample cubes were gradually filled with a clay slurry, letting water evaporate before each new filling. Measurements were made once cubes had been completely filled. Fisher-k values exceed 500 for both large and small cubes, and the α_{95} confidence cones are ~4°, which indicates that specimens record the magnetic field consistently. The inclinations of the specimens are ~10 - 15° shallower than the laboratory field and maybe attributed to refraction. The very shallow hard remanence component identified in the natural samples, therefore clearly occurred subsequent to acquisition of the original DRM (e.g. compaction, pDRM, chemical or viscous remagnetization).

Secular variation is apparent from the magnetostratigraphic record (from Figures 7.10; 7.14 – 7.19). Oscillatory swings are most obvious in the moving average of the declination and inclination records (Figure 7.16). The pattern of the intermediate and hard remanence components in moving averages of inclination are similar but differences reflect different grain responses to compaction. The shallower inclination of the hard remanence component is probably not due to hematite since based on the orthogonal three axis tests in Chapter 6 hematite contributes <10% to the NRM. It is likely that the shallow inclination hard remanence is due to compaction, at some time after the depositional remanence has been acquired. The DRM may have been ~10° shallower than the Earth's field as re-deposition experiments show. A moving average of Fisher means of the hard component indicates steady anticlockwise drift, completing two loops or cycles. A loop with small changes in declination and inclination is identified in the lower portion of the stratigraphic sequence (in the rhythmic sediments), whereas a loop with large changes in declination and inclination is recognized in the upper portion of the sediment column. Considering the loops representing secular variation in the Earth's field, the time period expired during the deposition of the sediment column studied could range from 600 – 2400 years (Lund, 1989).

References

Anson, G. L. and Kodama, K. P. 1987. Compaction induced shallowing of the post depositional remanent magnetization in a synthetic sediment. *Geophysical Journal of the Royal Astronomical Society,* 88, 673 – 692.

Antevs, E. 1951. Glacial clay in Steep Rock Lake, Ontario, Canada. *Geological Society of America Bulletin,* 62, 1223 – 1262.

As, J. A. and Zijderveld, J. D. A. 1958. Magnetic cleaning of rocks in paleomagnetic research. *Geophysical Journal of the Royal Astronomical Society* 1, 308 – 319.

Bakhmutov, V. G. and Zagniy, G. F. Secular variation of the geomagnetic field: data from the varved clays of Soviet Karelia. *Physics of the Earth and Planetary Interiors* 63, 121 – 134.

Banarjee, S. K., Lund, S. P. and Levi, S. 1979. Geomagnetic record in Minnesota lake sediments – absence of the Gothenburg and Erieau excursions. *Geology* 7, 588 – 591.

Bando, Y., Kiyama, M., Yamamoto, N., Takada, T., Shinjo, T. and Takaki, H. 1965. Magnetic properties of alpha-Fe_2O_3 fine particles. *Journal of the Physical Society of Japan,* 20, 2086.

Barton, C. E. 1982. Spectral analysis of palaeomagnetic time series and the geomagnetic spectrum. *Philosophical Transactions of the Royal Society of London, Series A,* 306, 203 – 209.

Barton, C. E. 1989. Geomagnetic secular variation: direction and intensity. In: *The Encyclopedia of Solid Earth Geophysics,* James, D. E. (ed.), Van Nostrand Reinhold, New York, pp. 560 – 577.

Batt. C. M. 1997. The British archaeomagnetic calibration curve: an objective treatment. *Archaeometry* 39, 153 – 168.

Blakemore, R. P. 1975. Magnetotactic bacteria. *Nature,* 190, 377 – 379.

Bloxham, J. 1992. The steady part of the secular variation of the Earth's magnetic field. *Journal of Geophysical Research,* 97, 19,565 – 19,579.

Borradaile, G. J. 1994. Low-temperature demagnetisation and ice-pressure demagnetisation in magnetite and hematite. *Geophysical Journal International* 116, 571 – 584.

Borradaile, G. J. 1996. Experimental stress remagnetization of magnetite. *Tectonophysics* 261, 229 – 248.

Borradaile, G. J. 2003. *Statistics of Earth Science Data.* Springer-Verlag, Berlin, 351pp.

Borradaile, G. J. and Stupavsky, M. 1995. Anisotropy of magnetic susceptibility: Measurement schemes. *Gephysical Research Letters,* 22, 1957 – 1960.

Borradaile, G. J. and Almqvist, B. S. 2006. Installation age of limestone masonry determined from its viscous remagnetization. *Geoarchaeology,* 1, 29 – 60.

Borradaile, G. B. and Jackson, M. 2004. Anisotropy of magnetic susceptibility (AMS): magnetic petrofabric of deformed rocks. In: Martin-Hernández, F., Lüneberg, C. M., Aubourg, C. and Jackson, M. (eds), *Magnetic Fabric: Methods and Applications.* Geological Society, Special Publication 238.

Borradaile, G. J., Fralick, P. W. and Lagroix, F. 1999. Acquisition of anhysteretic remanence and tensor subtraction from AMS isolates true paleocurrent grain alignments. *In:* Tarling, D. H. and Turner, P. (eds)

Palaeomagnetism and Diagenesis in Sediments, Geological Society, London, Special Publications, 151, 139 – 145.

Borradaile, G. J., Lagroix, F. and Trimble, D. 2001. Improved isolation of archaeomagnetic signals by combined low temperature and alternating field demagnetization. *Geophysical Journal International* 147, 176 – 182.

Borradaile, G. J. Lucas, K. and Middleton, R. S. 2004. Low-temperature demagnetization isolates stable magnetic vector components in magnetite-bearing diabase. *Geophysical Journal International* 157, 526 – 536.

Borradaile, G. J. and Middleton, R. S. 2006. Proterozoic paleomagnetism in the Nipigon Embayment of northern Ontario: Pillar Lake Lava, Waweig Troctolite and Gunflint Formation tuffs. *Precambrian Research,* 144, 69 – 91.

Breckenridge, A., Johnson, T. C., Beske-Diehl, S. and Mothersill, J. S. 2004. The timing of regional lateglacial events and post-glacial sedimentation rates from Lake Superior. *Quaternary Science Reviews* 23, 2355 – 2367.

Buchan, K. 1978. Magnetic overprinting in the Thanet gabbro complex, Ontario. *Canadian Journal of Earth Science* 15, 1407 – 1421.

Bullard, E. C., Freedman, C., Gellman, H. and Nixon, J. 1950. The westward drift of the Earth's magnetic field. *Philosophical Transactions of the Royal Society of London, Series A,* 243, 67 – 92.

Burwasser, G. J. 1977. Quaternary geology of the city of Thunder Bay and vicinity, district of Thunder Bay. *Ontario Geological Survery Report* GR164, 70p.

Butler, R. F. 1992. *Paleomagnetism: Magnetic domains to geologic terranes.* Blackwell, Oxford, 319pp.

Chang, S. R. and Kirschvink, J. L. 1989. Magnetofossils, the magnetization of sediments and the evolution of magnetite biomineralization. *Annual Review of Earth and Planetary Sciences,* 17, 169 – 195.

Chikazumi, S. 1964. *Physics of Magnetism.* John Wiley, NewYork, 554p.

Cisowski, S. 1981. Interacting vs. non-interacting single domain behavior in natural and synthetic samples. *Physics of the Earth and Planetary Interiors,* 26, 56 – 62.

Clark, A., Tarling, D. and Noël, M. 1988. Developments in archaeomagnetic dating in Great Britain. *Journal of Archaeological Science,* 15, 645 – 667.

Clayton. L. 1983. Chronology of Lake Agassiz draining to Lake Superior. In: Teller, J. T. and Clayton, L. eds., *Glacial Lake Agassiz*: Geological Association of Canada Special Paper 26, p.291-307.

Collinson, D. W. 1965. Origin of remanent magnetization and initial susceptibility of certain red sandstones. *Geophysical Journal of the Royal Astronomical Society* 9, 203 – 217.

Collinson, D. W. 1967. Chemical demagnetization. . In *Methods in Palaeomagnetism* (D. W. Collinson, K. M. Creer, S. K. Runcorn, Eds.), pp. 256 – 286, Elsevier, New York.

Collinson, D. W. 1983. *Methods in Rock Magnetism and Palaeomagnetism.* Chapman Hall, London, 503 pp.

Collombat, H., Rochette, P. and Kent, D. V. 1993. Detection and correction of inclination shallowing in deep sea sediments using the anisotropy of anhysteretic remanence. *Bulletin de la Société Géologique de France,* 164, 103 – 111.

Creer, K. M. 1959. A.C. demagnetization of unstable Triassic Keuper marls from S.W. England. *Geophysical Journal of the Royal Astronomical Society* 2, 261.

Creer, K. M. 1985. Review of lake sediment paleomagnetic data. *Geophysical Surveys* 7, 125 – 160.

Creer, K. M. and Tucholka, P. 1982. Construction of type curves of geomagnetic secular variation for dating lake sediments from east central North America. *Canadian Journal of Earth Sciences*, 19, 1106 – 1115.

Dankers, P. H. M. and Zijderveld, J. D. A. 1981. Alternating field demagnetization of rocks, and the problem of gyromagnetic remanence. *Earth and Planetary Science Letters* 53, 89 – 92.

Davis, D. W. and Sutcliffe, R. H. 1985. U-Pb ages from the Nipigon "Plate" (sic) and northern Lake Superior. *Geological Society of America Bulletin*, 96, 1572 – 1579.

Day, R., Fuller, M. and Schmidt, V. A. 1977. Hysteresis properties of titanomagnetites: grain size and composition dependence. *Physics of the Earth and Planetary Interiors*, 13, 260 – 267.

Deamer, G. A. and Kodama, K. P. 1990. Compaction-induced inclination shallowing in synthetic and natural clay-rich sediments. *Journal of Geophysical Research*, 95, 4511 – 4530.

Dekkers, M. J. 1988. *Some rockmagnetic parameters for natural goethite, pyrrhotite and fine-grained hematite*. PhD Thesis, University of Utrecht, 231 pp.

Dekkers, M. J. and Linssen, J. H. 1989. Rockmagnetic properties of fine-grained natural low-temperature haematite with reference to remanence acquisition mechanisms in red beds. *Geophysical Journal International*, 99, 1 – 18.

Diaz-Ricci, J. C. and Kirschvink, J. L. 1992. Magnetic domain state and coercivity predictions for biogenic greigite (Fe_3S_4): A comparison of theory with magnetosome observations. *Journal of Geophysical Research* 97, 17,309 – 17,315.

Dunlop, D. J. 1970. Hematite: intrinsic and defect ferromagnetism. *Science*, 169, 858 – 860.

Dunlop, D. J. 1971. Magnetic properties of fine-particle hematite. *Annales de Géophysique*, 27, 269 – 293.

Dunlop, D. 1979. On the use of Zijderveld vector diagrams in multicomponent paleomagnetic studies. *Physics of the Earth and Planetary Interiors* 20, 12 – 24.

Dunlop, D. J. 1986. Coercive forces and coercivity spectra of submicroscopic magnetites. *Earth and Planetary Science Letters*, 78, 288 – 295.

Dunlop, D. J. 2002a. Theory and application of the Day plot (M_{rs}/M_s versus H_{cr}/H_c) 1. Theoretical curves and tests using titanomagnetite data. *Journal of Geophysical Research*, 107, 10.1029/2001JB000486.

Dunlop, D. J. 2002b. Theory and application of the Day plot (M_{rs}/M_s versus H_{cr}/H_c) 2. Application to data for rocks, sediments and soils. *Journal of Geophysical Research*, 107, 10.1029/2001JB000487.

Dunlop, D. J. and Özdemir, Ö. 1993. Thermal demagnetization of VRM and pTRM of single domain magnetite: no evidence for anomalously high unblocking temperatures. *Geophysical Research Letters* 20, 1939 – 1942.

Dunlop, D. J. and Özdemir, Ö. 1997. *Rock Magnetism: Fundamentals and Frontiers*. Cambridge University Press, Cambridge, 573 pp.

Evans, M. E. and Heller, F. 1994. Magnetic enhancement and paleoclimate: Study of a loess/paleosol couplet across the Loess Plateau of China. *Geophysical Journal International,* 117, 257 – 264.

Evans, M. E. and Heller, F. 2003. *Environmental Magnetism.* Academic Press, Amsterdam, 299pp.

Evans, M. E. and Hoye, G. S. 2005. Archaeomagnetic results from southern Italy and their bearing on geomagnetic secular variation. *Physics of the Earth and Planetary Interiors,* 151, 155 – 162.

Fralick, P., Davis, D. W. and Kissin, S. A. 2002. The age of the Gunflint Formation, Ontario, Canada: single zircon U-Pb age determinations from

Fuller, M., Cisowski, S., Hart, M., Haston, R., Schmidtke, E. and Jarrard, R. 1988. NRM: IRM(s) demagnetization plots; an aid to the interpretation of natural remanent magnetization. *Geophysical Research Letters,* 15, 518 – 521.

Graham, J. W. 1949. The stability and significance of magnetism in sedimentary rocks. *Journal of Geophysical Research,* 54, 131 – 167.

Gravenor, C. P. and Coyle, D. A. 1984. Origin and magnetic fabric of glacial varves, Nottawasaga River, Ontario, Canada. *Canadian Journal of Earth Sciences* 22, 291 – 294.

Gravenor, C. P., Symons, D. T. A. and Coyle, D. A. 1984. Errors in the anisotropy of magnetic susceptibility and magnetic remanence of unconsolidated sediments produced by sampling methods. *Geophysical Research Letters* 1 (9), 836 – 839.

Green, J. C. 1983. Geologic and geochemical evidence for the development of the Middle Proterozoic (Keweenawan) Midcontinent Rift of North America. In: Morgan, P. and Baker, B. H. (Eds), *Processes of Continental Rifting. Tectonophysics,* 94, 413 – 437.

Griffiths, D. H., King, R. F., Rees, A. I. and Wright, A. E. Remanent magnetism of some recent varved sediments. *Proceedings of the Royal Society of London* 256, 359 – 383.

Hagee, V. L. and Olson, P. 1989. An analysis of paleomagnetic secular variation in the Holocene. *Physics of the Earth and Planetary Interiors,* 56, 266 – 284.

Halls, H. C. 1976. A least-squares method to find a remanence direction from converging remagnetization circles. *Geophysical Journal of the Royal Astronomical Society,* 132, 297 – 304.

Halls, H. C. 1978. The use of converging remagnetization circles in paleomagnetism. *Physics of the Earth and Planetary Interiors,* 16, 1 – 11.

Halls, H. C. 1979. Separation of multicomponent NRM: combined use of difference and resultant magnetization vectors. *Earth and Planetary Science Letters* 43, 303 – 308.

Hanna, R. L. and Verosub, K. L. 1988. A 3500-year paleomagnetic record of late Holocene secular variation from Blue Lake, Idaho. *Geophysical Research Letters,* 15, 685 – 688.

Hanna, R. L. and Verosub, K. L. 1989. A review of lacustrine paleomagnetic records from western North America: 0 – 40,000 years BP. *Physics of the Earth and Planetary Interiors* 56, 76 – 95.

Hartl, P. and Tauxe, L. 1996. A precursor to the Matuyama/Brunhes transition-field instability as recorded in pelagic sediments. *Earth and Planetary Science Letters* 138, 121 – 135.

Hillhouse, J. W. 1977. A method for the removal of rotational remanent magnetization acquired during alternating field demagnetization. *Geophysical Journal of the Royal Astronomical Society* 50, 29 – 34.

Hodych, J. P. 1991. Low-temperature demagnetization of saturation remanence in rocks bearing multidomain magnetite. *Physics of the Earth and Planetary Interiors*, 66, 144 – 152.

Hodych, J. P. 1996. Inferring domain state from magnetic hysteresis in high coercivity dolerites bearing magnetite with ilmenite lamellae. *Earth and Planetary Science Letters*, 132, 523 – 533.

Hodych, J. P. and Buchan, K. L. 1994. Early Silurian paleolatitude of the Springdale Group redbeds of central Newfoundland: a paleomagnetic determination with a remanence anisotropy test for inclination error.

Hoffman, K. and Day, R. 1978. Separation multi-component NRM: a general method. *Earth and Planetary Science Letters* 40, 433 – 438.

Hrouda, F. 1982. Magnetic anisotropy and its application in geology and geophysics. *Geophysical Surveys*, 5, 37 – 82.

Hudson, M. R., Reynolds, R. L. and Fishman, N. S. 1989. Synfolding magnetization on the Jurassic Preuss sandstone Wyoming-Idaho-Utah thrust belt. *Journal of Geophysical Research*, B94, 13, 13,681 – 13,705

Irving, E. and Major, A. 1964. Post depositional detrital remanent magnetization in a synthetic sediment. *Sedimentology* 3, 135 – 143.

Ising, G. 1941. On the magnetic properties of varved clay. *Arkiv för Matematik, Astronomi och Fysik*, 29, 1 – 37.

Ising, G. 1942. Den varviga lerans magnetiska egenskaper. *Geologiska Föreningens i Stockholm Förhandlingar*, 64, 126 – 142.

Jackson, M. 1991. Anisotropy of magnetic remanence: a brief review of mineralogical sources, physical origins, and geological applications, and comparison with susceptibility anisotropy. *Pure and Applied Geophysics*, 136, 1-28.

Jackson, M., Banarjee, S. K., Marvin, J. A., Lu, R. and Gruber, W. 1991. Detrital remanence, inclination errors, and anhysteretic remanence anisotropy: quantitative model and experimental results. *Geophysical Journal International*, 104, 95 – 103.

Katari, K. and Tauxe, L. 2000. Effects of pH and salinity on the intensity of magnetization in redeposited sediments. *Earth and Planetary Science Letters*, 181, 489 – 486.

Katari, K. and Bloxham, J. 2001. Effects of sediment aggregate size on DRM intensity: a new theory. *Earth and Planetary Science Letters*, 186, 113 -122.

Katari, K., Tauxe, L. and King. J. 2000. A reassessment of post-depositional remanent magnetism: preliminary experiments with natural sediments. *Earth and Planetary Science Letters*, 183, 147 – 160.

Kent, D. V. 1973. Post depositional remanent magnetism in deep sea sediments. *Nature*, 246, 32 – 34.

King, J. 1996. Magnetic properties of arrays of magnetite particles produced by the method of electron beam lithography (EBL). *PhD Thesis*, University of Edinburgh.

King, J., Banarjee, S. K. Marvin, J. and Özdemir, Ö. 1982. A comparison of different magnetic methods for determining the relative grain size of magnetite in natural materials: some results from lake sediments. *Earth and Planetary Science Letters* 59, 404 – 419.

King, R. F. 1955. The remanent magnetism of artificially deposited sediments. *Monthly Notices of the Royal Astronomical Society, Geophysical Supplement*, 7, 115 – 134.

Kirschvink, J. L. 1978. The Precambrian-Cambrian boundary problem: Paleomagnetic directions from the Amadeus Basin, central Australia. *Earth and Planetary Science Letters,* 40, 91 – 100.

Kirschvink, J. L. 1980. The least-squares line and plane and the analysis of palaeomagnetic data. *Geophysical Journal of the Royal Astronomical Society* 62, 699 – 718.

Kirschvink, J. L. and Lowenstam, H. A. 1979. Mineralization and magnetization of chiton teeth: paleomagnetic, sedimentologic and biologic implications of organic magnetite. *Earth and Planetary Science Letters,* 44, 193 – 204.

Kodama, K. P. and Sun, W. W. 1992. Magnetic anisotropy as a correction for compaction-caused paleomagnetic inclination shallowing. *Geophysical Journal International,* 111, 465 – 469.

Kovacheva, M. and Zagniy, G. 1985. Archaeomagnetic results from some prehistoric sites in Bulgaria. *Archaeometry,* 27, 179 – 184.

Kovacheva, M., Jordanova, N. and Karloukovski, V. 1998. Geomagnetic field variation as determined from Bulgarian archaeomagnetic data. Part II: The last 8000 years. *Surveys in Geophysics,* 19, 431 – 460.

Kruiver, P. P., Dekkers, M. J. and Langereis, C. G. 2000. Secular variation in Permian red beds from Dôme de Barrot, SE France. *Earth and Planetary Science Letters,* 179, 205 – 217.

Larson, E. E., Walker, T. R., Patterson, P. E., Hoblitt, R. P. and Rosenbaum, J. G. 1982. Paleomagnetism of the Moenkopi formation, Colorado Plateau: Basis for long-term model of acquisition of chemical remanent magnetism in red beds. *Journal of Geophysical Research,* 87, 1081 – 1106.

Lovley, D. R., Stoltz, J. F., Nord, G. L. and Phillips, E. J. P. 1987. Anaerobic production of magnetite by a dissimilatory iron-reducing microorganism. *Nature,* 330, 252 – 254.

Lowrie, W. 1990. Identification of ferromagnetic minerals in a rock by coercivity and unblocking temperature properties. *Geophysical Research Letters* 17, 159 – 162.

Lowrie, W. 1997. *Fundamentals of Geophysics.* Cambridge University Press, United Kingdom, 354 pp.

Lowrie, W. and Fuller, M. 1971. On the alternating field demagnetization characteristics of multidomain thermoremanent magnetization in magnetite. *Journal of Geophysical Research* 76, 6339 – 6349.

Løvlie, R. 1974. Post-depositional remanent magnetization in a re-deposited deep-sea sediment. *Earth and Planetary Science Letters* 21, 315 – 320.

Løvlie, R. and Torsvik, T. 1984. Magnetic remanence and fabric properties of laboratory-deposited hematite bearing sandstone. *Geophysical Research Letters* 11, 221 – 224.

Lu, R., Banarjee, S. and Marvin, J. 1990. Effects of clay mineralogy and the electrical conductivity of water on the acquisition of depositional remanent magnetism in sediments. *Journal of Geophysical Research B* 95, 4531 – 4538.

Lund, S. P. 1985. A comparison of the statistical secular variation recorded in some late Quaternary lava flows and sediments, and its implications. *Geophysical Research Letters,* 12, 251 – 254.

Lund, S. P. 1989. Paleomagnetic secular variation. In: *Encyclopedia of Solid Earth Geophysics,* edited by James, D. pp. 476 – 488. Von Nostrand Rheinhold, New York.

Lund, S. P. 1996. A comparison of Holocene paleomagnetic secular variation records from North America. *Journal of Geophysical Research,* 101, 8007 – 8024.

Lund, S. P. and Keigwin, L. 1994. Measurement of the degree of smoothing in sediment paleomagnetic secular variation records: an example from late Quaternary deep-sea sediments of the Bermuda Rise, western North Atlantic Ocean. *Earth and Planetary Science Letters* 122, 317 – 330.

Lund, S. P. and Banarjee, S. K. 1985. Late Quaternary paleomagnetic field secular variation from two Minnesota lakes. *Journal of Geophysical Research* 90, 803 – 825.

Lund, S. P., Liddicoat, J. C., Lajoie, K. R., Henyey, T. L. and Robinson, S. W. 1988. Paleomagnetic evidence for the long-term (10^4 year) memory and periodic behavior in the Earth's core dynamo process. *Geophysical Research Letters,* 15, 1101 – 1104.

Maher, L., Borradaile, G. J., Stewart, J. D. & O'Connor, M., 2000. Primary or secondary insertion of the Romanesque Frieze at Lincoln Cathedral, England? Magnetic considerations. *Archaeometry,* 42: 225-236.

Maksymchuk, V. 2001. A study of the geomagnetic secular variation in Europe. *Contributions of Geophysics and Geodesy* 31, 285 – 289.

McCabe, C., Jackson, M. and Ellwood, B. B. 1985. Magnetic anisotropy in the Trenton limestone: results of a new technique, anisotropy of anhysteretic susceptibility. *Geophysical Research Letters,* 12, 333 – 336.

McElhinny, M. W. and McFadden, P. L. 2000. *Paleomagnetism: Continents and oceans.* Harcourth/Academic Press, United States of America, 386pp.

McElhinny, M. W. and Senanayake, W. E. 1982. Variation in the geomagnetic dipole I: The past 50,000 years. *Journal of Geomagnetism and Geoelectricity* 34, 39 – 51.

Merrill, R. T. and McElhinny, M. W. 1977. Anomalies in the time-averaged paleomagnetic field and their implications for the lower mantle. *Reviews in Geophysics and Space Physics,* 13, 687 - .

Merrill, R. T. and McElhinny, M. W. 1983. *The Earth's Magnetic Field: Its History, Origin and Planetary Perspective.* Academic Press, London, 412 pp.

Merrill, R. T., McElhinny, M. W. and McFadden, P. L. 1998. *The magnetic field of the Earth: Paleomagnetism, the core, and the deep mantle.* Academic Press, United States of America, 531pp.

Middleton, M. F. and Schmidt, P. W. 1982. Paleothermometry of the Sydney basin. *Journal of Geophysical Research* 87, 5351 - 5359.

Minning, G. V., Cowan, W. R., Sharpe, D. R. and Warman, T. A. 1994. Quaternary geology and drift composition, Lake of the Woods region, northwestern Ontario. *Geological Survey of Canada Memoir,* 436, 216p.

Moskowitz, B. M., Frankel, R. B. and Bazylinski, D. A. 1993. Rock magnetic criteria for the detection of biogenic magnetite. *Earth and Planetary Science Letters* 120, 283 – 300.

Mothersill, J. 1979. The paleomagnetic record of the late quaternary sediments of Thunder Bay. *Canadian Journal of Earth Science,* 16, 1016 – 1023.

Mothersill, J. 1981. Late Quaternary paleomagnetic record of the Goderich Basin, Lake Huron. *Canadian Journal of Earth Sciences,* 18, 448 – 456.

Mothersill, J. 1985. Batchawana Bay, Lake Superior: late Quaternary sedimentary fill and paleomagnetic record. *Canadian Journal of Earth Sciences,* 22, 39 – 52.

Mothersill, J. 1988. Paleomagnetic dating of late glacial and postglacial sediments in Lake Superior. *Canadian Journal of Earth Sciences*, 25, 1791 – 1799.

Muxworthy A. R. and McClelland, E. 2000a. Review of the low-temperature magnetic properties of magnetite from a rock magnetic perspective. *Geophysical Journal International* 140, 101 – 114.

Muxworthy, A. R. and McClelland, E. 2000b. The causes of low-temperature demagnetization of remanence in multidomain magnetite. *Geophysical Journal International* 140, 115 – 131.

Mörner, N.-A. and Lanser, J. P. 1974. Gothenburg magnetic 'flip'. *Nature* 251, 408 – 409.

Mörner, N.-A., Lanser, J. P. and Hospers, J. 1971. Late Weichselian palaeomagnetic reversal. *Nature* 234, 173 – 174.

Nagata, T. 1961. *Rock Magnetism*. Mazuren, Tokyo.

Néel, L. 1955. Some theoretical aspects of rock-magnetism. *Advances in Physics* 4, 191 – 243.

Nielsen, E., McKillop, W. B. and McCoy, J. P. 1982. The age of the Hartmann moraine and the Campbell beach of Lake Agassiz in northwestern Ontario. *Canadian Journal of Earth Sciences*, 19, 1933 – 1937.

Nye, J. F. 1957. *Physical Properties of Crystals: Their Representation by Tensors and Matrices*. Oxford University Press, New York.

Ojala, A. E. K. and Saarinen, T. 2002. Palaeosecular variation of the Earth's magnetic field during the last 10,000 years based on the annually laminated sediment of Lake Nautajärvi, central Finland. *The Holocene* 12, 391 – 400.

Ojala, A. E. K. and Saarnisto, M. 1999. Comparative varve counting and magnetic properties of the 8400-yr sequence of an annually laminated sediment in Lake Valkiajärvi, central Finland. *Journal of Paleolimnology*, 22, 335 – 348.

Opdyke, N. D. and Channell, J. E. T. 1996. *Magnetic Stratigraphy*. Academic Press, Inc.

O'Reilly, W. 1984. *Rock and Mineral Magnetism*. Blackie, Glasgow, 230pp.

Ouliac, M. 1976. Removal of secondary magnetization from natural remanent magnetization of sedimentary rocks: alternating field or thermal demagnetization technique? *Earth and Planetary Science Letters* 29, 65 – 70.

Ozima, M., Ozima, M. and Akimoto, S. 1964. Low temperature characteristics of remanent magnetization of magnetite self-reversal and recovery phenomena of remanent magnetization. *Journal of Geomagnetism and Geoelectricity*, 16, 165 – 177.

Paasche, Ø., Løvlie, R., Olaf Dahl, S., Bakke, J. and Nesje, A. Bacterial magnetite in lake sediments: late glacial to Holocene climate and sedimentary changes in northern Norway. *Earth and Planetary Science Letters* 223, 319 – 333.

Pan, Y. X., Petersen, N., Davila, A. F., Zhang, L. M., Winklhofer, M., Liu, Q. S., Hanzlik, M. and Zhu, R. 2005. The detection of bacterial magnetite in recent sediments of Lake Chiemsee (southern Germany). *Earth and Planetary Science Letters*, 232, 109 – 123.

Pearce, G. W. and Karson, J. A. 1981. On pressure demagnetization. *Geophysical Research Letters*, 8, 725 – 728.

Pike, C. R., Roberts, A. P., Dekkers, M. J. and Verosub, K. L. 2001. An investigation of multi-domain hysteresis mechanisms using FORC diagrams. *Physics of the Earth and Planetary Interiors,* 126, 11 – 25.

Prest, V. K., Grant, D. R. and Rampton, V. N. 1968. Glacial Map of Canada: Geological Survey of Canada Map 1253A, Scale 1:5 000 000.

Pullaiah, G., Irving, E, Buchan, K. L. and Dunlop, D. J. 1975. Magnetization changes caused by burial and uplift. *Earth and Planetary Science Letters* 28, 133 – 143.

Rittenhouse, G. 1934. A laboratory study of an unusual series of varved clays from northern Ontario. *American Journal of Science,* 28, 110 – 120.

Roberts, A. P. and Winkelhofer, M. 2004. Why are geomagnetic excursions not always recorded in sediments? Constraints from post-depositional remanent magnetization lock-in modeling. *Earth and Planetary Science Letters* 345 – 359.

Roberts, A. P., Cui, Y. and Verosub, K. L. 1995. Wasp-waisted hysteresis loops: mineral magnetic characteristics and discrimination of components in mixed magnetic systems. *Journal of Geophysical Research,* 100, 17,909 – 17,924.

Roberts, A. P., Pike, C. R. and Verosub, K. L. 2000. First-order reversal curve diagrams: A new tool for characterizing the magnetic properties of natural samples. *Journal of Geophysical Research,* 105, 28,461 – 28,475.

Robertson, D. and France, D. 1994. Discrimination of remanence-carrying minerals in mixtures using isothermal remanent magnetisation acquisition curves. *Physics of the Earth and Planetary Science Letters,* 82, 223 – 234.

Roy, J. L. and Park, J. K. 1974. The magnetization of certain red beds: Vector analysis of chemical and thermal results. *Canadian Journal of Earth Sciences* 11, 437 – 471.

Sagnotti, L. and Winkler, A. 1999. Rock magnetism and palaeomagnetism of greigite-bearing mudstones in the Italian peninsula. *Earth and Planetary Science Letters* 165, 67 – 80.

Schmidt, P. W. 1993. Palaeomagnetic cleaning strategies. *Physics of the Earth and Planetary Interiors* 76, 169 – 178.

Snowball, I. F. 1991. Magnetic hysteresis properties of greigite (Fe_3S_4) and a new occurrence in Holocene sediments for Swedish Lappland. *Physics of the Earth and Planetary Interiors* 68, 32 – 40.

Snowball, I. F. 1994. Bacterial magnetite and the magnetic properties of sediments in a Swedish lake. *Earth and Planetary Science Letters* 126, 129 – 142.

Snowball, I. F. 1997a. Gyroremanent magnetization and the magnetic properties of greigite-bearing clays in southern Sweden. *Geophysical Journal International,* 129, 624 – 636.

Snowball, I. F. 1997b. The detection of single-domain greigite (Fe3S4) using rotational remanent magnetization (RRM) and the effective gyro field (*Bg*): mineral magnetic and paleomagnetic applications. *Geophysical Journal International,* 130, 704 – 716.

Snowball, I. and Torii, M. 1999. Incidence and significance of magnetic iron sulphides in Quaternary sediments and soils. In: *Quaternary Climates, Environments and Magnetism.* Eds. Maher, B. A. and Thompson, R. pp. 199 – 230. Cambridge University Press.

Sprowl, D. R. and Banarjee, S. K. 1985. High-resolution paleomagnetic record of geomagnetic field fluctuations from the varved sediments of Elk Lake, Minnesota. *Geology,* 13, 531 – 533.

Stacey, F. 1972. On the role of Brownian motion in the control of detrital remanent magnetization of sediments. *Pure and Applied Geophysics* 98, 139 – 145.

Stacey, F. D. and Banarjee, S. K. 1974. *The Physical Principles of Rock Magnetism.* Elsevier, Amsterdam, 195 pp.

Stephenson, A. 1980a. Gyromagnetism and the remanence acquired by a rotating rock in an alternating field. *Nature* 284, 48 – 49.

Stephenson, A. 1980b. A gyroremanent magnetization in anisotropic magnetic material. *Nature* 284, 49 – 51.

Stephenson, A. 1983. Changes in direction of the remanence of rocks produced by stationary alternating field demagnetization. *Geophysical Journal of the Royal Astronomical Society* 73, 213 – 239.

Stephenson, A. 1993. Three-axis static demagnetization alternating field demagnetization of rocks and the identification of natural remanent magnetization, gyroremanent magnetization, and anisotropy. *Journal of Geophysical Research* 98, 373 – 381.

Stephenson, A., Sadikun, S. and Potter, D. K. 1986. A theoretical and experimental comparison of the anisotropies of magnetic susceptibility and remanence in rocks and minerals. *Geophysical Journal of the Royal Astronomical Society,* 84, 185 – 200.

Sternberg, R. S. 1983. Archaeomagnetism in the southwest of North America. In: Creer, K. M., Tucholka, P. and Barton, C. E. (eds), *Geomagnetism of Baked Clays and Recent Sediments.* New York, Elsevier, 158 – 167.

Sun, W. W. and Kodama, K. P. 1992. Magnetic anisotropy, scanning electron microscopy, and X-ray pole figure goniometry study of inclination shallowing in a compacting clay-rich sediment. *Journal of Geophysical Research,* 97, 19,599 – 19,615.

Symons, D. T. A. and Cioppa, M. T. 2000. Crossover plots: a useful method for plotting data in paleomagnetism. *Geophysical Research Letters,* 27, 1779 – 1782.

Tan, X. and Kodama, K. P. 1998. Compaction-corrected inclinations from southern California Cretaceous marine sedimentary rocks indicate no paleolatitudinal offset for the Peninsular Ranges terrane. *Journal of Geophysical Research,* 103, 27,169 – 27,192.

Tan, X. and Kodama, K. P. 2003. An analytical solution for correcting paleomagnetic inclination error. *Geophysical Journal International,* 152, 228 – 236.

Tan, X., Kodama, K. P. and Fang, D. 2002. Laboratory depositional and compaction-caused inclination errors carried by haematite and their implications in identifying inclination error of natural remanence in red beds. *Geophysical Journal International,* 151, 475 – 486.

Tarling, D. H. 1983. *Paleomagnetism.* Chapman and Hall, London.

Tauxe, L. 1993. Sedimentary records of relative paleointensity of the geomagnetic field: Theory and practice. *Reviews of Geophysics* 31, 319 – 354.

Tauxe, L. and Kent, D. V. 1984. Properties of a detrital remanence carried by haematite from study of modern river deposits and laboratory redeposition experiments. *Geophysical Journal of the Royal Astronomical Society,* 77, 543 – 561.

Tauxe, L. and Bertram, H. N. 2002. Physical interpretation of hysteresis loops: micromagnetic modelling of fine particle magnetite. *Geochemistry, Geophysics and Geosystems,* DOI 10.1029/2001GC000280.

Tauxe, L., Mullender, T. A. T. and Pick, T. 1996. Pot-bellies, wasp-waists and superparamagnetism in magnetic hysteresis. *Journal of Geophysical Research,* 101, 571 – 583.

Teller, J. T. and Thorleifson, L. H. 1983. The Lake Agassiz-Lake Superior connection. In: Teller, J. T. and Clayton, L. eds., *Glacial Lake Agassiz*: Geological Association of Canada Special Paper 26, p.261-290.

Thompson, R. and Berglund, B. 1976. Late Weichselian geomagnetic 'reversal' as a possible example of the reinforcement syndrome. *Nature* 263, 490 – 491.

Thompson, R. and Oldfield, F. 1986. *Environmental Magnetism.* George Allen and Unwin, London.

Tucker, P. 1980. A grain mobility model of post-depositional realignment. *Geophysical Journal of the Royal Astronomical Society,* 63, 149 – 163.

Turner, G. and Thompson, R. 1981. Lake sediment record of the geomagnetic secular variation in Britain during Holocene times. *Geophysical Journal of the Royal Astronomical Society,* 65, 703 – 725.

Van der Voo, R. 1993. *Paleomagnetism of the Atlantic, Tethys and Iapetus Oceans.* Cambridge University Press, Great Britain, 411pp.

van Vreumingen, M. J. 1993a. The magnetization of some artificial suspensions while flocculating in a magnetic field. *Geophysical Journal International* 114, 601 – 606.

van Vreumingen, M. J. 1993b. The influence of salinity and flocculation upon the acquisition of remanent magnetization in some artificial sediments. *Geophysical Journal International* 114, 607 – 614.

Verosub, K. L. 1977. Depositional and postdepositional processes in the magnetization of sediments. *Reviews of Geophysics and Space Physics* 15, 129 – 143.

Verosub, K. 1979. Paleomagnetism of varved sediments from western New England: variability of the palaeomagnetic recorder. *Geophysical Research Letters,* 6, 241 – 244.

Verosub, K. and Banarjee, S. K. 1977. Geomagnetic excursions and their paleomagnetic record. *Reviews of Geophysics* 15, 145 – 155.

Vlag, P., Thouveny, N., Williamson, D., Rochette, P. and Ben-Atig, F. 1996. Evidence for a geomagnetic excursion recorded in the sediments of Lac St. Front, France: A link with the Laschamp excursion? *Journal of Geophysical Research* 101, 28,211 – 28,230.

Walton, D. 1996. Magnetic overprints and their removal. *Physics of the Earth and Planetary Interiors* 94, 145 – 148.

Walton, D., Shaw, J., Share, J. A. and Hakes, J. 1992. Microwave demagnetization. *Journal of Applied Physics* 71, 1549 – 1551.

Walton, D., Share, J., Rolph, T. C. and Shaw, J. 1993. Microwave magnetization. *Geophysical Research Letters* 20, 109 – 111.

Wang, D. and Van der Voo, R. 2004. The hysteresis properties of multidomain magnetite and titanomagnetite/titanomaghemite in mid-ocean ridge basalts. *Earth and Planetary Science Letters,* 220, 175-184.

Wasilewski, P. J. 1973. Magnetic hysteresis in natural materials. *Earth and Planetary Science Letters,* 20,

67 – 72.

Weiss, B. P., Kim, S. S., Kirschvink, J. L., Kopp, R. E., Sankaran, M., Kobayashi, A. and Komeili, A. 2004. Ferromagnetic resonance and low-temperature magnetic tests for biogenic magnetite. *Earth and Planetary Science Letters,* 224, 73 – 89.

Zhu, R. X., Coe, R. S. and Zhao, X. X. 1998. Sedimentary record of two geomagnetic excursions within the last 15,000 years in Beijing, China. *Journal of GeophysicalResearch* 103, 30,323 – 30,333.

Zijderveld, J. D. A. 1967. A.C. demagnetization of rocks. In *Methods in Palaeomagnetism* (D. W. Collinson, K. M. Creer, S. K. Runcorn, Eds.), pp. 256 – 286, Elsevier, New York.

Zoltai, S. C. 1961. Glacial history of part of northwestern Ontario. *Proceedings of the Geological Association of Canada,* 13, 61 – 83.

Zoltai, S. C. 1963. Glacial features of the Canadian Lakehead area. *Canadian Geographer,* 7, 101 – 115.

Zoltai, S. C. 1965. Glacial features of the Quetico-Nipigon area, Ontario. *Canadian Journal of Earth Sciences,* 2, 247 – 269.

Yamazaki, T., Abdeldayem, A. L. and Ikehara, K. 2003. Rock-magnetic changes with reduction diagenesis in Japan Sea sediments and preservation of geomagnetic secular variation in inclination during the last 30,000 years. *Earth Planets Space,* 55, 327 – 340.

Yu, Y., Dunlop, D. J. and Özdemir, Ö. 2003. On the resolution of multivectorial remanences. *Earth and Planetary Science Letters* 208, 13 – 26.

Özdemir, Ö. and Banarjee, S. K. 1984. High temperature stability of maghemite (γ-Fe_2O_3). *Geophysical Research Letters,* 11, 161 – 164.

Özdemir, Ö. and Dunlop, D. J. 1996. Thermoremanence and Néel temperature of goethite. Geophysical Research Letters 23, 921 – 924.

Appendix A: AMS data

Spec.	Dec	Incl	Min	Dec	Incl	Int	Dec	Inc	Max
SC001A	150.8	71.4	399.3	242.2	0.5	465.5	332.4	18.6	467.7
SC002A	127.4	78.2	388.9	257.3	7.6	443.9	348.5	8.9	446.8
SC003A	118.2	80	381.8	314.3	9.6	438	223.8	2.7	439.7
SC004A	137.2	83	381.3	39.8	0.9	442.9	309.7	7	451.4
SC005A	165.2	86.9	374	47	1.5	438.7	316.9	2.8	440.1
SC006A	138.2	83.7	385.9	337.9	5.9	445.6	247.7	2.1	448.3
SC007A	140.3	81.9	371.4	292.9	7.2	433.7	23.4	3.7	434.8
SC008A	165.3	83	372.5	44	3.6	430.8	313.7	5.9	435.4
SC009A	156.1	77.8	357.3	47.6	3.9	415.3	316.8	11.5	417.7
SC010A	128.8	84.3	348.4	237	1.8	390.8	327.2	5.4	395.4
SC011A	161.8	74	341.3	266.7	4.2	392.1	357.9	15.4	399.4
SC012A	143.8	72.8	398.4	6.2	12.9	444.4	273.6	11.2	450.1
SC013A	211.8	81.4	388.5	341.5	5.6	432.3	72.2	6.6	438
SC014A	160.5	66.8	370.1	2.3	21.7	421.6	269.2	7.8	425.1
SC015A	176.2	69.4	384.6	335.5	19.4	439.3	67.9	6.7	441.3
SC016A	144.8	68.9	380.2	33.5	8	436.8	300.6	19.4	438.7
SC017A	149.1	76.1	374	40.1	4.6	438	309.1	13.1	441
SC018A	160.3	70	398.5	47.4	8	469.5	314.7	18.2	470.8
SC019A	166.3	71.8	374.9	297.9	12.3	442.1	30.8	13.2	443.7
SC020A	173.5	70.2	366.9	82.1	0.5	434.9	352	19.8	440.7
SC021A	170.1	73.9	371.7	24.6	13.4	433.2	292.5	8.8	438.4
SC022A	156.3	72.9	351.8	39.8	7.8	422.8	307.6	15.1	424.3
SC023A	168.1	72.2	382.2	63.4	4.7	451.9	331.9	17.1	453.5
SC024A	175	70.9	390.3	30.6	15.8	455.5	297.6	10.6	457.9
SC025A	172.5	75.2	366.1	53.9	7.2	425.1	322.3	12.9	428.7
SC026A	180.3	62.5	368.4	25.7	25.1	422	290.8	10.3	425.5
SC027A	159.9	68.2	398.2	49.4	8	446.8	316.5	20.2	451.5
SC028A	177.5	70.7	372.4	23.1	17.5	430.4	290.7	7.8	435.9
SC029A	150.6	63.4	379.6	288.4	20.3	435.7	24.6	16.4	436.4
SC030A	171.4	75.5	351.8	45.7	8.6	410.4	313.9	11.6	415
SC031A	158	78.3	354.3	10.8	9.9	411.1	279.8	6.2	418.9
SC032A	175.7	72.6	375.3	45.8	11.3	438.7	313.2	13	444.9
SC033A	188.4	80.2	350.7	96.4	0.3	405.3	6.3	9.8	407.4
SC034A	197.7	84.2	353.5	88.1	2	405.5	357.9	5.5	407.8
SC035A	182	83.9	374.1	73.7	1.9	427.6	343.5	5.8	433.2
SC036A	185.2	79.9	371.7	78.9	2.9	431.5	348.4	9.7	433.3
SC037A	197.3	76	413.4	70.6	8.5	478.8	339	11	480.5
SC038A	182.7	73.2	399	69.1	6.9	468.4	337.2	15.3	473.1
SC039A	162.4	77.2	384.3	37.7	7.4	448.5	306.4	10.4	455.6
SC040A	166.4	79.1	388	70.4	1.1	448.8	340.2	10.9	455.4
SC041A	180.2	77.4	433.8	79.4	2.4	491.2	348.9	12.4	497.9
SC042A	210.3	78.9	446.6	39.2	11	495.3	308.9	1.7	507.2
SC043A	164.2	81.1	363.9	53.9	3.1	423.5	323.5	8.3	424.6
SC044A	201.6	82.6	381	318.5	3.4	444.7	48.9	6.6	445.2
SC045A	183.6	74	368	2.3	16	432.9	92.5	0.3	433.6
SC046A	190	77	426	17.1	12.9	493.6	286.7	1.6	497.1
SC047A	197.5	76.1	411.2	34.6	13.3	477.1	303.7	3.9	480.3

Spec.	Dec	Incl	Min	Dec	Incl	Int	Dec	Inc	Max
SC048A	252.8	82.8	428.1	9	3.2	495.1	99.3	6.4	498
SC049A	205.1	81.1	404.5	50.2	8.1	469	319.7	3.7	470.4
SC050A	228	87.2	437.6	78.1	2.4	510.3	348	1.4	513
SC051A	186.1	68	428.9	279.3	1.3	501.4	9.8	21.9	505
SC052A	179.9	70.7	440.6	273.7	1.3	507.3	4.2	19.3	510.1
SC053A	192.4	76	468.3	345	12.4	540.6	76.3	6.2	541.5
SC054A	180.3	80.2	428.3	21.5	9.1	493.6	290.9	3.5	495
SC055A	185.5	84	407.3	93.8	0.2	474.2	3.8	6	479.7
SC056A	201.6	82.7	448.4	75.3	4.4	522.2	344.8	5.9	523.8
SC057A	206.2	82.7	462.6	51.5	6.6	537.3	321.2	3.1	539.7
SC058A	227.7	84.1	459.4	79.8	5	532.7	349.5	3.1	536.4
SC059A	342.9	83.8	473.9	105.3	3.3	548	195.6	5.2	551.3
SC060A	324.3	87.2	614.1	109	2.3	705.1	199.1	1.6	707.5
SC061A	217	76.5	565.6	93.4	7.6	637.2	1.9	11.1	639.1
SC062A	216.4	84.2	426.4	86.4	3.7	501	356.1	4.4	504.7
SC063A	193.4	83	338.5	96.6	0.8	404	6.5	7	408.5
SC064A	173.5	83.7	531.3	308.4	4.4	625.9	38.8	4.4	626.4
SC065A	186.5	86.1	542.6	67.9	1.9	627.7	337.8	3.4	627.8
SC066A	157.8	85.4	3011.6	269	1.7	3205.8	359.2	4.3	3223.4
SC067A	95.5	86.4	3320.3	265.7	3.5	3579	355.7	0.6	3606.5
SC068A	41.4	86	435.4	268.4	2.7	523.4	178.2	2.9	525.2
SC069A	27.3	88.3	596.6	264	0.9	702.3	174	1.4	704.7
SC070A	112.9	86	3524.1	286.3	3.9	3744.2	16.3	0.5	3766
SC071A	136.6	85.6	3109.1	273.1	3.2	3335.3	3.2	3	3352.5
SC072A	6.6	84.1	759.2	259.3	1.8	868.4	169.1	5.7	874.2
SC073A	97	87.9	1427.1	266.5	2.1	1548.4	356.5	0.4	1553.3
SC074A	179.4	89.7	1782	301.7	0.1	1913.8	31.7	0.2	1923.4
SC075A	34.5	83.9	1074.9	264.9	3.9	1187.4	174.6	4.7	1189.8
SC076A	21	83.6	695.4	274.3	1.8	800	184.1	6.1	805.1
SC077A	79.6	83.9	972.2	272	6	1066.6	181.9	1.3	1073.9
SC078A	20.4	86.7	4711.7	230.3	2.9	4956.2	140.2	1.7	4972
SC203	253.89	80.3	4738.33	146.3	3	4984.19	55.79	9.19	5002.11
SC204A	232.39	77	4656.77	116.8	5.69	4895.5	25.7	11.6	4931.36
SC205	248.1	71	4580.27	132.1	8.599999	4815.76	39.5	16.79	4860.96
SC206	356.2	0.4	492.1	130.6	89.5	586.97	266.2	0.3	589.73
SC207	2.79	8.389999	465.42	245.89	71.9	549.48	95.18999	15.89	553.89
SC208A	4.3	4.3	485.49	108.8	73.4	568.71	273.1	16	572.29
SC209	182.19	1.5	530.56	274.79	59.7	629.49	91.3	30.29	633.72
SC210	357.79	8.69	470.78	250.19	63.2	558.43	91.9	25.2	560.84
SC211	186.3	18.29	533.05	59.2	61.2	598.96	283.7	21.39	603.84
SC212	0.2	1.1	567.18	263.6	80.8	664.66	90.4	9.099999	667.06
SC213	179.19	0.69	515.57	300	88.59	615.86	89.09	1.2	618.05
SC216A	184.39	0.2	481.77	274.79	68.18999	558.34	94.3	21.79	564.41
SC218	178.89	2.09	665.42	84.59	63.59	765.59	269.89	26.29	768.96
SC0401A	4.9	8.1	660.6	126.3	74.7	742.7	273	12.9	746.4
SC0401B	185.1	5.4	330.6	276.3	12.1	399.2	71.5	76.7	400.7
SC0401C	4.9	13.2	379.7	246.7	63.6	452.9	100.5	22.4	454
SC0401D	5.5	1.4	484.6	96.6	37	592.8	273.6	52.9	595.5
SC0401EA	6	0.6	1152.6	97	57.9	1266.3	275.7	32.1	1272.6

Spec.	Dec	Incl	Min	Dec	Incl	Int	Dec	Inc	Max
SC0401EB	186.6	4.1	1043.9	94.3	28.8	1141	283.9	60.8	1143.8
SC0401F	4.3	1.7	567.6	99.5	72.2	658.7	273.7	17.7	662.3
SC0401GA	1.2	7.5	3855.5	93.5	17.4	4064.7	248.7	71	4083.5
SC0401GB	2.2	10.5	3331.4	269.6	13.9	3519.3	128.1	72.4	3533.3
SC0401H	182.5	16.5	591.6	89.5	10.3	688.2	328.7	70.4	695.7
SC0402A	356.4	2.5	236	254.5	78.2	274.1	86.9	11.6	276.8
SC0402B	183	8.1	233.9	308.5	76.3	278.4	91.5	11	279.7
SC0402C	184.3	3.7	257.3	329.9	85.5	306.3	94.1	2.5	307.4
SC0402D	182.3	1.6	233.6	281.4	80	279	92	9.8	279.5
SC0402E	7.2	8.2	251.5	136.8	77.3	288.9	275.8	9.7	291.4

Appendix B: AARM data

Spec.	Orientation	Decl	Incl	Int (mA/m)
SC203	000/00	351.36	8.87	700.929
SC203	090/00	95.65	9.62	650.456
SC203	*/90	238.85	82.4	785.141
SC203	045/35.2	43.16	47.62	706.045
SC203	135/35.2	306.89	37.5	792.568
SC203	225/35.2	228.6	33.87	856.203
SC203	315/35.2	145.43	40.68	768.452
SC204	000/00	354.17	8.15	679.732
SC204	090/00	97.6	8.02	654.816
SC204	*/90	221.67	81.78	765.502
SC204	045/35.2	44.96	46.67	692.51
SC204	135/35.2	305.68	37.15	770.77
SC204	225/35.2	226.87	32.47	845.861
SC204	315/35.2	144.61	38.44	762.629
SC205	000/00	351.13	9.62	654.266
SC205	090/00	97.97	9.49	621.545
SC205	*/90	246.42	81.68	748.315
SC205	045/35.2	44.84	46.9	678.763
SC205	135/35.2	306.46	36.68	754.893
SC205	225/35.2	226.74	33.48	822.475
SC205	315/35.2	146.48	39.81	733.438
SC30504B	000/00	359.27	0.91	216.896
SC30504B	090/00	93.19	-1.79	217.111
SC30504B	*/90	253.06	85.1	146.995
SC30504B	045/35.2	43.24	25.98	190.244
SC30504B	135/35.2	311.4	25.14	204.114
SC30504B	225/35.2	225.7	22.01	207.422
SC30504B	315/35.2	134.06	24.32	195.714
SC30505A	000/00	359.47	0.65	208.648
SC30505A	090/00	91.37	-0.35	208.574
SC30505A	*/90	280.72	86.66	143.998
SC30505A	045/35.2	44.11	28.37	188.126
SC30505A	135/35.2	311.25	24.75	192.147
SC30505A	225/35.2	227.25	22.92	193.87
SC30505A	315/35.2	135.42	25.2	188.775
SC30505B	000/00	0.04	1.16	211.616
SC30505B	090/00	93.31	-1.98	218.772
SC30505B	*/90	285.03	86.43	147.128
SC30505B	045/35.2	44.83	27.09	189.541
SC30505B	135/35.2	312.23	25.51	201.4
SC30505B	225/35.2	228.7	23.43	197.541
SC30505B	315/35.2	133.83	22.58	194.277
SC30506A	000/00	359.13	1.38	245.917
SC30506A	090/00	92.14	-0.18	246.92
SC30506A	*/90	295.85	86.73	168.403
SC30506A	045/35.2	43.12	26.79	220.046
SC30506A	135/35.2	311.36	25.77	226.354

Spec.	Orientation	Decl	Incl	Int (mA/m)
SC30506A	225/35.2	227.14	21.94	225.867
SC30506A	315/35.2	133.46	25.94	221.944
SC30506B	000/00	0.42	1.25	282.573
SC30506B	090/00	92.33	-1.39	290.277
SC30506B	*/90	276.96	86.91	198.296
SC30506B	045/35.2	43.74	27.07	254.612
SC30506B	135/35.2	312.14	25.6	264.607
SC30506B	225/35.2	226.26	23.13	262.883
SC30506B	315/35.2	133.86	24.05	254.053
SC30510A	000/00	357.95	0.85	518.657
SC30510A	090/00	89.68	-4.5	475.927
SC30510A	*/90	294.68	81.8	391.708
SC30510A	045/35.2	39.84	28.81	452.455
SC30510A	135/35.2	311.17	27.47	504.49
SC30510A	225/35.2	229.32	26.4	480.229
SC30510A	315/35.2	135.27	28.48	432.607
SC30510B	000/00	355.04	-4.38	739.866
SC30510B	090/00	88.37	-8.74	621.158
SC30510B	*/90	296.81	79.55	525.145
SC30510B	045/35.2	36.01	28.58	596.861
SC30510B	135/35.2	313.48	24.88	702.413
SC30510B	225/35.2	232.83	23.95	657.925
SC30510B	315/35.2	137.52	29.1	564.197

Appendix C: AF demagnetization data

Spec.	Dec*	Incl*	Dec†	Incl†	Int (mA/m)	Size (cm3)	AF demag (mT)
SC001A	225.41	7.3	353.41	7.3	31.884	8	0
SC001A	226.63	5.83	354.63	5.83	32.346	8	2
SC001A	227.88	5.51	355.88	5.51	32.993	8	5
SC001A	232.05	3.62	0.05	3.62	31.928	8	10
SC001A	233.84	-2.23	1.84	-2.23	29.361	8	20
SC001A	235.59	-4.01	3.59	-4.01	26.991	8	30
SC001A	235.68	-4.75	3.68	-4.75	24.498	8	40
SC001A	236.47	-4.75	4.47	-4.75	20.059	8	60
SC001A	237.43	-4.74	5.43	-4.74	16.389	8	80
SC001A	238.21	-3.33	6.21	-3.33	14.387	8	100
SC001A	238.96	-4.76	6.96	-4.76	13.209	8	130
SC001A	239.92	-1.92	7.92	-1.92	12.305	8	160
SC002A	209.54	31.75	337.54	31.75	33.054	8	0
SC002A	210.21	29.25	338.21	29.25	33.231	8	2
SC002A	213.99	28.94	341.99	28.94	33.196	8	5
SC002A	216.98	25.65	344.98	25.65	30.358	8	10
SC002A	219	21	347	21	26.574	8	20
SC002A	218.54	19.69	346.54	19.69	24.244	8	30
SC002A	218.88	18.39	346.88	18.39	21.744	8	40
SC002A	219.65	16.32	347.65	16.32	17.032	8	60
SC002A	221.92	15.99	349.92	15.99	13.048	8	80
SC002A	222.16	13.05	350.16	13.05	11.065	8	100
SC002A	223.24	13.76	351.24	13.76	9.759	8	130
SC002A	223.99	10.05	351.99	10.05	9.116	8	160
SC003A	153.43	14.89	281.43	14.89	35.993	8	0
SC003A	153.42	14.68	281.42	14.68	35.565	8	2
SC003A	153.88	15.4	281.88	15.4	33.931	8	5
SC003A	153.92	14.03	281.92	14.03	30.722	8	10
SC003A	151.53	11.69	279.53	11.69	27.555	8	20
SC003A	151.44	9.96	279.44	9.96	25.288	8	30
SC003A	152.05	8.36	280.05	8.36	22.851	8	40
SC003A	153.72	6.74	281.72	6.74	18.233	8	60
SC003A	154.02	6.57	282.02	6.57	14.048	8	80
SC003A	154.89	7.73	282.89	7.73	11.333	8	100
SC003A	158.16	5.53	286.16	5.53	9.932	8	130
SC003A	160.55	5.8	288.55	5.8	8.887	8	160
SC004A	165.68	40.43	293.68	40.43	32.86	8	0
SC004A	165.56	38.07	293.56	38.07	32.167	8	2
SC004A	164.41	37.07	292.41	37.07	32.405	8	5
SC004A	161.67	34.74	289.67	34.74	29.829	8	10
SC004A	160.22	30.94	288.22	30.94	26.045	8	20
SC004A	159.84	28.4	287.84	28.4	23.335	8	30
SC004A	157.96	27.94	285.96	27.94	20.857	8	40
SC004A	159.41	24.9	287.41	24.9	16.586	8	60

SC004A	165.05	25.09	293.05	25.09	13.316	8	80
SC004A	165.9	23.05	293.9	23.05	11.157	8	100
SC004A	175.84	23.64	303.84	23.64	9.195	8	130
SC004A	179.5	21.19	307.5	21.19	8.418	8	160
SC005A	173.98	46.82	301.98	46.82	26.247	8	0
SC005A	174.29	45.83	302.29	45.83	26.83	8	2
SC005A	172.88	43.37	300.88	43.37	27.625	8	5
SC005A	171.85	42.14	299.85	42.14	26.295	8	10
SC005A	169.28	40.08	297.28	40.08	23.501	8	20
SC005A	167.46	38.7	295.46	38.7	20.822	8	30
SC005A	167.56	37.72	295.56	37.72	18.761	8	40
SC005A	168.27	37.21	296.27	37.21	14.748	8	60
SC005A	169.48	35.79	297.48	35.79	11.871	8	80
SC005A	172.11	34.32	300.11	34.32	10.372	8	100
SC006A	174.23	26.52	302.23	26.52	32.881	8	0
SC006A	175.5	26.32	303.5	26.32	32.174	8	2
SC006A	177.87	24.75	305.87	24.75	32.024	8	5
SC006A	178.03	21.4	306.03	21.4	30.024	8	10
SC006A	177.31	17.26	305.31	17.26	27.498	8	20
SC006A	175.75	17.09	303.75	17.09	24.719	8	30
SC006A	176.23	15.61	304.23	15.61	22.343	8	40
SC006A	177.05	13.29	305.05	13.29	17.829	8	60
SC006A	177.7	14.93	305.7	14.93	14.69	8	80
SC006A	181.9	11.62	309.9	11.62	8.24	8	180
SC007A	184.13	25.15	312.13	25.15	29.207	8	0
SC007A	185.8	25.2	313.8	25.2	29.567	8	2
SC007A	187.49	24.44	315.49	24.44	29.774	8	5
SC007A	187.37	21.79	315.37	21.79	28.507	8	10
SC007A	184.94	20.57	312.94	20.57	25.94	8	20
SC007A	186.55	20.19	314.55	20.19	23.039	8	30
SC007A	186.84	19.72	314.84	19.72	20.433	8	40
SC007A	187.02	19.21	315.02	19.21	16.993	8	60
SC007A	187.94	17.32	315.94	17.32	14.162	8	80
SC007A	189.96	17.29	317.96	17.29	12.452	8	100
SC008A	194.53	19.52	322.53	19.52	32.457	8	0
SC008A	196.1	19.95	324.1	19.95	32.838	8	2
SC008A	198.38	18.87	326.38	18.87	33.462	8	5
SC008A	201.26	15.13	329.26	15.13	32.033	8	10
SC008A	200.91	10.89	328.91	10.89	28.487	8	20
SC008A	200.58	9.97	328.58	9.97	25.599	8	30
SC008A	200.58	9.2	328.58	9.2	23.503	8	40
SC008A	202.11	7.75	330.11	7.75	19.656	8	60
SC008A	203.36	8.1	331.36	8.1	15.97	8	80
SC008A	206.01	8.4	334.01	8.4	13.294	8	100
SC009A	204.52	18.19	332.52	18.19	35.243	8	0

SC009A	206.63	18.51	334.63	18.51	35.604	8	2
SC009A	209.73	17.37	337.73	17.37	35.578	8	5
SC009A	211.57	14.32	339.57	14.32	33.53	8	10
SC009A	212.27	9.77	340.27	9.77	30.123	8	20
SC009A	213.15	8.35	341.15	8.35	26.9	8	30
SC009A	212.76	6.97	340.76	6.97	24.351	8	40
SC009A	213.36	5.68	341.36	5.68	20.205	8	40
SC009A	214.1	6.52	342.1	6.52	17.113	8	80
SC009A	215.27	6.86	343.27	6.86	14.943	8	100
SC010A	249.79	35.63	17.79	35.63	30.152	8	0
SC010A	249.34	35.14	17.34	35.14	29.891	8	2
SC010A	246.79	34.09	14.79	34.09	29.171	8	5
SC010A	249.46	29.92	17.46	29.92	27.201	8	10
SC010A	250.51	27.08	18.51	27.08	24.057	8	20
SC010A	250.6	25.7	18.6	25.7	21.979	8	30
SC010A	249.71	26.38	17.71	26.38	19.202	8	40
SC010A	252.28	22.74	20.28	22.74	16.193	8	60
SC010A	249.76	24.61	17.76	24.61	13.041	8	80
SC010A	248.56	22.72	16.56	22.72	11.09	8	100
SC011A	276.14	56.78	44.14	56.78	26.591	8	0
SC011A	273.34	57.18	41.34	57.18	26.132	8	2
SC011A	270.05	55.72	38.05	55.72	25.428	8	5
SC011A	273.22	55.63	41.22	55.63	23.83	8	10
SC011A	277.06	54.84	45.06	54.84	20.854	8	20
SC011A	279.13	55.29	47.13	55.29	18.635	8	30
SC011A	278.64	53.92	46.64	53.92	16.56	8	40
SC011A	278.6	51.06	46.6	51.06	13.395	8	60
SC011A	277.1	47	45.1	47	11.131	8	80
SC011A	272.66	45.01	40.66	45.01	10.133	8	100
SC011A	268.46	40.08	36.46	40.08	8.891	8	140
SC011A	267.64	35.81	35.64	35.81	8.238	8	180
SC012A	262.47	42.96	27.47	42.96	35.447	8	0
SC012A	263.07	41.08	28.07	41.08	37.255	8	2
SC012A	264.19	39.54	29.19	39.54	37.696	8	5
SC012A	266.88	35.83	31.88	35.83	37.099	8	10
SC012A	270.71	35.61	35.71	35.61	34.212	8	20
SC012A	272.14	34.05	37.14	34.05	30.754	8	30
SC012A	272.08	33.54	37.08	33.54	27.684	8	40
SC012A	272.05	30.96	37.05	30.96	22.366	8	60
SC012A	267.51	30.95	32.51	30.95	18.413	8	80
SC012A	262.94	28.73	27.94	28.73	15.196	8	100
SC012A	259.98	27.32	24.98	27.32	12	8	140
SC012A	255.46	25.18	20.46	25.18	11.489	8	180
SC013A	239.2	29.65	4.2	29.65	33.433	8	0
SC013A	240.98	28.92	5.98	28.92	35.192	8	2
SC013A	243.12	28.11	8.12	28.11	35.65	8	5

SC013A	244.88	25.69	9.88	25.69	34.8	8	10
SC013A	246.72	24.65	11.72	24.65	31.613	8	20
SC013A	246.83	22.94	11.83	22.94	28.275	8	30
SC013A	247.44	22.46	12.44	22.46	25.365	8	40
SC013A	247.99	21.09	12.99	21.09	20.622	8	60
SC013A	248.37	19.89	13.37	19.89	16.567	8	80
SC013A	249.49	18.9	14.49	18.9	13.69	8	100
SC013A	250.79	19.57	15.79	19.57	11.163	8	140
SC013A	252.1	17.66	17.1	17.66	9.958	8	180
SC014A	214.33	41.59	339.33	41.59	30.772	8	0
SC014A	215.3	40.83	340.3	40.83	30.981	8	2
SC014A	219.13	40.45	344.13	40.45	31.276	8	5
SC014A	223.66	37.83	348.66	37.83	29.547	8	5
SC014A	224.34	36.76	349.34	36.76	26.277	8	20
SC014A	227.38	35.96	352.38	35.96	24.113	8	30
SC014A	226.85	35.11	351.85	35.11	21.535	8	40
SC014A	230.19	33.45	355.19	33.45	17.344	8	60
SC014A	232.51	29.76	357.51	29.76	14.16	8	80
SC014A	234.5	26.04	359.5	26.04	12.775	8	100
SC014A	236.48	23.81	1.48	23.81	11.73	8	140
SC014A	237.19	20.99	2.19	20.99	10.997	8	180
SC015A	248.98	33.27	13.98	33.27	37.51	8	0
SC015A	247.01	32.73	12.01	32.73	37.409	8	2
SC015A	245.56	32.69	10.56	32.69	37.261	8	5
SC015A	246.31	30.12	11.31	30.12	35.63	8	10
SC015A	249.44	28.98	14.44	28.98	32.313	8	20
SC015A	250.13	28.57	15.13	28.57	29.19	8	30
SC015A	251.13	28.68	16.13	28.68	26.437	8	40
SC015A	252.69	26.07	17.69	26.07	22.17	8	60
SC015A	252.28	23.79	17.28	23.79	19.043	8	80
SC015A	252.44	22.25	17.44	22.25	16.639	8	100
SC015A	251.64	19.83	16.64	19.83	14.53	8	140
SC015A	251.57	18.43	16.57	18.43	13.369	8	180
SC016A	274.67	42.56	39.67	42.56	44.187	8	0
SC016A	271.32	42.29	36.32	42.29	43.878	8	2
SC016A	269.61	40.29	34.61	40.29	43.168	8	5
SC016A	271.41	39.23	36.41	39.23	41.097	8	10
SC016A	274.16	36.58	39.16	36.58	37.716	8	20
SC016A	274.33	35.27	39.33	35.27	34.889	8	30
SC016A	275.03	35.79	40.03	35.79	31.675	8	40
SC016A	273.38	34.05	38.38	34.05	25.478	8	60
SC016A	270.97	31.49	35.97	31.49	21.235	8	80
SC016A	266.29	31.49	31.29	31.49	18.068	8	100
SC016A	263	27.28	28	27.28	15.476	8	140
SC016A	258.26	24.52	23.26	24.52	14.143	8	180
SC017A	264.51	29.42	29.51	29.42	47.936	8	0

SC017A	263.76	29.44	28.76	29.44	47.664	8	2
SC017A	262.84	28.15	27.84	28.15	47.523	8	5
SC017A	261.47	25.25	26.47	25.25	46.081	8	10
SC017A	262.98	23.58	27.98	23.58	43.068	8	20
SC017A	263.28	24.44	28.28	24.44	40.08	8	30
SC017A	263.23	22.26	28.23	22.26	37.122	8	40
SC017A	263.52	22.12	28.52	22.12	29.738	8	60
SC017A	263.01	21.72	28.01	21.72	24.237	8	80
SC017A	262.16	21.42	27.16	21.42	21.1	8	100
SC017A	259.88	19.69	24.88	19.69	17.602	8	140
SC017A	256.55	18.87	21.55	18.87	15.711	8	180
SC018A	253.61	44.39	18.61	44.39	40.445	8	0
SC018A	252.31	44.05	17.31	44.05	39.843	8	2
SC018A	249.02	41.89	14.02	41.89	39.016	8	5
SC018A	253.08	40.77	18.08	40.77	36.163	8	10
SC018A	254.04	40.31	19.04	40.31	32.625	8	20
SC018A	256.11	39.22	21.11	39.22	29.717	8	30
SC018A	254.46	38.46	19.46	38.46	26.897	8	40
SC018A	255.38	35.99	20.38	35.99	22.053	8	60
SC018A	255.84	33.81	20.84	33.81	18.774	8	80
SC018A	256.38	31.52	21.38	31.52	16.866	8	100
SC018A	253.92	27.79	18.92	27.79	14.672	8	140
SC018A	254.63	24.93	19.63	24.93	13.745	8	180
SC019A	256.12	37.72	21.12	37.72	45.188	8	0
SC019A	253.68	38.73	18.68	38.73	44.93	8	2
SC019A	251.78	38.61	16.78	38.61	44.499	8	5
SC019A	253.67	37.13	18.67	37.13	42.741	8	10
SC019A	255.53	35.44	20.53	35.44	39.213	8	20
SC019A	256.61	33.78	21.61	33.78	36.033	8	30
SC019A	257.52	34.36	22.52	34.36	32.908	8	40
SC019A	257.12	33.77	22.12	33.77	26.857	8	60
SC019A	258.08	31.19	23.08	31.19	22.407	8	80
SC019A	256.71	31.37	21.71	31.37	18.839	8	100
SC019A	255.85	25.05	20.85	25.05	16.752	8	140
SC019A	256.65	23.97	21.65	23.97	15.229	8	180
SC020A	232.16	49.23	357.16	49.23	36.455	8	0
SC020A	232.48	47.97	357.48	47.97	35.341	8	2
SC020A	232.88	48.01	357.88	48.01	34.376	8	5
SC020A	237.1	46.18	2.1	46.18	31.853	8	10
SC020A	238.58	44.74	3.58	44.74	28.009	8	20
SC020A	239.1	45.13	4.1	45.13	25.694	8	30
SC020A	239.99	43.46	4.99	43.46	23.303	8	40
SC020A	241.27	42.82	6.27	42.82	19.504	8	60
SC020A	242.44	39.1	7.44	39.1	16.194	8	80
SC020A	247.04	36.83	12.04	36.83	14.058	8	100
SC020A	250.64	31.86	15.64	31.86	12.577	8	140
SC020A	249.84	28.44	14.84	28.44	12.018	8	180

SC021A	259.4	55.26	24.4	55.26	39.371	8	0
SC021A	258.89	53.85	23.89	53.85	39.211	8	2
SC021A	254.21	54.17	19.21	54.17	39.043	8	5
SC021A	255.42	56.23	20.42	56.23	36.678	8	10
SC021A	259.13	56.77	24.13	56.77	32.839	8	20
SC021A	257.17	57.97	22.17	57.97	29.76	8	30
SC021A	260.35	55.97	25.35	55.97	26.648	8	40
SC021A	262.4	55.62	27.4	55.62	21.8	8	60
SC021A	260.11	50.72	25.11	50.72	17.985	8	80
SC021A	260.47	46.95	25.47	46.95	15.304	8	100
SC021A	257.37	38.8	22.37	38.8	13.011	8	140
SC021A	257.32	34.64	22.32	34.64	12.215	8	180
SC022A	321.15	54.87	86.15	54.87	39.135	8	0
SC022A	319	56.16	84	56.16	38.924	8	2
SC022A	316.64	57.34	81.64	57.34	37.67	8	5
SC022A	317.54	57.67	82.54	57.67	35.92	8	10
SC022A	323.54	56.66	88.54	56.66	33.161	8	20
SC022A	326.48	55.92	91.48	55.92	30.773	8	30
SC022A	326.81	54.54	91.81	54.54	27.685	8	40
SC022A	321.97	56.45	86.97	56.45	22.45	8	60
SC022A	315.92	54.67	80.92	54.67	17.911	8	80
SC022A	306.19	53.15	71.19	53.15	14.56	8	100
SC022A	288.64	47.04	53.64	47.04	11.629	8	140
SC022A	281.5	46.27	46.5	46.27	10.454	8	180
SC023A	343.49	68.83	108.49	68.83	36.194	8	0
SC023A	335.01	69.04	100.01	69.04	36.806	8	2
SC023A	327.58	67.42	92.58	67.42	36.13	8	5
SC023A	327.71	63.4	92.71	63.4	35.265	8	10
SC023A	326.7	62.89	91.7	62.89	34.931	8	20
SC023A	321.79	63.15	86.79	63.15	33.847	8	30
SC023A	321.81	62.79	86.81	62.79	31.153	8	40
SC023A	316.11	63.18	81.11	63.18	24.598	8	60
SC023A	310.55	60.31	75.55	60.31	20.208	8	80
SC023A	301.85	57.64	66.85	57.64	16.679	8	100
SC023A	290.64	50.31	55.64	50.31	13.308	8	140
SC023A	284.64	47.24	49.64	47.24	11.765	8	180
SC024A	287.28	54.11	52.28	54.11	40.269	8	0
SC024A	287.52	52.18	52.52	52.18	40.518	8	2
SC024A	286.13	50.46	51.13	50.46	41.507	8	5
SC024A	289.84	46.46	54.84	46.46	41.557	8	10
SC024A	294.62	44.26	59.62	44.26	38.536	8	20
SC024A	292.9	43.58	57.9	43.58	35.671	8	30
SC024A	293.81	42.78	58.81	42.78	32.557	8	40
SC024A	293.55	41.5	58.55	41.5	26.613	8	60
SC024A	291.99	39.78	56.99	39.78	22.147	8	80
SC024A	289.06	37.92	54.06	37.92	19.231	8	100

SC024A	283.43	34.96	48.43	34.96	16.122	8	140
SC024A	280.47	32.91	45.47	32.91	14.452	8	180
SC025A	292.54	42.98	57.54	42.98	41.417	8	0
SC025A	290.42	42.94	55.42	42.94	40.663	8	2
SC025A	286.97	43.18	51.97	43.18	39.834	8	5
SC025A	287.79	40.75	52.79	40.75	38.154	8	10
SC025A	291.03	37.56	56.03	37.56	34.875	8	20
SC025A	292.11	37.64	57.11	37.64	32.06	8	30
SC025A	292.63	36.03	57.63	36.03	29.245	8	40
SC025A	292.02	35.64	57.02	35.64	23.829	8	60
SC025A	289.31	36.78	54.31	36.78	19.947	8	80
SC025A	285.91	34.7	50.91	34.7	16.886	8	100
SC025A	282.12	31.79	47.12	31.79	14.193	8	140
SC025A	278.61	30.39	43.61	30.39	13.029	8	180
SC026A	233.69	31.06	358.69	31.06	42.907	8	0
SC026A	233.95	29.59	358.95	29.59	43.928	8	2
SC026A	235.67	28.57	0.67	28.57	44.505	8	5
SC026A	237.67	26.89	2.67	26.89	42.755	8	10
SC026A	240.05	25.58	5.05	25.58	39.079	8	20
SC026A	241.18	24.85	6.18	24.85	35.355	8	30
SC026A	242.16	25.81	7.16	25.81	32	8	40
SC026A	243.98	24.18	8.98	24.18	26.178	8	60
SC026A	245.57	21.66	10.57	21.66	22.358	8	80
SC026A	247.46	20.75	12.46	20.75	19.627	8	100
SC026A	249.25	19.07	14.25	19.07	17.128	8	140
SC026A	250.1	19.64	15.1	19.64	15.85	8	180
SC027A	266.84	62.04	33.84	62.04	37.495	8	2
SC027A	260.68	62.1	27.68	62.1	36.976	8	5
SC027A	263.23	61.72	30.23	61.72	35.721	8	10
SC027A	266.68	60.2	33.68	60.2	32.479	8	20
SC027A	269.16	61.94	36.16	61.94	29.993	8	30
SC027A	270.91	59.65	37.91	59.65	27.196	8	40
SC027A	269.02	58.28	36.02	58.28	21.885	8	60
SC027A	267.38	53.88	34.38	53.88	17.951	8	80
SC027A	267.08	52.37	34.08	52.37	15.559	8	100
SC027A	263.08	44.86	30.08	44.86	12.68	8	140
SC027A	259.26	37.58	26.26	37.58	11.946	8	180
SC028A	302.27	58.99	69.27	58.99	36.444	8	0
SC028A	299.81	58.1	66.81	58.1	35.862	8	2
SC028A	299.15	58.99	66.15	58.99	34.94	8	5
SC028A	295.14	59.74	62.14	59.74	32.422	8	10
SC028A	301.78	58.56	68.78	58.56	29.427	8	20
SC028A	301.36	57.04	68.36	57.04	26.861	8	30
SC028A	304.15	56.49	71.15	56.49	24.616	8	40
SC028A	302.63	54.93	69.63	54.93	20.119	8	60
SC028A	296.81	53.53	63.81	53.53	16.616	8	80

SC028A	290.71	47.38	57.71	47.38	14.082	8	100
SC028A	283.91	41.51	50.91	41.51	12.335	8	140
SC028A	280.51	36.58	47.51	36.58	11.356	8	180
SC029A	288.84	76.93	55.84	76.93	39.538	8	0
SC029A	301.61	78.05	68.61	78.05	39.318	8	2
SC029A	286.09	72.96	53.09	72.96	40.024	8	5
SC029A	291.16	70.73	58.16	70.73	39.152	8	10
SC029A	297.66	69.88	64.66	69.88	36.523	8	20
SC029A	302.51	68.94	69.51	68.94	33.592	8	30
SC029A	300.03	69.15	67.03	69.15	30.569	8	40
SC029A	294.27	66.53	61.27	66.53	24.211	8	60
SC029A	287.56	64.66	54.56	64.66	19.192	8	80
SC029A	280.06	62.69	47.06	62.69	16.325	8	100
SC029A	265.96	53	32.96	53	13.494	8	140
SC029A	262.32	47.37	29.32	47.37	12.138	8	180
SC030A	295.98	52.47	62.98	52.47	46.548	8	0
SC030A	292.62	52.97	59.62	52.97	46.176	8	2
SC030A	289.45	53.35	56.45	53.35	44.753	8	5
SC030A	290.25	53.52	57.25	53.52	41.866	8	10
SC030A	292.33	52.64	59.33	52.64	38.586	8	20
SC030A	293.22	53.7	60.22	53.7	35.75	8	30
SC030A	293.93	52.63	60.93	52.63	32.384	8	40
SC030A	291.19	50.41	58.19	50.41	26.18	8	60
SC030A	288.39	47.2	55.39	47.2	20.613	8	80
SC030A	285.31	47.1	52.31	47.1	17.552	8	100
SC030A	276.2	42.7	43.2	42.7	14.287	8	140
SC030A	275.56	41.94	42.56	41.94	12.819	8	180
SC031A	270.34	49.29	37.34	49.29	42.106	8	0
SC031A	268.29	50.62	35.29	50.62	41.929	8	2
SC031A	265.87	50.22	32.87	50.22	40.929	8	5
SC031A	264.91	49.69	31.91	49.69	38.911	8	10
SC031A	268.01	50.82	35.01	50.82	35.61	8	20
SC031A	269.97	49.44	36.97	49.44	32.636	8	30
SC031A	270.14	49.09	37.14	49.09	29.099	8	40
SC031A	268.37	48.34	35.37	48.34	23.784	8	60
SC031A	267.04	46.96	34.04	46.96	19.575	8	80
SC031A	266.8	44.47	33.8	44.47	16.482	8	100
SC031A	259.77	41.63	26.77	41.63	13.087	8	140
SC031A	255.28	40.18	22.28	40.18	11.907	8	180
SC032A	194.39	74.37	321.39	74.37	32.126	8	0
SC032A	183.7	70.97	310.7	70.97	32.8	8	2
SC032A	183.22	71.77	310.22	71.77	31.374	8	5
SC032A	181.99	70.51	308.99	70.51	28.83	8	10
SC032A	173.5	70.32	300.5	70.32	25.053	8	20
SC032A	172.32	72.34	299.32	72.34	22.993	8	30
SC032A	171.57	71.32	298.57	71.32	20.579	8	40

SC032A	178.32	72.33	305.32	72.33	16.827	8	60
SC032A	189.59	71.49	316.59	71.49	13.487	8	80
SC032A	206.65	71.8	333.65	71.8	11.163	8	100
SC032A	225.96	64.73	352.96	64.73	9.068	8	140
SC032A	244.27	59.82	11.27	59.82	8.381	8	180
SC033A	67.94	62.83	194.94	62.83	32.944	8	0
SC033A	68.55	61.6	195.55	61.6	31.961	8	2
SC033A	70.28	58.18	197.28	58.18	30.655	8	5
SC033A	71.98	56.21	198.98	56.21	28.645	8	10
SC033A	71.83	50.67	198.83	50.67	26.205	8	20
SC033A	70.41	49.7	197.41	49.7	24.576	8	30
SC033A	70.56	46.85	197.56	46.85	22.401	8	40
SC033A	70.59	48.9	197.59	48.9	18.244	8	60
SC033A	69.28	48.93	196.28	48.93	14.427	8	80
SC033A	70.19	50.46	197.19	50.46	11.869	8	100
SC033A	68.04	58.62	195.04	58.62	8.609	8	140
SC033A	62.48	60.35	189.48	60.35	6.832	8	180
SC034A	208.95	68.42	335.95	68.42	25.552	8	0
SC034A	218.3	68.98	345.3	68.98	26.193	8	2
SC034A	221.99	66.06	348.99	66.06	25.935	8	5
SC034A	228.5	66.13	355.5	66.13	24.025	8	10
SC034A	227.96	66.01	354.96	66.01	20.502	8	20
SC034A	228.26	65.15	355.26	65.15	18.68	8	30
SC034A	231.91	67.87	358.91	67.87	16.849	8	40
SC034A	229.92	66.48	356.92	66.48	13.765	8	60
SC034A	229.25	64.14	356.25	64.14	11.295	8	80
SC034A	229.68	62.87	356.68	62.87	9.614	8	100
SC034A	238.13	60.66	5.13	60.66	7.589	8	140
SC034A	242.92	60.36	9.92	60.36	6.937	8	180
SC035A	206.46	62.74	333.46	62.74	31.141	8	0
SC035A	210.67	62.83	337.67	62.83	31.682	8	2
SC035A	212.54	62.84	339.54	62.84	31.389	8	5
SC035A	211.27	62.61	338.27	62.61	29.219	8	10
SC035A	211.2	62.18	338.2	62.18	25.666	8	20
SC035A	208.22	62.56	335.22	62.56	23.235	8	30
SC035A	213.98	62.79	340.98	62.79	20.822	8	40
SC035A	211.93	62.98	338.93	62.98	17.066	8	60
SC035A	213.29	62.28	340.29	62.28	13.99	8	80
SC035A	214.22	62.25	341.22	62.25	11.444	8	100
SC035A	218.45	54.68	345.45	54.68	9.316	8	140
SC035A	225.37	52.84	352.37	52.84	8.61	8	180
SC036A	218.56	35.43	345.56	35.43	52.62	8	0
SC036A	219.24	35	346.24	35	53.024	8	2
SC036A	222.08	32.82	349.08	32.82	53.657	8	5
SC036A	221.64	31.39	348.64	31.39	52.229	8	10
SC036A	222.67	31.62	349.67	31.62	48.997	8	20

SC036A	222.4	29.72	349.4	29.72	44.754	8	30
SC036A	222.49	29.79	349.49	29.79	41.438	8	40
SC036A	224.51	28.76	351.51	28.76	33.317	8	60
SC036A	224.12	29.09	351.12	29.09	26.705	8	80
SC036A	226.93	28.04	353.93	28.04	22.169	8	100
SC036A	230.69	29.56	357.69	29.56	17.515	8	140
SC036A	235.04	27.91	2.04	27.91	15.564	8	180
SC037A	221.1	39.73	348.1	39.73	57.601	8	0
SC037A	217.42	38.66	344.42	38.66	57.65	8	2
SC037A	214.97	37.51	341.97	37.51	56.046	8	5
SC037A	212.44	37.57	339.44	37.57	53.605	8	10
SC037A	211.61	37.49	338.61	37.49	49.364	8	20
SC037A	211.49	36.77	338.49	36.77	45.659	8	30
SC037A	210.97	37.93	337.97	37.93	41.94	8	40
SC037A	214.17	37.84	341.17	37.84	34.093	8	60
SC037A	214.93	35.96	341.93	35.96	26.605	8	80
SC037A	219.61	35.91	346.61	35.91	21.8	8	100
SC037A	227.1	32.63	354.1	32.63	17.413	8	140
SC037A	234.41	32.57	1.41	32.57	15.879	8	180
SC038A	223.39	37.04	336.39	37.04	32.844	8	0
SC038A	221.21	37.02	334.21	37.02	33.398	8	2
SC038A	218.33	34.17	331.33	34.17	33.245	8	5
SC038A	216.08	30.24	329.08	30.24	31.254	8	10
SC038A	212.58	29.23	325.58	29.23	27.677	8	20
SC038A	214.76	27.9	327.76	27.9	25.077	8	30
SC038A	214.18	27.02	327.18	27.02	22.585	8	40
SC038A	216.34	25.27	329.34	25.27	18.697	8	60
SC038A	222.99	26.15	335.99	26.15	15.611	8	80
SC038A	227.37	24.45	340.37	24.45	13.488	8	100
SC038A	236.61	20.84	349.61	20.84	11.979	8	140
SC038A	242.8	19.62	355.8	19.62	11.488	8	180
SC039A	172.18	36.26	285.18	36.26	31.565	8	0
SC039A	171.66	37.62	284.66	37.62	32.144	8	2
SC039A	172.92	36.62	285.92	36.62	32.676	8	5
SC039A	168.19	35.6	281.19	35.6	31.115	8	10
SC039A	166.06	33.56	279.06	33.56	27.867	8	20
SC039A	164.38	33.47	277.38	33.47	25.056	8	30
SC039A	165.58	32.82	278.58	32.82	22.526	8	40
SC039A	167.74	32.16	280.74	32.16	17.712	8	60
SC039A	176.03	32.67	289.03	32.67	14.096	8	80
SC039A	182.56	33.49	295.56	33.49	11.483	8	100
SC039A	195.21	32.93	308.21	32.93	9.31	8	140
SC039A	207.03	34.22	320.03	34.22	8.444	8	180
SC040A	142.6	24.47	255.6	24.47	47.161	8	0
SC040A	141.9	24.68	254.9	24.68	46.844	8	2
SC040A	143.03	23.32	256.03	23.32	45.481	8	5

SC040A	141.47	20.74	254.47	20.74	43.421	8	10
SC040A	139.26	18.59	252.26	18.59	40.326	8	20
SC040A	137.6	17.93	250.6	17.93	37.28	8	30
SC040A	138.41	17.14	251.41	17.14	33.164	8	40
SC040A	138.14	17.46	251.14	17.46	26.139	8	60
SC040A	138.81	18.08	251.81	18.08	19.797	8	80
SC040A	139.76	18.1	252.76	18.1	15.634	8	100
SC040A	140.86	20	253.86	20	11.034	8	140
SC040A	146.8	19.79	259.8	19.79	9.406	8	180
SC041A	142.86	54.25	255.86	54.25	20.257	8	0
SC041A	147.01	53.74	260.01	53.74	20.39	8	2
SC041A	153.23	53.83	266.23	53.83	19.221	8	5
SC041A	153.33	50.02	266.33	50.02	17.156	8	10
SC041A	147.22	46.26	260.22	46.26	14.579	8	20
SC041A	143.64	45.33	256.64	45.33	12.926	8	30
SC041A	145.29	44.33	258.29	44.33	11.581	8	40
SC041A	147.88	45.34	260.88	45.34	8.972	8	60
SC041A	154.81	46.17	267.81	46.17	7.453	8	80
SC041A	164.28	47.37	277.28	47.37	5.924	8	100
SC041A	189.85	52.14	302.85	52.14	5.067	8	140
SC041A	216.01	50.18	329.01	50.18	4.576	8	180
SC042A	236.3	40.8	349.3	40.8	42.535	8	0
SC042A	240.18	40.93	353.18	40.93	43.27	8	2
SC042A	239.25	38.74	352.25	38.74	43.772	8	5
SC042A	238.23	37.04	351.23	37.04	42.339	8	10
SC042A	246.93	29.28	359.93	29.28	36.291	8	20
SC042A	254.25	23.18	7.25	23.18	29.845	8	30
SC042A	258.49	19.57	11.49	19.57	27.549	8	40
SC042A	262.15	16.19	15.15	16.19	22.397	8	60
SC042A	262.14	17.25	15.14	17.25	19.028	8	80
SC042A	262.77	17.35	15.77	17.35	16.752	8	100
SC042A	264.56	18.13	17.56	18.13	13.601	8	140
SC042A	264.25	19.15	17.25	19.15	12.091	8	180
SC043A	258.79	20.96	11.79	20.96	46.034	8	0
SC043A	257.43	20.74	10.43	20.74	45.55	8	2
SC043A	254.95	21.34	7.95	21.34	45.798	8	5
SC043A	253.94	19.09	6.94	19.09	43.793	8	10
SC043A	252.63	16.73	5.63	16.73	40.697	8	20
SC043A	254.91	15.56	7.91	15.56	37.76	8	30
SC043A	254.6	14.24	7.6	14.24	34.721	8	40
SC043A	253.03	14.81	6.03	14.81	28.247	8	60
SC043A	252.5	14.16	5.5	14.16	23.408	8	80
SC043A	251.22	14.75	4.22	14.75	20.212	8	100
SC043A	252.21	14.93	5.21	14.93	16.6	8	140
SC043A	249.7	14.85	2.7	14.85	14.789	8	180
SC044A	263.47	14.28	16.47	14.28	39.945	8	0

SC044A	259.69	16.77	12.69	16.77	31.725	8	2
SC044A	259.27	12.76	12.27	12.76	39.567	8	5
SC044A	257.75	10.35	10.75	10.35	37.922	8	10
SC044A	257.76	7.29	10.76	7.29	35.203	8	20
SC044A	258.91	7.17	11.91	7.17	31.619	8	30
SC044A	258.46	6.8	11.46	6.8	29.383	8	40
SC044A	261.83	5.79	14.83	5.79	23.615	8	60
SC044A	260.23	5.39	13.23	5.39	20.453	8	80
SC044A	259.85	6.54	12.85	6.54	17.883	8	100
SC044A	260.39	6.61	13.39	6.61	14.999	8	140
SC044A	263.57	6.44	16.57	6.44	13.338	8	180
SC045A	275.95	21.96	28.95	21.96	43.793	8	0
SC045A	273.81	20.8	26.81	20.8	42.217	8	2
SC045A	271.94	20.39	24.94	20.39	41.456	8	5
SC045A	273.06	20.01	26.06	20.01	40.058	8	10
SC045A	275.5	18.2	28.5	18.2	37.474	8	20
SC045A	276.5	16.1	29.5	16.1	34.856	8	30
SC045A	276.93	16.4	29.93	16.4	31.952	8	40
SC045A	276.36	15.74	29.36	15.74	26.779	8	60
SC045A	275.38	15.86	28.38	15.86	22.304	8	80
SC045A	273.91	15.15	26.91	15.15	19.695	8	100
SC045A	272.42	13.22	25.42	13.22	17.194	8	140
SC045A	271.9	13.01	24.9	13.01	16.437	8	180
SC046A	264.16	24.95	17.16	24.95	42.379	8	0
SC046A	262.3	26.33	15.3	26.33	42.397	8	2
SC046A	261.69	24.82	14.69	24.82	41.606	8	5
SC046A	260.59	24.15	13.59	24.15	39.377	8	10
SC046A	261.5	20.89	14.5	20.89	35.998	8	20
SC046A	262.48	20.75	15.48	20.75	33.169	8	30
SC046A	263.53	19.07	16.53	19.07	30.086	8	40
SC046A	264.09	18.34	17.09	18.34	25.209	8	60
SC046A	263.16	18.4	16.16	18.4	21.507	8	80
SC046A	263.16	17.6	16.16	17.6	19.467	8	100
SC046A	264.36	16.94	17.36	16.94	17.469	8	140
SC046A	265.73	16.66	18.73	16.66	16.863	8	180
SC047A	282.98	23.5	35.98	23.5	81.694	8	0
SC047A	282.49	23.77	35.49	23.77	82.465	8	2
SC047A	280.9	23.82	33.9	23.82	82.189	8	5
SC047A	281.76	23.01	34.76	23.01	80.672	8	10
SC047A	282.01	22.71	35.01	22.71	76.411	8	20
SC047A	282.27	21.27	35.27	21.27	71.623	8	30
SC047A	283.29	21.74	36.29	21.74	65.766	8	40
SC047A	283.96	20.98	36.96	20.98	52.849	8	60
SC047A	283.25	20.52	36.25	20.52	42.232	8	80
SC047A	282.33	19.18	35.33	19.18	35.274	8	100
SC047A	279.3	17.65	32.3	17.65	27.207	8	140
SC047A	279.06	17.2	32.06	17.2	24.058	8	180

SC048A	115.71	49.46	228.71	49.46	47.531	8	0
SC048A	116.86	52.24	229.86	52.24	47.052	8	2
SC048A	119.96	50.55	232.96	50.55	47.135	8	5
SC048A	118.45	49.12	231.45	49.12	46.333	8	10
SC048A	118.41	45.28	231.41	45.28	44.321	8	20
SC048A	116.06	44.09	229.06	44.09	42.138	8	30
SC048A	115.03	43.6	228.03	43.6	38.971	8	40
SC048A	113.96	43.72	226.96	43.72	30.639	8	60
SC048A	114.29	46.71	227.29	46.71	22.668	8	80
SC048A	113.07	51	226.07	51	17.035	8	100
SC048A	106.57	59.6	219.57	59.6	11.34	8	140
SC048A	101.43	69.26	214.43	69.26	9.094	8	180
SC049A	313.94	40.02	66.94	40.02	34.995	8	0
SC049A	312.87	40.01	65.87	40.01	33.616	8	2
SC049A	309.22	40.83	62.22	40.83	31.824	8	5
SC049A	309.81	40.62	62.81	40.62	28.808	8	10
SC049A	313.19	37.75	66.19	37.75	26.033	8	20
SC049A	317.76	35.86	70.76	35.86	24.134	8	30
SC049A	318.68	35.15	71.68	35.15	22.106	8	40
SC049A	317.96	34.26	70.96	34.26	18.229	8	60
SC049A	312.13	32.92	65.13	32.92	15.23	8	80
SC049A	306.41	31.87	59.41	31.87	13.419	8	100
SC049A	300.46	29.76	53.46	29.76	11.827	8	140
SC049A	299.81	27.82	52.81	27.82	11.474	8	180
SC050A	272.34	62.29	25.34	62.29	99.044	8	0
SC050A	269.65	63.07	22.65	63.07	99.348	8	2
SC050A	266.13	62.7	19.13	62.7	97.523	8	5
SC050A	268.23	62.86	21.23	62.86	93.802	8	10
SC050A	268.45	61.35	21.45	61.35	87.767	8	20
SC050A	269.46	60.03	22.46	60.03	82.28	8	30
SC050A	268.55	60.24	21.55	60.24	74.656	8	40
SC050A	268.84	59.85	21.84	59.85	59.529	8	60
SC050A	263.69	60.05	16.69	60.05	45.121	8	80
SC050A	263.93	58.05	16.93	58.05	35.861	8	100
SC050A	257.59	54.76	10.59	54.76	25.617	8	140
SC050A	257.32	53.96	10.32	53.96	21.311	8	180
SC051A	270.47	20.71	26.47	20.71	43.745	8	0
SC051A	270.44	19.38	26.44	19.38	43.599	8	2
SC051A	269.37	18.72	25.37	18.72	42.323	8	5
SC051A	269.21	16.97	25.21	16.97	40.33	8	10
SC051A	270.21	16.21	26.21	16.21	36.997	8	20
SC051A	272.2	14.89	28.2	14.89	34.501	8	30
SC051A	272.76	13.87	28.76	13.87	31.794	8	40
SC051A	272.62	13.73	28.62	13.73	26.441	8	60
SC051A	270.23	13.05	26.23	13.05	23.321	8	80
SC051A	269.17	12.9	25.17	12.9	21.45	8	100

SC051A	268.4	10.73	24.4	10.73	20.719	8	140
SC051A	268.87	9.46	24.87	9.46	20.868	8	180
SC052A	266.19	63.58	22.19	63.58	61.237	8	0
SC052A	263.04	62.15	19.04	62.15	62.007	8	2
SC052A	260.83	62.03	16.83	62.03	61.233	8	5
SC052A	257.47	63.53	13.47	63.53	58.293	8	10
SC052A	261.53	63.57	17.53	63.57	54.007	8	20
SC052A	263.31	63.79	19.31	63.79	50.39	8	30
SC052A	263.12	63.01	19.12	63.01	46.196	8	40
SC052A	265.29	62.08	21.29	62.08	38.142	8	60
SC052A	262.29	59	18.29	59	30.184	8	80
SC052A	262.64	54.25	18.64	54.25	24.648	8	100
SC052A	261.68	44.83	17.68	44.83	20.551	8	140
SC052A	261.38	39.66	17.38	39.66	19.381	8	180
SC053A	103.46	47.15	219.46	47.15	61.074	8	0
SC053A	103.97	47.92	219.97	47.92	60.6	8	2
SC053A	105.94	48.5	221.94	48.5	59.284	8	5
SC053A	106.01	46.46	222.01	46.46	57.52	8	10
SC053A	103.79	44.75	219.79	44.75	56.365	8	15
SC053A	102.99	44.56	218.99	44.56	55.174	8	20
SC053A	103.49	43.29	219.49	43.29	53.378	8	25
SC053A	102.81	42.8	218.81	42.8	51.829	8	30
SC053A	102.78	42.18	218.78	42.18	50.068	8	35
SC053A	101.46	42.34	217.46	42.34	47.887	8	40
SC053A	100.73	42.54	216.73	42.54	42.911	8	50
SC053A	101.52	43.26	217.52	43.26	38.077	8	60
SC053A	101.28	45.95	217.28	45.95	28.116	8	80
SC053A	104.41	52.36	220.41	52.36	20.719	8	100
SC053A	112.86	60.87	228.86	60.87	15.912	8	120
SC053A	116.71	71.15	232.71	71.15	12.926	8	140
SC053A	136.43	78.23	252.43	78.23	11.363	8	160
SC053A	194.04	82.77	310.04	82.77	9.932	8	180
SC054A	280.8	26.33	36.8	26.33	37.747	8	0
SC054A	278.93	27.44	34.93	27.44	36.893	8	2
SC054A	274.21	27.09	30.21	27.09	35.265	8	5
SC054A	272.87	26.06	28.87	26.06	32.288	8	10
SC054A	273.14	24.54	29.14	24.54	29.203	8	20
SC054A	273.38	22	29.38	22	26.609	8	30
SC054A	273.78	21.53	29.78	21.53	24.306	8	40
SC054A	274.68	20.78	30.68	20.78	20.282	8	60
SC054A	274.46	21.52	30.46	21.52	17.106	8	80
SC054A	275.88	20.24	31.88	20.24	15.014	8	100
SC054A	272.24	19.17	28.24	19.17	13.535	8	140
SC054A	275.6	19.75	31.6	19.75	12.376	8	180
SC055A	304.99	42.55	60.99	42.55	32.388	8	0
SC055A	304.54	41.88	60.54	41.88	32.227	8	2

SC055A	302.85	43.44	58.85	43.44	30.909	8	5
SC055A	303.84	43.03	59.84	43.03	28.115	8	10
SC055A	306.62	40.63	62.62	40.63	25.132	8	20
SC055A	307.74	38.43	63.74	38.43	23.133	8	30
SC055A	302.13	41.19	58.13	41.19	19.795	8	40
SC055A	309.17	37.73	65.17	37.73	17.516	8	60
SC055A	301.29	37.78	57.29	37.78	14.506	8	80
SC055A	295.64	38.31	51.64	38.31	12.484	8	100
SC055A	285.35	35.18	41.35	35.18	10.555	8	140
SC055A	280.86	33.38	36.86	33.38	9.605	8	180
SC056A	274.68	55.97	30.68	55.97	95.335	8	0
SC056A	273.41	55.05	29.41	55.05	95.695	8	2
SC056A	274.44	56.28	30.44	56.28	94.536	8	5
SC056A	274.56	56.29	30.56	56.29	91.093	8	10
SC056A	275.14	56.68	31.14	56.68	85.631	8	20
SC056A	277.45	56.37	33.45	56.37	79.498	8	30
SC056A	278.94	54.61	34.94	54.61	73.364	8	40
SC056A	276.62	54.67	32.62	54.67	58.339	8	60
SC056A	275.05	54.17	31.05	54.17	44.814	8	80
SC056A	272.03	53.58	28.03	53.58	35.372	8	100
SC056A	267.84	49.61	23.84	49.61	25.619	8	140
SC056A	266.25	48.3	22.25	48.3	22.139	8	180
SC057A	237.93	52.07	353.93	52.07	114.832	8	0
SC057A	236.57	50.87	352.57	50.87	114.075	8	2
SC057A	235.41	51.8	351.41	51.8	113.706	8	5
SC057A	233.45	50.51	349.45	50.51	109.682	8	10
SC057A	230.98	49.77	346.98	49.77	102.232	8	20
SC057A	233.79	49.81	349.79	49.81	94.942	8	30
SC057A	234.35	49.87	350.35	49.87	87.45	8	40
SC057A	235.92	49.15	351.92	49.15	69.876	8	60
SC057A	234.72	47.99	350.72	47.99	53.281	8	80
SC057A	237.02	47.05	353.02	47.05	42.262	8	100
SC057A	242.44	44.88	358.44	44.88	30.739	8	140
SC057A	247.75	41.8	3.75	41.8	25.889	8	180
SC058A	224.01	55.63	340.01	55.63	87.425	8	0
SC058A	222.33	54.77	338.33	54.77	86.115	8	2
SC058A	221.12	53.96	337.12	53.96	85.465	8	5
SC058A	217.49	54.16	333.49	54.16	83.314	8	10
SC058A	217.46	54.67	333.46	54.67	78.226	8	20
SC058A	217.76	53.95	333.76	53.95	72.298	8	30
SC058A	218.88	53.41	334.88	53.41	66.128	8	40
SC058A	219.38	53.87	335.38	53.87	52.723	8	60
SC058A	220.73	54.87	336.73	54.87	40.862	8	80
SC058A	226.27	53.01	342.27	53.01	32.121	8	100
SC058A	232.94	53.09	348.94	53.09	23.023	8	140
SC058A	239.7	52.78	355.7	52.78	19.01	8	180

SC059A	242.82	48.4	358.82	48.4	52.502	8	0
SC059A	242.43	48.53	358.43	48.53	52.576	8	2
SC059A	241.9	47.36	357.9	47.36	53.334	8	5
SC059A	241.94	44.33	357.94	44.33	51.35	8	10
SC059A	240.65	43.95	356.65	43.95	47.708	8	20
SC059A	240.37	44.29	356.37	44.29	43.922	8	30
SC059A	240.28	43.99	356.28	43.99	40.034	8	40
SC059A	242.18	43.87	358.18	43.87	31.896	8	60
SC059A	245.56	46.09	1.56	46.09	24.603	8	80
SC059A	246.56	48.67	2.56	48.67	19.67	8	100
SC059A	254.8	52.93	10.8	52.93	13.352	8	140
SC059A	253.71	56.14	9.71	56.14	10.906	8	180
SC060A	246.56	50.7	2.56	50.7	194.507	8	0
SC060A	245.42	51.33	1.42	51.33	194.209	8	2
SC060A	245.03	50.58	1.03	50.58	193.364	8	5
SC060A	244	51.22	360	51.22	188.863	8	10
SC060A	243.25	50.49	359.25	50.49	176.967	8	20
SC060A	243.26	50.26	359.26	50.26	160.912	8	30
SC060A	243.09	49.88	359.09	49.88	143.604	8	40
SC060A	243.43	50.57	359.43	50.57	109.989	8	60
SC060A	243.14	51.59	359.14	51.59	81.936	8	80
SC060A	243.29	50.86	359.29	50.86	63.216	8	100
SC060A	242.15	52.24	358.15	52.24	45.322	8	140
SC060A	248.27	53.73	4.27	53.73	37.48	8	180
SC061A	249.91	43.5	5.91	43.5	181.027	8	0
SC061A	249.38	43.91	5.38	43.91	178.686	8	2
SC061A	248.82	44.09	4.82	44.09	175.977	8	5
SC061A	249.72	44.55	5.72	44.55	170.017	8	10
SC061A	251.19	44	7.19	44	159.234	8	20
SC061A	250.79	42.95	6.79	42.95	142.461	8	30
SC061A	251.74	42.31	7.74	42.31	125.949	8	40
SC061A	252.12	40.74	8.12	40.74	92.148	8	60
SC061A	253.01	40.13	9.01	40.13	67.165	8	80
SC061A	254.61	40.25	10.61	40.25	51.359	8	100
SC061A	258.1	37.18	14.1	37.18	37.055	8	140
SC061A	260.97	36.83	16.97	36.83	30.835	8	180
SC062A	266.8	36.1	22.8	36.1	131.946	8	0
SC062A	266.56	36.1	22.56	36.1	131.429	8	2
SC062A	267.77	36.16	23.77	36.16	129.104	8	5
SC062A	266.78	35.15	22.78	35.15	125.644	8	10
SC062A	268.11	33.54	24.11	33.54	117.715	8	20
SC062A	266.64	33.5	22.64	33.5	108.86	8	30
SC062A	267.9	32.72	23.9	32.72	97.654	8	40
SC062A	266.92	32	22.92	32	74.857	8	60
SC062A	266.03	32.86	22.03	32.86	55.519	8	80
SC062A	266.02	33.13	22.02	33.13	43.21	8	100
SC062A	262.96	31.94	18.96	31.94	31.425	8	140

SC062A	261.08	32.07	17.08	32.07	25.711	8	180
SC063A	280.11	27.32	36.11	27.32	43.465	8	0
SC063A	278.43	28.73	34.43	28.73	43.566	8	2
SC063A	274.61	28.24	30.61	28.24	42.499	8	5
SC063A	274.02	27.56	30.02	27.56	40.094	8	10
SC063A	275.06	26.06	31.06	26.06	37.267	8	20
SC063A	275.7	24.43	31.7	24.43	34.099	8	30
SC063A	276.56	21.66	32.56	21.66	30.856	8	40
SC063A	275.51	22.63	31.51	22.63	24.317	8	60
SC063A	275.18	22.99	31.18	22.99	19.705	8	80
SC063A	273.68	23.29	29.68	23.29	15.976	8	100
SC063A	272.37	26.11	28.37	26.11	11.806	8	140
SC063A	271.54	24.71	27.54	24.71	11.059	8	180
SC064A	261.28	30.62	20.28	30.62	109.624	8	0
SC064A	261.22	29.52	20.22	29.52	108.962	8	2
SC064A	259.99	29.52	18.99	29.52	108.313	8	5
SC064A	261.18	28.01	20.18	28.01	103.926	8	10
SC064A	261.76	28.58	20.76	28.58	100.061	8	15
SC064A	261.64	25.75	20.64	25.75	95.661	8	20
SC064A	263.51	26.66	22.51	26.66	91.442	8	25
SC064A	262.93	26.29	21.93	26.29	86.392	8	30
SC064A	262.61	25.37	21.61	25.37	80.579	8	35
SC064A	262.95	24.49	21.95	24.49	74.853	8	40
SC064A	262.5	25.09	21.5	25.09	51.19	8	60
SC064A	261.72	24.22	20.72	24.22	34.058	8	80
SC064A	260.45	24.09	19.45	24.09	25.166	8	100
SC064A	259.03	24.36	18.03	24.36	20.088	8	120
SC064A	261.08	21.66	20.08	21.66	17.901	8	140
SC064A	260.03	21.46	19.03	21.46	16.723	8	160
SC064A	258.6	20.83	17.6	20.83	15.759	8	180
SC065A	254.48	28.84	13.48	28.84	126.422	8	0
SC065A	255.63	29.74	14.63	29.74	123.882	8	2
SC065A	256.83	28.26	15.83	28.26	125.891	8	5
SC065A	257.36	26.96	16.36	26.96	122.604	8	10
SC065A	257.84	27.26	16.84	27.26	118.384	8	15
SC065A	258.2	25.71	17.2	25.71	113.747	8	20
SC065A	257.59	26	16.59	26	109.557	8	25
SC065A	258.37	24.47	17.37	24.47	104.145	8	30
SC065A	257.71	24.45	16.71	24.45	97.507	8	35
SC065A	258.54	24.17	17.54	24.17	90.736	8	40
SC065A	257.46	24.53	16.46	24.53	62.838	8	60
SC065A	257.23	22.15	16.23	22.15	39.966	8	80
SC065A	256.43	23.26	15.43	23.26	28.199	8	100
SC065A	256.03	23.81	15.03	23.81	22.382	8	120
SC065A	256.52	23.65	15.52	23.65	19.057	8	140
SC065A	256.74	22.33	15.74	22.33	17.604	8	160
SC065A	78.14	-23.07	197.14	-23.07	4.83	8	180

SC066A	243.46	43.65	2.46	43.65	1108.001	8	0
SC066A	245.1	42.86	4.1	42.86	1103.982	8	2
SC066A	244.98	43.47	3.98	43.47	1088.045	8	5
SC066A	244.87	43.18	3.87	43.18	1063.546	8	10
SC066A	244.27	42.03	3.27	42.03	1033.99	8	15
SC066A	243.97	42.81	2.97	42.81	985.732	8	20
SC066A	244.39	43.54	3.39	43.54	935.408	8	25
SC066A	244.28	42.51	3.28	42.51	868.43	8	30
SC066A	244.27	43.16	3.27	43.16	791.547	8	35
SC066A	244.79	42.48	3.79	42.48	711.79	8	40
SC066A	242.66	43.42	1.66	43.42	453.124	8	60
SC066A	244.59	42.76	3.59	42.76	282.529	8	80
SC066A	245.19	42.76	4.19	42.76	189.634	8	100
SC066A	244.12	43.28	3.12	43.28	138.949	8	120
SC066A	240.9	46.43	359.9	46.43	106.372	8	140
SC066A	244.15	42.89	3.15	42.89	91.499	8	160
SC066A	244.2	42.79	3.2	42.79	83.492	8	180
SC067A	246.21	32.65	5.21	32.65	814.69	8	0
SC067A	245.91	33.3	4.91	33.3	817.32	8	2
SC067A	246.01	33.55	5.01	33.55	806.522	8	5
SC067A	244.39	32.49	3.39	32.49	785.032	8	10
SC067A	245.09	33.06	4.09	33.06	756.75	8	15
SC067A	244.4	32.61	3.4	32.61	716.694	8	20
SC067A	244.53	33.01	3.53	33.01	669.119	8	25
SC067A	245.84	33.41	4.84	33.41	610.8	8	30
SC067A	244.87	33.02	3.87	33.02	556.223	8	35
SC067A	245.16	33.56	4.16	33.56	500.644	8	40
SC067A	245.07	33.91	4.07	33.91	320.754	8	60
SC067A	245.57	33.22	4.57	33.22	203.752	8	80
SC067A	244.42	33.82	3.42	33.82	140.187	8	100
SC067A	243.95	32.71	2.95	32.71	102.123	8	120
SC067A	243.78	32.74	2.78	32.74	80.414	8	140
SC067A	243.71	33.47	2.71	33.47	65.92	8	160
SC067A	242.41	34.17	1.41	34.17	57.581	8	180
SC068A	273.13	31.43	32.13	31.43	64.726	8	0
SC068A	270.32	29.51	29.32	29.51	64.904	8	2
SC068A	267.98	28.51	26.98	28.51	62.621	8	5
SC068A	266.81	27.62	25.81	27.62	59.096	8	10
SC068A	267.7	24.69	26.7	24.69	53.751	8	20
SC068A	267.54	23.36	26.54	23.36	45.806	8	30
SC068A	268.73	24.53	27.73	24.53	39.247	8	40
SC068A	266.42	21.99	25.42	21.99	26.136	8	60
SC068A	266.88	22.19	25.88	22.19	17.874	8	80
SC068A	264.75	25.43	23.75	25.43	11.834	8	100
SC068A	259.83	26.53	18.83	26.53	7.817	8	140
SC068A	258.6	29.06	17.6	29.06	6.502	8	180

SC069A	269.31	29.34	28.31	29.34	103.134	8	0
SC069A	268.48	29.48	27.48	29.48	103.228	8	2
SC069A	267.2	28.68	26.2	28.68	101.974	8	5
SC069A	266.23	27.37	25.23	27.37	96.907	8	10
SC069A	266.16	25.48	25.16	25.48	88.168	8	20
SC069A	266.24	22.47	25.24	22.47	79.564	8	30
SC069A	266.68	23.64	25.68	23.64	67.973	8	40
SC069A	265.5	23.04	24.5	23.04	45.638	8	60
SC069A	265.16	24.68	24.16	24.68	29.908	8	80
SC069A	262.77	24.87	21.77	24.87	20.252	8	100
SC069A	258.57	28.83	17.57	28.83	12.614	8	140
SC069A	252.13	30.4	11.13	30.4	10.418	8	180
SC070A	247.63	39.54	6.63	39.54	1439.398	8	0
SC070A	247.53	38.88	6.53	38.88	1428.516	8	2
SC070A	246.29	38.4	5.29	38.4	1414.096	8	5
SC070A	247.19	39.25	6.19	39.25	1386.379	8	10
SC070A	247.1	38.04	6.1	38.04	1298.8	8	20
SC070A	248.15	39.69	7.15	39.69	1142.55	8	30
SC070A	247.64	39.32	6.64	39.32	954.064	8	40
SC070A	246.57	40.05	5.57	40.05	608.212	8	60
SC070A	246.06	39.76	5.06	39.76	386.832	8	80
SC070A	245.58	40.29	4.58	40.29	259.603	8	100
SC070A	245.4	40.95	4.4	40.95	152.768	8	140
SC070A	244.39	42.97	3.39	42.97	110.591	8	180
SC071A	246.91	33.56	5.91	33.56	1189.313	8	0
SC071A	246.96	34.09	5.96	34.09	1184.664	8	2
SC071A	247.7	34.51	6.7	34.51	1176.668	8	5
SC071A	247.4	33.66	6.4	33.66	1155.572	8	10
SC071A	247.24	33.36	6.24	33.36	1088.251	8	20
SC071A	246.79	33.82	5.79	33.82	955.237	8	30
SC071A	245.46	33.72	4.46	33.72	794.907	8	40
SC071A	245.63	34.88	4.63	34.88	509.009	8	60
SC071A	245.92	34.71	4.92	34.71	319.148	8	80
SC071A	246.11	35.69	5.11	35.69	213.305	8	100
SC071A	245.22	36.54	4.22	36.54	124.269	8	140
SC071A	244.45	38.01	3.45	38.01	91.764	8	180
SC072A	253.6	36.06	12.6	36.06	214.672	8	0
SC072A	254.09	35.4	13.09	35.4	213.635	8	2
SC072A	252.75	36.29	11.75	36.29	214.213	8	5
SC072A	253.24	35.11	12.24	35.11	207.184	8	10
SC072A	253.49	34.61	12.49	34.61	193.666	8	20
SC072A	253.49	34.63	12.49	34.63	173.97	8	30
SC072A	253.6	34.34	12.6	34.34	148.68	8	40
SC072A	253.44	35.9	12.44	35.9	97.538	8	60
SC072A	253.47	36.71	12.47	36.71	61.589	8	80
SC072A	253.11	37.41	12.11	37.41	40.368	8	100
SC072A	250.73	41.27	9.73	41.27	24.452	8	140

SC072A	248.64	42.68	7.64	42.68	17.637	8	180
SC073A	250.35	45.29	9.35	45.29	621.298	8	0
SC073A	250.43	44.09	9.43	44.09	618.008	8	2
SC073A	251.09	44.05	10.09	44.05	617.487	8	5
SC073A	250.49	43.03	9.49	43.03	609.892	8	10
SC073A	252.36	43.57	11.36	43.57	579.359	8	20
SC073A	251.55	44.14	10.55	44.14	520.534	8	30
SC073A	249.44	44.44	8.44	44.44	450.414	8	40
SC073A	250.97	44.23	9.97	44.23	298.106	8	60
SC073A	248.38	44.37	7.38	44.37	187.868	8	80
SC073A	248.19	44.32	7.19	44.32	126.312	8	100
SC073A	248.35	44.07	7.35	44.07	72.745	8	140
SC073A	247.74	43.67	6.74	43.67	53.563	8	180
SC074A	250.08	41.25	9.08	41.25	806.992	8	0
SC074A	248.54	41.85	7.54	41.85	817.262	8	2
SC074A	248.29	41.45	7.29	41.45	808.539	8	5
SC074A	248.52	41.03	7.52	41.03	789.133	8	10
SC074A	249	41.17	8	41.17	750.567	8	20
SC074A	247.7	40.46	6.7	40.46	682.137	8	30
SC074A	248.21	42.07	7.21	42.07	586.544	8	40
SC074A	248.09	41.4	7.09	41.4	391.486	8	60
SC074A	248.48	40.01	7.48	40.01	246.603	8	80
SC074A	248.91	40.23	7.91	40.23	162.721	8	100
SC074A	247.38	42.12	6.38	42.12	91.814	8	140
SC074A	247.39	41.44	6.39	41.44	65.964	8	180
SC075A	255.69	38.23	14.69	38.23	520.539	8	0
SC075A	254.66	38.49	13.66	38.49	518.065	8	2
SC075A	254.84	37.52	13.84	37.52	516.408	8	5
SC075A	256	37.57	15	37.57	509.091	8	10
SC075A	255.26	37.2	14.26	37.2	485.725	8	20
SC075A	254.73	37.39	13.73	37.39	443.477	8	30
SC075A	255.02	37.93	14.02	37.93	385.148	8	40
SC075A	254.93	37.75	13.93	37.75	251.962	8	60
SC075A	254.35	38.79	13.35	38.79	155.318	8	80
SC075A	255.02	38.17	14.02	38.17	101.202	8	100
SC075A	251.95	41.92	10.95	41.92	54.829	8	140
SC075A	249.55	42.47	8.55	42.47	39.541	8	180
SC076A	257.59	47.32	16.59	47.32	254.55	8	0
SC076A	257.99	47.47	16.99	47.47	254.245	8	2
SC076A	259.28	47.67	18.28	47.67	252.546	8	5
SC076A	258.28	46.47	17.28	46.47	233.39	8	20
SC076A	259.3	47.06	18.3	47.06	211.848	8	30
SC076A	258.49	48.02	17.49	48.02	181.379	8	40
SC076A	258.97	48.72	17.97	48.72	118.771	8	60
SC076A	258.58	48.08	17.58	48.08	72.459	8	80
SC076A	255.28	48.44	14.28	48.44	47.723	8	100

SC076A	256.25	51.8	15.25	51.8	28.753	8	140
SC076A	250.77	54.83	9.77	54.83	21.857	8	180
SC077A	245.5	46.8	4.5	46.8	416.302	8	0
SC077A	245.72	47.84	4.72	47.84	410.225	8	2
SC077A	247.19	47.57	6.19	47.57	403.725	8	5
SC077A	247.07	46.17	6.07	46.17	403.792	8	10
SC077A	245.6	46.23	4.6	46.23	388.85	8	15
SC077A	246.57	46.9	5.57	46.9	384.764	8	20
SC077A	246.95	46.93	5.95	46.93	370.773	8	25
SC077A	246.91	47.85	5.91	47.85	348.585	8	30
SC077A	245.45	46.61	4.45	46.61	324.183	8	35
SC077A	247.21	48.25	6.21	48.25	299.922	8	40
SC077A	246.26	47.52	5.26	47.52	197.631	8	60
SC077A	245.07	47.02	4.07	47.02	122.452	8	80
SC077A	245.63	47.64	4.63	47.64	80.553	8	100
SC077A	245.98	45.77	4.98	45.77	57.176	8	120
SC077A	242.31	47.45	1.31	47.45	44.822	8	140
SC077A	242.87	47.72	1.87	47.72	36.359	8	160
SC077A	244.1	47.48	3.1	47.48	31.907	8	180

* - Declination and inclination before orientation
correction
† - Declination and inclination after orientation
correction

Appendix D: hysteresis data

Spec. run#1	Hc	Hcr	Hcr/Hc	Mr	Ms	Mr/Ms	Correction	Notes
Sc001a	27.25	70.49	2.59	34.42	106.3	0.3237	-240.2	red clay
sc002a	27.74	70.48	2.54	62.11	188.8	0.3289	-516.5	red clay
sc003a	21.91	65.71	3.00	6.319	23.54	0.2684	-21.08	red clay
sc004a	22.8	72.08	3.16	15.56	57.56	0.2703	-162.3	red clay
sc005a	22.98	66.3	2.89	19.28	62.93	0.3063	-192.6	red clay
sc006a	24.19	67.79	2.80	32.38	102.1	0.3173	-333.2	red clay
sc007a	24.58	70.41	2.86	11.32	37.67	0.3004	-68.9	red clay
sc008a	23.57	65.89	2.80	11.45	35.39	0.3234	-95.41	red clay
sc009a	23.76	69.85	2.94	14.23	46.34	0.3071	-122.9	red clay
sc010a	21.89	68	3.11	8.607	30	0.2869	-54.7	red clay
sc011a	22.08	67.74	3.07	9.66	33.82	0.2856	-71.07	red clay
sc012a	22.32	62.86	2.82	18.09	62.57	0.2892	-147.2	red clay
sc013a	22.76	67.82	2.98	10.77	35.89	0.3001	-78.11	red clay
sc014a	23.94	66.57	2.78	15.05	47.28	0.3183	-97.36	red clay
sc015a	23.61	66.23	2.81	16.67	52.9	0.3152	-138.8	red clay
sc016a	23.92	68.45	2.86	16.73	55.32	0.3032	-150.5	red clay
sc017a	22.21	68.58	3.09	10.01	35.23	0.2841	-74.61	red clay
sc018a	19.7	62.67	3.18	9.292	34.47	0.2696	-24.88	red clay
sc019a	23.05	66.68	2.89	12.5	40.19	0.3109	-84.6	red clay
sc020a	21.41	63.91	2.99	11.58	40.25	0.2877	-88.33	red clay
sc021a	23.03	67.48	2.93	11.54	40.36	0.2859	-72	red clay
sc022a	20.14	65.91	3.27	7.044	26.93	0.2616	-40.35	red clay
sc023a	22.69	67.15	2.96	14.01	46.82	0.2993	-113.9	red clay
sc024a	20.05	65.94	3.29	10.5	37.66	0.2788	-97.88	red clay
sc025a	21.3	66.16	3.11	11.26	39.41	0.2857	-96.03	red clay
sc026a	19.69	63.68	3.23	10.11	37.03	0.273	-78.21	red clay
sc027a	21.83	61.49	2.82	8.025	28.17	0.2849	-46.15	red clay
sc028a	23.17	65.78	2.84	12.07	37.23	0.3242	-85.22	red clay
sc029a	18.23	60.05	3.29	5.801	21.78	0.2664	-20.29	red clay
sc030a	21.17	69.4	3.28	9.561	35.01	0.2731	-66.37	red clay
sc031a	20.55	64.13	3.12	10.62	34.56	0.3073	-75.51	red clay
sc032a	22.99	69.02	3.00	13.62	42.32	0.3219	-100.3	red clay
sc033a	21.21	76.16	3.59	9.113	34.41	0.2649	-80.45	red clay
sc034a	19.93	68.03	3.41	12.67	35.88	0.3531	-109.6	red clay
sc035a	22.74	68.45	3.01	8.672	30.86	0.281	-45.29	red clay
sc036a	23.69	66.53	2.81	12.23	38.36	0.319	-74.36	red clay
sc037a	23.1	64.99	2.81	7.181	24.07	0.2984	-22.77	red clay
sc038a	24.06	67.52	2.81	10.36	35.44	0.2924	-50.45	red clay
sc039a	21.76	61.83	2.84	8.304	28.2	0.2945	-38.67	red clay
sc040a	20.51	65.41	3.19	9.242	30.82	0.2998	-72.59	red clay
sc041a	20.73	67.51	3.26	17.43	63.19	0.2758	-201.5	red clay
sc042a	24.35	70.25	2.89	20.16	64.55	0.3123	-199.4	red clay
sc043a	25.44	70.41	2.77	18.02	55.62	0.3239	-148.3	red clay
sc044a	25.37	74.06	2.92	20.41	68.71	0.297	-214.7	red clay
sc045a	26.45	70.17	2.65	15.37	45.79	0.3356	-92.37	red clay
sc046a	25.25	68.88	2.73	10.33	32.79	0.3151	-38.77	red clay

Spec.	Hc	Hcr	Hcr/Hc	Mr	Ms	Mr/Ms	Correction	Notes
sc047a	35.22	71.27	2.02	38.26	99.77	0.3834	-216.3	red clay
sc048a	26.89	69.13	2.57	14.62	43.78	0.3339	-72.36	red clay
sc049a	26.84	69.85	2.60	18.54	56.45	0.3285	-96.51	red clay
sc050a	26.05	71.45	2.74	13.61	45.47	0.2993	-53.8	red clay
sc051a	23.95	67.94	2.84	11.44	37.78	0.3028	-36.33	red clay
sc052a	22.6	68.55	3.03	8.266	30.75	0.2688	-15.91	red clay
sc053a	27.85	68.33	2.45	34.85	102.9	0.3388	-170.2	red clay
sc054a	25.23	68.74	2.72	25.97	79.65	0.326	-155	red clay
sc055a	21.7	64.8	2.99	14.78	48.31	0.306	-62.24	red clay
sc056a	16.34	60.14	3.68	5.874	21.79	0.2696	14.03	red clay
sc057a	25.25	71.25	2.82	16.12	54.6	0.2953	-56.49	red clay
sc058a	26.21	68.07	2.60	17.95	54.41	0.3239	-57.02	red clay
sc059a	27.01	67.44	2.50	20.77	61.5	0.3377	-77.73	red clay
sc060a1	22.2	56.15	2.53	35.38	155.3	0.2279	-52.79	upper silt/clay laminae
sc060a2	23.11	61.15	2.65	18.6	62.44	0.2979	-70.64	red clay
sc060a3	24.24	56.1	2.31	52.39	219.5	0.2387	-52.65	lower silt
sc060a4	22.58	56.05	2.48	24.93	98.94	0.2543	-45.14	lower silt/clay laminae
sc061a	25.27	59.14	2.34	35.34	125.8	0.2808	-100.6	silt/clay lam.
sc062a	16.55	60.47	3.65	8.776	37.96	0.2312	-27.46	silt/clay lam.
sc063a	20.18	62.8	3.11	14.19	45.39	0.3127	-110.2	clay
sc064a	15.13	49.48	3.27	6.236	23.94	0.2605	-5.436	clay
sc065a	22.15	56.63	2.56	15.13	48.86	0.3097	-72.76	clay
sc066a	23.9	53.09	2.22	254.8	1076	0.2369	-97.73	silt
sc067a	20.2	48.3	2.39	82.46	424.4	0.1943	-29.68	silt
sc068a	21.63	54.2	2.51	22.98	74.64	0.3078	-212.3	clay
sc069a	23.36	55.5	2.38	18.95	59.64	0.3178	-124.6	clay
sc070a	27.29	58.38	2.14	189.8	780	0.2433	-142.7	silt
sc071a	27.72	58.5	2.11	83.21	332.5	0.2502	-59.73	silt
sc072a	25.87	59.26	2.29	16.25	51.98	0.3125	-65.58	upper clay
sc073a1	13.35	48.72	3.65	7.372	28.51	0.2586	-104.9	clay
sc073a2	28.24	58.2	2.06	150.3	563.3	0.2668	-111.5	silt
sc074a1	14.11	48.2	3.42	7.107	29.18	0.2436	-81.1	upper clay
sc074a2	28.4	57.68	2.03	111	410.7	0.2702	-67.02	middle silt
sc074a3	12.6	44.91	3.56	10.62	44.8	0.237	-173.4	lower clay
sc075a1	12.91	48.58	3.76	8.131	35.49	0.2291	-129	upper clay
sc075a2	26.27	56.89	2.17	44.61	177.5	0.2514	-15.81	middle silt
sc075a3	23.95	55.39	2.31	10.41	35.07	0.2969	-18.48	lower clay
sc076a1	13.9	43.37	3.12	10.18	37.32	0.2728	-148.3	upper clay
sc076a2	29.43	58.55	1.99	47.96	169.1	0.2836	-13.7	silt
sc077a1	13.22	41.45	3.14	12.1	45.45	0.2663	-174.9	upper clay
sc077a2	29.11	59	2.03	86.96	318.2	0.2733	-52.64	middle silt
sc077a3	25.38	61.82	2.44	6.39	23.34	0.2737	-142.4	lower clay
sc078a1	21.04	50.64	2.41	132.2	692.3	0.191	-62.01	silt
sc078a2	16.88	42.64	2.53	3.635	18.6	0.1954	28.72	sand lens
run#2								
sc001a	24.05	63.85	2.65	15.23	52.84	0.2881	-76.44	red clay
sc002a	22.59	61.72	2.73	10.76	38.29	0.281	-38.25	red clay

Spec.	Hc	Hcr	Hcr/Hc	Mr	Ms	Mr/Ms	Correction	Notes
sc003a	23.6	62.29	2.64	17.63	57.51	0.3065	-112.9	red clay
sc004a	21.23	59.3	2.79	9.848	34.39	0.2864	-41.4	red clay
sc005a	19.48	55.65	2.86	7.328	26.99	0.2715	-24.77	red clay
sc006a	19.48	55.95	2.87	6.196	22.93	0.2702	-11.85	red clay
sc007a	23.18	63.36	2.73	11.93	39.23	0.3042	-65.37	red clay
sc008a	23.41	64.81	2.77	15.44	48.78	0.3164	-110.5	red clay
sc009a	22.54	62.91	2.79	14.01	45.19	0.3101	-112.4	red clay
sc010a	21.29	60.84	2.86	11.24	36.99	0.3039	-76.42	red clay
sc011a	21.88	62.11	2.84	8.795	29.05	0.3027	-60.48	red clay
sc012a	20.88	60.24	2.89	10.25	34.84	0.2942	-68.91	red clay
sc013a	23.25	64.92	2.79	18.22	57.8	0.3153	-149.6	red clay
sc014a	22.05	64.55	2.93	10.52	37.74	0.2788	-75.37	red clay
sc015a	18.57	58.1	3.13	9.402	35.36	0.2659	-53.81	red clay
sc016a	17.42	54.92	3.15	7.379	30.65	0.2408	-23.37	red clay
sc017a	17.7	59.22	3.35	8.044	33.19	0.2423	-35.35	red clay
sc018a	21.8	63.36	2.91	17.57	57.74	0.3043	-132.3	red clay
sc019a	15.9	51.87	3.26	5.292	21.12	0.2505	0.7229	red clay
sc020a	19.26	62.37	3.24	10.52	39.96	0.2632	-84.54	red clay
sc021a	21.66	61.8	2.85	14.3	46.68	0.3063	-105.2	red clay
sc022a	17.81	57.28	3.22	6.698	25.09	0.2669	-17.06	red clay
sc023a	18.55	58.05	3.13	8.446	31.01	0.2724	-37.88	red clay
sc024a	16.37	57.72	3.53	7.682	33.69	0.228	-64.23	red clay
sc025a	19.8	60.52	3.06	9.268	32.55	0.2847	-58.85	red clay
sc026a	19.37	61.87	3.19	10.7	36.35	0.2943	-84.51	red clay
sc027a	23.05	65.35	2.84	19.51	63.08	0.3093	-155.4	red clay
sc028a	20.5	61.33	2.99	10.56	36.59	0.2885	-61.89	red clay
sc029a	21.23	65.2	3.07	17.02	60.6	0.2808	-152.6	red clay
sc030a	19.02	62.41	3.28	9.605	37.44	0.2565	-57.83	red clay
sc031a	18.19	61.26	3.37	9.136	35.86	0.2548	-65.54	red clay
sc032a	22.3	67.05	3.01	15.41	50.77	0.3034	-122.7	red clay
sc033a	21.65	66.45	3.07	13.4	45.55	0.2942	-104.9	red clay
sc034a	22.07	64.26	2.91	12.56	40.6	0.3093	-85.78	red clay
sc035a	26.22	66.76	2.55	25.08	77.19	0.325	-156.8	red clay
sc036a	26.78	67.96	2.54	33.17	99.44	0.3335	-222.2	red clay
sc037a	17.09	55.7	3.26	4.69	19.89	0.2358	-1.977	red clay
sc038a	26.68	67.09	2.51	23.21	68.99	0.3365	-140.7	red clay
sc039a	18.83	57.08	3.03	5.29	19.98	0.2647	-462.1	red clay
sc040a	18.87	61.64	3.27	14.48	52.69	0.2747	-133.9	red clay
sc041a	17.7	62.06	3.51	18.2	66.11	0.2753	-187	red clay
sc042a	18.66	63.96	3.43	17.19	60.87	0.2823	-146.2	red clay
sc043a	16.01	63.48	3.97	11.32	48.09	0.2353	-99.93	red clay
sc044a	20.88	64.9	3.11	19.85	67.19	0.2955	-141.6	red clay
sc045a	21.63	64.34	2.97	14.56	49.43	0.2945	-77.17	red clay
sc046a	24.05	66.34	2.76	27.31	86.01	0.3175	-166	red clay
sc047a	26.38	68.97	2.61	31.63	95.93	0.3297	-183.9	red clay
sc048a	25.23	71.79	2.85	20.53	73.84	0.278	-110.4	red clay
sc049a	22.63	69.82	3.09	21.53	77.72	0.277	-140	red clay
sc050a	23.15	67.03	2.90	21.25	70.65	0.3008	-119.8	red clay
sc051a	26.59	69.14	2.60	28.2	88.69	0.318	-155.2	red clay

Spec.	Hc	Hcr	Hcr/Hc	Mr	Ms	Mr/Ms	Correction	Notes
sc052a	23	65.33	2.84	19.34	63.79	0.3031	-94.62	red clay
sc053a	27.38	67.6	2.47	36.39	110.1	0.3306	-180.4	red clay
sc054a	21.34	69.54	3.26	17.22	65.52	0.2628	-113.6	red clay
sc055a	24.49	71.69	2.93	25.81	90.19	0.2861	-165.2	red clay
sc056a	25.87	68.35	2.64	24.02	76.26	0.315	-115.3	red clay
sc057a	29.22	70.61	2.42	45.05	136.2	0.3309	-222.4	red clay
sc058a	28.37	68.59	2.42	38.3	115.7	0.331	-177	red clay
sc059a	28.73	68.54	2.39	37.02	109	0.3395	-176.7	red clay
sc060a1	28.57	60.94	2.13	60.88	195.2	0.312	-153.4	upper silt/clay lam.
sc060a2	24.36	60.68	2.49	35.29	125.8	0.2805	-146.6	middle clay
sc060a3	24.72	56.86	2.30	70.34	287.9	0.2443	-75.86	lower silt/clay lam.
sc061a1	23.55	59	2.51	44.58	166.4	0.2679	-187.4	silt/clay lam.
sc061a2	25.01	58.55	2.34	53.97	202.4	0.2667	-154.2	silt/clay lam.
sc062a1	21.02	55.23	2.63	31.37	132	0.2376	-110.8	silt/clay lam.
sc062a2	21.93	63.75	2.91	20.42	67.41	0.3029	-126.7	predominantely silt
sc063a1	23.53	64.65	2.75	28.31	89.8	0.3152	-187.4	upper clay/silt lam.
sc063a2	19.71	66.12	3.35	21.12	75.03	0.2815	-210.3	lower clay
sc064a	24.54	56.37	2.30	50.64	147.3	0.3438	-360.3	clay
sc065a	23.67	56.57	2.39	34.23	103.3	0.3315	-228.5	clay
sc066a	27.18	57.05	2.10	218.4	844.8	0.2586	-151.2	silt
sc067a	21.24	50.74	2.39	287.9	1476	0.1951	-191.1	silt
sc068a	17.24	48.93	2.84	20.25	70.45	0.2875	-206.3	clay
sc069a	22.52	58.51	2.60	31.34	114.2	0.2744	-168.2	clay
sc070a	24.03	56.22	2.34	69.43	316	0.2197	-22.17	silt
sc071a	25.52	53.85	2.11	330.8	1349	0.2452	-224.2	silt
sc072a1	16.28	48.09	2.95	26.52	95.27	0.2783	-354.9	upper clay
sc072a2	26.34	57.42	2.18	55.67	211.9	0.2627	-72.01	lower silt
sc072a3	26.48	56.19	2.12	143.1	557.7	0.2565	-199.8	lower silt
sc073a1	12.97	43.13	3.33	14.21	55.11	0.2579	-214.8	upper clay
sc073a2	26.33	56.37	2.14	305.2	1242	0.2457	-217.5	middle silt
sc073a3	13.19	47.35	3.59	18.92	74.42	0.2543	-315.5	lower clay
sc074a1	14.43	46.99	3.26	11.6	46.46	0.2497	-131.1	upper clay
sc074a2	27.39	58.42	2.13	235.8	952	0.2477	-175.1	middle silt
sc074a3	11.6	40.44	3.49	9.09	43.73	0.2079	-86.95	lower clay
sc075a1	11.72	41.68	3.56	11.2	51.2	0.2188	-143.4	upper clay
sc075a2	31.01	59.81	1.93	78.19	241.1	0.3242	-121.3	middle silt
sc075a3	22.4	51.95	2.32	43.43	140.9	0.3081	-280.4	lower clay
sc076a1	11.38	40.22	3.53	11.34	47.72	0.2376	-188.1	upper clay
sc076a2	28.56	57.82	2.02	187.3	681.1	0.2751	-134.2	lower silt
sc077a1	15.44	47.73	3.09	19.6	75.24	0.2605	-243.8	upper clay
sc077a2	28.61	58.29	2.04	149.3	542.3	0.2753	-133.7	middle silt
sc077a3	17.22	47.37	2.75	12.07	63.95	0.1888	-176	lower clay
sc078a	23.17	54.29	2.34	281.4	1392	0.2021	-183.2	silt
run#3								
sc005a	20.95	64.11	3.060	15.6	54.92	0.284	-142.5	red clay

Spec.	Hc	Hcr	Hcr/Hc	Mr	Ms	Mr/Ms	Correction	Notes
sc006a	20.24	60.87	3.007	8.931	30.51	0.2927	-51.83	red clay
sc007a	22.34	63.56	2.845	12.47	41.14	0.3031	-77.69	red clay
sc008a	21.07	56.85	2.698	9.372	35.8	0.2618	-74.62	red clay
sc009a	21.49	63.15	2.939	10.24	33.3	0.3074	-69.92	red clay
sc010a	19.66	62.57	3.183	17.4	61.69	0.282	-173.8	red clay
sc011a	18.28	62.49	3.418	8.994	34.21	0.2629	-63.46	red clay
sc012a	21.22	64.77	3.052	19.89	69.99	0.2842	-191.1	red clay
sc013a	19.82	62.48	3.152	18.13	62.53	0.2899	-168.6	red clay
sc014a	19.38	62.85	3.243	14.24	52.22	0.2726	-111.4	red clay
sc015a	21.09	62.64	2.970	17.35	57.23	0.3032	-124	red clay
sc016a	16.09	57.98	3.603	9.369	39.24	0.2388	-54.22	red clay
sc017a	19.35	61.02	3.153	13.99	49.42	0.283	-96.56	red clay
sc018a	19.63	65.58	3.341	17.46	64.41	0.271	-177.9	red clay
sc019a	19.25	62.89	3.267	13.2	48.59	0.2717	-100.2	red clay
sc020a	16.44	56.21	3.419	9.314	41.29	0.2256	-51.28	red clay
sc021a	20.34	64.62	3.177	17.5	65.68	0.2665	-159.1	red clay
sc022a	18.42	59.56	3.233	12.37	43.92	0.2817	-82.59	red clay
sc023a	19.88	62	3.119	16.79	58.76	0.2858	-134.3	red clay
sc024a	19.03	60.6	3.184	11.55	44.08	0.262	-86.16	red clay
sc025a	17.55	59.96	3.417	15.31	59.9	0.2556	-121.5	red clay
sc026a	16.05	58.17	3.624	13.29	55.78	0.2382	-102.5	red clay
sc027a	17.45	59.98	3.437	14.08	54.65	0.2577	-90.89	red clay
sc028a	17.79	59.94	3.369	14.23	54.75	0.2599	-92.88	red clay
sc029a	17.01	63.12	3.711	17.77	77.13	0.2304	-186.1	red clay
sc030a	16.92	63.99	3.782	14.13	63.33	0.2232	-130.7	red clay
sc031a	13.92	55.17	3.963	9.204	41.8	0.2202	-54.55	red clay
sc032a	19.03	62.67	3.293	17.56	62.95	0.279	-139.1	red clay
sc033a	17.92	61.43	3.428	13.93	51.26	0.2718	-93.66	red clay
sc034a	19.82	62.54	3.155	19.95	67.8	0.2943	-154.4	red clay
sc035a	18.03	60.68	3.366	13.66	51.87	0.2633	-79.77	red clay
sc036a	21.73	63.43	2.919	19.58	67.41	0.2904	-101.4	red clay
sc037a	8.282	36.57	4.416	3.266	22.94	0.1424	18.18	diamagnetic
sc038a	16.27	59.83	3.677	10.92	46.71	0.2337	-68.21	red clay
sc039a	19.42	61.9	3.187	17.05	62.76	0.2717	-125	red clay
sc040a	16.04	60.99	3.802	10.43	45.27	0.2303	-92.69	red clay
sc041a	15.53	58.94	3.795	9.735	40.53	0.2402	-79.85	red clay
sc042a	21.56	65.15	3.022	22.51	72.04	0.3125	-191.5	red clay
sc043a	19.7	68.46	3.475	16.86	63.65	0.2649	-168.8	red clay
sc044a	22.91	67.13	2.930	24.84	79.55	0.3122	-193.1	red clay
sc045a	22.02	71.32	3.239	20.3	73.52	0.2761	-159.9	red clay
sc046a	22.3	67.28	3.017	17.27	58.19	0.2967	-94.66	red clay
sc047a	27.01	68.5	2.536	37.76	110.3	0.3424	-212.6	red clay
sc048a	23.68	66.94	2.827	22.79	71	0.321	-132.2	red clay
sc049a	24.86	67.8	2.727	27.42	84.01	0.3264	-160.4	red clay
sc050a	25.2	68.46	2.717	27.44	85.15	0.3223	-155.2	red clay
sc051a	24.4	66.85	2.740	25.39	80.3	0.3162	-142	red clay
sc052a	24.78	67.78	2.735	25.02	78.14	0.3203	-135.2	red clay
sc053a	23.86	69.34	2.906	40.56	119.3	0.3398	-198.5	red clay
sc054a	24.09	69.83	2.899	25.37	84.35	0.3007	-165.9	red clay

Spec.	Hc	Hcr	Hcr/Hc	Mr	Ms	Mr/Ms	Correction	Notes
sc055a	23.47	70.01	2.983	20.74	71.17	0.2915	-115.4	red clay
sc056a	27.45	69.27	2.523	35.48	105.7	0.3357	-200.2	red clay
sc057a	26.7	75.11	2.813	28.83	102.3	0.2819	-156.5	red clay
sc058a	26.2	73.31	2.798	24.71	85.74	0.2882	-114.8	red clay
sc059a	27.27	66.36	2.433	33.53	103.5	0.3239	-135.6	red clay
sc060a1	21.46	55.57	2.589	36.56	161.4	0.2264	-80.03	upper silt/clay lam.
sc060a2	25.71	68.11	2.649	29.46	110.7	0.266	-112.5	middle clay
sc060a3	24.98	57.02	2.283	53.79	221.2	0.2431	-58.59	lower silt/clay lam.
sc061a1	23.83	57.03	2.393	48.34	177.2	0.2727	-186.3	silt/clay lam.
sc061a2	23.5	56.1	2.387	55.4	219.8	0.252	-166.2	silt/clay lam.
sc062a1	19.93	55.22	2.771	14.78	60.35	0.2448	-38.72	silt/clay lam.
sc062a2	23.65	62.75	2.653	18.66	62.6	0.2981	-83.63	predominantely silt
sc063a1	23.26	63.45	2.728	22.58	72.98	0.3094	-139.7	upper clay/silt lam.
sc063a2	19.33	66.36	3.433	16.39	63.86	0.2566	-171	lower clay
sc064a	22.33	55.95	2.506	19	61.17	0.3106	-102.8	clay
sc065a	26.2	57.76	2.205	36.07	104.7	0.3445	-203	clay
sc066a	27.06	57.32	2.118	229.4	906.3	0.2531	-168.6	silt
sc067a	19.26	47.93	2.489	48.93	221.6	0.2208	-186.4	silt
sc068a	16.6	47.85	2.883	18.39	68.18	0.2698	-196.8	clay
sc069a	24.07	56.16	2.333	44.33	134.9	0.3285	-333.5	clay
sc070a	22.69	51.79	2.283	251.6	1150	0.2188	-212.2	silt
sc071a	25.62	54.47	2.126	275.4	1136	0.2425	-204.3	silt
sc072a1	16.89	49.38	2.924	24.05	87.06	0.2763	-287.7	upper clay
sc072a2	27.52	59.65	2.168	133.8	532.6	0.2512	-194.8	lower silt
sc072a3	26.2	57.51	2.195	140.1	592.5	0.2365	-100.4	lower silt
sc073a1	14.19	44.2	3.115	17.51	68.9	0.2541	-253.2	upper clay
sc073a2	26.76	57.73	2.157	190.4	787.8	0.2417	-126.2	middle silt
sc073a3	14.11	46.62	3.304	13.27	53.97	0.2458	-169.1	lower clay
sc074a1	13.41	47.04	3.508	17.33	70.11	0.2472	-314	upper clay
sc074a2	29.39	58.57	1.993	226.1	796.4	0.2839	-233.8	middle silt
sc074a3	13.68	43.1	3.151	22.31	85.94	0.2596	-286.3	lower clay
sc075a1	11.87	40.68	3.427	17.16	73.39	0.2338	-255.8	upper clay
sc075a2	28.75	57.24	1.991	107.3	363.4	0.2954	-149.6	middle silt
sc075a3	18.99	49.65	2.615	25.19	87.83	0.2868	-191	lower clay
sc076a1	11.31	40.22	3.556	19.54	82.84	0.2359	-340	upper clay
sc076a2	27.74	57.61	2.077	135.7	510.3	0.2659	-89.05	lower silt
sc077a1	13.42	46.46	3.462	14.11	67.38	0.2094	-157.3	upper clay
sc077a2	28.87	59.02	2.044	135	487	0.2772	-115.7	middle silt
sc077a3	8.045	36.88	4.584	38.26	583.8	0.0655	-244.3	lower clay
sc078a	21.16	52.04	2.459	260.2	1414	0.184	-161.1	silt

Appendix E1: Paleosecular variation records from North America

Baffin Island (seven records)
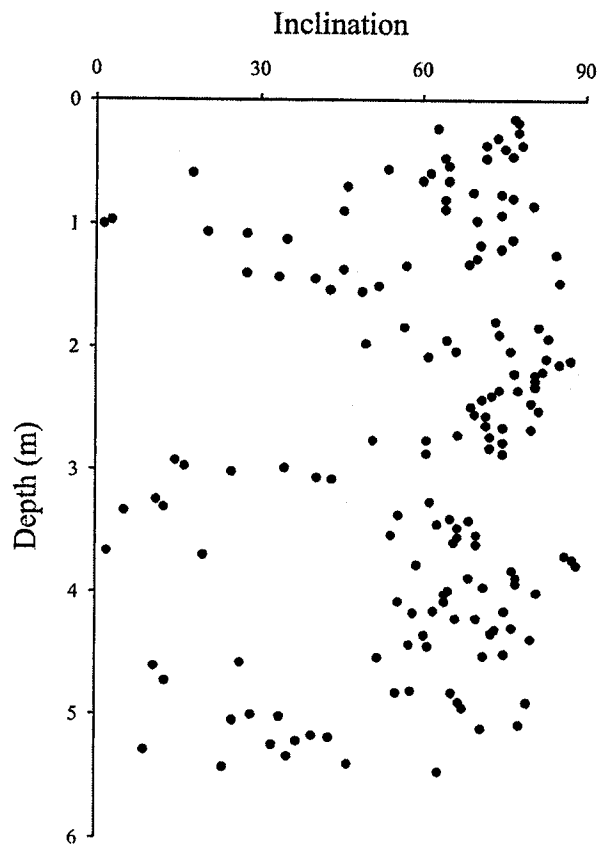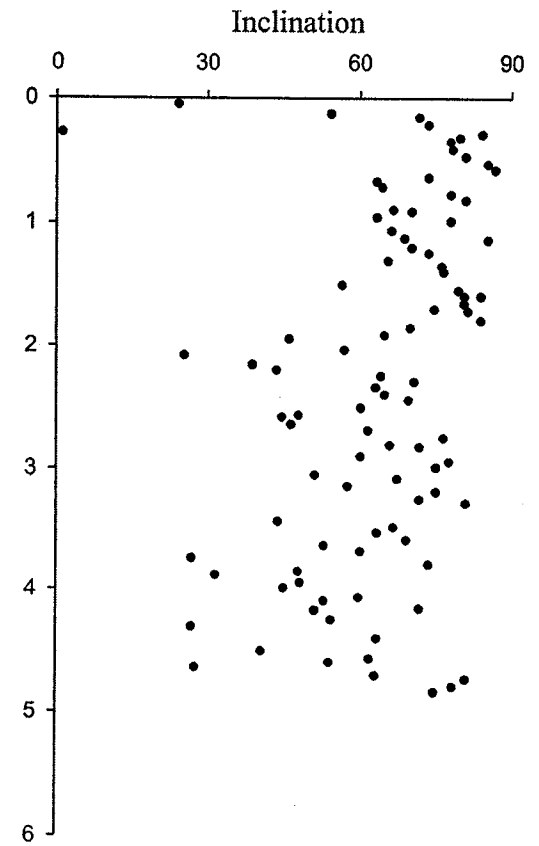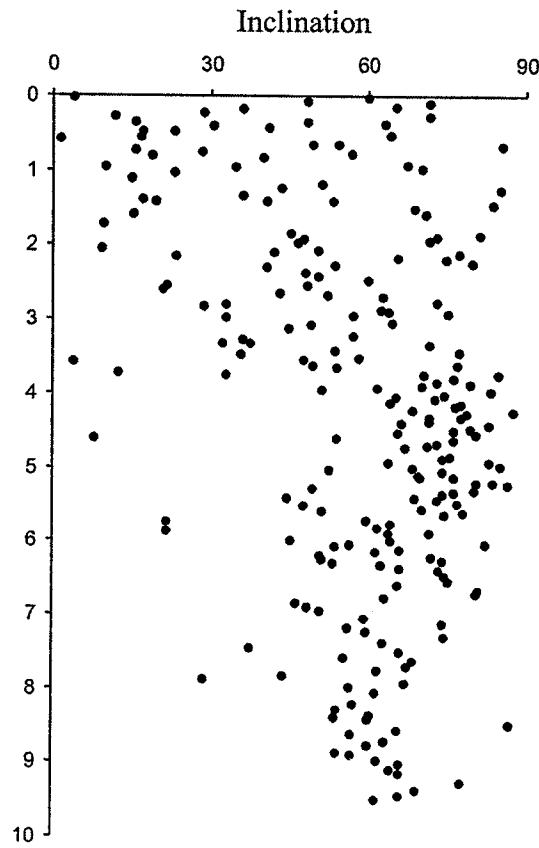
(Andrews et al., 1986)

Baffin Island (seven records)

(Andrews et al., 1986)

Baffin Island (seven records)

Inclination
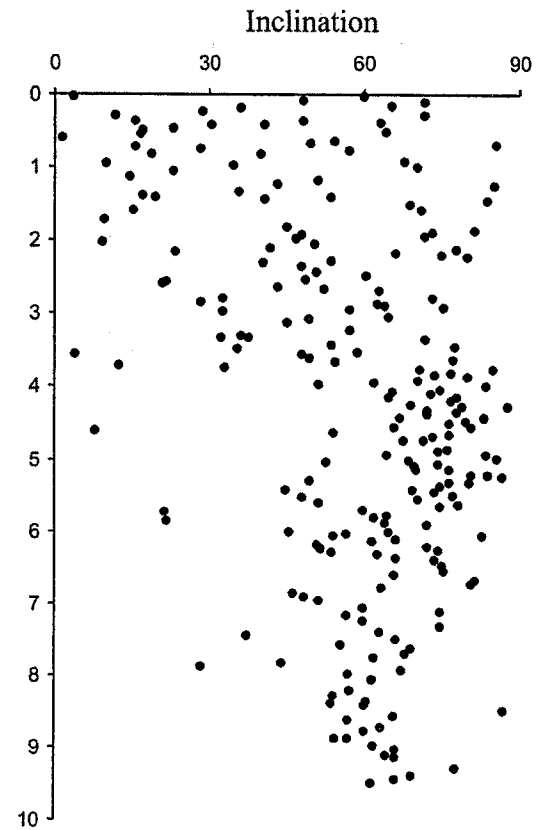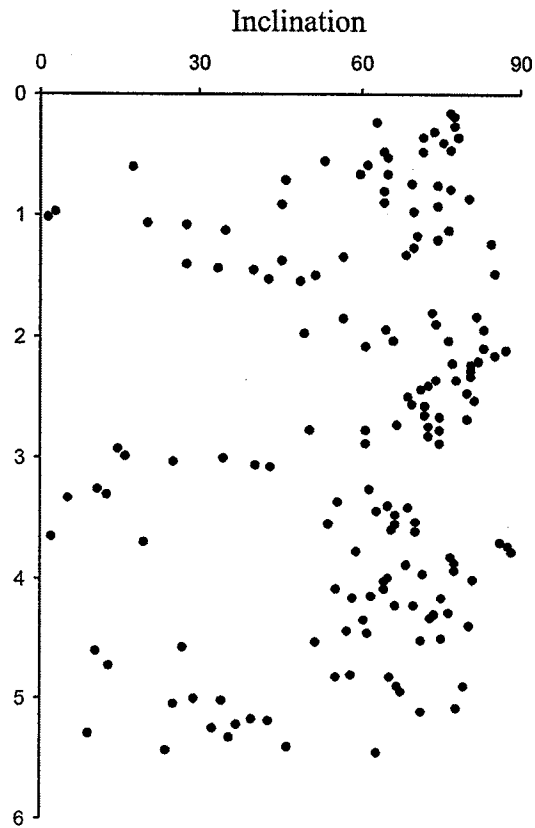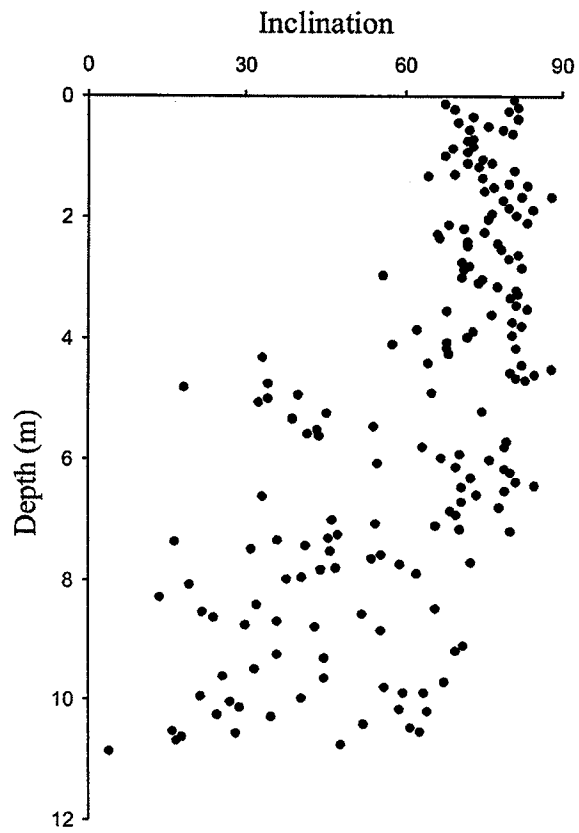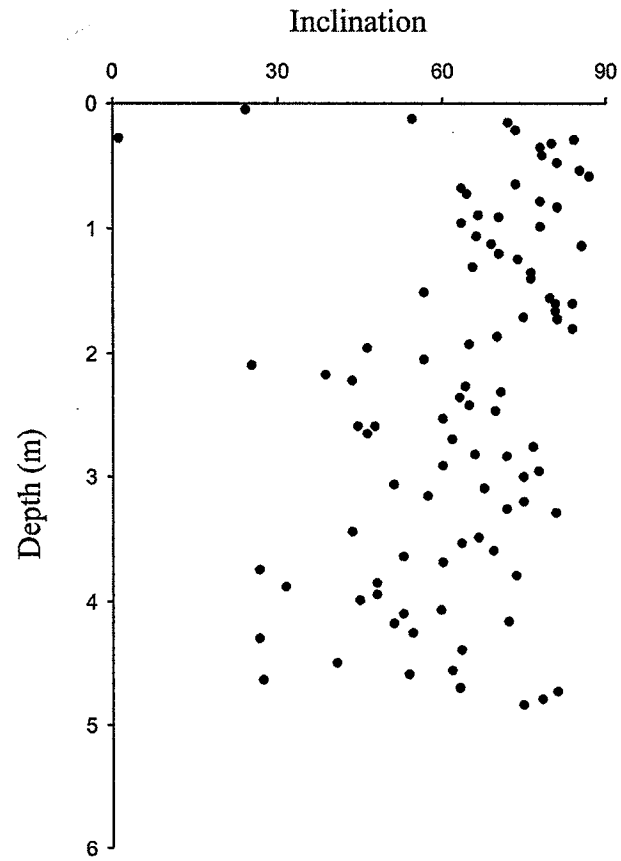
(Andrews et al., 1986)

Lake St. Croix (Minnesota)
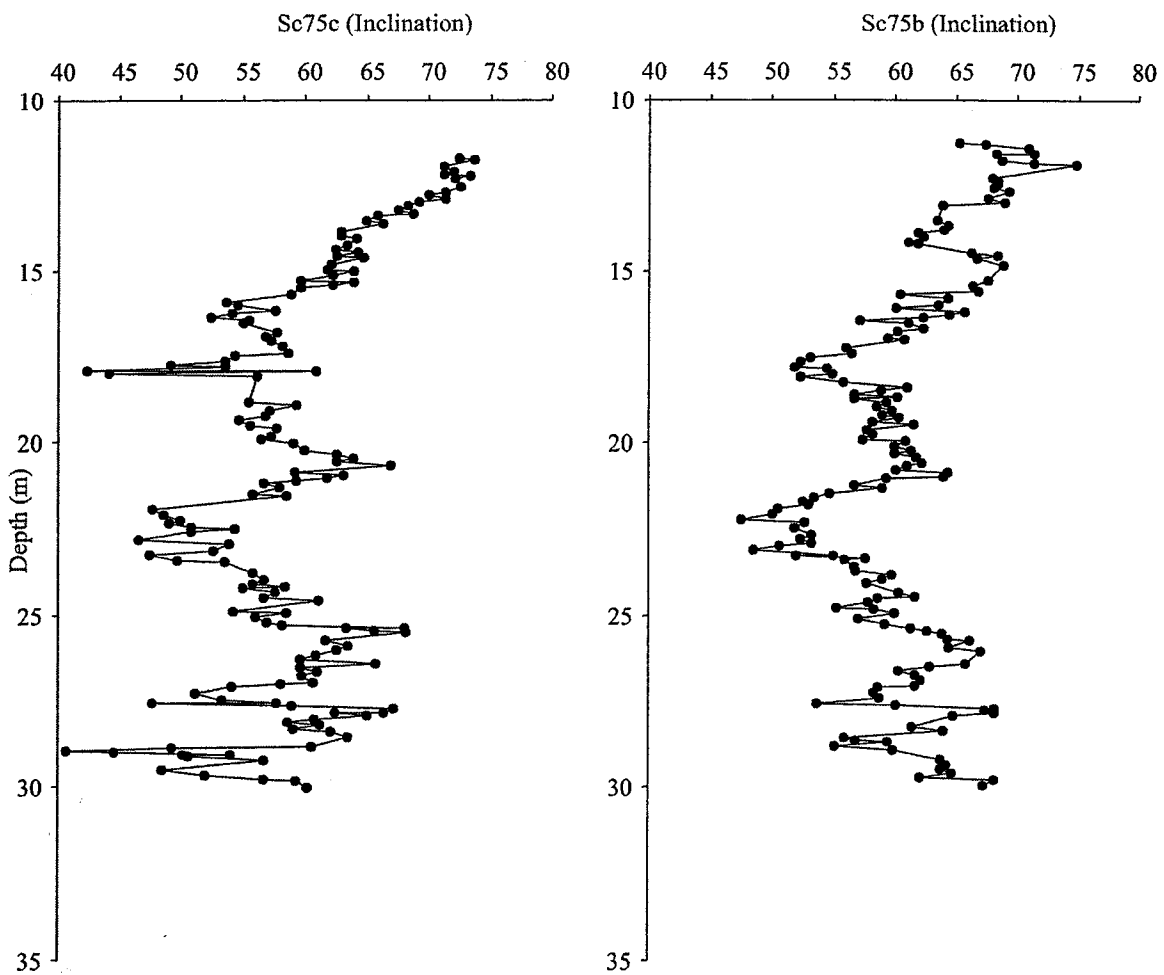
(Banarjee et al., 1979)

Lake sediment records from Hanna and Verosub (1989)
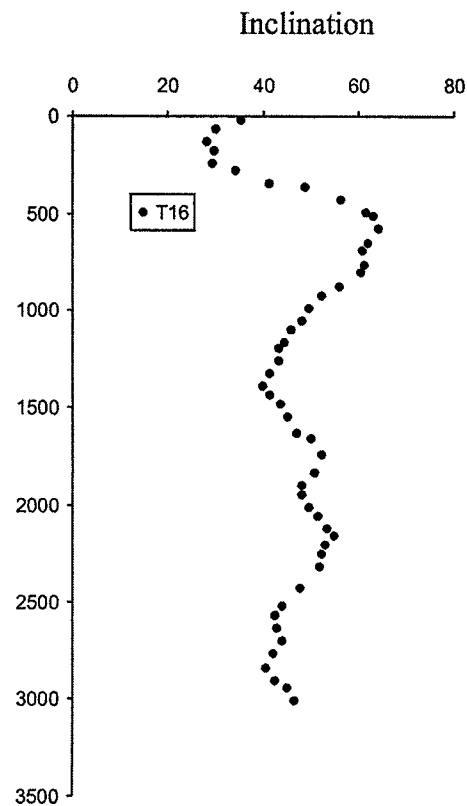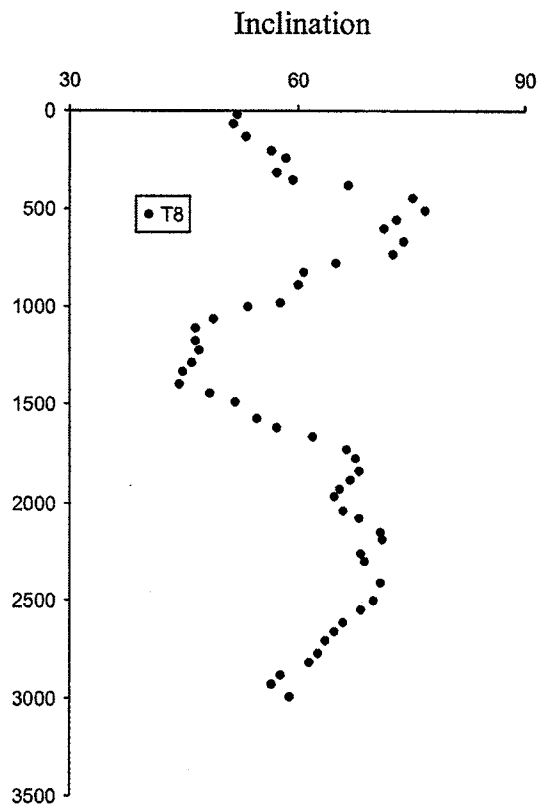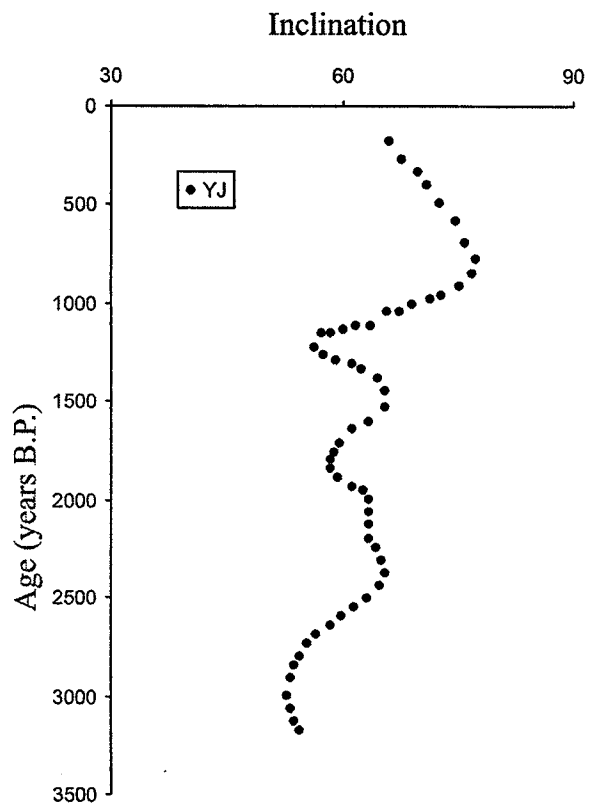
Lake sediment records from Hanna and Verosub (1989)
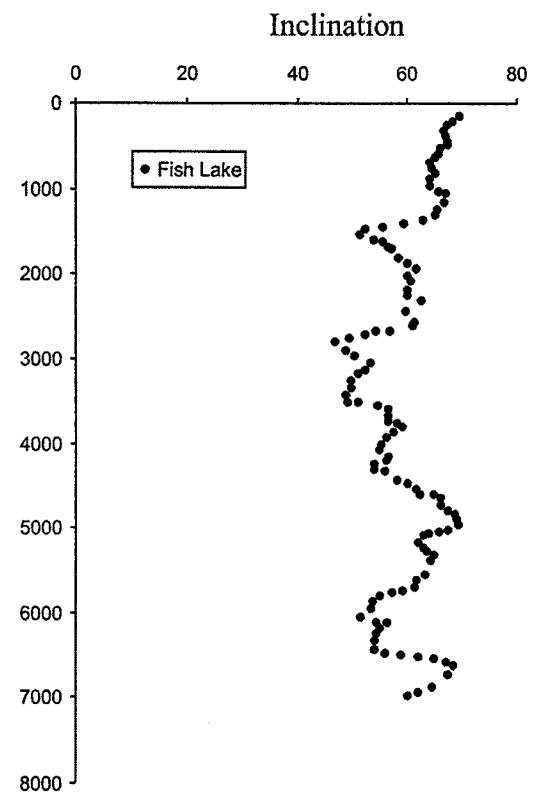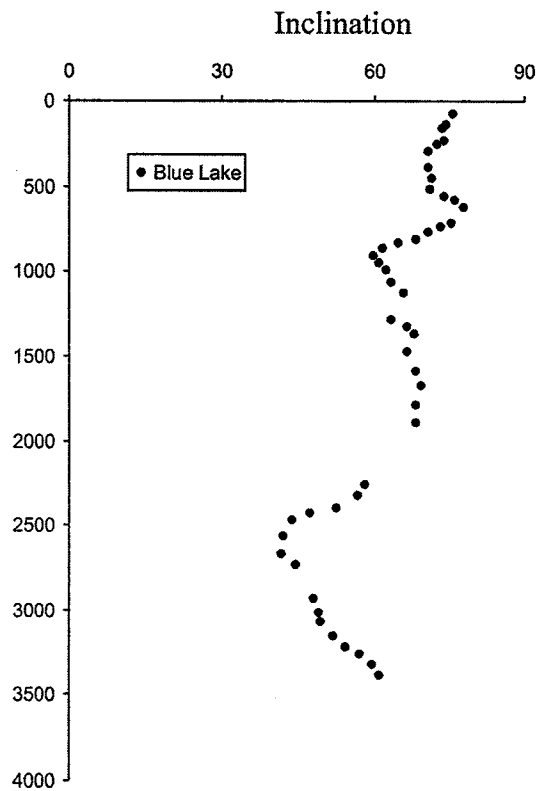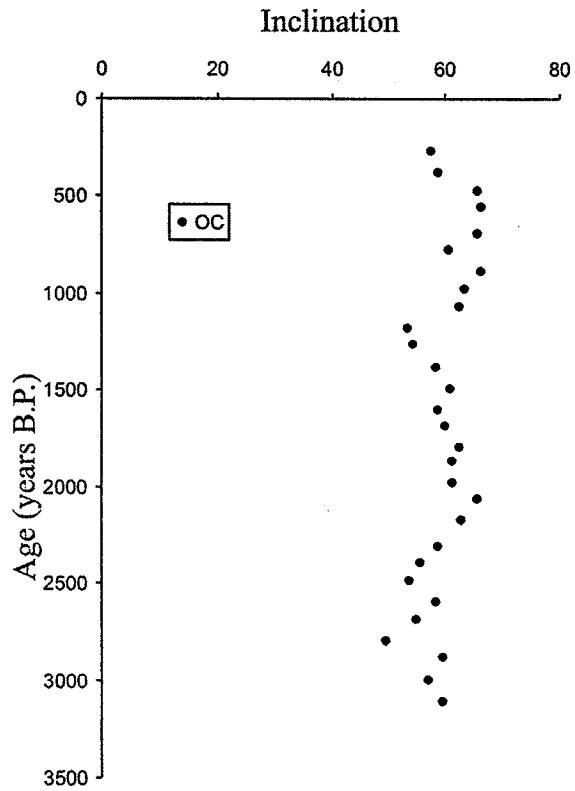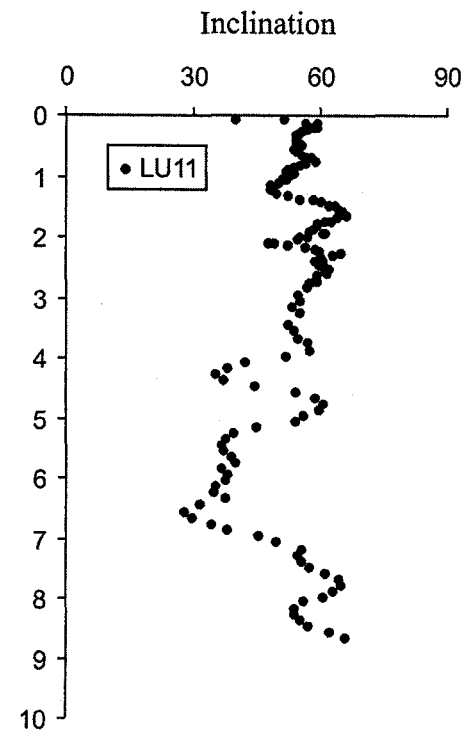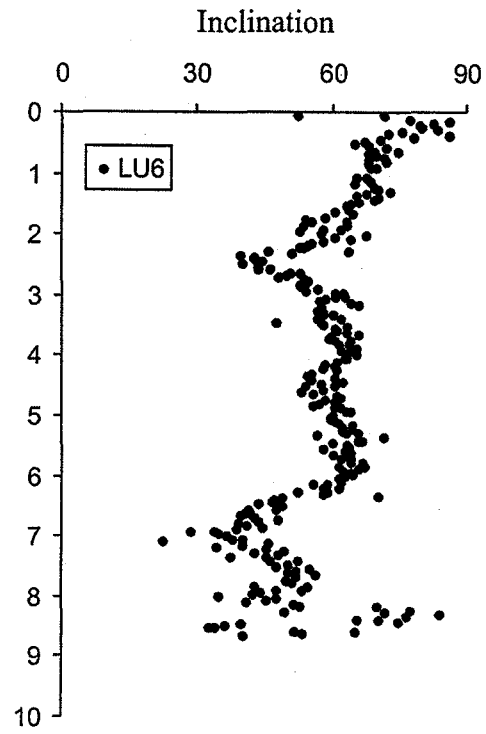
Lake sediment records from Hanna and Verosub (1989)
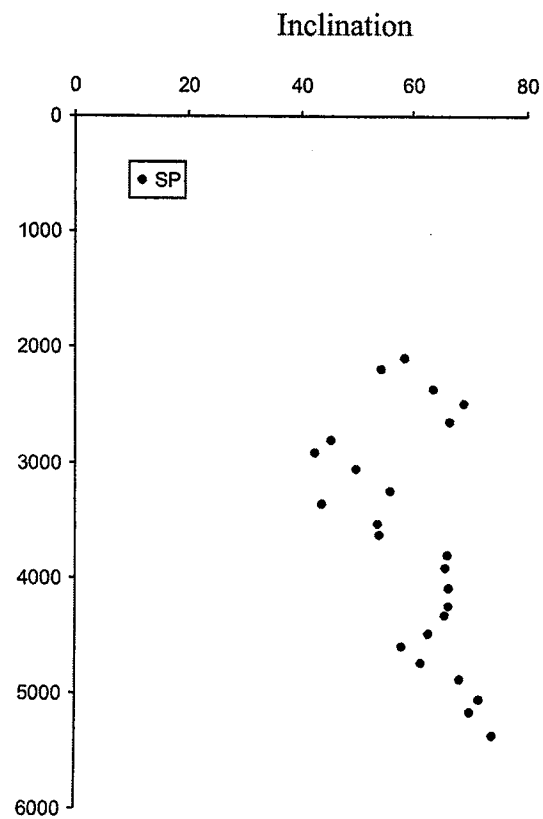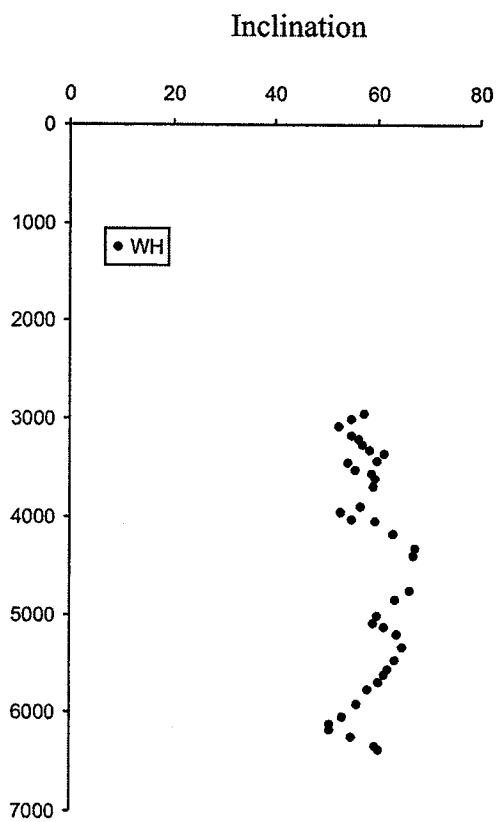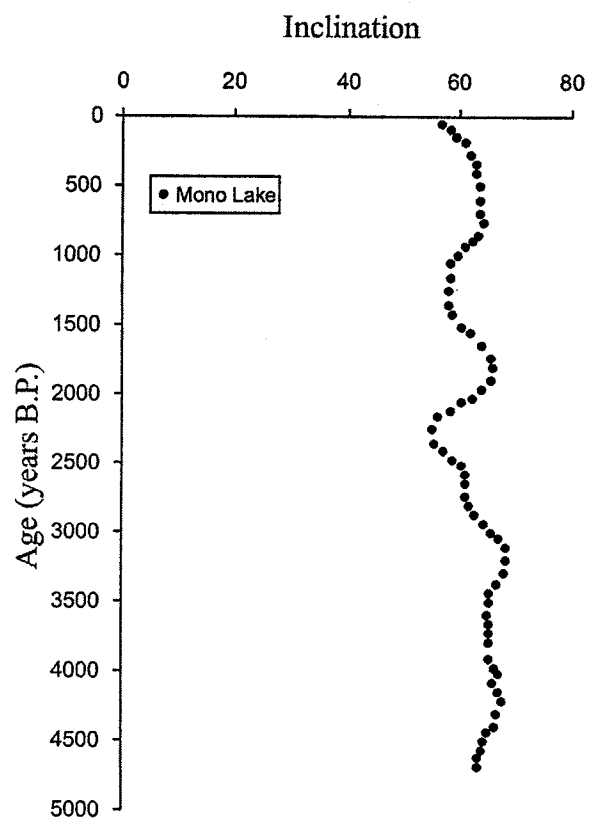
Lake Huron (four records)
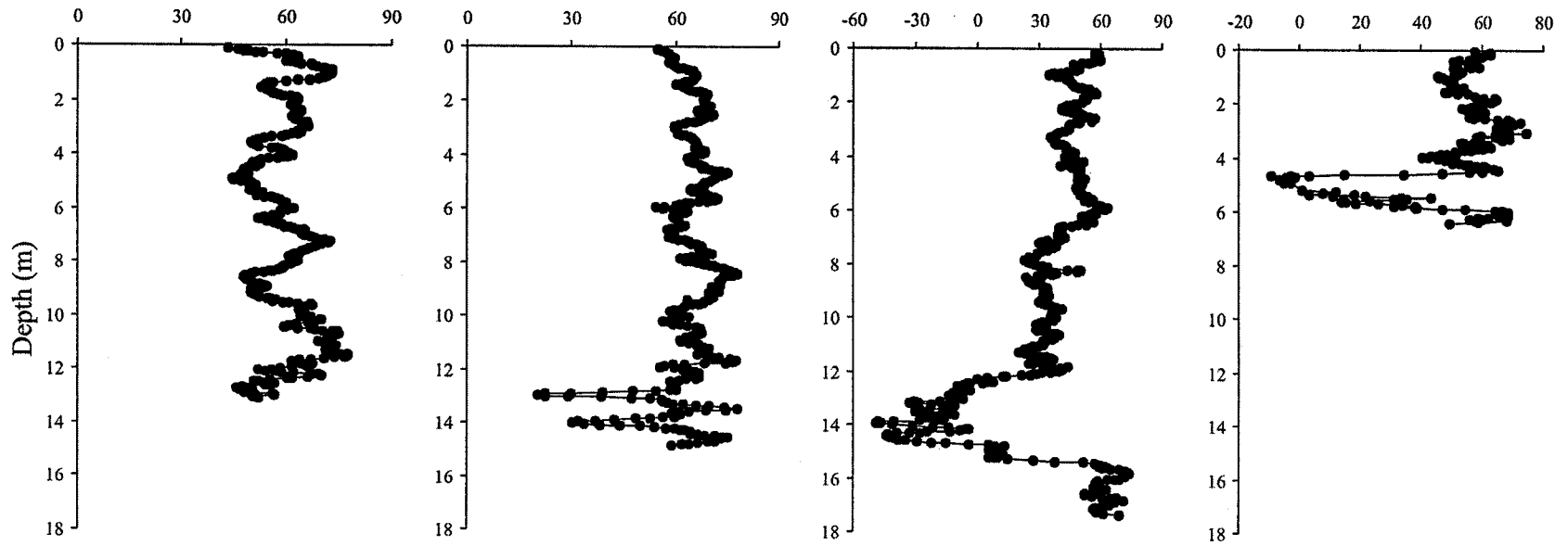
(Mothersill, 1981)

Lake Superior (Mothersill, 1988)
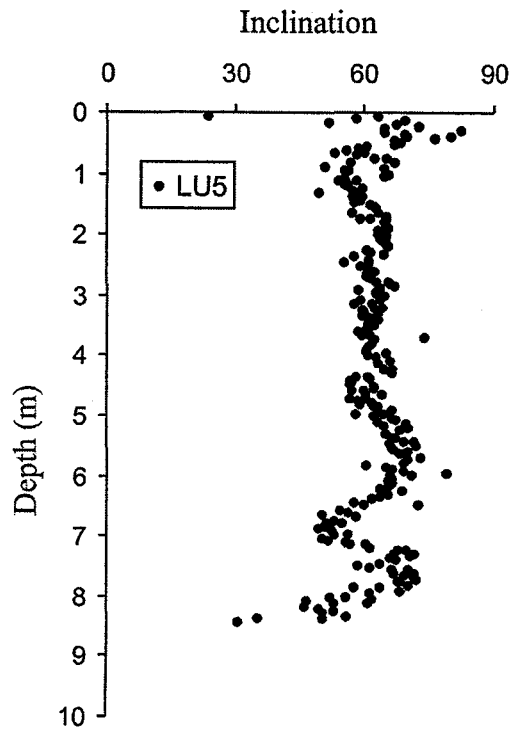
Lake Superior (Mothersill, 1988)
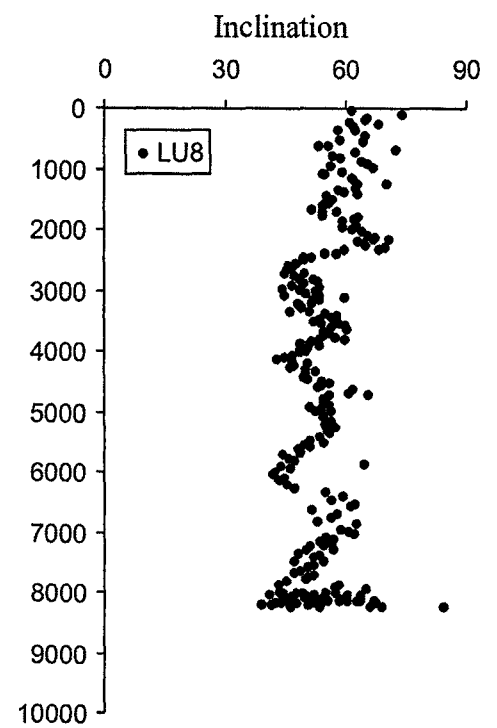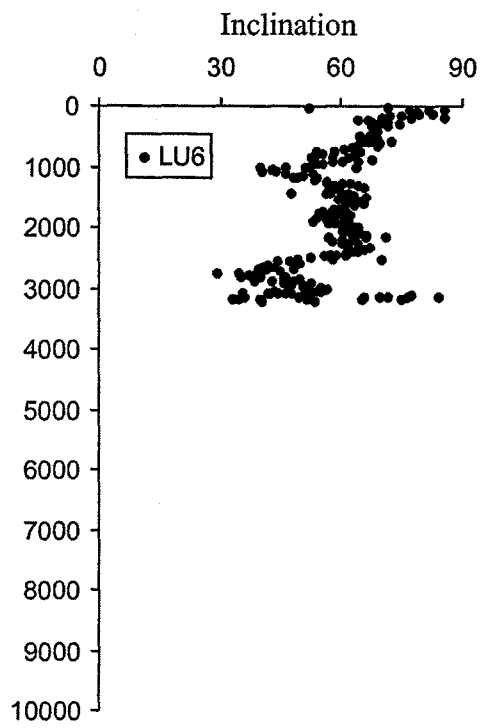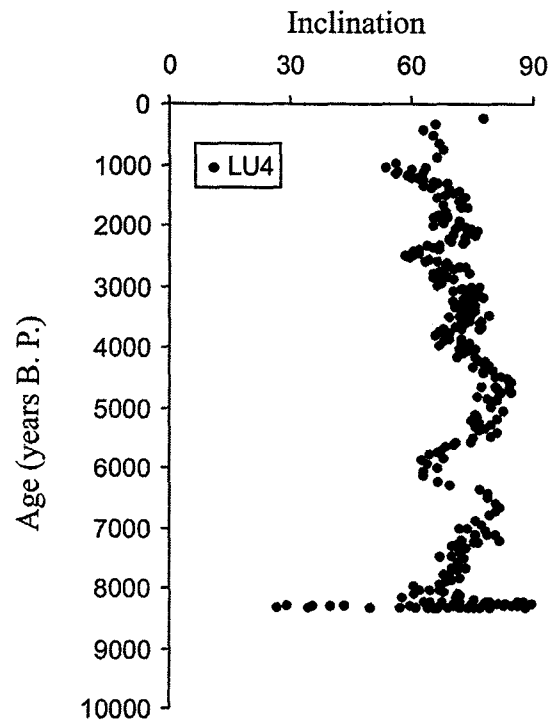
Lake Superior (Mothersill, 1988)
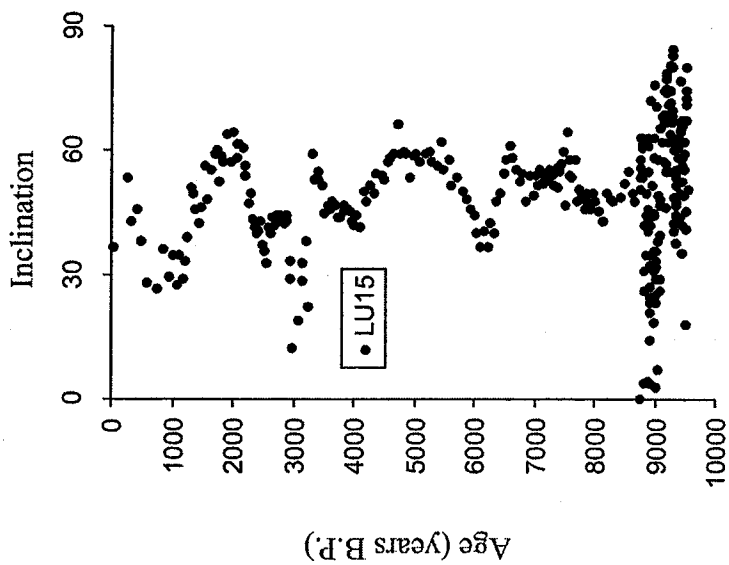
Lake Erie (two records)

(Mothersill, 2003)

Elk Lake

Inclination
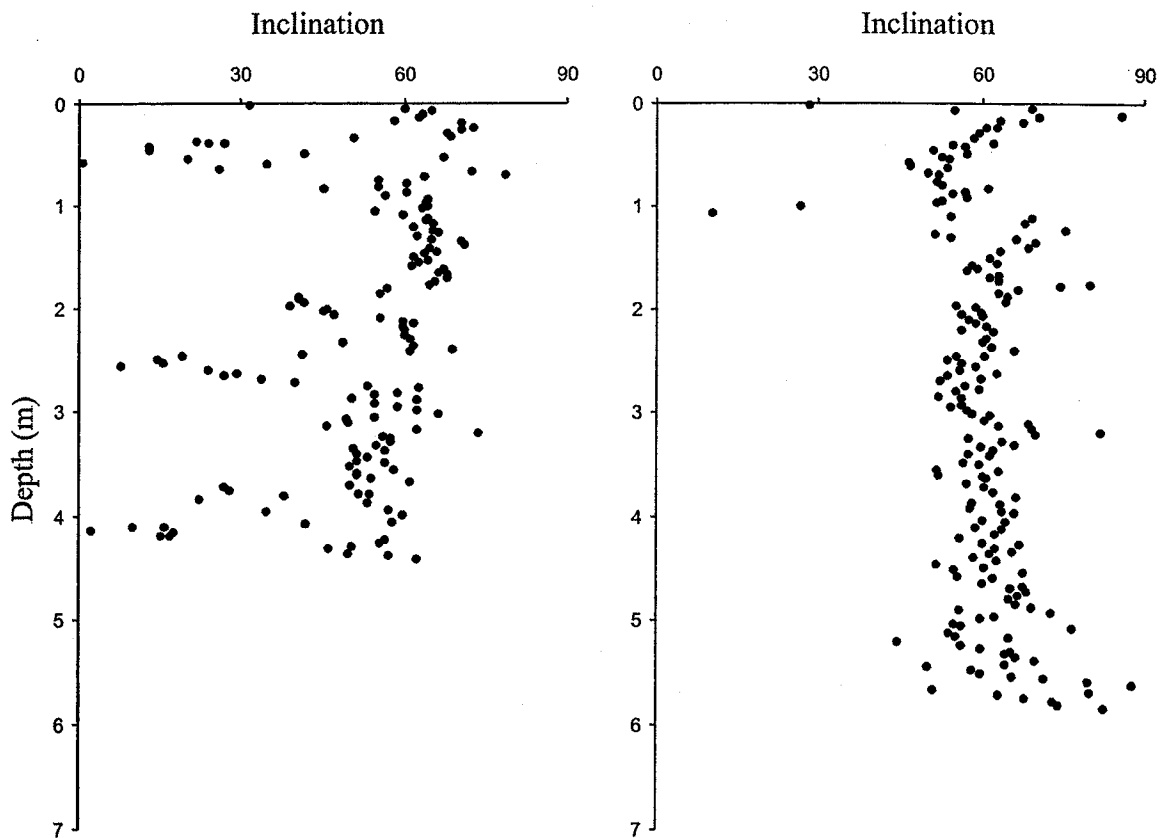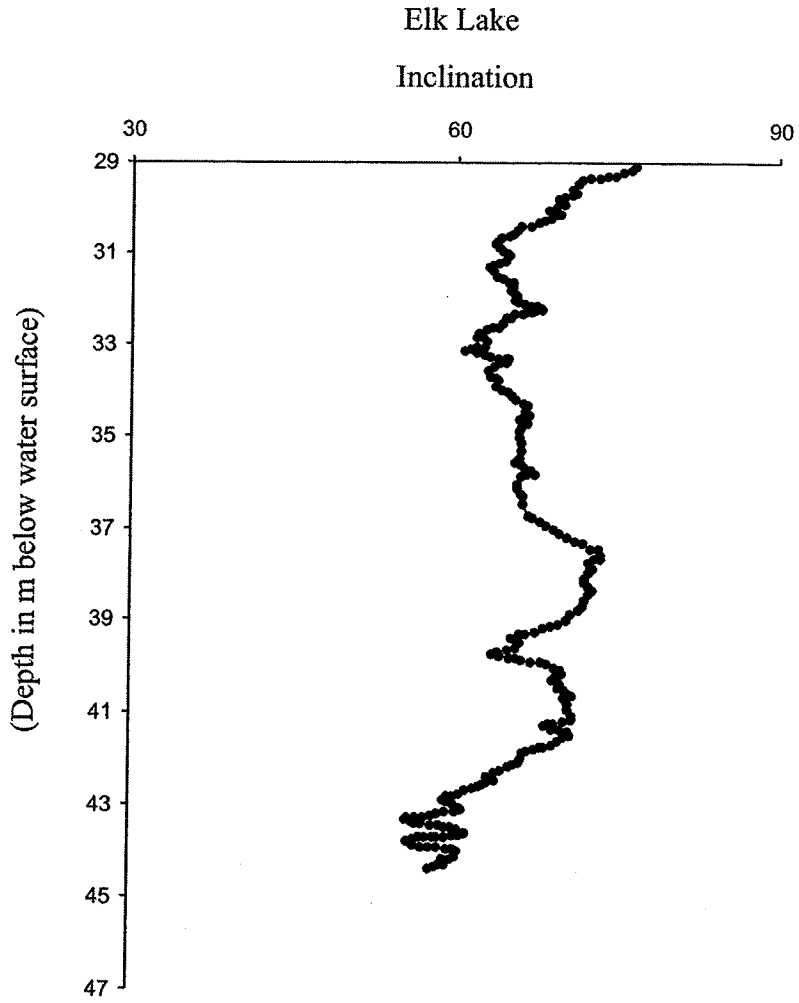
(Sprowl and Banarjee, 1989)

Fish Lake
(catchment: weathered basalt, tephra)

Inclination

Age (years B.P.)
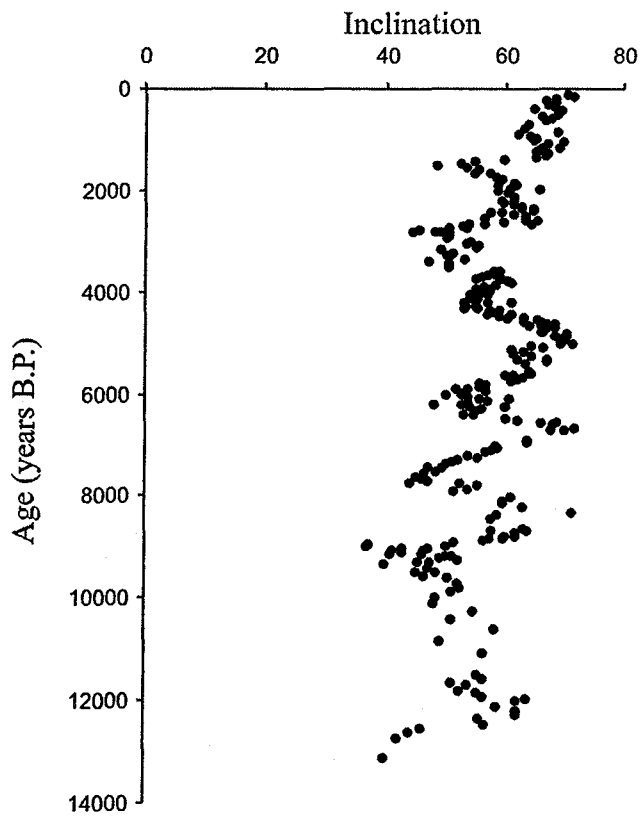
(Verosub et al., 1986)

Lake Michigan

Inclination
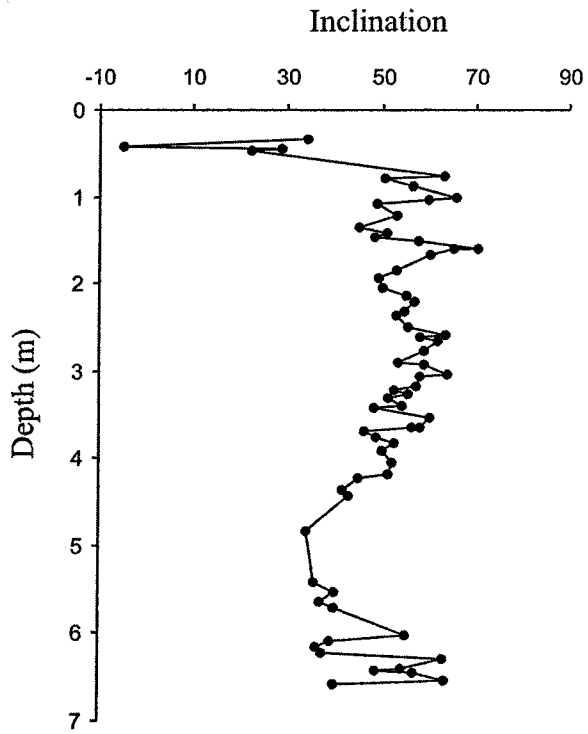
(Vitorello and Van der Voo, 1977)

Lake Lama (Frank et al., 2002)
North Central Sibera
69.5degN, 90.2degE
GAD=79.4degN
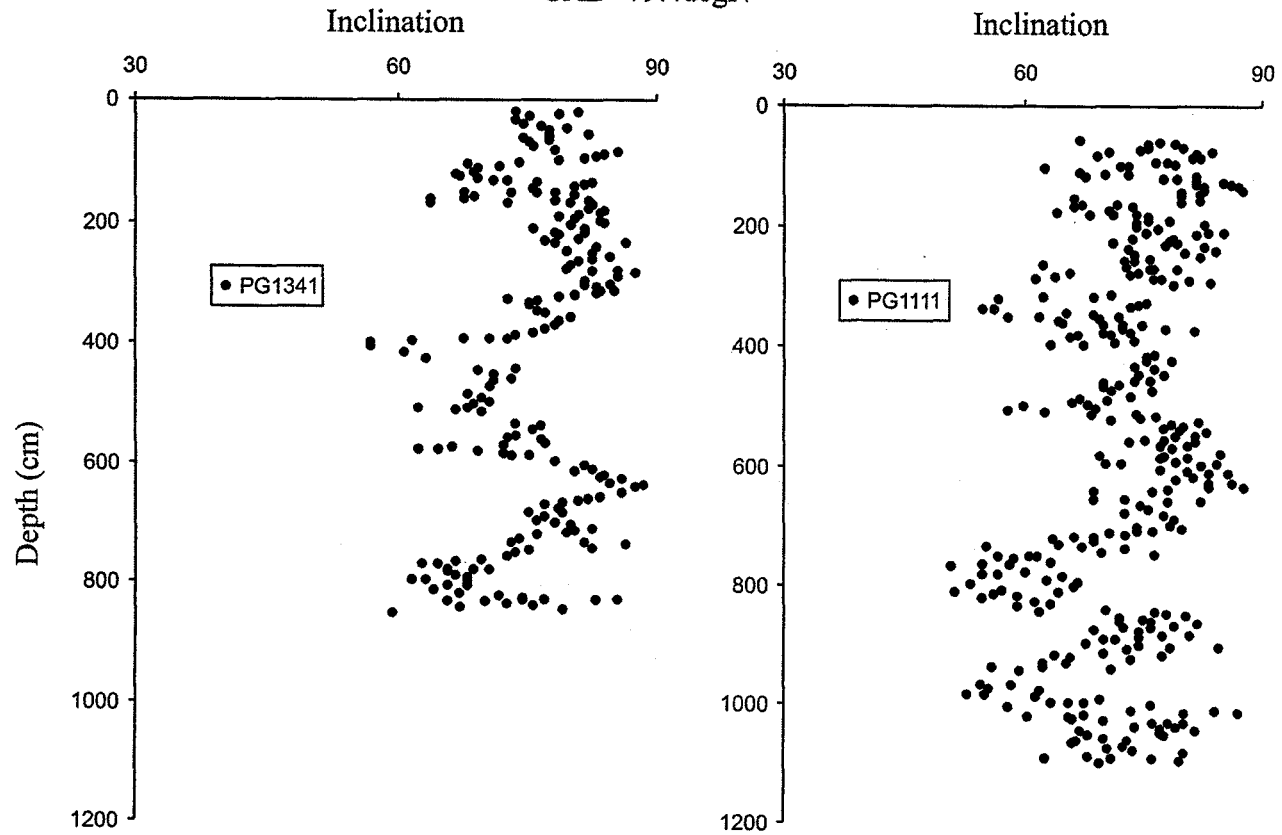
Birkat ram (Golan Heights), crater lake, Israel
(Frank, Schwab and Negendank, 2002)
33deg15'N, 35deg40'E
GAD=52.7deg
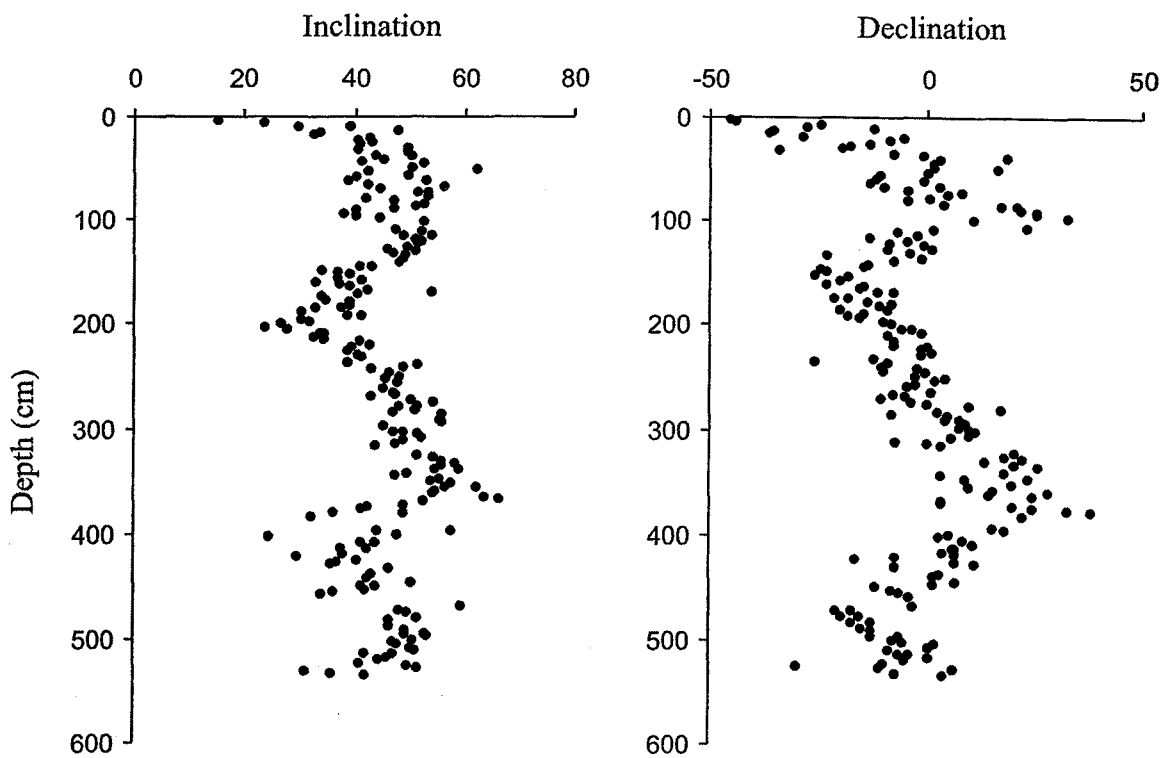
Lithology: Mainly Quaternary Pyroclastica and basalt catchment
Homogenous dark brown sediments, fine grained clastic with clay
mineralsand intercalated layers of calcareous microfossils

Lake Lisan (Paleo Dead Sea)

Inclination
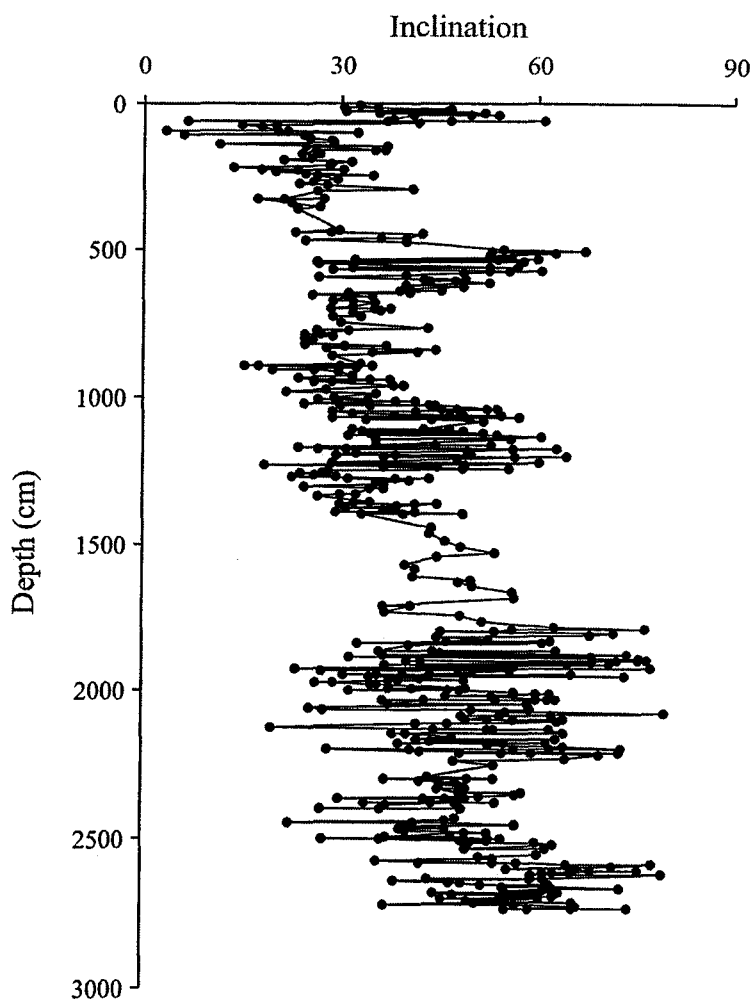
lithology: alternating layers of aragonite, dark detritus
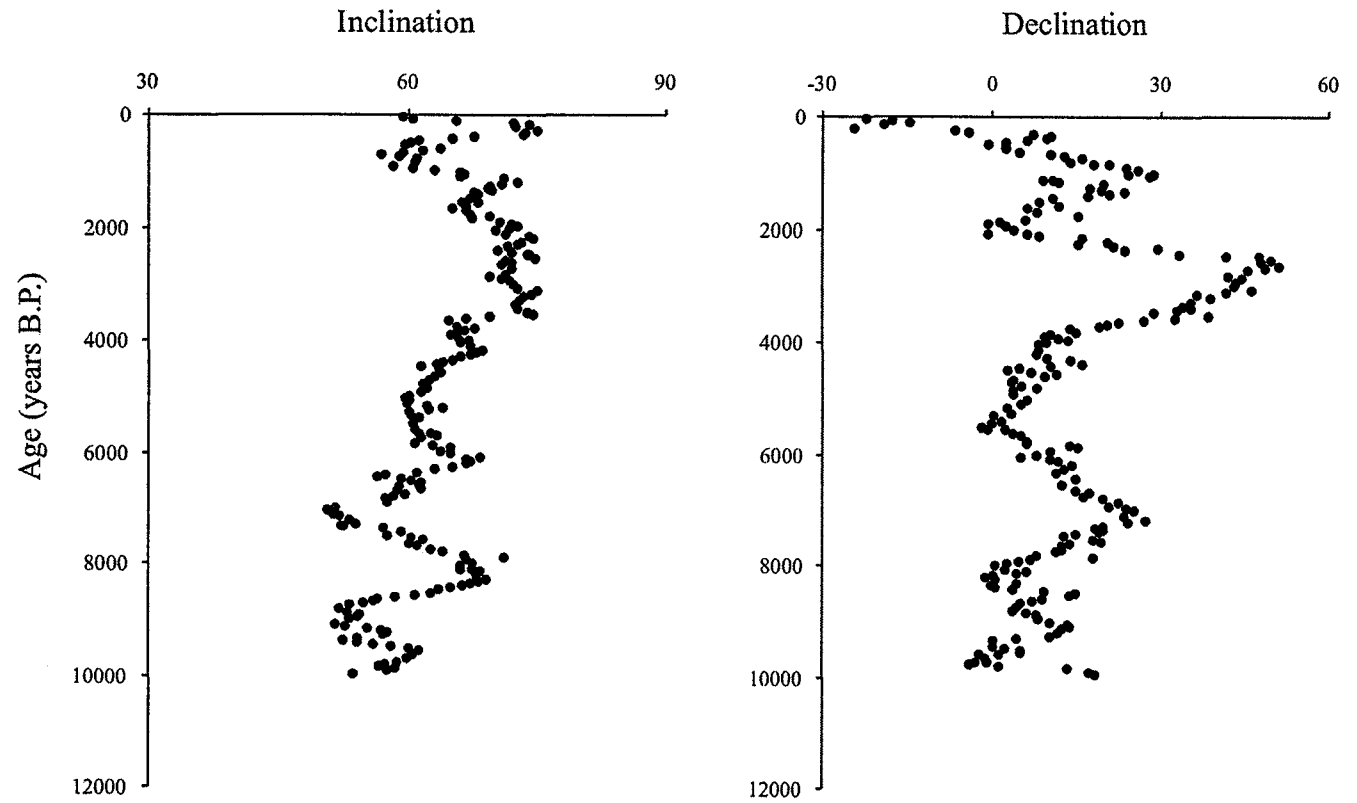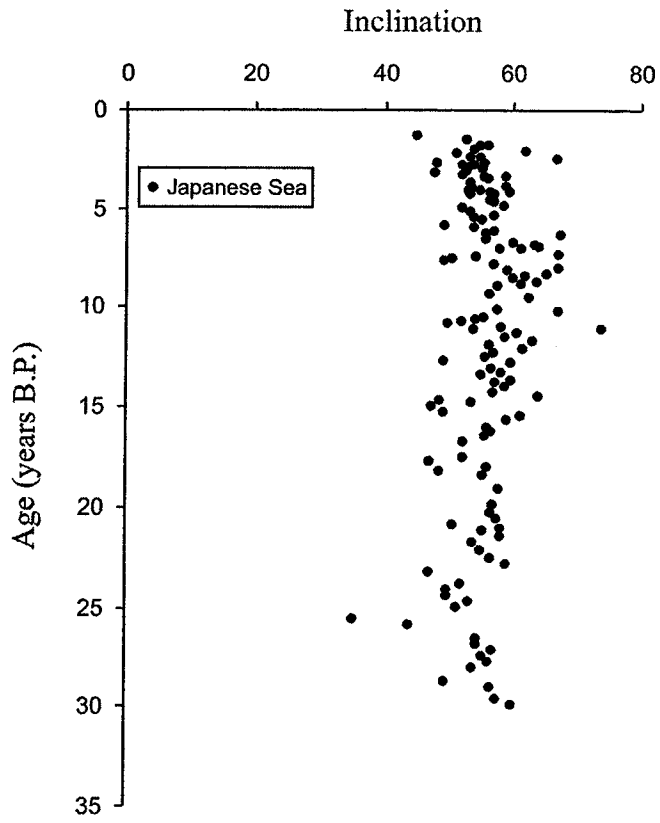few thick clastic layers and gypsum

Lac du Bouchet (Thouveny, 1990)
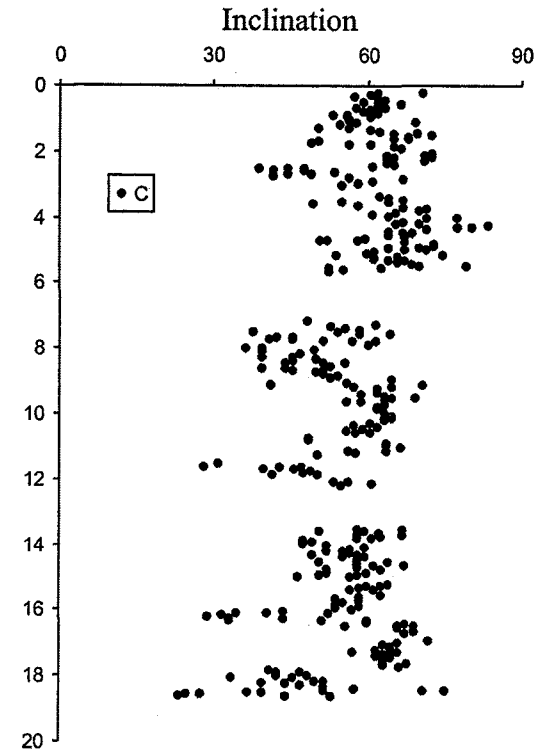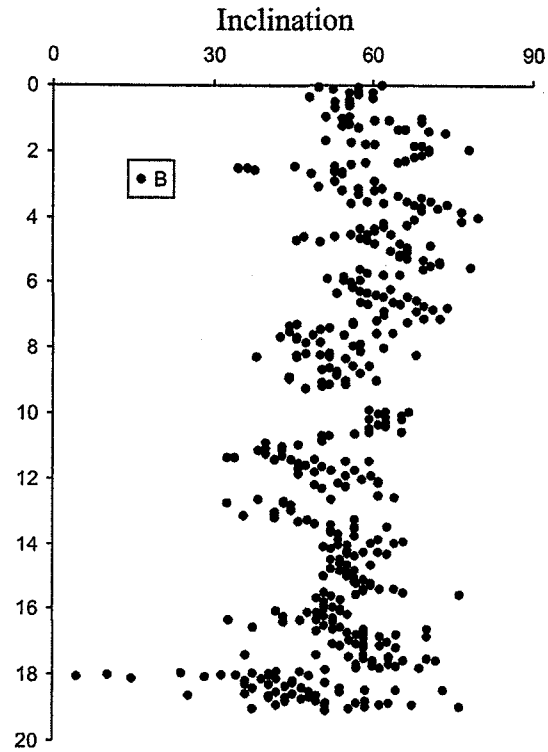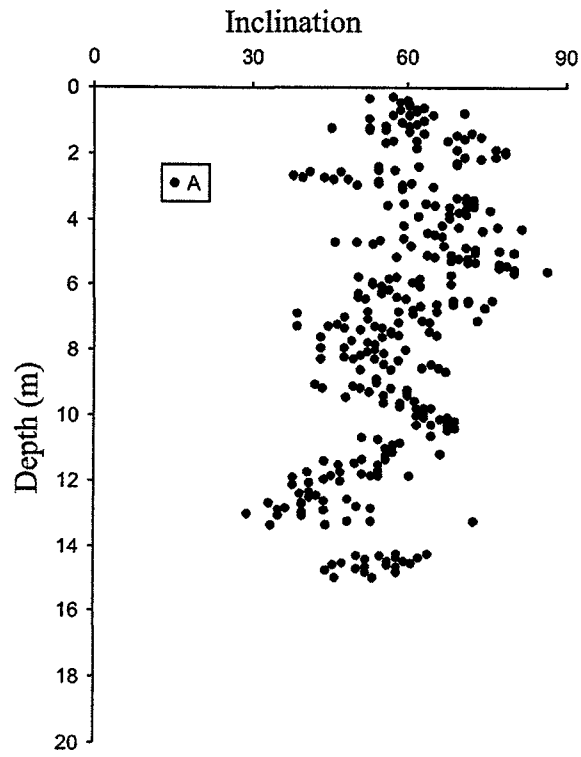
Lac du Bouchet (Thouveny, 1990)
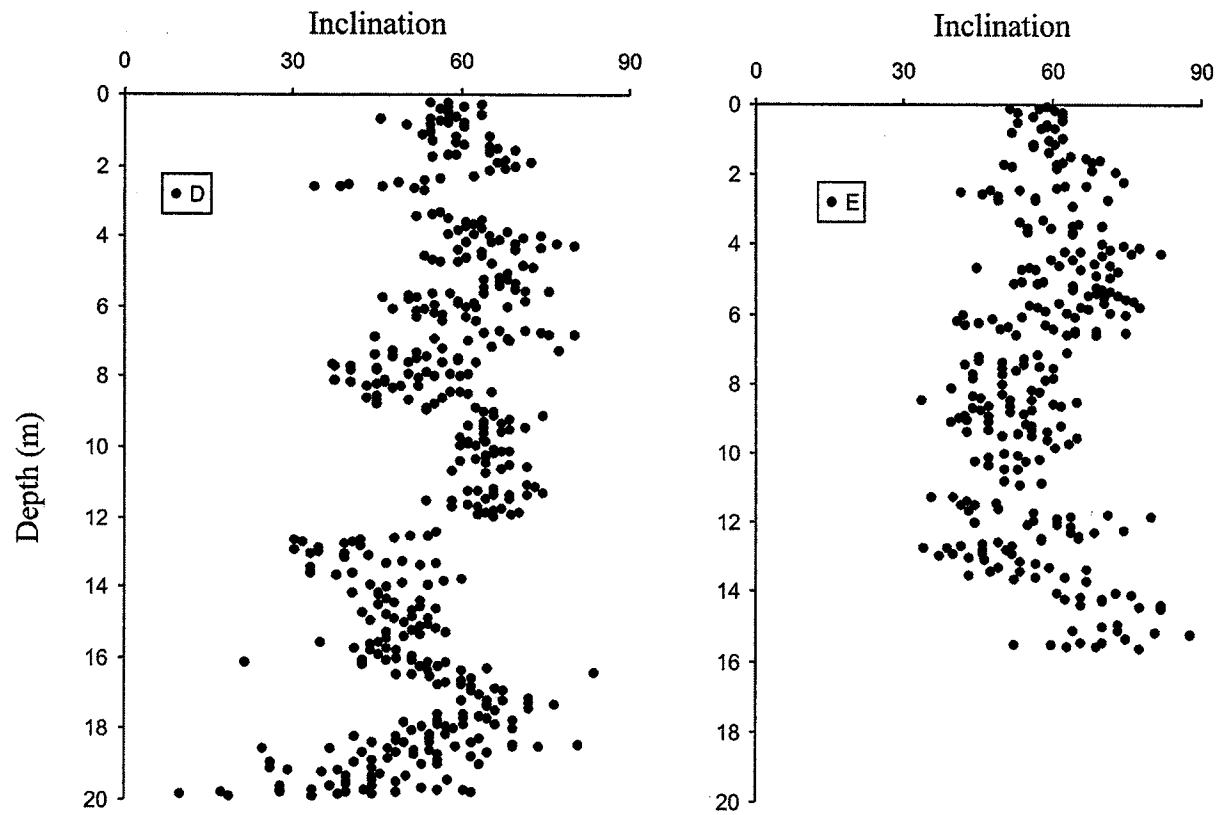
British secular variation curve (Turner and Thompson, 1982)
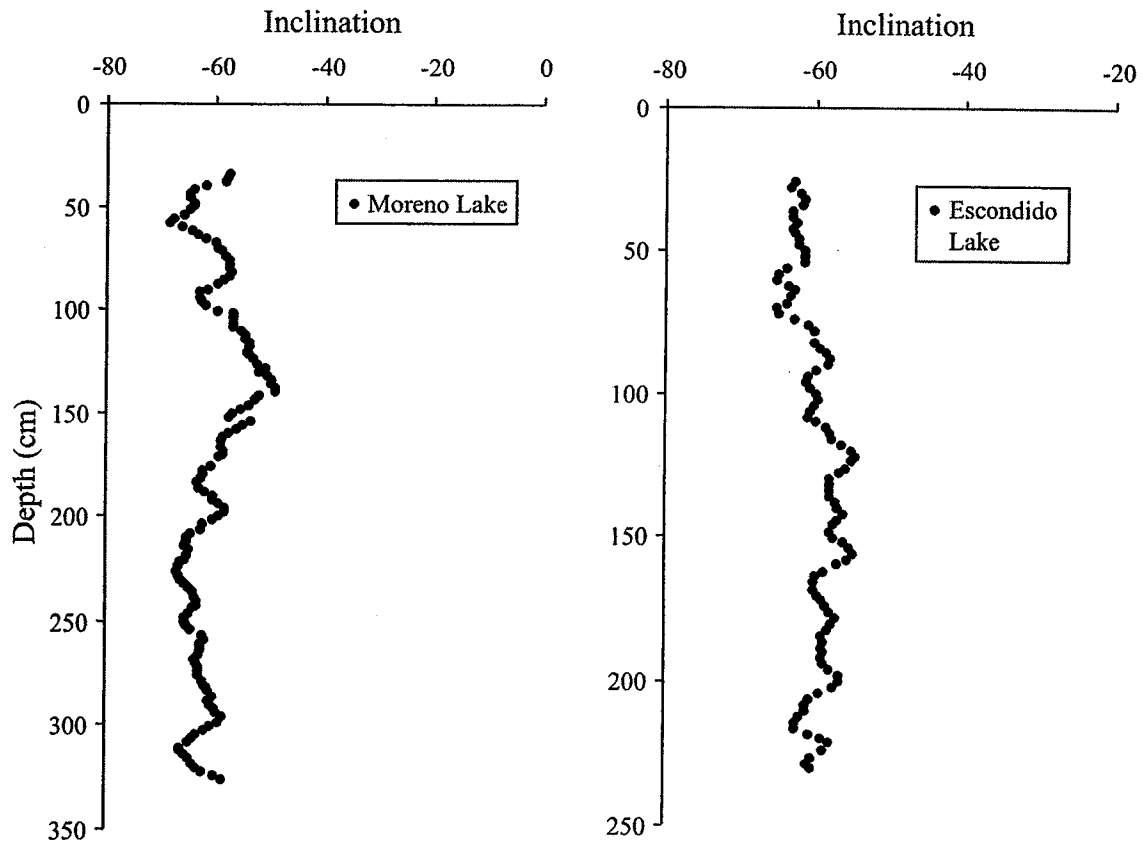
Inclination

Declination

Age (years B.P.)

Japanese Sea (Yamazaki et al., 2003)

Appendix E3: Paleosecular variation records from South America

Argentina
(Gogorza et al., 2002)

Argentina
(Gogorza et al., 2002)